2013-12-13

Characterizing the Relationship Between Energy Metabolism and Mesenchymal Stem Cell Therapy in the Infarcted Heart

Hughey, Curtis

UNIVERSITY OF CALGARY

Characterizing the Relationship Between Energy Metabolism and Mesenchymal Stem Cell Therapy in the Infarcted Heart

by

Curtis Connor Hughey

A THESIS

SUBMITTED TO THE FACULTY OF GRADUATE STUDIES

IN PARTIAL FULFILMENT OF THE REQUIREMENTS FOR THE

DEGREE OF DOCTOR OF PHILOSOPHY

DEPARTMENT OF BIOCHEMSITRY AND MOLECULAR BIOLOGY

CALGARY, ALBERTA

DECEMBER, 2013

Abstract

Objective: A constant provision of adenosine triphosphate (ATP) is of necessity for cardiac contraction. If the heart progresses towards failure following a myocardial infarction (MI) it may undergo metabolic alterations that have the potential to compromise its ability to meet energetic demands. The main focus of this dissertation was to evaluate the efficacy of mesenchymal stem cell (MSC) transplantation to mitigate abnormalities in energy metabolism that contribute to ATP synthesis post-MI in the presence and absence of diet-induced insulin resistance.

Methods: C57BL/6 mice were chow or high-fat fed prior to induction of a MI via chronic ligation of the left anterior descending coronary artery. Post-ligation, MSCs were transplanted via intramyocardial injection. Serial echocardiography was performed prior to and up to 28 days post-MI to evaluate cardiac systolic function. Hyperinsulinemic-euglycemic clamps coupled with the administration of isotopic tracers were employed post-MI to assess systemic insulin sensitivity and insulin-mediated, tissue-specific substrate uptake in the conscious, unrestrained mouse. High-resolution respirometry was utilized to evaluate cardiac mitochondrial function in saponin-permeabilized cardiac fibers. Western blotting was completed to assist in identifying molecular mechanisms through which the MSC therapy may modulate cardiac and systemic metabolic phenotypes.

Results: The improved systolic performance in MSC-treated mice was associated with a lessening of non-pathological *in vivo* insulin-stimulated cardiac glucose uptake. The

changes in glucose uptake may have been via the MSC-mediated alterations in fatty acid availability/utilization. MSC therapy preserved fatty acid uptake in the absence of diet-induced insulin resistance. Conversely, the cell-based treatment reduced circulating non-esterified fatty acid concentration in high-fat fed mice. Additionally, potential impairments in insulin signalling may have been minimized as indicated by conservation of the p-Akt/Akt ratio. Down-stream of glucose uptake, the administration of MSCs conferred protective effects to mitochondrial oxidative phosphorylation efficiency, maximal function and mitochondrial content.

Conclusions: The experiments conducted in this dissertation provide insight into the utility of MSC transplantation as a metabolic therapy for the metabolic perturbations that characterize insulin resistance in the infarcted heart. Also, these studies propose potential mechanisms of action that lead to an enhanced energetic and functional state in the infarcted heart following MSC transplantation.

Acknowledgements

The journey towards completing this dissertation has been a series of personal and professional successes and failures. Times of elation have been tempered by periods of frustration and self-doubt. However, the sum of these moments has brought forth a sense of pride in the work completed.

Importantly, the work presented in this thesis has not been though solitary actions. As such, I am pleased to have the opportunity to express my thanks to those who have assisted my scientific endeavours and made my years as a graduate student some of my most profound to date.

Firstly, I would like to express my deepest appreciation to my supervisor, Dr. Jane Shearer. With patience, Dr. Shearer has been able to balance providing mentorship with scientific independence. Furthermore, she has opened my eyes to qualities away from the bench that promote success as an academic researcher. Her maddening attention to detail when evaluating written prose, oral presentations and visual aids has drove me to finally invest care into communicating my scientific work. Undoubtedly, Dr. Shearer's efforts will have a lasting effect throughout my professional life.

I am indebted to Dr. Darrell Belke and Dr. Dustin Hittel for their guidance given as supervisory committee members. Dr. Belke has spent countless hours demonstrating and discussing experimental techniques and challenging me to contemplate the strengths and weaknesses of each. Conversations with Dr. Hittel have been insightful as he has the rare ability to think big and his enthusiasm for science is contagious.

I would like to particularly thank Virginia Berry for her role as lab manager. Without complaint, Virginia has undertaken the lion's share of less glamorous laboratory

tasks during my tenure in Dr. Shearer's laboratory. More importantly, Virginia has been as invested in the success of my scientific work as I have. Such a quality is rare in a co-worker and I am very fortunate to have been the recipient of her support.

I have largely benefited from my time in Dr. David Wasserman's laboratory at Vanderbilt University. Aside from enjoying his humour in the midst of long hours and challenging experiments, I have developed a great appreciation for collaboration, high research standards and transparency in the scientific process under his teaching.

A special thanks to Freyja James, Deanna Bracy, Lianli Ma for their technical expertise during the completion of my experiments.

Thank you to the Canadian Institutes of Health Research and the Killam Trusts for their funding support.

I am extremely grateful for the Dr. David Severson's efforts invested on my candidacy and dissertation examination committees.

Much gratitude goes to Dr. Paul Fedak for serving on my candidacy examination committee.

Dr. Gianni Parise receives my appreciation for his role on my thesis examination committee.

I must acknowledge my parents, sister and grandparents for their support and encouragement.

To my parents

Table of Contents

Abstract ii
Acknowledgements iv
Dedication vi
Table of Contents vii
List of Tables xi
List of Figures and Illustrations xii
List of Symbols, Abbreviations and Nomenclature xiv
Epigraph xvii

CHAPTER ONE: INTRODUCTION 1
1.1 Background 1
1.2 Objectives 3
1.3 Hypotheses 3
1.4 Presentation 4

CHAPTER TWO: LITERATURE REVIEW 6
2.1 Overview of cardiac substrate metabolism for energy provision 6
2.2 Cardiac glucose uptake 6
2.3 Insulin-stimulated glucose uptake 7
2.3.1 Insulin-stimulated glucose transport 7
2.3.2 Insulin-stimulated glucose phosphorylation 12
2.4 Influence of fatty acid availability on glucose uptake 13
2.5 Mitochondrial oxidative phosphorylation 17
2.5.1 Glucose provision of reducing equivalents 17
2.5.2 Fatty acid provision of reducing equivalents 17
2.5.3 Mitochondrial electron transport and ATP synthesis 18
2.5.4 Transcriptional control of electron transport chain complexes 19
2.5.5 Mitochondrial oxidative phosphorylation uncoupling 21
2.6 Significance of alterations in energy metabolism on cardiac function 23
2.7 Myocardial infarction and cardiac metabolism 24
2.7.1 Overview of heart failure 24
2.7.2 Myocardial infarction and heart failure 25
2.7.3 Glucose metabolism in the infarcted heart 26
2.7.4 Regulation of glucose metabolism in the infarcted heart 27
2.7.5 Insulin-stimulated glucose uptake in the infarcted heart 29
2.7.6 Mitochondria in the infarcted heart 30
2.8 Type 2 diabetes and cardiac metabolism 34
2.8.1 Overview of diabetic cardiomyopathy 34
2.8.2 Glucose metabolism in the diabetic heart 35
2.8.3 Regulation of glucose uptake in the diabetic heart 36
2.8.4 Insulin-stimulated glucose uptake in the diabetic heart 37
2.8.5 Mitochondria in the diabetic heart 38
2.9 Mesenchymal stem cell transplantation and cardiac metabolism 41
2.9.1 Overview of bone marrow-derived mesenchymal stem cells 41

2.9.2 Mesenchymal stem cell transplantation in regenerative medicine 43
2.9.3 In vivo use of mesenchymal stem cell therapy for the infarcted heart 44
2.9.4 Mesenchymal stem cell therapy for glucose metabolism in the infarcted heart 46
2.9.5 Mesenchymal stem cell therapy for mitochondria in the infarcted heart 48
2.9.6 In vivo use of MSCs for diabetic cardiomyopathy and the diabetic infarcted heart 48
2.9.7 Mesenchymal stem cell therapy for glucose metabolism in the diabetic heart 49

CHAPTER THREE: THE ROLE OF MESENCHYMAL STEM CELL TRANSPLANTATION IN MINIMIZING ENERGY METABOLISM ABNORMALITIES IN THE INFARCTED HEART EXIHIBITING MILD SYSTOLIC DYSFUNCTION 51
3.1 Introduction 51
3.2 Materials and Methods 53
3.2.1 Animal characteristics and myocardial infarction 54
3.2.2 Mesenchymal stem cells 55
3.2.3 Echocardiography 55
3.2.4 Catheterization procedures 55
3.2.5 Hyperinsulinemic-euglycemic clamp 56
3.2.6 Plasma and tissue analyses 57
3.2.7 Whole body and tissue-specific substrate kinetics 58
3.2.8 Mitochondrial respiration and enzymatic measurements 59
3.2.9 Immunoblotting and immunostaining 60
3.2.10 Quantitative real-time PCR 62
3.2.11 Statistical analyses 62
3.3 Results 62
3.3.1 Metabolic characteristics 62
3.3.2 Cardiovascular parameters 63
3.3.3 Metabolic indices of cardiac-specific glucose and fatty acid metabolism 67
3.3.4 Metabolic indices of whole body and peripheral tissue glucose metabolism. 70
3.3.5 Metabolic indices of whole body and peripheral tissue long-chain fatty acid metabolism 73
3.3.6 Cardiac mitochondrial function 74
3.4 Discussion 77
3.5 Conclusion 81

CHAPTER FOUR: THE ROLE OF MESENCHYMAL STEM CELL TRANSPLANTATION IN MINIMIZING ENERGY METABOLISM ABNORMALITIES IN THE INFARCTED HEART EXIHIBITING SEVERE SYSTOLIC DYSFUNCTION 84
4.1 Introduction 84
4.2 Materials and methods 86
4.2.1 Animals and myocardial infarction 87
4.2.2 Mesenchymal stem cells 88
4.2.3 Cardiac function 88

4.2.4 Chronic catheterization procedures 88
4.2.5 Hyperinsulinemic-euglycemic clamps and isotopic tracer administration..... 89
4.2.6 Plasma analyses 90
4.2.7 Tissue-specific substrate kinetics 90
4.2.8 Mitochondrial oxygen consumption and enzymatic activity..... 90
4.2.9 Immunoblotting 91
4.2.10 Statistical analyses 91
4.3 Results 92
4.3.1 Stem cell administration minimizes cardiac contractile dysfunction 92
4.3.2 MSC therapy dampens impairment in glucose uptake in the infarcted heart. 94
4.3.3 Diminishing impairments in regulators of glucose uptake by MSC transplantation 97
4.3.4 Potential for increased peripheral tissue glucose uptake post-MSC therapy.. 99
4.3.5 MSC transplantation preserves mitochondrial content and improves efficiency 101
4.4 Discussion 104
4.5 Conclusion 107

CHAPTER FIVE: THE ROLE OF MESENCHYMAL STEM CELL TRANSPLANTATION IN MINIMIZING ENERGY METABOLISM ABNORMALITIES IN THE DIET-INDUCED INSULIN RESISTANT/INFARCTED HEART 109
5.1 Introduction 109
5.2 Materials and methods 111
5.2.1 Animal characteristics and myocardial infarction 113
5.2.2 Mesenchymal stem cells 113
5.2.3 Echocardiography 114
5.2.4 Catheterization procedures 114
5.2.5 Hyperinsulinemic-euglycemic clamp 114
5.2.6 Plasma analyses 115
5.2.7 Tissue-specific substrate kinetics 115
5.2.8 Mitochondrial respiration and enzymatic measurements 115
5.2.9 Immunoblotting 116
5.2.10 Statistical analyses 117
5.3 Results 117
5.3.1 Stem cell therapy promotes improvement in cardiac contractile function ... 117
5.3.2 Enhanced insulin-stimulated cardiac glucose utilization in MSC-treated mice 122
5.3.3 MSC transplantation augments mitochondrial physiology 124
5.3.4 Reduced fasting plasma glucose and fatty acids following MSC administration 127
5.3.5 Systemic insulin sensitivity elevated by MSC injection 128
5.3.6 Increased peripheral tissue glucose uptake post-MSC therapy 129
5.4 Discussion 132
5.5 Conclusion 136

CHAPTER SIX: CHARACTERIZING MITOCHONDRIAL OXIDATIVE PHOSPHORYLATION IN 'SUPERHEALER' MESENCHYMAL STEM CELLS 139
6.1 Introduction 139
6.2 Materials and methods 140
6.2.1 Mesenchymal stem cells and cardiac myocytes 140
6.2.2 Mitochondrial respiration 141
6.2.3 Glucose deprivation and ischemic culture conditions 142
6.2.4 Flow cytometry 143
6.2.5 Statistical analyses 144
6.3 Results 144
6.3.1 Elevated intact MRL-MSC oxygen consumption 144
6.3.2 Superior permeabilized MRL-MSC oxygen flux 147
6.3.3 Increased MRL-MSC viability following glucose and oxygen deprivation. 149
6.4 Discussion 152
6.5 Conclusion 156

CHAPTER SEVEN: CONCLUSIONS AND GENERAL DISCUSSION 158
7.1 Introduction 158
7.2 Strengths and limitations of experimental protocols 159
7.2.1 Left anterior descending coronary artery ligation model 159
7.2.2 Dietary intervention 161
7.2.3 Intramyocardial injection of mesenchymal stem cells 163
7.2.4 Echocardiography 165
7.2.5 Hyperinsulinemic-euglycemic clamp 166
7.2.6 Permeabilized fibers and cells 168
7.3 Overall summary and interpretation of results 170
7.3.1 Insulin-stimulated glucose uptake 170
7.3.2 Cardiac mitochondria 174
7.3.3 Mesenchymal stem cell oxidative phosphorylation 178
7.4 Future directions 179
7.5 Conclusions and significance 182

REFERENCES 183

APPENDIX A 235

APPENDIX B 237

List of Tables

Table 3.1 Biometric characteristics of C57BL/6 mice 63

Table 3.2 Cardiovascular parameters in the conscious C57BL/6 mice 64

Table 4.1 Cardiovascular parameters in conscious C57BL/6 mice 93

Table 4.2 Biometric characteristics of C57BL/6 mice 101

Table 5.1 Cardiovascular parameters in conscious high-fat fed C57BL/6 mice 119

Table 5.2 Biometric characteristics of high-fat fed C57BL/6 mice 128

Table B.1 Proportion of mouse mortality following the ligation surgery in chapter four and five 237

List of Figures and Illustrations

Figure 2.1 Schematic of glucose uptake 7

Figure 2.2 Schematic of insulin-mediated GLUT4 exocytosis..... 10

Figure 2.3 Schematic of glucose-fatty acid cycle 16

Figure 2.4 Schematic of oxidative phosphorylation 19

Figure 3.1 Schematic representation of experimental procedures and timelines..... 53

Figure 3.2 Cardiac functional and structural indices 66

Figure 3.3 Cardiac metabolic indices..... 68

Figure 3.4 Metabolic regulators of substrate metabolism and capillary density 69

Figure 3.5 Insulin sensitivity and plasma substrates during the insulin clamp..... 71

Figure 3.6 Whole body and peripheral tissue glucose utilization 72

Figure 3.7 Whole body and peripheral tissue long-chain fatty acid utilization 74

Figure 3.8 Peri-infarct mitochondria..... 76

Figure 3.9 Schematic representation of metabolic signalling pathways that may be influenced by MSC transplantation following a MI 82

Figure 4.1 Schematic representation of experimental procedures and timelines..... 86

Figure 4.2 Cardiac functional and hypertrophic indices 94

Figure 4.3 Insulin-stimulated whole body disposal and cardiac-specific glucose uptake 96

Figure 4.4 Mediators of cardiac glucose uptake 98

Figure 4.5 Insulin-stimulated peripheral tissue glucose uptake..... 100

Figure 4.6 Cardiac mitochondrial function and characteristics 103

Figure 4.7 Schematic representation of metabolic signalling pathways that may be influenced by MSC transplantation following a MI 108

Figure 5.1 Schematic representation of experimental procedures and timeline 112

Figure 5.2 Cardiac functional and hypertrophic indices 121

Figure 5.3 Regional insulin-stimulated cardiac glucose uptake 123

Figure 5.4 Cardiac mitochondrial function and characteristics 126

Figure 5.5 Whole body insulin sensitivity and blood glucose during the insulin clamp 129

Figure 5.6 Insulin-stimulated peripheral tissue glucose utilization 131

Figure 5.7 Schematic representation of metabolic signalling pathways that may be influenced by MSC transplantation following a MI 138

Figure 6.1 Oxygen flux in intact mesenchymal stem cells 146

Figure 6.2 Oxygen flux in permeabilized mesenchymal stem cells 148

Figure 6.3 MSC survival following 48 hours of limited glucose and oxygen 151

Figure 6.4 Schematic representation of mitochondrial physiology that may influence MSC viability upon transplantation into the infarcted heart 157

Figure 7.1 Fractional shortening following 20 weeks of high-fat feeding 162

Figure A.1 Representative saponin-permeabilized, left ventricle, fiber bundle oxygen consumption experiment 235

List of Symbols, Abbreviations and Nomenclature

Symbol	Definition
[^{125}I]-BMIPP	[^{125}I]-15-(ρ-iodophenyl)-3-R,S-methylpentadecanoic acid
2-[^{14}C]DG	2-[^{14}C]deoxyglucose
^{31}P-MR	Phosphorus 31 magnetic resonance
5-AZA	5-aza-cytidine
AD	Acyl-CoA dehydrogenase
ADP	Adenosine diphosphate
Akt	Protein kinase B
αMEM	Alpha minimum essential medium
ANP	Atrial natriuretic peptide
ANT	Adenine nucleotide translocase
ATP	Adenosine triphosphate
CD	Cluster of differentiation
CI	Complex 1/ NADH:coenzyme Q oxidoreductase
CII	Complex 2/succinate dehydrogenase
CIII	Complex 3/coenzyme Q:cytochrome c oxidoreductase
CIV	Complex 4/cytochrome c oxidase
CV	Complex 5/ATP synthase
CoA	Coenzyme A
COX II	Cytochrome c oxidase subunit 2
COX IV	Cytochrome c oxidase subunit 4
CPT1	Carnitine palmitoyltransferase 1
CSA	Citrate synthase activity
DMEM	Dulbecco's modified eagle medium
DNA	Deoxyribonucleic acid
DTA	Diphtheria toxin A
EF	Ejection fraction
ETC	Electron transport chain
ETS	Electron transport system
FABP	Fatty acid binding protein
FACS	Fatty acyl-CoA synthase
$FADH_2$	Reduced flavine adenine dinucleotide
FATP	Fatty acid transport protein
FAT/CD36	Fatty acid translocase/cluster of differentiation 36
FBS	Fetal bovine serum
FCCP	Carbonyl cyanide-p-trifluoromethoxyphenylhydraz-one
FCR	Flux control ratio
FS	Fractional shortening
G	Glucose
G6P	Glucose 6-phosphate
GAPDH	Glyceraldehyde-3-phosphate dehydrogenase
GDP	Guanosine diphosphate
GIR	Glucose infusion rate

GLUT	Glucose transporter
GPx	Glutathione peroxidase
GSV	GLUT4 storage vesicle
HFF	High-fat fed
HK	Hexokinase
HLA-DR	Human leukocyte antigen-D-related
HR	Heart rate
HRP	Horseradish peroxidase
Insulin clamp	Hyperinsulinemic-euglycemic clamp
I	Insulin
iPS	Induced-pluripotent stem cells
IR	Insulin receptor
IRS	Insulin receptor substrate
IVSd	Interventricular septal thickness (diastole)
IVSs	Interventricular septal thickness (systole)
LAD	Left anterior descending coronary artery
LCAD	Long chain acyl-CoA dehydrogenase
LCFA	Long chain fatty acid
LEAK	Proton leak-mediated respiration
LV	Remote left ventricle
LVIDd	Left ventricle end-diastolic dimension
LVIDs	Left ventricle end-systolic dimension
LVPWd	Left ventricle posterior wall thickness (diastole)
LVPWs	Left ventricle posterior wall thickness (systole)
MCAD	Medium chain acyl-CoA dehydrogenase
MCR_g	Whole-body glucose clearance
MCR_f	Whole-body long-chain fatty acid clearance
MEF2C	Myocyte enhancer factor 2C
MHC	Myosin heavy chain
MI	Myocardial Infarction
MI+MSC	Myocardial infarction + mesenchymal stem cells
MI+PBS	Myocardial infarction + phosphate buffered saline
MiR05	Mitochondrial respiration medium
mRNA	Messenger ribonucleic acid
MSC	Mesenchymal stem cell
mtDNA	Mitochondrial deoxyribonucleic acid
mTORC2	Mammalian target of rapamycin complex 2
MVO_2	Myocardial oxygen consumption
NADH	Nicotinamide adenine dinucleotide (reduced)
nDNA	Nuclear deoxyribonucleic acid
NEFA	Non-esterified fatty acids
NRF	Nuclear respiratory factor
OXPHOS	Oxidative phosphorylation
PBS	Phospho-buffered saline
PCr	Phosphocreatine
PDGF	Platelet-derived growth factor

PDH	Pyruvate dehydrogenase
PDK	Pyruvate dehydrogenase kinase
PDK-1	3-phosphoinositide dependent protein kinase-1
PD-MSC	Placenta-derived mesenchymal stem cell
PECAM-1	Platelet endothelial cell adhesion molecule 1
PFK	Phosphofructokinase
PGC-1α	Peroxisome proliferator-activated receptor γ coactivator-1alpha
PI	Peri-infarct region of left ventricle
PI3K	Phosphatidylinositol 3-kinase
PIP2	Phosphatidylinositol (4,5)P2
PIP3	Phosphatidylinositol (3,4,5)P3
PM	Plasma membrane
PPAR	Peroxisome proliferator activated receptor
pO_2	Partial pressure of oxygen
P/O	Phosphate/oxygen ratio
PVA	Pressure-volume area
RCR	Respiratory control ratio
R_{DMEM}	Routine respiration in Dulbecco's Modified Eagle Medium
R_f	Metabolic index of fatty acid uptake
R_g	Metabolic index of glucose uptake
R_{MiR05}	Routine respiration in MiR05
ROS	Reactive oxygen species
RT-RCR	Reverse transcription-polymerase chain reaction
Sca1	Stem cell antigen 1
SCR	Succinate control ratio
sFRP	Secreted frizzled-related protein
STZ	Streptozotocin
TCA cycle	Tricarboxylic acid cycle
TEM	Transmission electron microscopy
TFAM	Mitochondrial transcription factor A
TFB1M	Mitochondrial transcription factor B1
TFB2M	Mitochondrial transcription factor B2
UCP	Uncoupling protein
$V_{0/CI}$	State 2 respiration supported by complex I substrates
VDAC	Voltage-dependent anion channel
VLCAD	Very long chain acyl-CoA dehydrogenase
V_{MAX-CI}	State 3 respiration supported by complex I substrates
$V_{MAX-CI+CII}$	State 3 respiration via convergent electron input through complex I and II
WT	Wild type
Wnt	Int/wingless

Epigraph

Obviously [Albert Einstein] had never worked on oxidative phosphorylation.

~Dr. Efraim Racker in conversation, 1963

CHAPTER ONE: INTRODUCTION

1.1 Background

A myocardial infarction (MI) represents cardiac tissue necrosis resulting from prolonged and/or extensive ischemia. In Canada, approximately 70, 000 MI events occur each year and 19, 000 individuals die from this condition (87). More than half of the 30-day mortality happens prior to arrival at the hospital (87). For those that do receive hospital treatment, immediate management performed by healthcare practitioners have reduced the number of individuals who succumb to the MI event itself by one-third between 1994 and 2004, however, the manifestation of heart failure is still a concern (60, 87). The regional loss of functioning cardiac myocytes compromises the ability of the heart to pump blood to peripheral sites and may initiate adaptive mechanisms in an attempt to preserve cardiac function (322). The mechanisms include changes in the genomic, proteomic and cellular characteristics of the myocardium that often present as altered cardiac shape, size and function (322). Although these alterations appear to be initially adaptive, the chronic activation of compensatory mechanisms may become maladaptive exhibiting a progressive impairment in the capacity of the ventricle to fill with or eject blood; otherwise known as heart failure (82). Of particular interest to this thesis is the perturbed cardiac substrate and mitochondrial metabolism post-MI that limits efficient ATP synthesis for contraction and potentially exacerbates remodelling progression (5, 146, 230, 328, 342).

Additional concern is for the nearly 2.4 million Canadians that have been diagnosed diabetes mellitus as of 2009 and the new documented cases occurring each

year occur at an incidence rate of approximately 6 out of 1000 individuals (246). Diabetes mellitus is a group of metabolic diseases characterized by hyperglycemia organized into two forms (1). The first classification, termed type 1 diabetes, accounts for approximately 5-10% of all individuals with diabetes mellitus (1). Type 1 diabetes occurs when cell-mediated autoimmune destruction of pancreatic β-cells results in an insulin deficiency requiring hormone replacement therapy (1). Type 2 diabetes is the predominant form (90-95%) characterized by a combination of insulin resistance and β-cell insulin secretion deficiency (1). In relation to the heart, diabetes mellitus has been implicated as a powerful predictor of experiencing an MI event (234, 292) and substantially elevates the prevalence of heart failure in post-MI survivors (76).

Recognizing the positive relationship between infarct size and likelihood of developing heart failure, researchers in regenerative medicine have become excited by the possibly of replacing lost tissue via administration of exogenous cells (216). Experimental study has identified cell-based therapies to reduce infarct size and improve systolic function (114). However, cell transplantation has been less than adequate at replacing the lost cells; which may be due to poor cell viability in the infarcted heart (118, 269). This inadequate cell survival is the result, in part, of being transplanted into a host environment with compromised oxygen and substrate supply (118, 269). Rather than replenishing the necrotic tissue, growing reports suggest the exogenous cells secrete soluble factors and elicit beneficial functional outcomes via paracrine-mediated mechanisms (114). The possibility that the factors released preserve non-pathological cardiac energetics as a means of reducing cardiac dysfunction remains largely under-investigated and unclear.

1.2 Objectives

Based on the observations that cardiac energy metabolism and provision is altered in the infarcted heart and cell viability is compromised by a potential lack of substrate supply upon transplantation, the general objective is to identify whether energy metabolism is both influenced by and influences cell transplantation following a MI. Specifically, employing *in vivo* and *in vitro* experimental models this dissertation aims to:

1. Characterize the effects of mesenchymal stem cell (MSC) transplantation on cardiac insulin-stimulated substrate uptake following a MI in the presence and absence of diet-induced insulin resistance.
2. Describe the influence of MSC transplantation on cardiac mitochondrial oxidative phosphorylation (OXPHOS) function in the presence and absence of diet-induced insulin resistance post-MI.
3. Evaluate the molecular mediators through which MSC transplantation may effect cardiac substrate utilization and mitochondrial physiology.
4. Identify mitochondrial OXPHOS characteristics that may assist MSCs maintain viability upon transplantation into the infarcted heart.

1.3 Hypotheses

1. The post-MI heart would be characterized by a reduction in abnormal insulin-stimulated glucose uptake following MSC transplantation. Also, the minimization of pathological glucose utilization would be associated with

preservation of components involved in insulin signalling and/or normalization of the competitive influence of fatty acid utilization.

2. Mitochondrial efficiency, maximal OXPHOS capacity and density in the infarcted heart would be rescued by the MSC administration. This mitoprotection would be associated with preservation of transcription factor coactivator, peroxisome proliferator-activated receptor gamma coactivator-1alpha, and the mitochondrial regulatory targets of this effector.
3. The added insult to insulin signalling and/or elevated fatty acid utilization induced by diet-induced insulin resistance would compromise the therapeutic effect of MSC therapy on cardiac, insulin-stimulated glucose and mitochondrial metabolism following a MI.
4. A cell type that exhibits mitochondrial OXPHOS flexibility would be associated with improved survival when substrate availability is limited.

1.4 Presentation

The remaining chapters of this dissertation are arranged in the following manner: Chapter two is a literature review. Chapter three through six are manuscripts that have been accepted for publication. Each of these chapters contains a brief introduction, methodology details, experimental results and a focused discussion. Chapter 3 is a manuscript characterizing the metabolic influence of MSCs on the infarcted heart exhibiting modest systolic dysfunction induced by ligating the left anterior descending coronary artery (LAD) relatively low (towards the apex of the heart). Chapter four is a manuscript that describes energy metabolism in the infarcted heart with severe systolic

dysfunction (induced through an LAD ligation closer to the atria) and receiving MSC therapy. Chapter five is a manuscript discussing the efficacy of MSC transplantation to minimize metabolic abnormalities in the infarcted heart in the presence of diet-induced insulin resistance. Chapter six is a study that shifts focus slightly and evaluates mitochondrial characteristics of MSCs that may enhance the viability of these exogenous cells upon transplantation into the infarcted heart. Chapter seven provides strengths/limitations, general conclusions and proposes future experimental endeavours based on the findings of the preceding four chapters.

CHAPTER TWO: LITERATURE REVIEW

2.1 Overview of cardiac substrate metabolism for energy provision

The heart is continually contracting to ensure proper blood pressure and provision. It has been estimated that 60–70% of adenosine triphosphate (ATP) utilized fuels cardiac contraction and 30–40% of ATP hydrolysis sustains sarcoplasmic reticulum Ca^{2+}-ATPase and the function of other ion pumps (315, 317). Furthermore, cardiac ATP content (~5 μmol/g wet wt) is low and rapid ATP hydrolysis (~0.5 μmol/g wet wt/s at rest) creates a situation whereby the ATP storage in the heart undergoes complete turnover within about 10 seconds (152, 315). To satisfy the constant requirement for ATP, the heart exhibits incredible metabolic flexibility, displayed by the ability to utilize a variety of substrates including fatty acids and glucose in response to alterations in physiological factors such as oxygen, substrates and hormones. Under normoxic, non-pathological conditions the heart predominantly utilizes fatty acids (60-90%) and glucose (10-40%) (152). Furthermore, the majority of this ATP is synthesized by mitochondrial oxidative phosphorylation (OXPHOS) (195, 315).

2.2 Cardiac glucose uptake

Glucose uptake is a multi-factorial process whereby glucose moves from the circulatory system to the intracellular space where it is trapped (Figure 2.1) (352). To be metabolized, arterial blood glucose transfers to the interstitium to the intracellular space and finally becomes phosphorylated to glucose 6-phosphate (G6P). The ability of glucose to travel from blood in the circulatory system to the interstitium is largely

controlled by blood glucose concentration, blood flow to the tissue, the recruitment of capillaries, and the permeability of the endothelium to glucose. Membrane glucose transporter (GLUT) content and translocation determine the movement of glucose into the cell. The ability to phosphorylate glucose is contributed to by hexokinase (HK) number, intracellular compartmentalization, and concentrations of intracellular HK inhibitors. Other intracellular factors may influence glucose uptake, however, regulators downstream of glucose uptake likely influence these three steps (352). This dissertation conceptualizes glucose uptake into these steps and is interested in the regulatory influence of insulin stimulation, a myocardial infarction (MI) and substrate availability on the membrane and intracellular stages of glucose utilization.

Figure 2.1 Schematic of glucose uptake

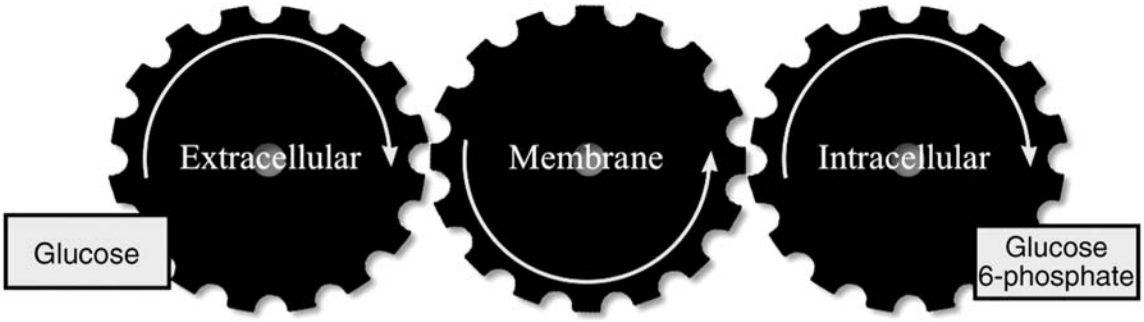

Adapted from Wasserman et al. (352)

2.3 Insulin-stimulated glucose uptake

2.3.1 Insulin-stimulated glucose transport

An extensively investigated area of glucose uptake is glucose transport. In 1948, LeFerve was investigating the uptake of glucose into human red blood cells (180).

LeFerve was the first to hypothesize that there must be a component in the lipid bilayer of a cell that is required for the transport of glucose to the intracellular space (333). The identification that a protein component in the membrane of erythrocytes is responsible for glucose transport was not accomplished until the 1970s (18, 160). In 1985, Mueckler et al. (221) identified the first glucose transporter (GLUT1) using human HepG2 hepatoma cells. Since the identification of GLUT1, a total of fourteen glucose transporters (GLUT1-14) have been discovered (333).

The extensive number of GLUT isoforms has spurred many clinical and experimental studies to evaluate their regulation at the transcriptional, translational and post-translational levels. Of particular interest is GLUT4, which is currently accepted as the predominant transporter of insulin-stimulated glucose uptake. Experimental data indicates the GLUT4 is the most abundant glucose transporter in the adult heart. In the C57BL/6J mouse, GLUT4 expression in the left ventricle was approximately 10-fold greater than the next highest glucose transporter (GLUT1) (6). The identification and characterization of the GLUT4 gene and associated regulatory regions has allowed for thorough investigation of GLUT4 transcription (159). Several transcription factors and co-activators have been found to promote or repress GLUT4 expression (159). However, peroxisome proliferator-activated receptor gamma coactivator-1alpha (PGC-1α) is appealing given its role in not only stimulating GLUT4 transcription but also mitochondrial protein expression (159). PGC-1α has been characterized as a co-activator: a protein that elevates the transcription rate via interaction with transcription factors, however, it does not directly bind to the gene regulatory region itself (159). Michael et al. (214) documented the role of PGC-1α in the expression of GLUT4 by

overexpressing PGC-1α in L6 myotubes. L6 myotubes generally display poor expression of PGC-1α and GLUT4 compared to *in vivo* muscle (214). However, the ectopic expression of PGC-1α enhanced GLUT4 messenger ribonucleic acid (mRNA) and protein (214). Additionally, the authors report PGC-1α likely interacts with the transcription factor myocyte enhancer factor 2C (MEF2C), a transcription factor required for full promoter activity (214). Phenotypically, the PGC-1α overexpression enhanced basal and insulin-stimulated glucose uptake due to larger total and membrane bound pools of GLUT4 (214).

At the post-translational level, the absence of insulin action elicits less than 1% of total myocyte GLUT4 content to be localized to the cell membrane (309). The remaining GLUT4 reside largely within GLUT4 storage vesicles (GSVs) found in the cytosol that do not cycle to the cell membrane in the absence of a stimulatory signal (187). In contrast, in the presence of insulin, experimental models have identified the fraction of cellular GLUT4 present at the sarcolemma to be approximately 40% (309). The regulation of GLUT4-mediated glucose uptake occurs due to intrinsic GLUT4 activity as well as GLUT4 endocytosis and exocytosis (187). Insulin appears to mediate glucose uptake primarily through GSV exocytosis and thus GLUT4 translocation to the plasma membrane (187). Several signalling cascades have been reported to influence GLUT4 exocytosis, however, in muscle, the phosphatidylinositol 3-kinase (PI3K)-dependent signalling pathway is one of the most comprehensively studied means of insulin action (Figure 2.2). A main hub of PI3K signalling that connects insulin binding at the plasma membrane to downstream regulators of GLUT4 translocation is protein kinase B (Akt)

(187). In fact, knockdown and knockout studies employing Chinese hamster ovarian cells and 3T3-L1 adipocytes have identified Akt is required for insulin-mediated glucose uptake (161). Additionally, constitutively active Akt can almost match the effect of insulin in 3T3-L1 adipocytes (171, 232). Akt describes a family of three serine/threonine-specific protein kinases that play a role in cell growth, metabolism and survival (126). The Akt2 isoform of the Akt family is the primary mediator of insulin-stimulated GLUT4 translocation following phosphorylation of Thr308 and/or Ser473 residues (126).

Figure 2.2 Schematic of insulin-mediated GLUT4 exocytosis

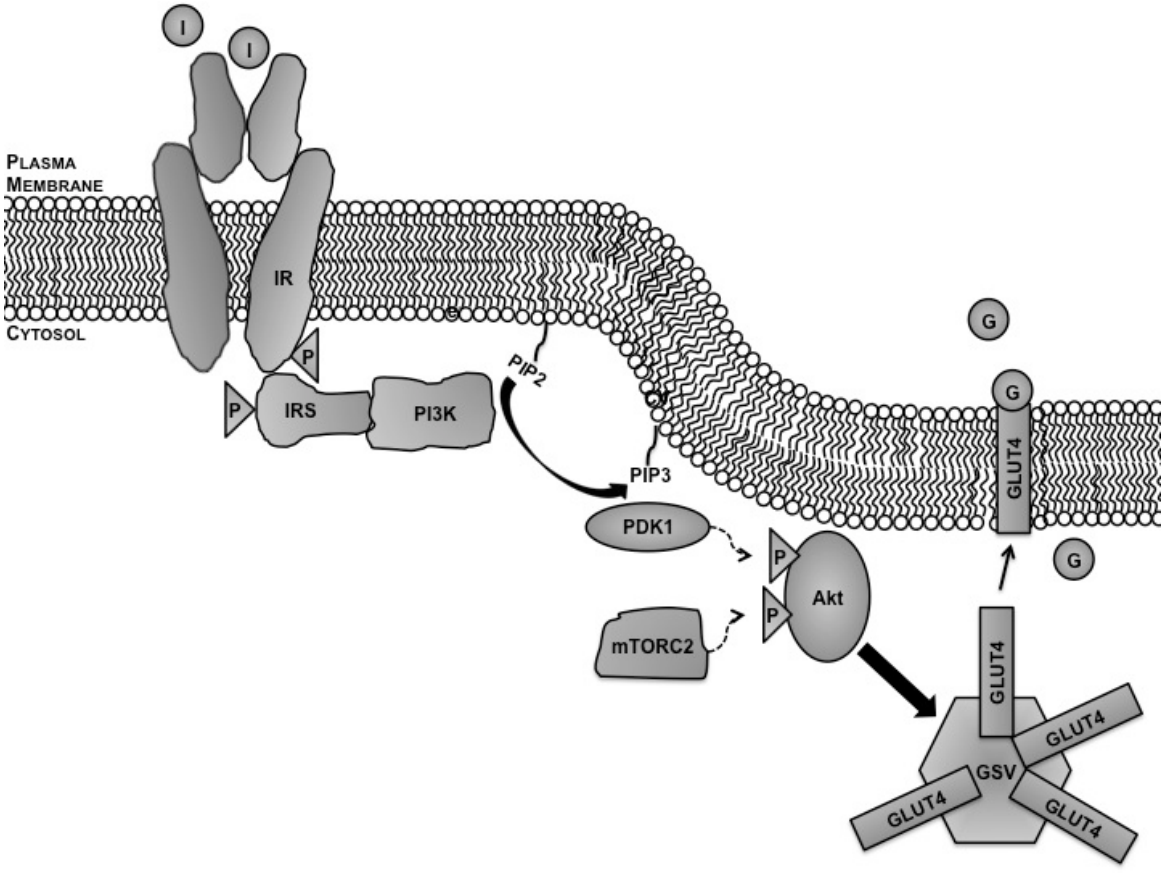

Figure 2.2: Insulin signalling is stimulated following binding of insulin (I) with the insulin receptor (IR) at the plasma membrane (PM) (187). This promotes IR tyrosine kinase activity that phosphorylates the insulin receptor substrate (IRS) proteins (187). Following phosphorylation, IRS proteins recruit and activate phosphatidylinositol 3-kinase (PI3K) (187). PI3K catalyses the reaction of phosphatidylinositol (4,5)P2 (PIP2) to phosphatidylinositol (3,4,5)P3 (PIP3) on the cytosolic surface of the PM (187). PIP3 functions as a docking area for Akt, which upon binding precipitates a conformational change in Akt (187). This structure change allows for phosphorylation at Thr308 by 3-phosphoinositide dependent protein kinase-1 (PDK1) (187). A second site, Ser473, is phosphorylated by the complex of mammalian target of rapamycin complex 2 (mTORC2) (187). Once phosphorylated, Akt mediates GLUT4 exocytosis (187).

Transgenic animal models support glucose transport as an important component of glucose uptake. Fam et al. (81) employed hyperinsulinemic-euglycemic clamps coupled to the administration of an isotopic glucose tracer to evaluate tissue-specific uptake in muscle-specific GLUT4 knockout mice on a C57BL/6J background. The authors reported that insulin-stimulated glucose uptake in the heart was depressed (81). Also, overexpression of GLUT4, at various levels, in transgenic mice increases insulin-mediated glucose disposal (206, 263, 338). However, the fold increase in whole body glucose utilization was always lower than that of GLUT4 protein expression (351). Given this, regulation of glucose uptake under insulin-stimulated conditions is likely significantly influenced by other physiological mechanisms such as blood flow and glucose phosphorylation.

2.3.2 Insulin-stimulated glucose phosphorylation

The phosphorylation of glucose to G6P is the final reaction in the glucose uptake pathway that is catalyzed by HK in muscle (94). This phosphorylation step renders the incoming glucose polar, preventing it from escaping the intracellular space through the glucose transporters and thus trapping it in the cell for subsequent metabolic destinations (312). The HK family consists of four isoforms with HKII, and to a lesser extent HKI, being predominant in the heart (312, 357, 358). Under basal conditions, a greater proportion of HKII resides in the cytosol and while a larger percentage of HKI is bound to the mitochondrial outer membrane (313). However, HKII action appears to be particularly responsive to insulin. Upon insulin stimulation, HKII translocation to the outer mitochondrial membrane exceeds that of HKI (313). Similar to GLUT4 translocation, insulin promotes this HK movement to the outer mitochondrial membrane through Akt activation (312). In HeLa cells, Pastorino et al. (241) report that inhibition of Akt induced dissociation between HKII and the outer mitochondrial membrane. While Akt activation is upstream of HK translocation, the direct target of Akt remains unknown (203). Growing experimental reports suggest that insulin-stimulated glucose uptake may be limited by glucose phosphorylation to a greater extent than glucose transport. In 1961, Morgan and colleagues (219) employed a perfused, rat heart model to identify that glucose phosphorylation is rate-limiting under insulin-stimulated conditions. More recently, transgenic mouse models have allowed for the manipulation of genes involved in glucose transport and phosphorylation individually or in conjunction to determine the *in vivo* regulatory influence of these steps in muscle glucose uptake under insulin stimulated conditions. Fueger et al. (95) performed hyperinsulinemic-euglycemic clamps

coupled to the administration of an isotopic glucose tracer to evaluate muscle glucose uptake in the conscious, unrestrained mouse. The study employed four groups: a wild type (WT) C57BL/6J mouse, a partial (50%) GLUT4 deletion in skeletal muscle group ($GLUT4^{+/-}$), an HKII skeletal muscle overexpression group (HK^{Tg}) and a $GLUT4^{+/-}$, HK^{Tg} group (95). The WT, $GLUT4^{+/-}$ and $GLUT4^{+/-}$, HK^{Tg} groups displayed comparable insulin-stimulated muscle glucose uptake (95). The HK^{Tg} mice exhibited an elevated glucose uptake in the soleus, gastrocnemius and superficial vastus lateralis (95). The data suggests that glucose transport does not impede muscle glucose uptake with as much as a 50% reduction in GLUT4 under insulin-stimulated conditions (95). The limitation of glucose phosphorylation on glucose uptake is overcome by overexpression of HKII (95). Also, only when the barrier of glucose phosphorylation is reduced due to HKII overexpression, glucose transport becomes rate limiting (95). A follow-up study identified that a 50% reduction in HKII accrued a reduction in insulin-mediated cardiac glucose uptake *in vivo* (96). Together these results indicate that HKII content and subsequently glucose phosphorylation poses an important rate-limiting step in the regulation of glucose uptake in response to insulin (94, 95).

2.4 Influence of fatty acid availability on glucose uptake

In 1963, Randle et al. (258) proposed the "glucose-fatty acid cycle" (later termed the Randle Cycle) to describe the reciprocal competition between glucose and non-esterified fatty acids for substrate oxidation in the mitochondria. More specifically, in the isolated, perfused heart, Randle and colleagues identified that the utilization of one substrate impeded the use of the other substrate depending on their availability in the

presence or absence of hormonal regulation such as insulin (258). Extensive studies by Randle and colleagues as well as others identified the mechanisms by which fatty acids could impair glucose metabolism. Inhibition of glucose utilization occurred at several glycolytic steps including glucose uptake, phosphofructokinase (PFK) and pyruvate dehydrogenase (PDH) (Figure 2.3) (257, 258, 318).

The primary site of inhibition is thought to occur at PDH with glucose uptake and PFK playing a secondary role (134, 257). Fatty acid oxidation promotes an increase in mitochondrial ratios of acetyl coenzyme A (acetyl-CoA)-to-CoA and reduced nicotinamide adenine dinucleotide (NADH)-to-oxidized nicotinamide adenine dinucleotide (NAD^+) (134). Both acetyl-CoA and NADH regulate PDH activity via stimulation of pyruvate dehydrogenase kinase (PDK) (134). Activated PDK subsequently phosphorylates and inhibits PDH (134). The accumulation of acetyl-CoA can also promote the increase in citrate levels (134). Citrate has been reported to reduce PFK activity via allosteric inhibition in the heart (134, 240). Of particular interest to this dissertation is the role of fatty acid availability plays in reducing glucose uptake. However, the mechanisms haven't been completely elucidated as of yet (134, 257). Randle and colleagues proposed that glucose uptake was inhibited via regulation of hexokinase (257). By impairing PFK, G6P could accumulate and impede HK function (134). While HK has been reported to be regulated by its product, some question whether fatty acid metabolism inhibits glucose uptake via glucose phosphorylation (134). This is due to GLUT4 being the rate-limiting step in glucose uptake in the absence of insulin (351). As previously indicated, glucose phosphorylation is rate limiting in the presence

of insulin (351). In speculation, under insulin-stimulated conditions, HK may indeed be the regulatory site by which fatty acids metabolism inhibits glucose uptake.

Figure 2.3 Schematic of glucose-fatty acid cycle

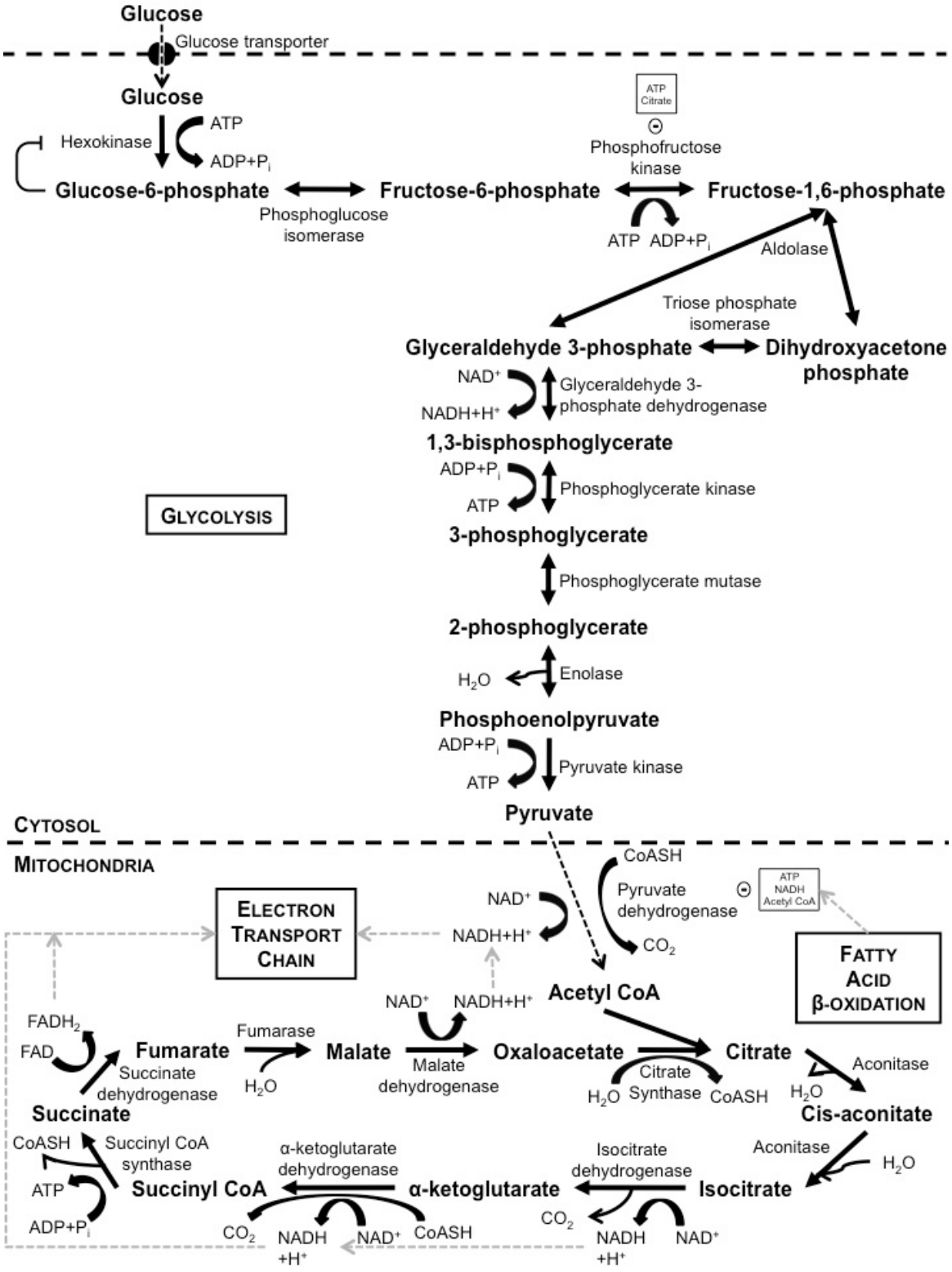

2.5 Mitochondrial oxidative phosphorylation

2.5.1 Glucose provision of reducing equivalents

If G6P is destined for glycolysis, it is converted to pyruvate (152). Pyruvate generated from glycolysis has three fates: conversion to lactate, decarboxylation to acetyl-CoA or carboxylation to oxaloacetate or malate (315). Decarboxylation occurs as pyruvate is transported to the mitochondrial matrix via a transcarboxylate carrier situated in the inner mitochondrial membrane and pyruvate is decarboxylated by PDH in a reaction synthesizing acetyl-CoA and NADH (315). Acetyl-CoA enters the tricarboxylic acid (TCA) cycle where reducing equivalents such as reduced flavine adenine dinucleotide ($FADH_2$) and NADH are synthesized in addition to ATP (315).

2.5.2 Fatty acid provision of reducing equivalents

As fatty acids appear in the cytosolic compartment of cardiac myocytes they are bound by a cytosolic isoform of fatty acid binding protein (FABP) (315). Additionally, the fatty acids are activated by esterification to a fatty acyl-CoA by an intracellular fatty acyl-CoA synthase (FACS) and bound to an acyl-CoA binding protein (152). The fatty acyl-CoA has several metabolic fates including use for phospholipid synthesis, triglycerides and fatty acid β-oxidation (152). If fated to be catabolized for energy provision, β-oxidation occurs. The fatty acyl-CoA must be first transported across the mitochondrial membranes (166). In the mitochondrial matrix the fatty acyl-CoA molecules are sequentially relieved of 2 carbons through the β-oxidation process (74). For saturated fatty acids, this process is sequential series of four reactions involving an acyl-CoA dehydrogenase (AD), enoyl-CoA hydratase, 3-hydroxyacyl-CoA

dehydrogenase and 3-ketoacyl-CoA thiolase (74). Each cycle of the described 4 steps liberates 2 carbons forming acetyl-CoA as well as one NADH and $FADH_2$ (74).

2.5.3 Mitochondrial electron transport and ATP synthesis

Mitochondria use reducing equivalents produced via substrate utilization to provide electrons to the electron transport chain (ETC) (Figure 2.4) (270). The ETC consists of four protein complexes (I-IV) and two electron carriers, coenzyme Q and cytochrome c (199). Electrons may enter the ETC at complex I (CI; NADH-coenzyme Q oxidoreductase), complex II (CII; succinate-coenzyme Q oxidoreductase) or complex III (CIII; coenzyme Q-cytochrome c oxidoreductase) (108). These electrons are transported via a series of oxidation-reduction reactions to complex IV (CIV; cytochrome c oxidase) where oxygen is reduced to water (199). The transport of electrons through the ETC to oxygen drives the pumping of protons out of the mitochondrial matrix by CI, CIII and CIV into the mitochondrial intermembrane space (107). This induces a proton electrochemical gradient that creates a proton motive force able to mediate adenosine diphosphate (ADP) phosphorylation, forming ATP via ATP synthase (CV) rotary catalysis (306).

Figure 2.4 Schematic of oxidative phosphorylation

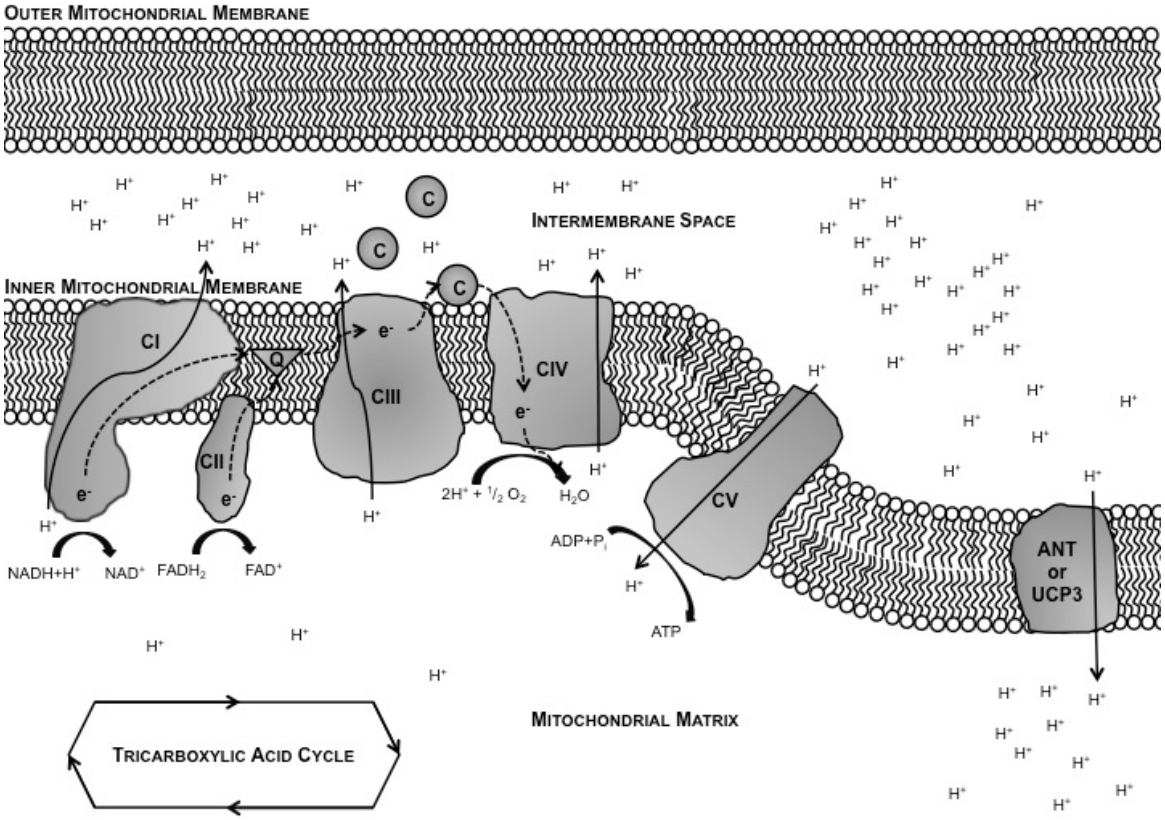

Figure 2.3: ANT, adenine nucleotide translocase; c, cytochrome c; CI, complex I; CII, complex II; CIII, complex III; CIV, complex IV; e^-, electron; H^+, proton; UCP3, uncoupling protein 3.

2.5.4 Transcriptional control of electron transport chain complexes

Mitochondria are semi-autonomous organelles that contain their own deoxyribonucleic acid (mtDNA) (268, 288, 289). mtDNA is a 16.5 kb, double stranded, circular, multicopy genome that contains 37 genes for 13 OXPHOS subunits (CI, CIII, CIV, CV), 22 transfer RNAs and 2 ribosomal RNAs (268, 288, 289). Nuclear DNA

(nDNA) expresses the remaining and majority of ETC complex subunits (268, 288, 289). The formation OXPHOS complexes involve the elaborate spatiotemporal coordination of expressing ETC proteins encoded by the nuclear and mitochondrial genome (268, 288, 289). Additionally, OXPHOS protein subunits transcribed by nDNA must be translated, imported into the mitochondria, assembled with mtDNA-encoded subunits into protein complexes and incorporated into the inner mitochondrial membrane (268, 288, 289).

To assist in coordination, mtDNA transcription is completed by nDNA-encoded products (164). Three activating transcription factors being expressed by the nuclear genome have been identified. Two, mitochondrial transcription factor B1 and B2 (TFB1M and TFB2M), are transcription-specific factors (268). The third, mitochondrial transcription factor A (TFAM), has also being implicated in mtDNA replication and maintenance processes (42). TFAM, TFB1M and TFB2M expression is promoted by nuclear respiratory factors 1 and 2 (NRF-1 and NRF-2) (106, 287, 347). NRF-1 is a nuclear transcription factor identified after characterization of cytochrome c and CIV gene promoters (78, 286). NRF-2 was later discovered during the evaluation of CIV subunit IV expression (COX IV) (286, 348). Further studies have reported NRF-1 and NRF-2 to play a role in the transcriptional control of the majority of the nuclear-encoded ETC complex and ATP synthase subunits as well as proteins involved in import and assembly (164). As such, the nuclear respiratory factors are important in synchronizing the nuclear and mitochondrial genome for proper mitochondrial biogenesis and metabolism.

Further regulation of mitochondrial protein transcription occurs in response to coactivators such as PGC-1α. Wu et al. (364) overexpressed PGC-1α in myoblasts

observing a 1.9-fold elevation in mitochondrial oxygen consumption, two- to three-fold increase in ATP synthase β subunit, CIV subunit II (COX II), COX IV and cytochrome c mRNA levels and a significant elevation in COX IV and cytochrome c protein. Furthermore, the overexpression of PGC-1α was associated with stimulation of mitochondrial biogenesis. The myoblasts with the elevated co-activator displayed higher mtDNA and mitochondrial content (364). In additional experimental analysis, Wu et al. (364) identified that PGC-1α enhances TFAM promoter activity and the presence of NRF-1 was required. The authors concluded that PGC-1α promotes mitochondrial biogenesis and OXPHOS function in a NRF-1-dependent fashion (364). Of note, PGC-1α functions similarly in cultured, cardiac myocytes (184).

2.5.5 Mitochondrial oxidative phosphorylation uncoupling

Mitochondrial OXPHOS displays inefficiencies in that it is not completely coupled. Mitochondrial coupling efficiency has been defined as the proportion of the respiratory rate that mediates ATP synthesis (68). Experimental evidence indicates that protons have the ability to leak across the inner mitochondrial membrane and lessen the proton motive force and stimulate oxygen flux independently of ATP synthase action (68).

Brookes et al. (36) identified that liposomes made from inner mitochondrial membrane phospholipids were permeable to protons, however, it was concluded that a negligible proportion of proton leak would be contributed by the lipid bilayer *in vivo*. Rather, proteins and/or protein complexes in the inner mitochondrial membrane mediate proton leak. The protein complex, adenine nuclease translocase (ANT), is the primary

mediator of basal proton leak (34). Additionally, ANT-mediated proton conductance is largely dependent on total content but not activity (34). ANT is a transmembrane protein found in the inner mitochondrial membrane (336). In mammals, four ANT isoforms (ANT1-4) have been identified with the exception of rodents where only three have been reported (ANT1, 2, 4) (336). In addition to the role of ANT in proton conductance, ANT exchanges exogenous ADP with ATP from the mitochondrial matrix in a 1:1 ratio (336). This allows the transfer of ATP to the cytosol and the appearance of ADP in the mitochondrial matrix for phosphorylation via OXPHOS.

Proton movement across the inner mitochondrial membrane can also be induced (68). Uncoupling proteins (UCPs) are the most widely investigated inducible uncouplers (68). UCPs exist as a family of three isoforms (UCP1-3) (68). UCP1 is predominantly found in brown adipose tissue (15). UCP2 has been identified in the kidney, pancreas, spleen, and thymus (68, 244). UCP3 is present in brown adipose tissue, skeletal muscle and the heart (28). The expression of UCP3 in the heart makes it of particular interest in the current dissertation as it may influence the efficiency of mitochondrial ATP provision. It is generally believed that UCP3 does not influence basal proton leak (41, 59). However, UCP3-mediated proton conductance in cardiac mitochondria can be activated by reactive alkenals and pharmacological ligands (68). Additionally, fatty acids have been reported to activate UCP3 uncoupling in liposomes reconstituted from the inner mitochondrial membrane (75). The expression of UCP3 is promoted by a number of transcription factors including the peroxisome proliferator-activated receptor (PPAR) family (310). The PPAR transcription factor family are nuclear receptors consisting of three isoforms: PPARα, PPARβ and PPARγ (20, 140). In the heart, PPARα and PPARβ

are highly expressed with the role PPARα receiving greater evaluation (140). In addition, Puigserver et al. (256) initially identified PGC-1α as a coactivator of PPARγ in brown adipose tissue; a tissue with significant UCP expression.

2.6 Significance of alterations in energy metabolism on cardiac function

Growing reports are providing evidence that cardiac bioenergetics influence contractile function. Cardiac mechanical efficiency is determined by the ability to convert metabolic energy into hydraulic energy (cardiac external work) (317, 355). In experimental practice, cardiac mechanical efficiency is represented by the cardiac work/myocardial oxygen consumption ratio (MVO_2) (195). Cardiac work is often obtained from the pressure-volume area (PVA) (131, 317). Under constant contractility, there is a linear relationship between oxygen consumption and cardiac work (152). Additionally, in aerobic conditions, the heart meets greater than 95% of its energetic demands through oxidative metabolism of fatty acids and glucose (195). Thus, oxygen consumption provides a surrogate measure of energy input.

Interestingly, the specific substrate catabolized for oxidative energy provision influences cardiac mechanical efficiency (174, 315). MVO_2 is consistently higher when the heart is metabolizing fatty acids to a greater extent than glucose (174, 315). This increase in MVO_2 during a greater reliance on fatty acid oxidation results in reduced cardiac mechanical efficiency as defined by the PVA-MVO_2 relationship (174). The mechanisms responsible for the impaired mechanical efficiency when depending on fatty acids for ATP provision are not completely clear. One reason may be that higher oxygen cost for fatty acid oxidation compared to glucose oxidation as explained by the reduced

phosphorus/oxygen (P/O) ratio (145, 152, 195, 315, 326, 342). The P/O ratio refers to the number of ATP molecules generated per oxygen atom reduced during OXPHOS (83). P/O ratios differ depending on the reducing equivalent used (83). Specifically, the P/O ratio is 2.5 and 1.5 for NADH and $FADH_2$, respectively (83). Although oxidation of fatty acids result in greater absolute ATP generation, a greater proportion of the ATP generated by fatty acids is derived from $FADH_2$ which has a lower P/O ratio (314). Additionally, fatty acids exhibit the ability to uncouple mitochondrial OXPHOS resulting in greater oxygen consumption that does not result in ATP synthesis (29).

2.7 Myocardial infarction and cardiac metabolism

2.7.1 Overview of heart failure

As previously stated, heart failure is defined as "any structural or functional cardiac disorder that impairs the ability of the ventricle to fill with or eject blood" (139). But rather than a single entity, heart failure is a progressive process of cardiac remodelling characterized by genetic, molecular, interstitial and cellular changes that manifest clinically as structural and functional alterations following injury and/or dysfunction (52, 82). Such initial insults may include coronary artery disease (ischemic heart disease), diabetes, hypertension, myocarditis and congenital malformations (82, 139). For basic scientists, Fedak et al. (82) have provided a concise organization of the progress from insult to heart failure into three stages. Notably, the stages emphasize systolic dysfunction, however, Fedak and colleagues do emphasize alterations in diastolic function are of importance as well (82). The first stage is that of preserved function, identified as a condition where the heart is subjected to injury or increased mechanical

load resulting in an initial depression in systolic function (82). In response, adaptive mechanisms are activated to maintain global cardiac function (82). Stage 2, compensated dysfunction, is described as the situation where the injury, increased mechanical load and activated adaptive mechanisms become maladaptive (82). The shape and structure of the heart is augmented by pathological hypertrophy (increased heart mass) and chamber dilation (82). Furthermore, global cardiac contraction is perturbed (82). The final stage is decompensated heart failure characterized by extensive global dysfunction (82). This is a period of severe morbidity and mortality with the majority of patients requiring hospitalization to maintain the peripheral perfusion required to survive (82). Not unexpectedly, gross alterations in cardiac geometry are observed. These aberrations include a pronounced sphere shape of the ventricle(s), chamber dilation and cardiac wall thinning (82). The duration of each stage is variable, the progression from one to the next is not distinct, and transition from one stage to the next may never occur.

2.7.2 Myocardial infarction and heart failure

Of those individuals diagnosed with heart failure approximately two-thirds have a history of ischemic heart disease (139, 315). Cardiac ischemia represents a condition of imbalance between cardiac oxygen supply and demand (248, 303). If the oxygen mismatch is extensive and prolonged in duration a MI event will occur. Heart failure manifestation, in the setting of coronary artery disease, is often a result of a MI event (104, 139). As such, this literature review will focus on cardiac pathology associated with a MI. Importantly, experimental evidence will not be limited to overt heart failure, but will include all stages of cardiac remodelling following the chronic MI event from preserved function to decompensated heart failure.

Attention has been given to cardiac bioenergetics in the infarcted heart due to the need for oxygen to generate a large proportion of cardiac ATP required to sustain contraction. Early work by Tian et al. (334) assessed the PVA-MVO_2 relationship in rats eight weeks post-MI to identify alterations in cardiac mechanoenergetics. Intriguingly, cardiac efficiency was improved in the heart following a MI (334). Since the findings of Tian and colleagues (334), experimental investigation has aimed to determine whether the perturbations in energy metabolism throughout the remodelling process are adaptive or maladaptive and to identify potential therapeutic targets in metabolic pathways.

2.7.3 Glucose metabolism in the infarcted heart

The improved functional efficiency observed by Tian and colleagues (334) has been attributed to the infarcted heart potentially exhibiting an initial switch in reliance from fatty acids to glucose. Gnecchi et al. (113) evaluated *ex vivo* cardiac energetics in a chronically infarcted, rodent model. Basal, cardiac, glucose uptake was elevated at three days and two weeks following the MI (113). Alternatively, Amorim and colleagues (10) report that *ex vivo*, cardiac, glucose uptake was unchanged in the absence of insulin two weeks post-MI in rats. Of note, both of these studies evaluated cardiac metabolism prior to the onset of indicators of cardiac remodelling such as hypertrophy (10, 113). In agreement with Amorim and colleagues, Murray et al. (226) report that 10 weeks post-infarct, cardiac glucose uptake in the isolated, perfused heart of rats was unchanged. Added complexity to identifying a metabolic pattern following a MI is the observation that regional differences may exist. Maki et al. (204) evaluated glucose uptake in humans with total LAD occlusion. In the absence of alterations in blood flow, regions of the heart with dysfunctional contraction exhibited an increase in basal glucose uptake (204).

As such, following a MI cardiac glucose uptake in the non-infarcted heart appears to be unchanged or elevated.

To date, fewer studies have evaluated glucose oxidation in the infarcted heart. Amorim et al. (10) assessed cardiac metabolism in rat hearts displaying impaired systolic function in the absence of hypertrophy. Cardiac glucose oxidation was unchanged two weeks post-MI *ex vivo* (10). Chandler et al. (48) employed a moderate severity coronary microembolization-induced heart failure model in dogs to assess cardiac metabolism. The authors reported that glucose oxidation was preserved (48). In contrast, Remondino et al. (262) reported augmentation of cardiac glucose oxidation following the induction of a chronic infarct in rats. Eight weeks post-MI, in the isolated, perfused heart, the contribution of glucose oxidation to total oxidative metabolism in the non-infarcted myocardium was significantly elevated in the infarcted animals (262). Remondino and colleagues (262) identified the infarcted hearts displayed pathological hypertrophy as indicated by cardiac atrial natriuretic peptide (ANP) expression and the heart weight-to-body weight. However, the authors were hesitant to suggest the presence of heart failure. The results suggest that during cardiac remodelling but prior to overt failure the post-MI heart may be characterized by an increase in glucose oxidation. Of note, almost unanimously, overt heart failure of various origins appears to be characterized by the severe depression in glucose and fatty acid utilization (144, 145, 230, 342).

2.7.4 Regulation of glucose metabolism in the infarcted heart

The exact alterations in cardiac glucose uptake and oxidation following a MI in the absence of insulin remain inconclusive. However, as previously stated, the general hypothesis is that glucose metabolism may be elevated during cardiac remodelling prior

to being depressed in end-stage heart failure (315). The changes in cardiac metabolism post-MI have been proposed to be the result of alterations at the transcriptional, translational and/or post-translational level. One area of interest in the current dissertation is the alterations in the content of key regulators of metabolism. A limited number of experimental studies have identified that the basal glucose transporter, GLUT1, mRNA and protein are increased in the infarcted heart (242, 275). However, the potential switch towards heightened glucose utilization appears to be due to reduced competition from fatty acid utilization as described by the "glucose-fatty acid cycle" (152, 315). The involvement of the PPAR/PGC-1α axis in this metabolic switch has been extensively studied. As previously indicated, PPARα and PPARβ are highly expressed in the heart with the role of PPARα in fatty acid metabolism receiving the most attention (140). PPARα promotes the expression of genes involved in fatty acid uptake (FATP, fatty acid transport protein; FAT/CD36, fatty acid translocase/CD36; FABP and FACS), transport of fatty acids into mitochondria (CPT1, carnitine palmitoyltransferase 1) and mitochondrial β-oxidation (MCAD, medium chain AD; LCAD, long chain AD; VLCAD, very long chain AD) (35, 116, 220, 343). Additional investigation has confirmed PGC-1α to enhance fatty acid metabolism gene regulation by PPARα and PPARβ (71, 344). In terms of cardiac remodelling, multiple models of experimental cardiomyopathy including that mediated by a MI report reductions in cardiac PPARα and PGC-1α mRNA and/or protein (10, 19, 100, 101, 280). In agreement, targets of PPARα and PGC-1α involved in fatty acid utilization are depressed in the failing heart (140). More specifically, in the infarcted heart, targets that exhibit

down-regulated mRNA and/or protein include FABP, FACS, CPT1, MCAD, LCAD, and VLCAD (10, 61, 123, 262, 275). These molecular changes parallel changes in the metabolic phenotype on the infarcted heart as animal studies have described a depression in fatty acid oxidation rates following a MI (10, 123). As such, the increased reliance on glucose for energy provision in the infarcted heart is, in part, the result of a decline in the inhibitory effect of fatty acid utilization on glucose metabolism.

2.7.5 Insulin-stimulated glucose uptake in the infarcted heart

Studies evaluating the influence of a MI on insulin-stimulated glucose metabolism in the heart do not observe the same pattern as basal glucose utilization. Murray et al. (226) report that insulin-stimulated glucose uptake was reduced in perfused rat hearts ten weeks post-MI. Two weeks following a MI in rats, Amorim et al. (10) reported cardiac glucose uptake in the presence of insulin was unchanged, however, insulin-stimulated glucose oxidation was depressed. Additionally, in humans experiencing a MI, regions of the heart demonstrating contractile dysfunction exhibit a decline in insulin-mediated glucose uptake independent of impaired blood supply (204). Based on the few studies performed, it appears as though a MI and subsequent pathology may promote cardiac insulin resistance, which for the purposes of this dissertation is defined as the impaired ability of exogenously administered or endogenous insulin to increase glucose utilization in an experimental group to a comparable extent as that of a control group.

Abnormalities in glucose transport and phosphorylation also support the hypothesis that impaired insulin-mediated glucose uptake is a consequence of a MI. GLUT4 protein has been reported to decline in rodent LAD ligation models (226, 275). Given the role of GLUT4 in insulin-mediated glucose transport, a decline in this glucose

transporter may compromise glucose uptake in the presence of insulin. Also utilizing a chronically infarcted rat model, Yeih et al. (368) identified irregularities in HK characteristics. Four weeks following the MI event, the mitochondrial HK activity-to-cytosolic HK activity ratio was reduced (368). Concurrently, the cytosolic HK activity-to-whole cell HK activity ratio was enhanced (368). Together, these results suggest the ability of HK to translocate from the cytosol to the outer mitochondrial membrane is impaired. Another observation was that the mitochondrial HK activity-to-citrate synthase activity was increased post-MI (368). This may indicate that the HK binding to the mitochondria display a greater activation to compensate for the reduced translocation (368). Notably, insulin-stimulated glucose uptake was not evaluated. As such, it cannot be definitively concluded that alterations in the glucose phosphorylation step of insulin-mediated glucose uptake regulate the previously observed insulin resistance post-MI.

2.7.6 Mitochondria in the infarcted heart

In addition to aberrations in cardiac substrate utilization, it has been proposed that mitochondrial electron transport and OXPHOS in the infarcted and failing heart may be compromised. Employing phosphorus 31 magnetic resonance (^{31}P-MR) spectroscopy to assess *in vivo* high-energy phosphates, the phosphocreatine (PCr)-to-ATP ratio has been reported to be depressed in the peri-infarct region and left ventricle of chronically infarcted animal models (84, 85, 133, 369). The decline in the PCr/ATP ratio is concerning because it is a ratio reflecting OXPHOS, energy efficiency and ventricular function in cardiomyopathies (85, 369). Furthermore, given as much as 95% of cardiac ATP provision arises from oxidative metabolism (315), mitochondrial ATP synthesis is

of importance and the OXPHOS impairments associated with ischemic cardiomyopathies warrant close evaluation to determine their role in energetic dysfunction.

A frequently used technique to identify mitochondrial and, potentially, ATP provision impairments in a variety of pathologies is respirometric assessment. The measurement of oxygen consumption in samples provides an excellent screening approach that includes not only structural membrane defects but also biochemical insults that encompass alterations in the enzymatic systems of membrane transport, electron transport and coupling of ADP phosphorylation (109). Two commonly employed indicators of mitochondrial function and efficiency are the respiratory control ratio (RCR) and the P/O ratio (33). The RCR is obtained from oxygen consumption measures by dividing oxygen flux in the presence of ADP (state 3) by oxygen consumption in the absence of ADP (state 2/4) (33). Oxygen flux in the presence of ADP is controlled by ATP turnover (ANT, phosphate transporter and ATP synthase) and substrate oxidation (substrate uptake, substrate catabolism, electron transport through the ETC, oxygen concentration and pool sizes of cytochrome c and ubiquinone) (33). Oxygen flux in the absence of ADP largely represents respiration controlled by proton leak, electron slip, and contaminating ATPase activity (33) (See APPENDIX A for representative respirometric measures). As such, the use of the RCR is an effective means of identifying alterations in mitochondrial function because it is influenced by almost every OXPHOS contributor (33). Both animal models of cardiomyopathy and human heart failure resulting from ischemic insult exhibit a decline in cardiac RCR (122, 153, 154, 175, 274, 295, 296). A reoccurring characteristic identified is a reduction in ADP-stimulated oxygen flux supported by substrates donating reducing equivalents to CI (122,

153, 154, 175, 274, 285, 295, 296). This suggests that the lower RCR may be the result of dysfunction in ETC. In agreement, specific abnormalities that have been observed include mitochondrial OXPHOS complex structural abnormalities (272) and a reduction in the content or enzymatic activity of OXPHOS CI, CIII, CIV and ATP synthase (122, 133, 142, 175, 274, 295, 296). However, alterations in mitochondrial oxygen flux, OXPHOS complex content and/or enzymatic activity are not always reported (265, 266). Also, while mitochondrial and ETC aberrations are a common characteristic, there is no consensus as to the site(s) of impairment in the ETC following a MI and in the failing heart. It has been proposed that early post-MI or following mild ischemic insult the decline in integrative OXPHOS function is the result of structural alterations (273, 274). However, as the heart nears overt failure a decline in OXPHOS complex expression and content becomes readily apparent (122, 133, 175, 273). It should be noted that although the aforementioned insults are proposed to compromise the OXPHOS ability of cardiac myocyte, ATP provision and contractile function, experimental evaluation has yet to confirm such speculation (270, 315).

The second index of coupling efficiency, the P/O ratio, refers to the maximum number of ATP molecules synthesized as a pair of electron transfers through the ETC from the substrate to oxygen (83). Given this, the P/O ratio is quite stable for a given substrate and does not identify dysfunction in the ETC (33). However, the ratio is quite sensitive to proton leak-mediated oxygen consumption given ATP is not synthesized under such a situation (33). Animal models employing a chronic infarction model have reported the P/O ratio to be unaffected (122, 274) or to decline (224, 264). Although ANT and UCPs have been identified as mediators of proton leak, few studies have

investigated these OXPHOS uncouplers in post-MI remodelling and their relation to the depressed P/O ratio. One such study performed by Murray et al. (224) observed the cardiac systolic performance to decline in parallel with the P/O ratio in rat, cardiac mitochondria isolated ten weeks following the infarct procedure. In addition, UCP3 protein was elevated in the injured heart (224). Together, the results suggest UCP3 levels increase, compromise the efficiency of mitochondrial ATP provision and potentially exaggerate cardiac dysfunction following ischemic insult. In contrast, there are indirect observations that suggest that ANT-stimulated proton leak declines post-MI. Animal studies indicate oxygen flux in the absence of ADP can be lower when an extended length of time is allowed between insult and experimental evaluation (153, 295). Given these conflicting findings, the role of proton leak on mitochondrial uncoupling and cardiac mechanical efficiency in the chronically infarcted heart is incompletely understood.

Absolute energy provision may also be affected by changes in mitochondrial density. Two-dimensional transmission electron microscopy (TEM) is considered the gold standard for measuring mitochondrial fraction area, however, several surrogate markers of mitochondrial content are often utilized in practice to evaluate mitochondrial density including citrate synthase activity, mtDNA copy number and OXPHOS complex activities (179). Whether post-infarct remodelling is associated with a decline in mitochondrial biogenesis is unclear as biomarkers of mitochondrial density remain unchanged (113, 122, 266, 274, 368) as often as they are reported to decline (61, 153, 165, 175, 264, 265). Interestingly, the reports suggesting mitochondrial content does not decline in the post-infarcted heart were conducted from two days through eight weeks

following insult (113, 266, 274, 368). In contrast, studies assessing mitochondrial density eight to sixteen weeks into the post-MI remodelling process conclude mitochondrial markers are lowered (165, 175, 264, 265). Furthermore, the reports indicating a decline in mitochondrial levels identify the induction of pathological hypertrophy with greater regularity (61, 113, 122, 153, 165, 175, 264-266, 274, 368). Thus, it appears as though the loss of mitochondria following a MI is a characteristic that occurs late in the compensated dysfunction and/or overt heart failure stage. In agreement, promoters of mitochondrial gene transcription and mitochondrial biogenesis have been observed to decline post-MI. NRF-1, NRF-2, TFAM and PGC-1α have been reported to lessen following a MI as indicated by mRNA or protein assessment (10, 154, 319).

2.8 Type 2 diabetes and cardiac metabolism

2.8.1 Overview of diabetic cardiomyopathy

Individuals with diabetes mellitus are at a two- to four-fold greater risk for the development of cardiovascular disease, including coronary artery disease, compared to non-diabetic peers (132, 157, 292). However, Rubler et al. (279) described the phenomena whereby four diabetic patients exhibited heart failure in the absence of coronary artery disease. Subsequent work by Regan and colleagues (261) reported similar characteristics in a subset of diabetic patients. Population studies have also identified an elevated risk of heart failure in individuals diagnosed with diabetes even after controlling for age, cholesterol, hypertension, obesity and coronary artery disease (127, 157). These reports have lead to the term diabetic cardiomyopathy being used to describe "a distinct entity characterized by the presence of abnormal myocardial

performance or structure in the absence of coronary artery disease, hypertension, and significant valvular disease" (330). Recently, diabetic cardiomyopathy has been used to describe the diastolic dysfunction that often precedes systolic abnormalities present in up to 60% of type 2 diabetic individuals (24, 40). In addition to cardiac systolic and diastolic impairments, the mechanical efficiency of the heart may be compromised. Peterson et al. (250) evaluated cardiac work and MVO_2 in women with glucose intolerance and insulin resistance. The authors reported that women with metabolic dysfunction displayed a depression in left ventricle efficiency due to higher MVO_2 without a similar elevation in cardiac work (250). Declines in cardiac efficiency are also observed in animal models of type 2 diabetes (30-32, 38, 210). As such, deviations in cardiac glucose utilization, fatty acid metabolism and/or mitochondrial OXPHOS have been proposed to contribute to diabetic cardiomyopathy and may add increased complexity to the cardiac metabolic phenotype if a MI is sustained.

2.8.2 Glucose metabolism in the diabetic heart

Given that rodents are relatively resistant to the development of atherosclerosis (363), utilization of rodent models of diabetes to identify perturbations that may promote cardiac dysfunction without influence of coronary artery disease (diabetic cardiomyopathy) are invaluable (23, 293). Hafstad et al. (117) found 12 to 16 week-old db/db (leptin receptor deficient) mice displayed a reduction in basal glucose uptake in an isolated, working heart model. In contrast, *in vivo,* cardiac glucose uptake in mice is not inhibited. Shearer et al. (299) elegantly employed saline-infused, euglycemic clamps coupled to isotopic tracer administration in 13 week high-fat fed (HFF) mice and reported comparable rates of cardiac glucose uptake. Utilizing a similar model, Fueger et al. (96)

found cardiac glucose uptake to be similar following 16 weeks of HFF. A possible contributor to the conflicting results between *ex vivo* and *in vivo* techniques is hyperinsulinemia. The saline-infused, euglycemic clamps control for the influence of glucose concentration on glucose uptake, however, arterial insulin levels were higher in the mice fed the high-fat diet compared to the control diet (96, 298, 299). As such, the elevated insulin levels may provide a compensatory mechanism to maintain glucose uptake in these studies. Beyond glucose uptake, HFF C57BL/6 (361, 371), db/db (2, 3, 22, 117) and ob/ob (leptin deficient) (210) mice exhibit a decline in *ex vivo*, cardiac glycolysis and glucose oxidation in the absence of insulin. Of note, the greater reliance of fatty acids as a substrate is rarely contested. Both fatty acid uptake (200, 299) and oxidation (2, 3, 22, 117, 210, 361) are often reported to increase in animal models of insulin resistance and diabetes. Thus, in the insulin resistant heart, glucose uptake and downstream metabolic fates appear to be impeded.

2.8.3 Regulation of glucose uptake in the diabetic heart

Substrate availability has been proposed to influence the decrease in glucose utilization and reciprocal elevation in fatty acid uptake and oxidation. Increases in arterial free fatty acids and triglycerides are commonly observed in human subjects with type 2 diabetes (267). This characteristic hyperlipidemia is not lost in animal models of diabetes (38, 200, 210, 298). Furthermore, fatty acids appear to have the ability to function as ligand activators of PPARα and thus promote the transcription of gene targets involved in fatty acid utilization (202). Not unexpectedly, the cardiac expression of FABP, FAT/CD36, MCAD, LCAD, VLCAD and PDK has been reported to increase (38, 45, 299, 361) in animal studies. Thus, the higher supply of fatty acids often associated

with insulin resistance and type 2 diabetes may contribute, in part, to this substrate shift via the Randle cycle (194).

2.8.4 Insulin-stimulated glucose uptake in the diabetic heart

The pattern of insulin-stimulated glucose uptake largely mirrors that of basal conditions. A decline in insulin-mediated, cardiac glucose uptake has been consistently demonstrated in diet-induced and monogenic insulin resistant animal studies (96, 117, 239, 299, 361). Several mechanisms may be responsible for the depressed glucose uptake in the presence of insulin. The role of the Randle cycle in response to hyperlipidemia and transcriptional increases in mediators of fatty acid metabolism, as described above, have been put forth (115). Also, impairments in glucose transport may have a profound impact. Total GLUT4 protein in the heart has been reported to decline in HFF animals (239, 361). Reductions in membrane GLUT4 have been exhibited suggesting impairments in GLUT4 translocation and/or insulin signalling (63). Support for insulin signalling alterations are often presented as reductions in the phosphorylation of insulin receptor substrate (IRS) and Akt proteins (63, 181, 210, 239). Together, these abnormalities suggest that insulin signalling may be compromised.

Alterations in glucose phosphorylation may also contribute to insulin resistance. Fueger et al. (96) identified that 16 weeks of high-fat feeding in mice promoted a lowering of cardiac HKII. Hyperinsulinemic-euglycemic clamps coupled to isotopic glucose tracers displayed a decline in cardiac glucose uptake in these mice (96). Moreover, this phenotype closely matched that of mice displaying a 50% reduction in HKII and fed a low fat diet. Given glucose phosphorylation is regarded as a rate-limiting

step in the glucose uptake process under insulin-stimulated conditions, the role of HK proteins cannot be dismissed in the diabetic heart.

2.8.5 Mitochondria in the diabetic heart

Similar to studies evaluating energetics post-MI, evaluating ^{31}P-MR spectra of high-energy phosphates in the hearts of individuals diagnosed with type 2 diabetes provides indirect evidence for potentially impaired ATP provision. Diamant et al. (66) assessed the PCr-to-ATP ratio in men with type 2 diabetes in the absence of systolic dysfunction and pathological hypertrophy. The hearts of the type 2 diabetes group displayed a reduction in the PCr-to-ATP ratio (66). Furthermore, the decline in this energetic marker correlated well with contractile dysfunction in diastole (66). In agreement, Scheuremann-Freestone et al. (291) observed a decline in the PCr-to-ATP ratio in the hearts of type 2 diabetic men with no evidence of cardiac dysfunction. Together, these findings indicate that metabolic dysfunction may precede and contribute to diabetic cardiomyopathy.

Arguably, the most direct support of mitochondrial alterations in human diabetic hearts comes from the work of Anderson et al. (11) evaluating oxygen flux in saponin-permeabilized atrial fibers. In the presence of ADP, oxygen flux supported by palmitoyl-carnitine was depressed the diabetic group (11). Also, state 3 respiration receiving reducing equivalents from glutamate and malate was lower in type 2 diabetic hearts (11). The work of Anderson and colleagues (11) provides a strong indication that the maximal capacity of cardiac mitochondria to oxidize lipid and non-lipid substrates is impeded in individuals with type 2 diabetes.

Due to difficulty in obtaining samples, the evaluation of cardiac mitochondria in human subjects with type 2 diabetes or associated metabolic abnormalities is limited (72). The use of animal models mimicking metabolic aberrations associated with type 2 diabetes have allowed the work exploring cardiac mitochondria function in humans to be extended (40). In agreement with human atrial respiration measures, a decline in ADP-stimulated oxygen flux is commonly reported (31, 32, 177, 264). In 1983, Kuo et al. found state 3 respiration to be impaired in mitochondria isolated from hearts of db/db mice (177). Also, saponin-permeabilized fibers sampled from glucose-perfused db/db and ob/ob hearts exhibit a lower ADP-stimulated oxygen flux supported by a combination of glutamate and malate, pyruvate and malate or palmitoyl-carnitine and malate (31, 32). The impairment in mitochondrial oxygen consumption is not limited to genetic models of diabetes. Following 16 weeks of high-fat feeding, cardiac mitochondria isolated from rats displayed a reduction in state 3 respiration receiving reducing equivalents from palmitoyl-carnitine and malate or succinate (264). As such, a reduction in maximal mitochondrial capacity to oxidize lipid and non-lipid substrates is a common characteristic identified in both genetic and dietary models of insulin resistance and diabetes.

As previously stated, mitochondria evaluated from hearts perfused with only glucose display a reduction in ADP-stimulated oxygen flux. However, perfusion of hearts with glucose and palmitate prior to mitochondrial evaluation resulted in a preservation of maximal oxygen consumption measures in both HFF and db/db mice (30-32). This increase appears to be the result of fatty acid-induced proton leak as oxygen flux in the absence of ADP is elevated (30-32). Concurrently with the higher basal

oxygen flux, cardiac ATP synthesis and P/O ratios were depressed compared to control animals (31, 32). To identify a mechanism for this palmitate-induced uncoupling, Boudina et al. (32) evaluated proton leak in saponin-permeabilized fibers from db/db mice incubated with guanosine diphosphate (GDP), a known inhibitor of UCPs. In a series of experiments assessing the ability of GDP to impede cardiac proton leak the authors report that proton leak is elevated in db/db mice compared to controls animals and it is largely the result of UCPs. In addition, HFF and db/db mouse models with heightened circulating fatty acids exhibit an increase in cardiac UCP3 (30, 53, 225, 227). The combination of elevated uncoupling protein content and activation may provide a synergistic effect in reducing mitochondrial efficiency (32). Thus, the heart in animal models of diabetes is characterized by mitochondrial uncoupling, which has the potential to compromise energy provision and metabolic efficiency.

Additional mitochondrial aberrations that may compromise cardiac ATP synthesis in those with type 2 diabetes and/or associated metabolic impairments include changes in ETC proteins and mitochondrial content. In nine week-old ob/ob mice, cardiac CI, CIII and CIV subunit protein is depressed (31). Dong et al. (70) found cardiac mitochondrial density to be lower following 20 weeks of high-fat feeding in mice. Also, mediators of mitochondrial biogenesis and ETC protein transcription such as PGC-1α, NRF-1, NRF-2 and TFAM protein and/or mRNA were observed to decrease (70). However, the lessening of mitochondrial protein and content has been contested. Duncan et al. (73) employed an uncoupling protein-diphtheria toxin A (UCP-DTA) mouse model to assess mitochondria in the presence of metabolic insults. The UCP-DTA mouse is characterized by ablation of brown adipose tissue, increased appetite, obesity, hyperglycemia,

hyperlipidemia and hyperinsulinemia (72, 198). At 12 weeks of age, the UCP-DTA mice exhibited greater cardiac mitochondrial content as determined by TEM (73). Also, the protein of CIV and ATP synthase subunits was elevated (73). Further complexity in the mitochondrial alterations that associate with type 2 diabetes occurs as Boudina et al. (32) reported cardiac mitochondrial content and mtDNA to increase concurrently with a decline in TFAM, CII and ATP synthase subunit protein as well as PGC-1 and NRF-1 mRNA in eight to nine week old db/db mice. In light of these inconsistent reports it has been proposed that there are temporal mitochondrial changes in type 2 diabetes (72). More specifically, there may be an increase in mitochondria biogenesis in the early stages of metabolic derangement followed by a reduction under prolonged or severe insult (72). Support for a biphasic quality to mitochondria in the heart has been provided in the study of ob/ob and db/db animals (38). Four week-old ob/ob and db/db mice exhibit normoglycemia but are hyperinsulinemic (38). Hyperglycemia develops between four to eight weeks of age (38). Buchanan et al. (38) observed PGC-1α mRNA was elevated at four weeks of age in ob/ob mice compared to wild-type mice, however, at 16 weeks PGC-1α expression was similar between groups. In db/db animals, PGC-1α mRNA was comparable to controls at four weeks of age (38). In 16 week-old db/db mice, the expression of PGC-1α was depressed (38).

2.9 Mesenchymal stem cell transplantation and cardiac metabolism

2.9.1 Overview of bone marrow-derived mesenchymal stem cells

In general, stem cells are characterized by their capacity for self-renewal and potency (172, 176). Self-renewal describes the infinite proliferation of undifferentiated

cells independent of lineage commitment (172, 176). Potency refers to the ability of these uncommitted cells to differentiate into various cell lineages or tissue types (172, 176). In the 1960's, Friedenstein and colleagues described a rare non-hematopoietic cell population present in guinea pig bone marrow often credited as the initial identification of what is today considered a mesenchymal stem cell (MSC) (92, 93). This bone marrow cell population contained cells that were clonal, plastic adherent and exhibited osteogenic potential (92, 93). Subsequent animal experiments using similar cell populations evaluated their differentiation abilities and biological role in supporting hematopoiesis (162, 356). These studies led to Caplan (44) proposing the term MSC and their capacity to differentiate into all cell types derived from the mesoderm. In 1999, Pittenger et al. (253) identified bone marrow-derived human MSCs were able to be expanded in culture and maintain the ability to differentiate towards osteoblastic, adipolytic and chondrolytic lineages as well.

In an attempt to provide uniformity to the field, the International Society for Cellular Therapy stated that the dynamic cell population derived from bone marrow termed mesenchymal stem cells should be identified as multipotent mesenchymal stromal cells, of which, the mesenchymal stem cell is likely a subset (128, 129). Furthermore, a minimum criteria was put forth to experimentally identify human, bone marrow-derived, multipotent mesenchymal stromal cells (69). Firstly, the cells should adhere to plastic under culturing conditions (69). Also, specific surface antigens expressions should be observed. The surface molecules CD70, CD90, CD105 should be present in parallel with the absence of CD45, CD34, CD11 or CD14b, CD79α or CD19 and human leukocyte antigen-D-related (HLA-DR) expression (69). Finally, the cells should maintain capacity

for trilineage differentiation (69). More specifically, they display the ability to differentiate into osteoblasts, adipocytes and chondroblasts *in vitro* (69). Of note, these criteria established for bone marrow-derived human multipotent mesenchymal stromal cells may not apply consistently to those obtained from other species (245). Although these recommendations have gained traction in the scientific community, the term mesenchymal stem cell continues to receive more regular use (162).

2.9.2 Mesenchymal stem cell transplantation in regenerative medicine

Owing to a limited, innate capacity for regeneration of lost cardiac tissue, the post-MI necrotic region of the heart undergoes a healing process to form a scar for structural integrity (51, 168). The severely depressed contractile properties of the scar places added mechanical responsibility on the uninjured myocardium to preserve function (320). As such, regenerative medicine researchers have been excited by the possibility of using of exogenous cells to repopulate the lost tissue following a MI in an effort to restore function and prevent the transition to heart failure.

MSCs reputedly display immunoprivileged characteristics that make the use of this cell type attractive for cell transplantation purposes (112, 254, 356). MSCs lack the expression of major histocompatibility complex class II and co-stimulatory B7 and CD40 surface molecules (112, 254, 356). This phenotype allows MSCs to minimize being recognized by T cells and the target of subsequent adaptive immune response (27). Additionally, MSCs have been identified to suppress cell mediators of innate and adaptive immune response via cell-cell contact and the secretion of soluble factors (112, 254, 356). These unique characteristics provide promise for use of MSCs in not only autologous transplantation but allogeneic and xenogeneic transplantation.

Another quality of MSCs that lend well to use in regeneration of cardiac tissue is the multipotent differentiation capacity that extends beyond the trilineage potential. *In vitro* experiments incubating MSCs of rodent and human origin with demethylating agent 5-aza-cytidine (5-AZA) report potential cardiomyogenic differentiation (205, 356, 365). The treated MSCs expressed cardiac markers such as beta-myosin heavy chain (beta-MHC), desmin and alpha-cardiac actin protein (205, 356, 365). Additionally, mRNA expression of beta-MHC, desmin and alpha-cardiac actin and protein troponin T was higher than control MSCs (365). Interestingly, after prolonged incubation, the 5-AZA-treated cells started to adjoin via intercalated discs, form myotubes and contract spontaneously (205).

2.9.3 In vivo use of mesenchymal stem cell therapy for the infarcted heart

Promisingly, cell transplantation for the infarcted heart has elicited beneficial results such as a reduction in infarct size and left ventricle dysfunction in human subjects (149). In fact, randomized, controlled, clinical trials have been performed with the use of bone marrow cells in patients with an acute MI (138, 150, 156, 201, 212, 290, 331). Consistently, most trials reported a 3-4% improvement in ejection fraction (EF) when the bone marrow cells were administered post-MI (307, 337).

Bone marrow is comprised of several cell types with MSCs being a relatively minor component (0.001% to 0.01% of the nucleated cells) (254). On going clinical trials are expanding on the findings of total bone marrow administration and employing solely MSC treatments to investigate the safety and therapeutic efficacy of this cell type for ischemic cardiovascular diseases (259). Recently, two of these studies have been completed and the results published (120, 247). The first completed clinical trial by Hare

et al. (120) was a phase I randomized, double-blind, placebo-controlled trial to evaluate allogeneic bone marrow-derived MSC administration for patients within ten days of experiencing a first acute MI. The authors report approximately 5% increase in ejection fraction at 12 months compared to baseline (120). In the second trial, Penn et al. (247) executed a phase I, open–label study administering bone marrow-derived MSCs between two and five days post-MI. An 8.7% increase in ejection fraction was observed four months following MSC transplantation (247).

The decrease in infarct size and improvement in contractile function has also been displayed in animal experiments evaluating MSC therapy for the infarcted heart (112). Furthermore, experimental studies employing large and small animal models have provided insight into the mechanisms for these positive endpoints. Indeed, there is evidence that the exogenous cells can incorporate into the host tissue and differentiate towards the cardiomyogenic lineage (294, 305, 335). However, the occurrence and magnitude of these events are too low to explain the functional improvements following transplantation (114). Moreover, the majority of MSCs fail to engraft and/or survive upon transplantation into the infarcted heart (90, 335). For example, Toma et al. (335) administered human bone marrow-derived MSCs into the murine heart within 20 minutes of inducing a chronic MI. Only 0.44% of the administered cells were present four days following the MI surgery (335). The inability of transplanted cells to persist and remain viable is largely influenced by the host environment. The primary factors leading to cell death and poor engraftment in the infarcted heart are lack of extracellular matrix support, ischemia and acute inflammation following a MI (46, 118, 167, 269, 311).

In the absence of gross cell survival, engraftment and differentiation, the mechanisms promoting the beneficial results reported following cell transplantation has been subject to an increasing number of studies that suggest that cell-mediated paracrine effects are likely the major mechanism for the improvement in cardiac function and the attenuation or slowing of the remodelling process. The release of paracrine factors have a potential regulatory role in various processes including anti-apoptotic signalling and neovascularization as well as the modulation of inflammation, fibrosis, cardiac contractility, endogenous host regeneration and cardiac metabolism (114, 360).

2.9.4 Mesenchymal stem cell therapy for glucose metabolism in the infarcted heart

To date the influence of cell transplantation on cardiac glucose metabolism is largely unstudied. The available literature is conflicting in the assessment of glucose uptake. Gnecchi et al. (113) observed basal glucose uptake in the isolated, perfused, rat heart two weeks following LAD ligation and MSC transplantation. Although MSC-treated hearts exhibited greater glucose uptake than control hearts, glucose utilization was significantly lower than the untreated, infarcted hearts (113). The results suggest that MSC therapy prevents the early increase in glucose uptake post-MI. In contrast, Mazo and colleagues have published two studies that provide differing conclusions (208, 209). In the initial study, Mazo et al. (209) employed a rat LAD ligation model and assessed the effects of adipose-derived MSCs on cardiac glucose uptake one month post-transplantation and two months following the MI event. The authors show global glucose uptake in the heart to be increased in the MSC-treated hearts compared to MI-only animals (209). In the subsequent experiment Mazo et al. (208) administered bone marrow-derived MSCs five weeks following chronic LAD ligation in rats. Seventeen

weeks post-MI, global cardiac glucose uptake was elevated relative to the infarcted animals (208). Although the studies performed by Mazo and colleagues did not use sham animals, the results suggest MSC transplantation prevents a decline in glucose uptake following a MI.

There are several readily apparent reasons for the contrasting findings regarding glucose uptake. First, the studies undertaken by Mazo et al. (208, 209) allowed more time to elapse between MI and metabolic evaluation. Moreover, the degree of insult induced appeared to be greater as determined by contractile parameters (208, 209). This is particularly important given the biphasic behaviour of glucose uptake in the infarcted heart that eventually progresses to failure. Third, Gnecchi et al. (113) indicate that glucose uptake was evaluated in the surviving tissue only. Alternatively, Mazo et al. (208, 209) evaluated glucose uptake in the entire left ventricle including the injured myocardium. Also, Mazo and colleagues utilized isoflurane to sedate the rats during metabolic assessment (208, 209). This may have influenced results given that isoflurane promotes tissue glucose uptake (88) and the cell transplantation reduced infarct size (209). Based on these reports, the work completed in this dissertation aim to evaluate the MSC impact under differing degrees of insult and without the use of anaesthetics *in vivo*.

The interest in the ability of MSCs to minimize metabolic alteration post-MI has also been extended to clinical trials. The phase II trial, Intracoronary Human Wharton's Jelly- Derived Mesenchymal Stem Cells Transfer in Patients With Acute Myocardial Infarction (WJ-MSC-AMI) (NCT01291329), has recently been completed (259). Although results are not currently available, a primary outcome of the study was to evaluate cardiac metabolism and perfusion (259).

2.9.5 Mesenchymal stem cell therapy for mitochondria in the infarcted heart

The Zhang Laboratory at the University of Minnesota has provided much of the current knowledge of the bioenergetic influence MSC therapy exerts on the infarcted heart (85, 148, 369). All studies employ a chronic LAD ligation in swine and intramyocardial delivery of MSCs (85, 148, 369). Two studies report that approximately four weeks post-MI the surviving myocardium of MSC-treated hearts exhibited an improvement in the infarct border zone (~30%) and whole left ventricle (~16%) PCr-to-ATP ratio (85, 369). An improvement in this ratio suggests greater mitochondrial OXPHOS function mediated by the MSC administration. The most recent report from the Zhang laboratory evaluated energetics four months post-MI (148). Similarly, the PCr/ATP ratio was identified to be elevated in the MSC-treated hearts compared to the MI-only (148). Interestingly, nuclear-encoded CI subunits NDUFB6, NDUFB7 and NDUFB11 gene expression was depressed by the cell therapy (148). In speculation, MSC transplantation may confer more than simply a preservation mitochondrial function.

2.9.6 In vivo use of MSCs for diabetic cardiomyopathy and the diabetic infarcted heart

Two independent reports have assessed the effect of cell transplantation on cardiac dysfunction in streptozotocin (STZ)-induced diabetic rats (4, 229). STZ is toxic to pancreatic β-cells leading to cellular dysfunction and compromised insulin production (325). Given this, STZ-treated animals are often utilized to mimic type 1 diabetes (325). Abdel Aziz et al. (4) evaluated *ex vivo* cardiac function in rats receiving MSCs intravenously. Cell transplantation minimized the decline in heart rate, left ventricle developed pressure and contractility index (left ventricle $\Delta p/\Delta t$) induced by STZ (4). Similarly, improvement in cardiac systolic performance was observed using induced

pluripotent stem (iPS) cells in STZ-treated rats (229). Twenty-eight days following iPS cell administration fractional shortening was higher than the STZ-only animals (229).

A protective effect of exogenous cell transplantation has been observed in combined type 2 diabetic/infarcted hearts. Yan et al. (366) assessed the therapeutic efficacy of iPS cell administration in the db/db mouse heart following chronic LAD ligation. Echocardiography revealed that left ventricle contractile dysfunction, as indicated by fractional shortening and ejection fraction, was dampened 14 days post-MI (366).

2.9.7 Mesenchymal stem cell therapy for glucose metabolism in the diabetic heart

Early evidence suggests that cell therapy has the ability to modulate metabolic dysfunction in individuals with type 2 diabetes. A pilot clinical study conducted by Jiang et al. (155) investigated the effect of placenta-derived MSCs (PD-MSCs) on insulin and glucose abnormalities in type 2 diabetic men. Daily, exogenous insulin requirements were reduced up to six months following the last of three PD-MSC intravenous infusions (155). Additionally, glycosylated hemoglobin was depressed (155). Glycosylated hemoglobin is often used as a surrogate for chronic hyperglycemia, reflecting mean blood glucose concentration during the prior two to three months of time (1). Similar findings have been reported employing bone marrow-derived mononuclear cells (25, 26). Together these results suggest cell therapy has potential to aid in diseases of abnormal glucose control.

To date, a single study has evaluated the influence of cell-based therapy on insulin-stimulated glucose disposal as a mechanism through which the cell treatment reduces hyperglycemia as indicated by glycosylated hemoglobin. Si et al. (304)

employed hyperinsulinemic-euglycemic clamps to test whether MSC administration improves whole-body insulin sensitivity in STZ/high-fat diet-induced diabetic rodents. In addition to a reduction in fasting glucose concentration, it was reported that MSC therapy increased the glucose infusion rate (GIR; an index of whole body insulin sensitivity) (304). Moreover, skeletal muscle GLUT4, p-IRS-1 and p-Akt protein was elevated in the MSC-treated animals (304). The work presented in this thesis employs isotopic tracers to provide tissue-specific indexes of *in vivo* glucose uptake in addition to whole body GIR following MSC transplantation and aims to identify the whether cardiac muscle exhibits the same response to the exogenous cells that was reported in skeletal muscle.

[1]CHAPTER THREE: THE ROLE OF MESENCHYMAL STEM CELL TRANSPLANTATION IN MINIMIZING ENERGY METABOLISM ABNORMALITIES IN THE INFARCTED HEART EXIHIBITING MILD SYSTOLIC DYSFUNCTION

3.1 Introduction

To satisfy the continuous energetic demand of contractile function, fatty acids and to a lesser extent glucose are catabolized by mitochondria to synthesize ATP via oxidative phosphorylation (OXPHOS) (326). In response to physiological stressors, the heart must maintain an efficient means of energy provision. This is accomplished by the heart possessing metabolic flexibility, the ability to switch to the most appropriate substrate. Following a myocardial infarction (MI), the heart undergoes energetic alterations in which this adaptability is lost (173). This metabolic remodelling is characterized by a reduction in cardiac fatty acid utilization and an increased reliance on glucose. While the switch to glucose is initially adaptive, the prolonged dependence on a single substrate limits the heart from using the most appropriate substrate milieu in response to physiological stressors which compromises the heart's capacity for energy provision and promotes substrate toxicity. Shifts in substrate balance are often accompanied by mitochondrial insult. Mitochondrial content is reduced and existing mitochondria exhibit OXPHOS dysfunction (186). Consequently, satisfying cardiac

[1]A version of this chapter has been published. Hughey, C.C., Johnsen, V., Ma, L., James, F.D., Young, P.P., Wasserman, D.H., Rottman, J.N., Hittel, D.S., and Shearer, J. Mesenchymal Stem Cell Transplantation for the Infarcted Heart: A Role in Minimizing Abnormalities in Cardiac-Specific Energy Metabolism. *American Journal of Physiology - Endocrinology and Metabolism.* 2012 Jan;302(2):E163-72.

energetic requirements becomes exceedingly difficult and contractile dysfunction is perpetuated.

Research into the efficacy of stem cell therapy as a treatment post-MI is receiving substantial attention. Cell-based therapy promotes cellular viability, neovascularization and improves cardiac contractile performance following a MI (67, 114). Given the dynamic relationship between the aforementioned and energetics, manipulation of metabolism via stem cell therapy may represent an additional mechanism through which transplanted cells minimize myocardial contractile impairment. A limited number of existing reports indicate bone marrow-derived mesenchymal stem cell (MSC) therapy may modulate myocardial metabolism. *Ex vivo*, MSC transplantation blunted an increase in basal, cardiac glucose uptake two weeks post-MI in a rat model (113). Additionally, MSC transplantation into the infarcted swine heart maintained the peri-infarct phosphocreatine-to-ATP (PCr/ATP) ratio, a ratio reflecting OXPHOS regulation, energy efficiency and ventricular function in cardiomyopathies (85, 369). In contrast, Eun et al. (77) reported that MSC therapy does not restore cardiac glycolytic-related metabolites 7-11 days following a MI. The present study builds upon these initial findings characterizing the influence of MSC transplantation on *ex vivo*, basal, cardiac glucose uptake by assessing the *in vivo* effects of intramyocardial MSC injection on insulin sensitivity, insulin-stimulated substrate utilization and mitochondrial function following a MI in the conscious, unrestrained mouse. It was hypothesized MSC transplantation would prevent metabolic inflexibility and mitochondrial impairment.

3.2 Materials and Methods

See Figure 3.1 for a schematic of experimental outline.

Figure 3.1 Schematic representation of experimental procedures and timelines

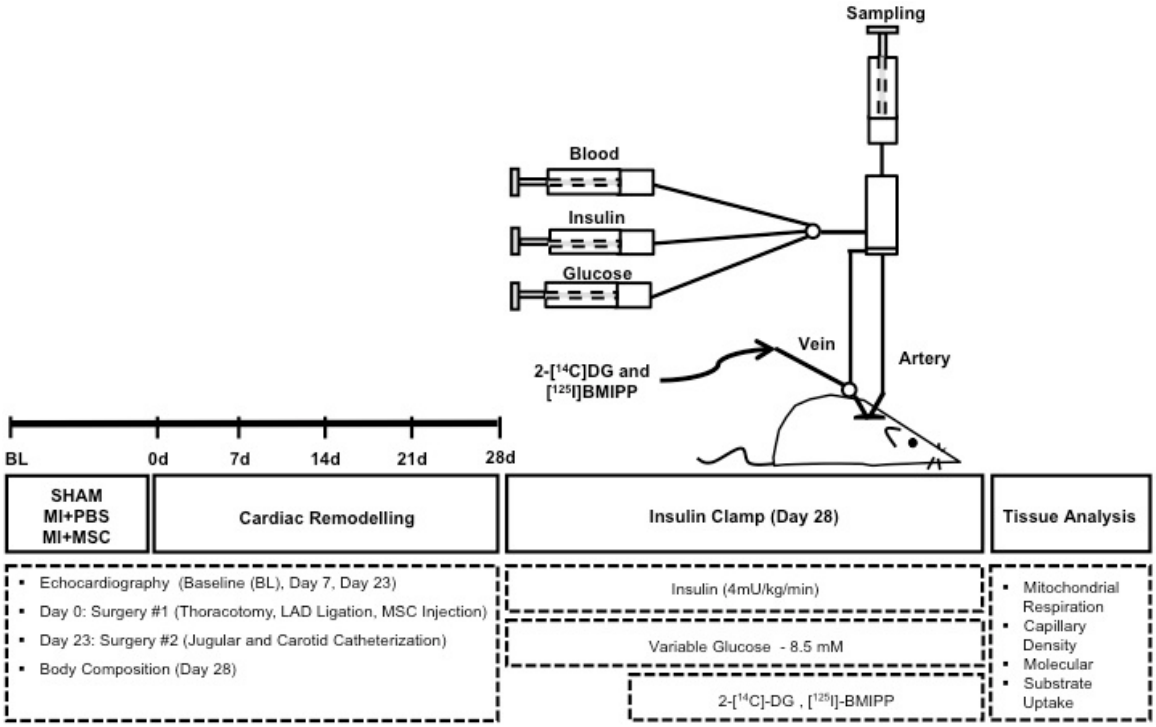

Figure 3.1: Echocardiography on conscious mice was performed at baseline (BL), seven and 23 days following ligation of the left anterior descending coronary artery (LAD). Arterial and jugular catheterization was performed 23 days following the LAD ligation for the sampling and infusion protocols of the hyperinsulinemic-euglycemic (insulin) clamp. Insulin clamps were performed following 5 days of recovery from the catheterization surgeries (28 days post-LAD ligation) to assess insulin action in the conscious, unrestrained mouse. Isotopic tracer (2-[^{14}C]deoxyglucose (2-[^{14}C]DG) and [^{125}I]-15-(ρ-iodophenyl)-3-R,S-methylpentadecanoic acid ([^{125}I]-BMIPP)) administration during the insulin clamps allowed for whole body and tissue-specific substrate uptake to be assessed *in vivo*. Additional experiments included evaluation of mitochondrial

respiration in permeabilized cardiac tissue, capillary density indicated by platelet endothelial cell adhesion molecule1 (PECAM-1) positive area and key molecular indexes of metabolism and myocardial remodelling by immunoblotting and RT-PCR.

3.2.1 Animal characteristics and myocardial infarction

Procedures were approved by the Vanderbilt University Animal Care and Use Committee and were performed according to the Guide for the Care and Use of Laboratory Animals published by the US National Institutes of Health (NIH Publication No. 85-23, revised 1996, A3227-01). C57BL/6J mice (Jackson Laboratories) were randomly separated into three groups: SHAM, MI + phosphate buffered saline (MI+PBS) and MI + mesenchymal stem cells (MI+MSC). A left anterior descending coronary artery (LAD) ligation model of MI was used. Briefly, at three months of age mice of each group were anaesthetized with 50 mg/kg sodium pentobarbital via intraperitoneal injection. All animals underwent a thoracotomy and a 7–0 silk suture was placed through the myocardium into anterolateral left ventricle wall followed by ligation of the LAD of mice in the MI+PBS and MI+MSC groups. Following the LAD ligation and visualization of the infarct manifestation via blanching, 15 μl of PBS, pH 7.2, was injected into the peri-infarct area of the MI+PBS group. 2.5×10^5 MSCs in 15 μl of PBS, pH 7.2, were injected into the peri-infarct area of the MI+MSC group. The experimental protocol of a single administration of 2.5×10^5 cells was employed as a result of previous work by the authors showing a modest reduction in infarct size with this experimental cell number (8). Intra-procedural anaesthesia adequacy was ensured by evaluating the respiratory and/or heart rate as well as the absence of withdrawal reflex for all surgical

procedures. The mice were fed a chow diet (5001 Laboratory Rodent Diet; Purina, Richmond, IN, USA) with ad libitum access to water.

3.2.2 Mesenchymal stem cells

Primary MSCs were generated and expanded in DMEM-LG (Biowhittaker), 10% defined FBS (HyClone, Mediatech; Cellgro), antibiotics, fungizone and 20 μg/ml PDGF as previously described (8, 339). The immunophenotype of MSCs was identified by FACS analysis as previously reported (8). MSCs were $CD44^+$ and $LY6A/E/Sca1^+$. The immunofluorescent staining confirmed the cells to be $CD45^-$, $CD14^-$, $CD11b^-$, $CD16/32^-$, $CD144^-$ and $CD146^-$. Confirmation of MSC phenotype (17, 339) was supported by identifying capacity for trilineage (osteoblast, adipocyte and chondrocyte) differentiation. Differentiation was performed as previously reported (8).

3.2.3 Echocardiography

M-mode echocardiography was performed prior to, seven and 23 days following the LAD ligation in conscious mice as previously described (79, 278).

3.2.4 Catheterization procedures

The catheterization procedures were performed 23 days post-MI as those previously described (299). Briefly, mice were anaesthetized with isoflurane and the carotid artery and jugular vein were catheterized for arterial sampling and venous infusions, respectively. The free ends of the catheters were tunnelled under the skin to the back of the neck where they were attached via stainless steel connectors to lines made of Micro-Renathane. These lines were exteriorized, flushed with saline containing 200 U/ml of heparin and 5mg/ml of ampicillin and then sealed with stainless steel plugs. Post-surgery, the mice were housed individually and given five days of post-operative

recovery prior to hyperinsulinemic-euglycemic (insulin) clamps. The post-operative recovery period ensured mice were within 10% of pre-surgical weight.

3.2.5 Hyperinsulinemic-euglycemic clamp

The insulin clamps were performed ensuring technical considerations previously described (13) were employed approximately twenty-eight days post-MI to ensure the infarct healing and scar formation was largely complete (89). Mice were fasted at 5:00 a.m., five hours prior to commencement of the insulin clamps at 10:00 a.m. Approximately one hour prior to the experiment, the Micro-Renathane tubing was connected to catheter leads and infusion syringes to allow the mice to acclimate to their environment. A baseline arterial blood sample (~100µl) was taken to measure arterial levels of plasma glucose, insulin, non-esterified fatty acids (NEFA) and hematocrit. The insulin clamp was initiated with a constant, continuous infusion of human insulin at 4 mU/kg/min maintained throughout the experiment (Humulin R; Eli Lilly). In the five hour-fasted mouse the insulin dose of 4 mU/kg/min and the corresponding plasma insulin concentration results in complete suppression of hepatic glucose production and increases the rate of glucose disposal approximately three-fold over basal conditions (13). This methodology allows assessment of insulin action on peripheral tissues at high physiological insulin levels. Stable euglycemia (plasma glucose: ~8.5 mM) was maintained during the insulin clamps by measuring blood glucose. Mice received saline-washed erythrocytes from donors for the duration of the insulin clamps (5 µl/minute of saline-washed erythrocytes) to prevent a fall of >10% hematocrit. In all mice, at t= 0 minutes, ~50 ul of arterial blood was sampled to determine arterial plasma glucose and NEFA. Immediately after sampling, a bolus containing 2-[^{14}C]DG (13 µCi) and [^{125}I]-

BMIPP (20 μCi) was administered into the jugular vein to provide an index of tissue-specific glucose and long chain fatty acid (LCFA) uptake and clearance. At t = 2, 5, 10, 15 and 20 minutes, ~50 μl of arterial blood was sampled to determine arterial plasma glucose, NEFA, 2-[^{14}C]DG and [^{125}I]-BMIPP. Hematocrit was also measured at t = 20 minutes. At t = 30 minutes, ~200 μl of arterial blood was taken for the measurement of arterial glucose, insulin, NEFA, 2-[^{14}C]DG and [^{125}I]-BMIPP. Plasma was stored at -20°C until analysis. Mice were then immobilized by cervical dislocation and tissues were rapidly excised for immediate analysis or flash frozen in liquid nitrogen, and stored at -80°C for future analysis. Tissues collected included the heart, gastrocnemius, superficial vastus lateralis and white adipose tissue from the epididymal deposits. For the heart, cardiac tissue was dissected into remote left ventricle and peri-infarct regions. For all experiments conducted in this dissertation, the left ventricle peri-infarct was defined as the cardiac tissue directly adjacent to the infarcted region up to 2 mm. The remote left ventricle was considered the left ventricular tissue beyond this 2 mm region.

3.2.6 Plasma and tissue analyses

Plasma and tissue [^{125}I]-BMIPP radioactivity was determined directly using a gamma (γ-) counter (Beckman Instruments). Plasma 2-[^{14}C]DG was assessed following deproteinization (298). Tissue phosphorylated 2-[^{14}C]DG (2-[^{14}C]DG-P) was measured using a liquid scintillation analyzer (PerkinElmer). Plasma insulin was assayed via double antibody method (218) and plasma NEFA were measured using a colorimetric assay (Wako Chemicals). Plasma glucose was determined from the same deproteinized sample used to determine 2-[^{14}C]DG radioactivity. Briefly, plasma glucose was determined spectrophotometrically (Molecular Devices) in a two-reaction process

measuring the arising reduced nicotinamide adenine dinucleotide phosphate (NADPH) at 340 nm. The reaction mixture included 2.84 mg/ml ATP, 200 mM Tris-HCl (pH7.4), 10 mM $MgCl_2$, 2.03 mg/ml NADP, 1.73 U/ml hexokinase and 0.86 U/ml glucose-6-phoshate dehydrogenase. The relationship between γ-radioactivity and β-emissions was established in the experimental counters.

3.2.7 Whole body and tissue-specific substrate kinetics

The metabolic index of glucose (R_g) and fatty acid (R_f) uptake was calculated (299) and expressed (276) as previously described. Briefly, glucose clearance (K_g) and R_g indices were calculated from the tissue accumulation of 2-[^{14}C]DG-P and the integral of the plasma 2-[^{14}C]DG concentration following the administration of a 2-[^{14}C]DG bolus. The relationships were defined as:

$$K_g = [2\text{-}[^{14}C]DG\text{-}P]_{tissue}\,(t) / \int_0^t [2\text{-}[^{14}C]DG]_{plasma}\,dt$$

$$R_g = K_g \times [Glucose]_{plasma}$$

Similarly, long chain fatty acid clearance (K_f) and R_f indices were calculated from the tissue accumulation of [^{125}I]-BMIPP and the integral of the plasma [^{125}I]-BMIPP concentration following the administration of a [^{125}I]-BMIPP bolus. The equations used were:

$$K_f = [[^{125}I]\text{-}BMIPP]_{tissue}\,(t) / \int_0^t [[^{125}I]\text{-}BMIPP]_{plasma}\,dt$$

$$R_g = K_f \times [NEFA]_{plasma}$$

Whole-body glucose (MCR_g) and fatty acid (MCR_f) clearance were determined as previously reported (301). MCRs were determined from the initial tracer dose administered (D) and the tracer disappearance in the plasma. The equations used were:

$$MCR_g = D/\int_0^t [2\text{-}[^{14}C]DG]_{plasma}(t)dt$$

$$MCR_f = D/\int_0^t [[^{125}I]\text{-}BMIPP]_{plasma}(t)dt$$

R_g for cardiac and peripheral tissues were expressed relative to R_g of the brain, which represents constant reservoir of glucose uptake under various physiological conditions (276). As a result of no tissue exhibiting constant fatty acid uptake, [^{125}I]-BMIPP accumulation in the tissue was expressed as absolute values. MCR values were expressed relative to the SHAM group.

3.2.8 Mitochondrial respiration and enzymatic measurements

Peri-infarct permeabilized fibers were prepared as described (178). In brief, cardiac samples were excised following the insulin clamp and permeabilized in buffer X (7.23 mM K_2EGTA, 2.77 mM CaK_2EGTA, 20 mM imidazole, 0.5 mM DTT, 20 mM taurine, 5.7 mM ATP, 14.3 mM PCr, 6.56 mM $MgCl_2$, 50 mM K-MES, 50 µg/ml saponin (pH 7.1)). Fiber bundles were washed in buffer Z (105 mM K-MES, 30 mM KCl, 10 mM K_2HPO_4, 5 mM $MgCl_2$, 5 g/L BSA, 1 mM EGTA (pH 7.1)). High resolution respirometry (Oroboros Instruments) was performed in duplicate at 37°C in buffer Z. Substrates included 10 mM glutamate plus 2 mM malate, 5 mM ADP and 10 mM succinate.

Peri-infarct citrate synthase activity was determined through adaptation of previous methods (125) at 25°C. Following slight modifications, peri-infarct NADH-cytochrome *c* oxidoreductase activity (CI+III) was determined as previously reported (183). Protein was determined using the Bradford method (BioRad).

3.2.9 Immunoblotting and immunostaining

Muscle samples were homogenized in a lysis buffer containing 50 mM HEPES (pH 7.5), 2 mM EDTA, 10% glycerol, 1% NP-40, 150 mM NaCl, 2 mM PMSF, 10 mM β-glycerophosphate, 1 mM $CaCl_2$, 1 mM $MgCl_2$, 2 mM Na_3VO_4, 10 mg/L Aprotinin, 10 mg/L Leupeptin, 3 mM Benzamidine, 10 mM NaF, and 20 mM NaP. Tissue homogenate was centrifuged (10 minutes at 1000 g and 4°C) and protein determination in the supernatant was assessed using the Bradford method (BioRad). Protein expression of glucose transporter 4 (GLUT4), hexokinase II (HKII), peroxisome proliferator-activated receptor gamma coactivator-1alpha (PGC-1α), glutathione peroxidase (GPx), mitochondrial oxidative phosphorylation complexes I to V (CI to CV), uncoupling protein 3 (UCP3) and adenine nucleotide translocase (ANT) in the peri-infarct region of cardiac tissue were determined. Proteins (20-30 ug) were resolved on NuPAGE 4-12% Bis-Tris gels (Invitrogen) and transferred to a polyvinylidene fluoride membrane. The membranes were blocked and subsequently probed with anti-UCP3 (Abcam, 1:1000) anti-ANT (Santa Cruz Biotechnology, 1:500), anti-GLUT4 (Abcam, 1:10,000), anti-hexokinase (Chemicon, 1:1000), anti-PGC-1α (Santa Cruz, 1:1000), anti-α-actin (Thermoscientific, 1:2000) and anti-VDAC (Abcam, 1:1000). OXPHOS complexes of the electron transport chain were determined using MitoProfile® Total OXPHOS Rodent WB Antibody Cocktail (MitoSciences, 1:500). Following incubation with HRP-

conjugated secondary antibodies, the membranes were exposed to a chemiluminescent HRP-substrate (Millipore) and imaging was performed using Chemigenius² BioImaging System (SynGene). Densitometry was completed using Gene Tools software (Syngene). Protein expression was normalized to voltage dependent anion channel (VDAC) expression; which has routinely been used as a mitochondrial loading control. α-actin was used as the control for GLUT4, HKII and PGC-1α.

Capillary density was assessed in 8 μm sections of formalin fixed paraffin-embedded cardiac tissue following immunofluorescence detection of platelet endothelial cell adhesion molecule1 (PECAM-1). For immunofluorescence, sections were washed with PBS and then incubated with a PBS-blocking buffer (1% BSA and 10% goat serum) for 30 minutes. The slides were then incubated with rabbit anti-PECAM-1 (Santa Cruz; 1:250) overnight at 4°C. The sections were washed three times and incubated with the fluorescently labeled secondary antibody (Alexa Fluor 546-labeled anti-rabbit IgG; Invitrogen) at room temperature for one hour. Sections were washed three times with PBS and mounted with Prolong Gold Antifade Reagent (Invitrogen). Quantification of vascularity (PECAM-1) in the heart was evaluated on nine to ten randomly chosen fields (objective 40x/0.75) from tissues obtained from mice by fluorescence microscopy. For confocal microscopy analysis, an Olympus BX61 W confocal microscope was used and images were generated using Fluorview 1000 software. The PECAM-1 positive area of tissue for each field was quantified using Image J by outlining tissue and calculating total area per field. Areas are expressed relative to the SHAM group for the infarct and remote left ventricle.

3.2.10 Quantitative real-time PCR

Total RNA was extracted from freeze-clamped heart tissue with Trizol reagent (Invitrogen). Reverse transcription, real-time PCR and data analysis were performed as previously described (300). Real-time PCR reactions were employed with Quantitect mouse atrial natriuretic peptide primer pairs (Qiagen) and the following mouse β-actin primers: forward (TGTTACCAACTGGGACGACA) and reverse (GGGGTGTTGAAGGTCTCAAA). β-actin was used as a housekeeping gene as it did not change between treatment groups. Relative gene expression levels are presented as the fold-change compared to the SHAM group, for which all levels were designated as 1.

3.2.11 Statistical analyses

ANOVAs were performed to detect statistical differences ($p < 0.05$). Differences within the ANOVA were determined using Tukey's post hoc test. All data are reported as means ± SEM.

3.3 Results

3.3.1 Metabolic characteristics

Prior to the initiation of the insulin clamps baseline metabolic parameters were evaluated (Table 3.1). Fasting concentrations of arterial plasma glucose, NEFA and insulin were similar between groups. Additionally, the experimental plasma insulin concentration in response to the constant insulin infusion was comparable for animals of each treatment group.

Table 3.1 Biometric characteristics of C57BL/6 mice

	SHAM	MI+PBS	MI+MSC
Fasting Plasma Glucose (mM)	6.2 +/- 0.8	6.2 +/- 0.3	5.8 +/- 0.5
Fasting Plasma NEFA (mM)	0.98+/- 0.09	1.12 +/- 0.11	1.13 +/- 0.22
Fasting Plasma Insulin (µU/ml)	33.2 +/- 4.7	24.7 +/- 2.9	22.5 +/- 3.3
Experimental Plasma Insulin (µU/ml)	79.8 +/- 8.4	80.8 +/- 11.1	99.9 +/- 13.0

Data are mean ± SEM for n=8-12 mice per group for plasma glucose; n=7-8 for plasma NEFA; n=11-15 for fasting plasma insulin; n= 9-16 for experimental plasma insulin.

3.3.2 Cardiovascular parameters

To gain insight into the impact of MSC therapy on left ventricle contractile performance, echocardiography was performed on conscious mice prior to, seven and 23 days post-MI. Functional abnormalities (Table 3.2) were observed in the MI+PBS group, indicative of left ventricle systolic impairment with depressed ejection fraction (Figure 3.2A) and fractional shortening (Figure 3.2B). The effects of MSC transplantation were manifested seven days post-surgery with preservation of fractional shortening (Figure 3.2B). At 23 days, the MSC transplantation blunted abnormalities in ventricular function. MI+PBS mice had a lower fractional shortening than the SHAM and MI+MSC animals (Figure 3.2B). However, fractional shortening was decreased in MSC-treated mice compared to the SHAM mice (Figure 3.2B). The data demonstrates MSC injection post-MI preserves left ventricle contractile performance. Indices of alterations in cardiac structure and geometry were evaluated. Post-MI hearts exhibited pathological hypertrophy as the heart weight-to-body weight ratio was increased (Figure 3.2C). MSC treatment normalized heart weight-to-body weight (Figure 3.2C). Additionally, cardiac

ANP gene expression was elevated in the MI+PBS mice (Figure 3.2D). Unexpectedly, ANP was further elevated in the MI+MSC animals (Figure 3.2D).

Table 3.2 Cardiovascular parameters in the conscious C57BL/6 mice

	Baseline			7 days			23 days		
	SHAM	**MI+ PBS**	**MI+ MSC**	**SHAM**	**MI+ PBS**	**MI+ MSC**	**SHAM**	**MI+ PBS**	**MI+ MSC**
HR (bpm)	694 ± 4	673 ± 7	676 ± 10	706 ± 13	685 ± 22	697 ± 6	700 ± 10	673 ± 18	692 ± 9
FS	0.500 ± 0.005	0.495 ± 0.002	0.503 ± 0.004	0.488± 0.005	0.376 ± 0.008*	0.466 ± 0.005†	0.484± 0.004	0.360 ± 0.009*	0.455 ± 0.007*†
EF	0.864 ± 0.004	0.866 ± 0.002	0.871 ± 0.003	0.858± 0.004	0.743 ± 0.01*	0.840 ± 0.004†	0.853± 0.004	0.723 ± 0.01*	0.828 ± 0.008†
IVSd (cm)	0.067 ± 0.001	0.066 ± 0.001	0.063 ± 0.001*†	0.071± 0.002	0.068 ± 0.002	0.068 ± 0.001	0.072± 0.002	0.073 ± 0.002	0.069 ± 0.002
LVIDd (cm)	0.287 ± 0.004	0.289 ± 0.002	0.293 ± 0.004	0.300± 0.005	0.340 ± 0.01*	0.301 ± 0.007†	0.290± 0.006	0.354 ± 0.009*	0.310 ± 0.008†
LVPWd (cm)	0.052 ± 0.001	0.054 ± 0.001	0.054 ± 0.001	0.060± 0.002	0.066 ± 0.002	0.064 ± 0.002	0.060± 0.002	0.062 ± 0.002	0.064 ± 0.002
IVSs (cm)	0.119 ± 0.002	0.116 ± 0.002	0.110 ± 0.002*	0.120± 0.001	0.106 ± 0.003*	0.115 ± 0.003	0.120± 0.002	0.114 ± 0.002	0.117 ± 0.004
LVIDs (cm)	0.145 ± 0.003	0.144 ± 0.001	0.146 ± 0.002	0.154± 0.003	0.213 ± 0.008*	0.16 ± 0.004†	0.150± 0.003	0.227 ± 0.008*	0.169 ± 0.006†
LVPWs (cm)	0.084 ± 0.001	0.081 ± 0.001	0.085 ± 0.002	0.085± 0.001	0.095 ± 0.003*	0.095 ± 0.002*	0.088± 0.002	0.090 ± 0.003	0.091 ± 0.002

*$p<0.05$ vs. SHAM at specified time point.

†$p<0.05$ vs. MI+PBS at specified time point.

Data are mean ± SEM for n=15-19 mice per group.

Abbreviations: HR, heart rate; FS, fractional shortening; EF, ejection fraction; IVSd, interventricular septal thickness in diastole; LVIDd, left ventricle (LV) end-diastolic dimension; LVPWd, LV posterior wall thickness in diastole; IVSs, interventricular septal thickness in systole; LVIDs, LV end-systolic dimension; LVPWs, LV posterior wall thickness in systole.

Figure 3.2 Cardiac functional and structural indices

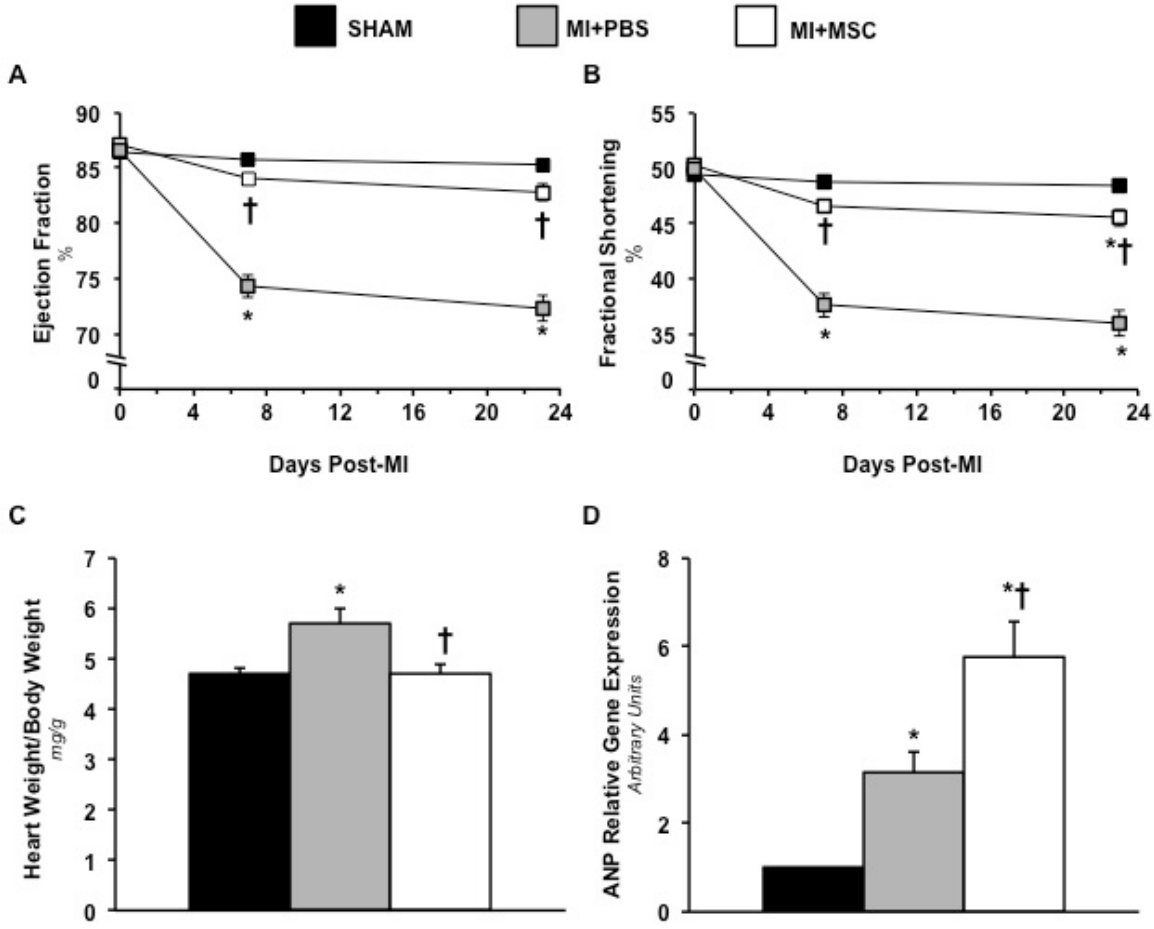

Figure 3.2: (A) Cardiac ejection fraction prior to, seven and 23 days following a MI. (B) Fractional shortening prior to, seven and 23 days following a MI. n=15-19 mice per group. (C) Heart weight-to-body weight ratio 28 days following a MI. n=12-18 mice per group. (D) Cardiac atrial natriuretic peptide (ANP) gene expression 28 days following a MI relative to the SHAM mice. n=6-7 mice per group. Data are mean ± S.E.M. *$p<0.05$ vs. SHAM. †$p<0.05$ vs. MI+PBS.

3.3.3 Metabolic indices of cardiac-specific glucose and fatty acid metabolism

Isotopic tracers were administered during insulin clamps in the conscious, unrestrained mouse to evaluate glucose and fatty acid uptake at high physiological insulin levels. Cardiac glucose uptake (R_g) exhibited regional differences in the infarcted heart. MI+PBS mice were found to have a similar peri-infarct glucose uptake compared to SHAM mice (Figure 3.3A). However, the remote left ventricle glucose utilization was elevated (Figure 3.3B). MSC therapy inhibited the increase in remote left ventricle glucose metabolism (Figure 3.3B). Similarly, insulin-stimulated cardiac fatty acid uptake (R_f) displayed site-specific differences following a MI. The peri-infarct fatty acid uptake was depressed and the remote left ventricle was unaltered in the MI+PBS animals (Figure 3.3C and 3.3D). More importantly, this is the first report to demonstrate MSC transplantation maintains peri-infarct fatty acid uptake post-MI (Figure 3.3C).

Given the alterations in substrate kinetics, protein levels of key regulators of substrate metabolism were evaluated. GLUT4 and HKII, key mediators in glucose transport and phosphorylation, were comparable (Figure 3.4A and 3.4B). However, PGC-1α, a transcriptional coactivator exhibiting a central role in the regulation of fatty acid oxidation, mitochondrial biogenesis and OXPHOS, was depressed post-MI (Figure 3.4A and 3.4B). Substrate uptake is also influenced by substrate availability, muscle blood flow and capillary recruitment (350). The depressed peri-infarct fatty acid utilization may be influenced by differences in vascularity given infarct PECAM-1 positive area was lower in MI+PBS mice (Figure 3.4C). However, aberrations in substrate utilization in the remote left ventricle were independent of vascular density as PECAM-1 positive area was similar between groups (Figure 3.4D).

Figure 3.3 Cardiac metabolic indices

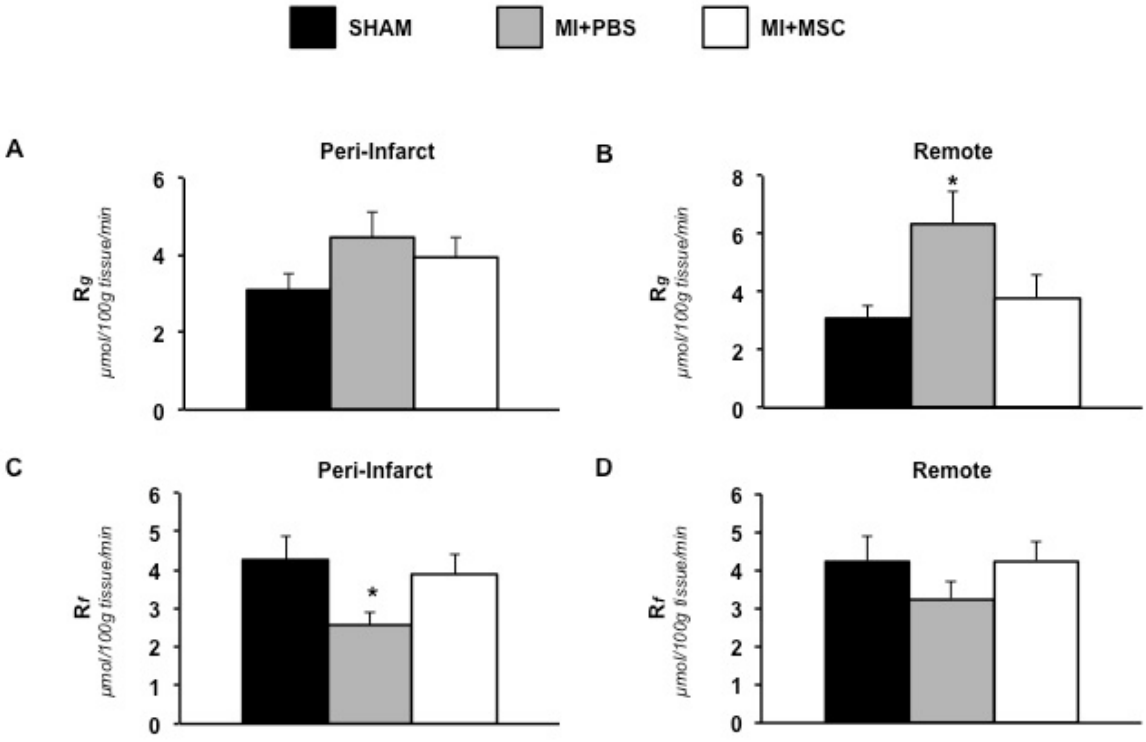

Figure 3.3: (A) Metabolic index of glucose uptake (R_g) in the peri-infarct. (B) Metabolic index of glucose uptake remote left ventricle. (C) Metabolic index of long chain fatty acid uptake (R_f) in the peri-infarct. (D) Metabolic index of long chain fatty acid uptake remote left ventricle. Cardiac R_g values are relative to brain R_g. n=8-12 mice per group. Data are mean ± S.E.M. *$p<0.05$ vs. SHAM.

Figure 3.4 Metabolic regulators of substrate metabolism and capillary density

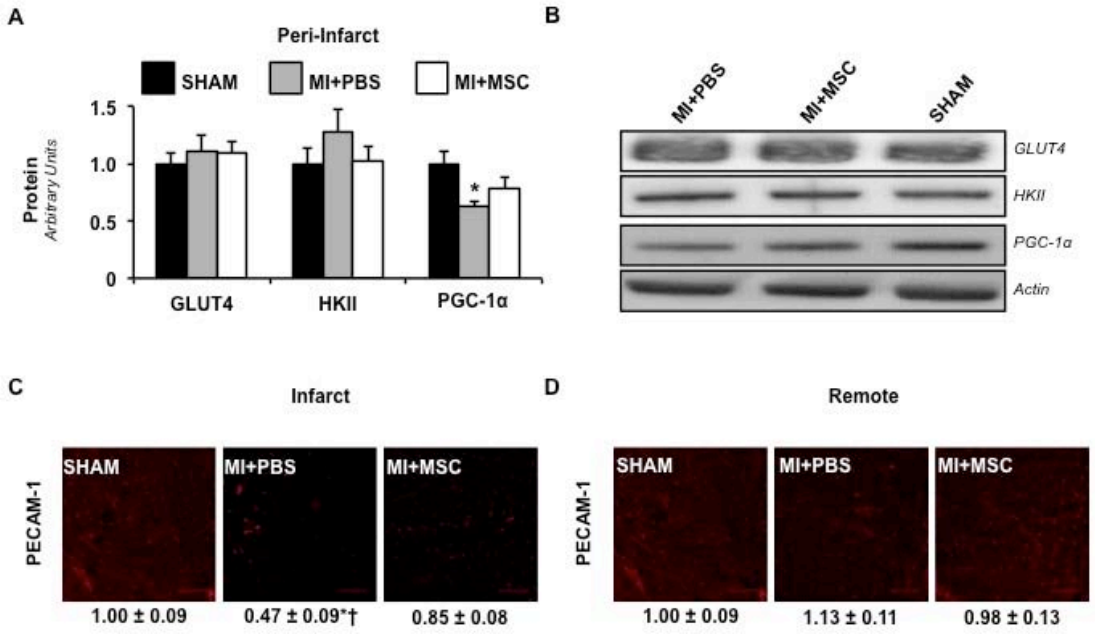

Figure 3.4: (A) Glucose transporter 4 (GLUT4), hexokinase II (HKII) and peroxisome proliferator-activated receptor gamma coactivator-1alpha (PGC-1α) from the peri-infarct region as determined by immunoblotting. (B) Representative immunoblotting performed to measure GLUT4, HKII, PGC-1α. Protein levels are normalized to actin content and are relative to the SHAM group. n=6-8 mice per group. (C) PECAM-1 immunofluorescence staining of the infarct. (D) PECAM-1 immunofluorescence staining of the remote left ventricle. Vascular density determined as the percentage of immunopositive PECAM-1 area/total tissue area. Values are relative to SHAM LV. n=9-10 mice per group. Scale bar, 50μm. Data are mean ± S.E.M. *p<0.05 vs. SHAM. Of note, the order presentation of the groups in panel B is different than the order presentation of the groups in panels A, C and D. The SHAM group presented in panels C and D are the same data set.

3.3.4 Metabolic indices of whole body and peripheral tissue glucose metabolism

To assess insulin sensitivity, insulin clamps were performed in conscious animals. Glucose infusion rate (Figure 3.5A) was not different between treatments, indicating no difference in whole body insulin sensitivity with MSC administration. Figures 3.5B and 3.5C represent a time-course of arterial plasma glucose and NEFA concentration during the insulin clamps and confirms stable euglycemia was achieved. Additionally, systemic glucose uptake was examined to evaluate whole body metabolic alterations following a MI and/or MSC therapy. Whole body clearance of glucose from the blood (MCR_g; Figure 3.6A) was comparable between groups. Peripheral tissue glucose uptake was assessed. Specifically, gastrocnemius (Figure 3.6B), superficial vastus lateralis (Figure 3.6C) and white adipose tissue (Figure 3.6D) substrate utilization was determined. As exhibited by whole body glucose clearance, peripheral tissue glucose utilization was similar between groups.

Figure 3.5 Insulin sensitivity and plasma substrates during the insulin clamp

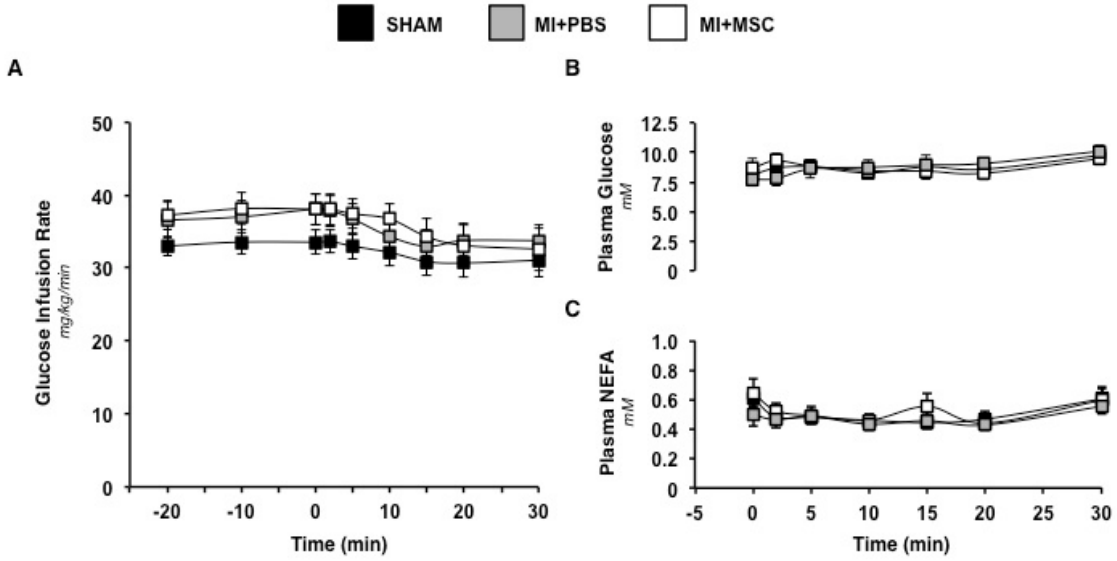

Figure 3.5: (A) Glucose infusion rate (GIR) during the insulin clamp. The GIR is equivalent to glucose disposal rate in response to insulin stimulation. The GIR is presented as a time course starting twenty minutes prior to administration of 2-[^{14}C]DG and [^{125}I]-BMIPP (-20 minute time point) until 30 minutes following 2-[^{14}C]DG and [^{125}I]-BMIPP infusion (30 minute time point). (B) Arterial, plasma glucose concentration following 2-[^{14}C]DG and [^{125}I]-BMIPP injection. (C) Arterial, plasma non-esterified fatty acids (NEFA) in mice following 2-[^{14}C]DG and [^{125}I]-BMIPP injection. Data are mean ± SEM for n=8-12 mice per group.

Figure 3.6 Whole body and peripheral tissue glucose utilization

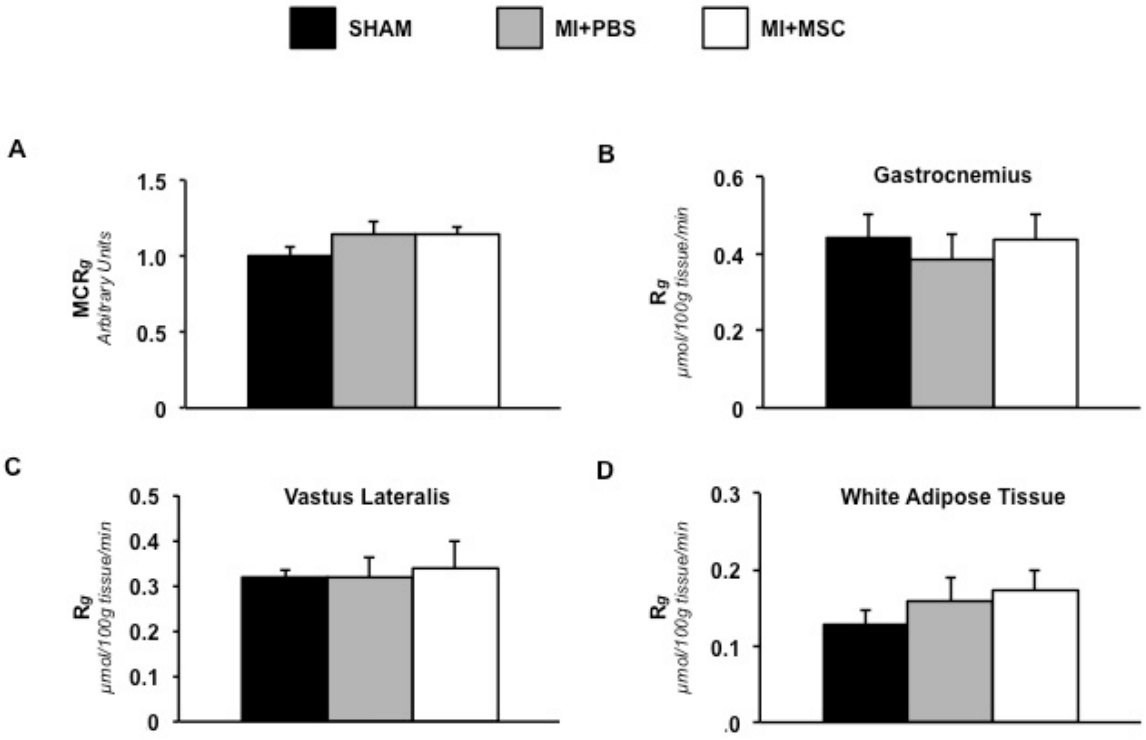

Figure 3.6: (A) Index of whole body glucose clearance rate (MCR_g). MCR_g values are relative to the SHAM group. SHAM values are set to an arbitrary value of one. (B) Metabolic index of glucose uptake (R_g) in the gastrocnemius. (C) Metabolic index of glucose uptake (R_g) in the superficial vastus lateralis. (D) Metabolic index of glucose uptake (R_g) in white adipose tissue. Tissue R_g values are relative to brain R_g. n=8-12 mice per group.

3.3.5 Metabolic indices of whole body and peripheral tissue long-chain fatty acid metabolism

Peripheral fatty acid metabolism was also evaluated following a MI and/or MSC transplantation. Whole body, LCFA clearance from the circulation (MCR_f; Figure 3.7A) was similar between groups. Identical to glucose utilization, peripheral tissue fatty acid uptake was assessed. Gastrocnemius (Figures 3.7B), superficial vastus lateralis (Figure 3.7C) and white adipose tissue (Figure 3.7D) fatty acid uptake kinetics were determined. Unexpectedly, gastrocnemius fatty acid uptake was significantly lower in the MI+PBS mice compared to the MSC-treated mice (Figure 3.7B).

Figure 3.7 Whole body and peripheral tissue long-chain fatty acid utilization

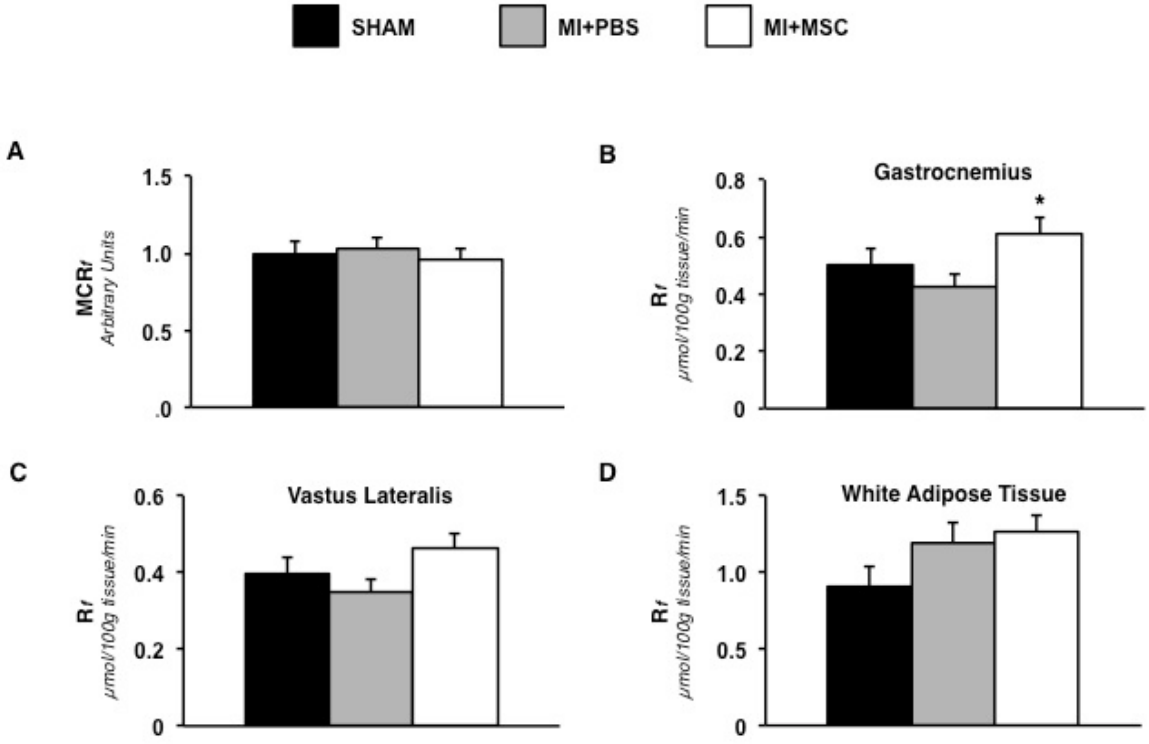

Figure 3.7: (A) Index of whole body long-chain fatty acid (LCFA) clearance rate (MCR_f). MCR_f values are relative to the SHAM group. SHAM values are set to an arbitrary value of one. (B) Metabolic index of LCFA uptake (R_f) in the gastrocnemius. (C) Metabolic index of LCFA uptake (R_f) in the superficial vastus lateralis. (D) Metabolic index of LCFA uptake (R_f) in white adipose tissue. n=8-11 mice per group. Data are mean ± S.E.M. *$p<0.05$ vs. MI+PBS.

3.3.6 Cardiac mitochondrial function

Because contractile function and substrate utilization are affected by energy metabolism, polarographic oxygen consumption measurements were performed using permeabilized cardiac fibers to evaluate the integrative function of OXPHOS. MSC

therapy lowered basal oxygen consumption through complex I (Figure 3.8A; V_0). Adenosine diphosphate (ADP)-stimulated oxygen consumption through complex I was reduced in MI+PBS and MI+MSC animals (Figure 3.8A; $V_{MAX\text{-}CI}$). Similarly, ADP-stimulated oxygen consumption via convergent electron flux was reduced in both treatment groups (Figure 3.8A; $V_{MAX\text{-}CI+CII}$). The succinate control ratio (SCR) was unchanged suggesting complex II is not responsible for the lower respiratory capacity (Figure 3.8B). Interestingly, the respiratory control ratio (RCR) was depressed in the MI+PBS mice (Figure 3.8B) compared to the MI+MSC mice. This indicates reduced coupling of ADP phosphorylation and oxygen consumption and translates into a decreased efficiency of mitochondrial OXPHOS in the infarcted mice. Citrate synthase activity was assessed to determine the influence of mitochondrial heterogeneity on the reduced oxygen flux. Citrate synthase activity was similar between groups excluding any effect of mitochondrial content on OXPHOS (Figure 3.8E). This prompted the evaluation of mitochondrial protein content. Protein expression of mitochondrial OXPHOS CI-CV and ANT were unchanged (Figures 3.8C and 3.8D). The absence of differences in many of the mitochondrial proteins did not account for the reduced oxygen flux following MSC therapy. However, a reduced CI+CIII activity (Figure 3.8F) provides a mechanism, in part, for the depressed oxygen flux through complex I in MI+MSC mice. Peri-infarct UCP3 was lower in the MI+PBS mice (Figures 3.8C and 3.8D), consistent with reduced fatty acid uptake. The lower UCP3 may be an adaptive response to depressed fatty acid utilization. In addition to generating ATP, mitochondria are a source of reactive oxygen species (ROS). The alterations in mitochondrial function

and efficiency provided rationale for cardiac antioxidant defense assessment. GPx, a ROS scavenger, exhibited lower protein levels in the MI+MSC mice (Figure 3.8C-D).

Figure 3.8 Peri-infarct mitochondria

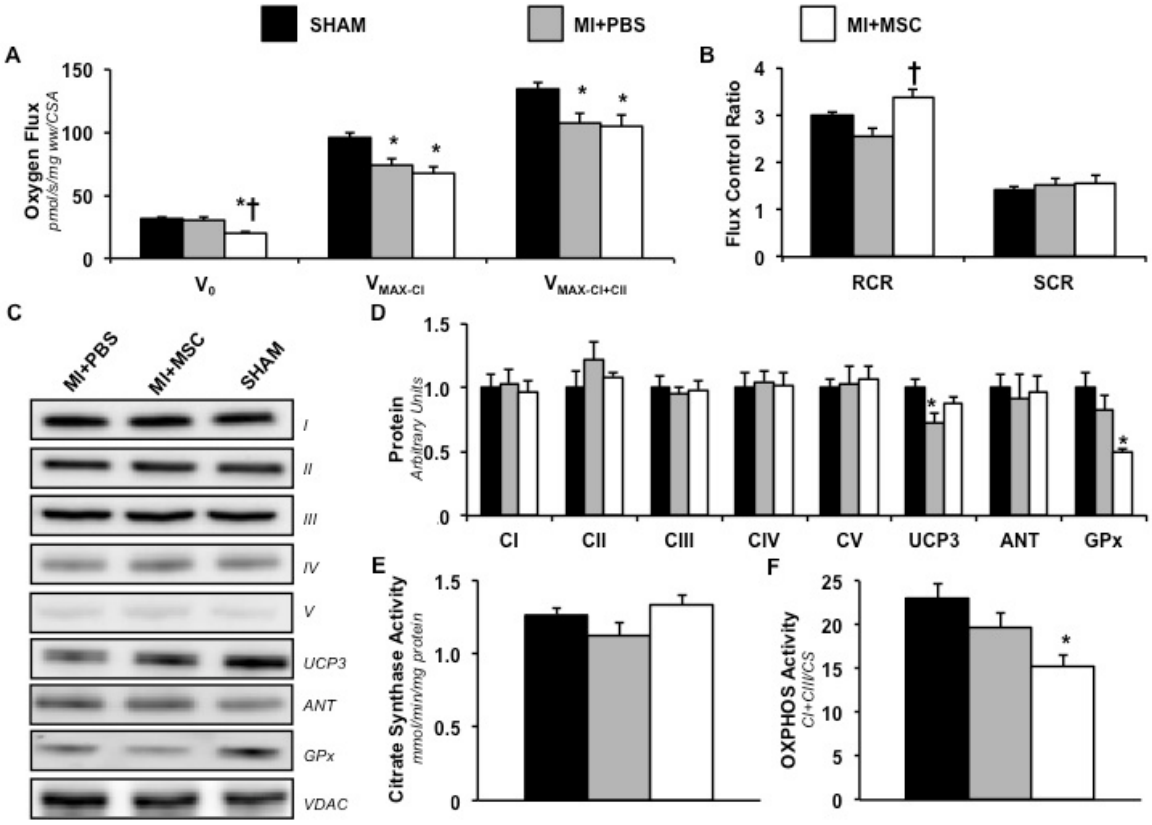

Figure 3.8: (A) Peri-infarct permeabilized cardiac fiber basal oxygen consumption supported by glutamate and malate (V_0), maximal oxygen consumption supported by glutamate and malate through complex I ($V_{MAX\text{-}CI}$) and maximal convergent oxygen consumption supported by glutamate, malate and succinate ($V_{MAX\text{-}CI+CII}$). (B) Respiratory control ratio (RCR; defined as $V_{MAX\text{-}CI}/V_0$) and Succinate Control Ratio (SCR; defined as $V_{MAX\text{-}CI+CII}/ V_{MAX\text{-}CI}$). n=8 mice per group. (C): Mitochondrial oxidative phosphorylation (OXPHOS) complexes, uncoupling protein 3 (UCP3), adenine

nucleotide translocase (ANT) and glutathione peroxidase (GPx) from the peri-infarct region as determined by immunoblotting. (D) Representative immunoblotting of OXPHOS complexes, UCP3, ANT, GPx and VDAC. Protein levels were normalized to VDAC content and are relative to the SHAM group. n=6 mice per group. Of note, the order presentation of the groups in panel D is different than the order presentation of the groups in panel C (E) citrate synthase activity (CSA) (mmol/min/mg protein). (F) Relative CI+CIII activity (nmol/min/mg protein) normalized to CSA. n=6-8 mice per group. Data are mean ± S.E.M. *$p<0.05$ vs. SHAM. †$p<0.05$ vs. MI+PBS.

3.4 Discussion

Metabolic remodelling is a hallmark characteristic post-MI (230). This study uniquely combines a series of technically challenging experiments to address the therapeutic value of MSCs as a metabolic modulator to rescue the infarcted heart from contractile and energetic alterations in the conscious mouse. We report regional differences in insulin-stimulated cardiac glucose uptake post-MI. The peri-infarct glucose uptake was comparable and the remote left ventricle glucose uptake was increased. Novel findings show that MSC transplantation normalized the deranged insulin-stimulated cardiac glucose uptake *in vivo*. This extends a recent report that MSC transplantation prevents increases in basal glucose uptake *ex vivo* (113). Additionally, insulin-stimulated fatty acid utilization exhibited site-specific alterations in the infarcted heart. A depression in the peri-infarct fatty acid uptake was observed, however, the remote left ventricle was unaffected. In agreement, a reduced utilization of fatty acids is an oft-reported alteration under basal conditions following a MI (123). Moreover, this is

the first study to show MSC treatment preserves *in vivo* peri-infarct fatty acid uptake. A growing number of reports postulate that fatty acids are required for optimal left ventricle function (341, 367). We found MSC therapy minimized left ventricle systolic dysfunction and pathological hypertrophy as indicated by improved fractional shortening and reduced heart weight-to-body weight body, respectively. Our findings suggest that in the early stages and/or presence of moderate insult post-MI, the maintenance of a metabolic network that can utilize both fatty acids and glucose has positive associations with improved cardiac structure and function.

The switch away from fatty acid utilization towards a glucose preference may be in response to alterations in substrate availability. Following a MI, capillary density is lost in the infarcted region (369). Our findings show that the infarcted region of the MI+PBS mice has a lower PECAM-1 positive area suggesting a reduction in capillary supply to the insulted region of the heart. The decline in infarct capillary density may contribute to the reduced peri-infarct fatty acid utilization in the untreated mice. In contrast, the transplantation of MSCs preserved capillary density in infarcted mouse heart and may assist in the maintenance of cardiac fatty acid uptake.

Alterations in substrate utilization may also be the result of abnormal molecular regulation. Of note, PGC-1α is a transcription factor co-activator that promotes the expression of target genes involved in fatty acid uptake and oxidation (184). Our results indicate PGC-1α protein levels were reduced in the peri-infarct region following a MI, however, levels were maintained in the peri-infarct region of MSC-treated mice. These results suggest MSC therapy inhibits the decline in PGC-1α. This could maintain activation of genes involved in fatty acid metabolism and assist in preserving fatty acid

utilization in the peri-infarct region of the MI+MSC mice. The decline in PGC-1α following a MI may also link abnormalities in cardiac fatty acid metabolism and mitochondrial function.

PGC-1α promotes mitochondrial biogenesis, respiration and OXPHOS coupling in addition to its role in fatty acid metabolism (184). Upon evaluation, maximal oxygen flux was reduced in the peri-infarct bundles of the infarct-only hearts. Our findings suggest the decline in ADP-stimulated respiration was unrelated to alterations in the individual electron transport complexes. Protein levels of mitochondrial CI-CIV as well as the enzymatic activity were unchanged in the MI+PBS mice. The reduction in maximal respiration in the absence of electron transport chain alterations suggests that the supramolecular complex structures or phosphorylation system is impaired. Further support for these alterations is the reduced RCR in the MI+PBS mice. This ratio represents coupling between ADP phosphorylation and oxygen consumption.

Of particular interest, cell-based therapy appears to elicit changes in cardiac mitochondria that do not completely normalize energetics. Recently, Eun et al. (77) reported that MSC transplantation into infarcted rat hearts produce ATP synthesis-related metabolite profiles significantly different than that of control and infarct-only animals. MSC transplantation has also been shown to reduce complex I subunit gene expression in the peri-infarct region four months post-MI (148). We did not identify differences in the protein levels of the OXPHOS complexes. This may be due to the current study determining alterations in complex I at four weeks post-MI rather than four months. Additionally, the contrasting findings may arise from the evaluation of different complex I subunits. However, in agreement with the previous report that MSC therapy augments

cardiac complex I characteristics, our data shows a reduced CI+CIII activity induced by the MSC treatment. This catalytic reduction in OXPHOS components contributes to the depressed oxygen flux in the peri-infarct fiber bundles following MSC injection. The causation for the lowered OXPHOS enzymatic activity is currently unknown. Jameel et al. (148) hypothesized that a reduction in regional wall stress and energetic demands following the cell-based therapy may result in the differential complex I subunit gene expression and may contribute to OXPHOS enzymatic alterations. In support, we observed cardiac ANP gene expression to be increased in the MI+MSC mice above that of the MI+PBS and SHAM animals. The biological functions of ANP include diuresis, natriuresis, hypotensive promotion as well as anti-hypertrophic and -fibrotic actions (281). In speculation, the large increase in ANP expression mediated by the MSC transplantation may have augmented wall stresses leading to complex I alterations. Additionally, previous work evaluating MSC administration into the infarcted swine heart has been reported to blunt the peri-infarct PCr/ATP ratio decline (85, 369). We found the RCR to be higher in MSC-treated mice compared to MI+PBS mice. This suggests MSCs preserve mitochondrial efficiency and ADP responsiveness for adequate high-energy phosphate provision to assist in the maintenance of the PCr/ATP ratio.

To date, little data is available concerning the influence of MSC transplantation on cardiac oxidative stress and antioxidant status. Of interest, Kim et al. (169) reported that human dermal fibroblasts treated with the conditioned culture medium of adipose-derived MSCs augments the activity of fibroblast GPx and superoxide dismutase. In agreement, our findings also show that MSC treatment influences the anti-oxidant defence systems of the heart. Specifically, MSC transplantation depressed GPx protein

levels in the peri-infarct region four weeks post-MI. Although preliminary, this may indicate cell-based therapies induce alterations in the anti-oxidant defence systems. Future work is warranted to identify the role of MSC transplantation on ROS production and whether MSCs minimize oxidative stress as a means of cardioprotection following a MI.

The therapeutic influence of intramyocardial administration of MSCs also extends beyond the heart. Fatty acid uptake by the gastrocnemius was lower in the MI+PBS mice compared to the MI+MSC animals. To our knowledge this is the first study to address *in vivo* skeletal muscle substrate utilization post-MI. As such, mechanisms for the depressed fatty acid uptake observed are currently unknown. Previous reports indicate PGC-1α expression is reduced in the gastrocnemius of a rat MI model (374). A reduction in PGC-1α may explain, in part, the observed depression in gastrocnemius fatty acid uptake.

3.5 Conclusion

These experiments are the first to combine a comprehensive *in vivo* approach for evaluating insulin sensitivity, substrate uptake and cardiac function with stem cell therapy following a standardized MI in the conscious mouse. The experimental approach required for these studies is technically demanding, but can be applied to a variety of murine models to further address mechanism. Our findings show MSCs exhibit therapeutic potential as a metabolic intervention that attenuates post-MI energetic abnormalities. Specifically, the MSC therapy inhibited a shift in substrate reliance towards glucose and increased mitochondrial ADP responsiveness for improved energetic

efficiency (Figure 3.9). This may preserve metabolic flexibility and improve the heart's ability to meet the energy demands of cardiac contraction.

Figure 3.9 Schematic representation of metabolic signalling pathways that may be influenced by MSC transplantation following a MI

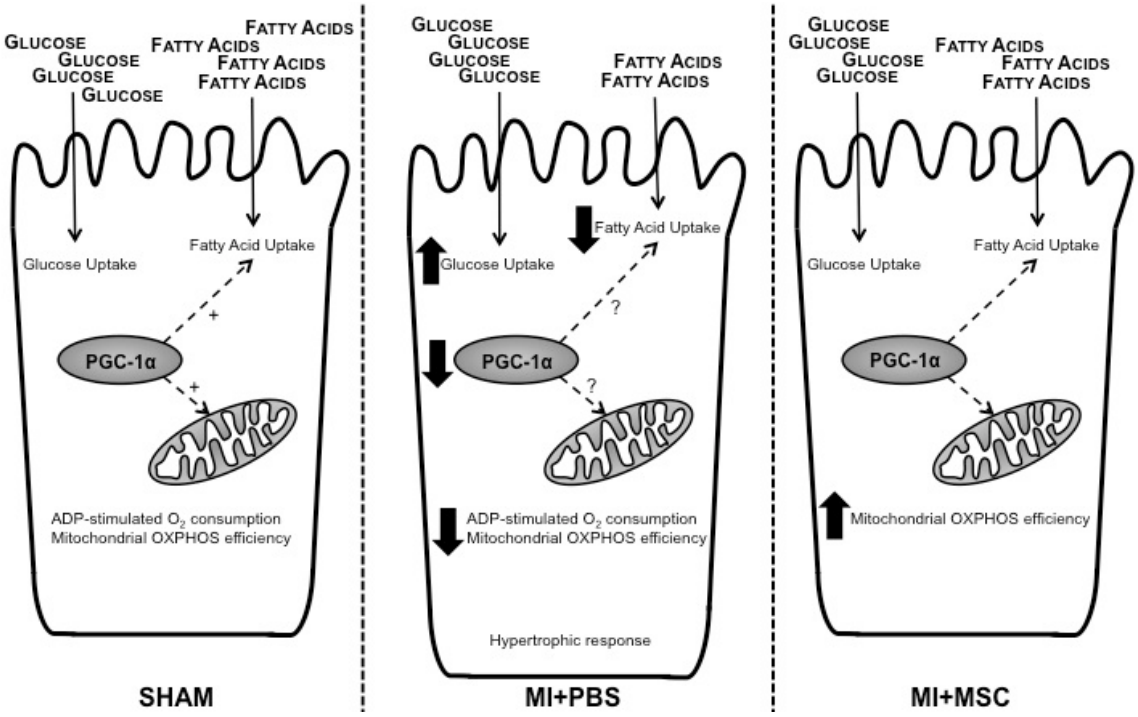

Figure 3.9: Twenty-eight days following a myocardial infarction (MI), hearts exhibited an increase in glucose uptake in the remote left ventricle and a decrease in fatty acid utilization in the peri-infarct region. Fatty acid uptake may be hindered by a reduction in vascular density in the infarct region or depression in peroxisome proliferator-activated receptor γ coactivator 1α (PGC-1α). Also, mitochondrial oxygen flux in response to ADP and the respiratory control ratio was compromised. Again, PGC-1α may contribute to these mitochondrial irregularities. MSC transplantation prevented the changes in

substrate utilization, vascular density, and PGC-1α. Also, mitochondrial efficiency was improved through a lowering of uncoupling.

[2]CHAPTER FOUR: THE ROLE OF MESENCHYMAL STEM CELL TRANSPLANTATION IN MINIMIZING ENERGY METABOLISM ABNORMALITIES IN THE INFARCTED HEART EXIHIBITING SEVERE SYSTOLIC DYSFUNCTION

4.1 Introduction

Following a myocardial infarction (MI) the heart undergoes remodelling that often augments its shape, size and function (322). Additionally, changes in cardiac structure and performance post-MI are routinely accompanied by metabolic abnormalities that limit the ability of the heart to meet the constant energetic requirements of contraction (230). The compromised capability to match energy supply and demand in the failing myocardium is, in part, the result of potentially impaired insulin signalling, a decline in insulin-mediated glucose uptake and the overall rate of glucose utilization being depressed (152, 188, 230). While the impediment in fuel delivery that accompanies insulin resistance may limit ATP synthesis, further detriment to energy provision is facilitated through alterations in mitochondria (271). Integrative mitochondrial oxidative phosphorylation (OXPHOS) may be repressed as indicated by a decline in ADP-stimulated oxygen consumption (285, 296). Additionally, defects in individual electron transport chain (ETC) complex activities (122) and a lowering of mitochondrial density have been reported in the post-infarcted heart (100). These adverse

---

[2] A version of this chapter has been accepted for publication. Hughey, C.C., James, F.D., Ma, L., Bracy, D.P., Wang, Z., Wasserman, D.H., Rottman, J.N., and Shearer, J. Diminishing impairments in glucose uptake, mitochondrial content and ADP-stimulated oxygen flux by mesenchymal stem cell therapy in the infarcted heart. *American Journal of Physiology-Cell Physiology*. In press.

mitochondrial characteristics are exacerbated by reduced peroxisome proliferator-activated receptor γ coactivator 1α (PGC-1α) in the infarcted and failing heart (50). PGC-1α is a master regulator that influences mitochondrial respiration and coupling (184, 185). Also, this co-activator promotes the transcription and replication of nuclear and mitochondrial DNA via nuclear respiratory factors (NRFs) and mitochondrial transcription factor A (TFAM) (364).

Cell-based treatments have been investigated as a therapeutic agent for repairing cardiac tissue and attenuating dysfunction in the infarcted heart. However, the efficacy of cell transplantation to minimize disparities in ATP supply/demand has been largely unstudied. Bone marrow mononuclear cell transplantation into the heart has been reported to enhance the cardiac p-Akt-to-Akt ratio following ischemia-reperfusion injury (197). This suggests potential utility in combating impaired insulin-mediated glucose uptake. Additionally, following a MI the surviving myocardium of mesenchymal stem cell (MSC)-treated hearts exhibited an elevation in the peri-infarct (~30%) and whole left ventricle (~16%) phosphocreatine (PCr)-to-ATP ratio (85). The PCr/ATP ratio reflects OXPHOS function, efficiency of myocardial energy provision, and correlates well with LV contractile function (85, 369).

The current report aimed to further these experimental studies indicating stem cell administration provides the post-infarcted heart relief from "energy starvation" by examining the conservation of metabolic function post-MI with MSC treatment. To uncover contributors to energy preservation with MSC administration, cardiac mitochondrial function, content, and regulators of mitochondrial biogenesis such as PGC-1α, NRF-1 and TFAM were assessed. Hyperinsulinemic-euglycemic clamps combined

with a radioactive glucose tracer provided indices of whole body and tissue-specific, insulin-stimulated glucose uptake *in vivo*. Together, these measures allowed for identification of potential means by which the transplanted cells improve cardiac ATP provision and act as a metabolic therapy for the infarcted heart.

4.2 Materials and methods

See Figure 4.1 for a schematic of experimental outline.

Figure 4.1 Schematic representation of experimental procedures and timelines

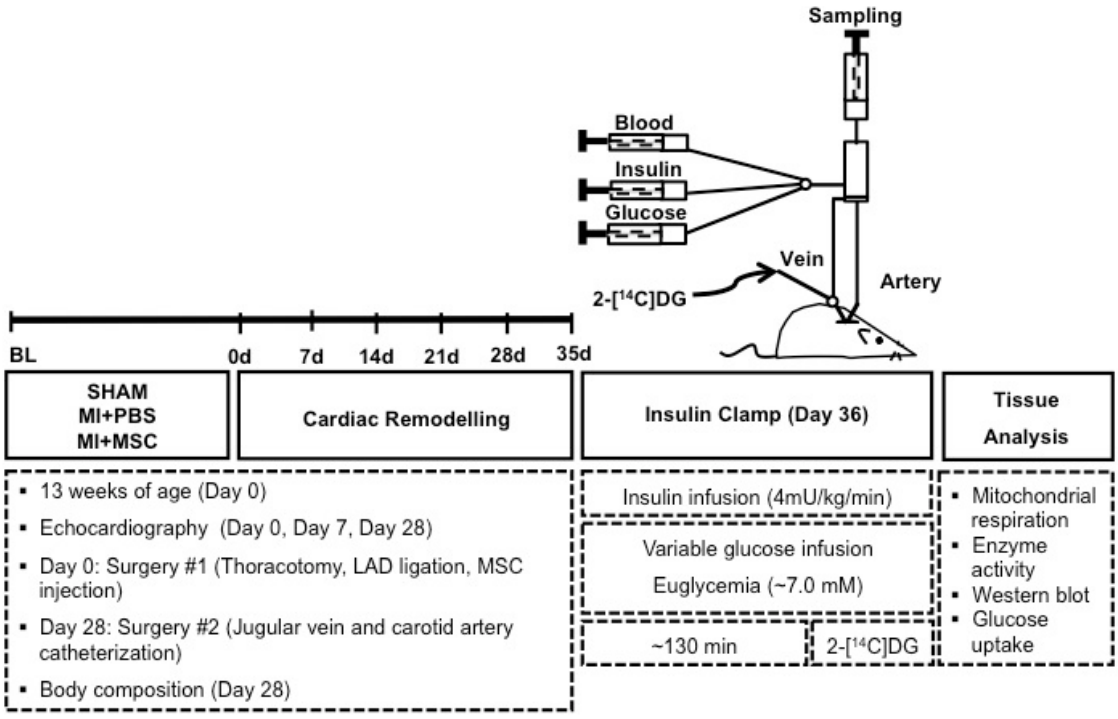

Figure 4.1: Echocardiography on conscious mice was performed prior to as well as seven and 28 days following ligation of the left anterior descending (LAD) coronary artery. Arterial and jugular chronic catheterization was performed 28 days following the myocardial infarction event for the arterial sampling and venous infusion protocols of the hyperinsulinemic-euglycemic (insulin) clamp. Insulin clamps were executed after seven

days of recovery from the catheterization surgeries (36 days post-infarct) to assess insulin sensitivity in the conscious, unrestrained mouse. Isotopic tracer (2-[^{14}C]deoxyglucose (2-[^{14}C]DG) administration during insulin clamps allowed for tissue-specific glucose uptake to be assessed *in vivo*. Additional experiments included evaluation of mitochondrial respiration in permeabilized cardiac fibers and regulators of metabolism by immunoblotting.

4.2.1 Animals and myocardial infarction

Procedures were approved by the Vanderbilt University Animal Care and Use Committee and performed according to the Guide for the Care and Use of Laboratory Animals published by the National Institutes of Health (NIH Publication No. 85-23, revised 1996, A3227-01).

Thirteen week-old, male C57BL/6J mice (Jackson Laboratories, Bar Harbour, ME, USA) were randomly separated into three groups: SHAM, MI + phosphate buffered saline (MI+PBS) and MI + mesenchymal stem cells (MI+MSC). A left anterior descending coronary artery (LAD) chronic ligation model was employed to induce a MI as previously described (137). Immediately following the ligation, 25 μl of PBS (pH 7.2) or 2.5×10^5 MSCs in 25 μl of PBS (pH 7.2) was administered via a single intramyocardial injection into the blanching peri-infarct area of the MI+PBS or MI+MSC mice, respectively. The mice were anesthetized with 50 mg/kg sodium pentobarbital via intraperitoneal injection prior to the surgeries. Adequate intra-procedural anaesthesia was confirmed by the absence of withdrawal reflex and evaluating respiratory and/or heart rate.

4.2.2 Mesenchymal stem cells

Human bone marrow-derived MSCs were purchased from the Center for the Preparation and Distribution of Adult Stem Cells (Texas A&M Health Science Center College of Medicine Institute for Regenerative, Temple, TX, USA) that provides standardized preparations of MSCs with NIH/NCRR (P40 RR 17447-06) support. The MSCs have been identified to consistently exhibit the capacity for osteoblast, adipocyte and chondrocyte lineage differentiation as well as be $CD90^+$, $CD105^+$, $CD49c^+$, $CD49f^+$, $CD166^+$, $CD59^+$, $CD29^+$, $CD44^+$, $CD45^-$, $CD34^-$, $CD117^-$ and $CD36^-$ (236). MSCs were cultured in alpha minimum essential medium (αMEM) with L-glutamine (Life Technologies, Burlington, ON, Canada), 16.5% defined FBS (HyClone, Logan, UT, USA), streptomycin (100 μg/ml) and penicillin (100 units/ml). All MSCs for injection were obtained from a single donor and passages 3-7 were utilized.

4.2.3 Cardiac function

Cardiac systolic function was evaluated by M-mode echocardiography in conscious mice prior to the LAD ligation procedures as well as seven and 28 days post-MI as previously described (79, 278).

4.2.4 Chronic catheterization procedures

In preparation for the hyperinsulinemic-euglycemic clamps (insulin clamps), the mice underwent chronic venous and arterial catheterization surgery 28 days post-ligation as previously described (137). The mice were housed individually for seven days post-catheterization to ensure the mice were within 10% of pre-surgical weight for use in the insulin clamps.

4.2.5 Hyperinsulinemic-euglycemic clamps and isotopic tracer administration

Insulin clamps were executed 36 days post-MI as previously described (13). Mice were fasted at 7:00 a.m. for five hours before the initiation of the experiments. One hour prior to the insulin clamps the mice were given an opportunity to acclimate to their environment by connecting the externalized mouse catheters to all catheter leads and infusion syringes. Just prior to insulin clamp commencement, an arterial blood sample was obtained for fasted plasma glucose, insulin, non-esterified fatty acids (NEFA) and hematocrit measures. To prevent a decline in hematocrit a continuous, venous administration of saline-washed erythrocytes (5 μl/minute) was performed. Each experiment maintained a constant, continuous infusion (4 mU/kg/min) of insulin for 133.17 ± 10.02 minutes. Euglycemia (~7.0 mM) was maintained during the insulin clamps. Once a stable glucose infusion rate (GIR) and euglycemia was a achieved for at least 30 minutes arterial blood was sampled for glucose concentration (t=0 minutes). Following this sample, a bolus containing 2-[^{14}C]DG (13 μCi) was administered via the jugular vein to provide an index of tissue-specific glucose uptake. At t = 2, 5, 10, 15, 20 minutes, arterial blood was sampled to determine glucose and 2-[^{14}C]DG. At t = 30 minutes, arterial blood was taken for the measurement of glucose, experimental insulin, 2-[^{14}C]DG and hematocrit. Plasma samples were stored at -20°C until analysis. Once the insulin clamp was completed mice were sacrificed via cervical dislocation. Tissues (heart, soleus, gastrocnemius, superficial vastus lateralis and white adipose tissue from epididymal deposits) were immediately excised for analysis or stored at -80°C.

4.2.6 Plasma analyses

Plasma insulin was evaluated by a double antibody method as previously performed (218). Plasma NEFAs (NEFA C kit; Wako Chemicals, Richmond, VA, USA) and glucose were determined spectrophotometrically (Molecular Devices, Sunnyvale, CA) as previously described (137). Plasma 2-[^{14}C]DG was assessed as previously outlined (298).

4.2.7 Tissue-specific substrate kinetics

Tissue 2-[^{14}C]DG and phosphorylated 2-[^{14}C]DG (2-[^{14}C]DG-P) were evaluated as previously described (298). The metabolic index of glucose (R_g) uptake was calculated (299) and expressed (276) as previously outlined. R_g for tissues were expressed relative to the brain R_g, which represents constant reservoir of glucose uptake (276).

4.2.8 Mitochondrial oxygen consumption and enzymatic activity

Saponin-permeabilized, cardiac fibers from the peri-infarct area were prepared as described (136). High-resolution respirometry (Oroboros Instruments, Innsbruck, Austria) was performed in duplicate at 37°C in MiR05 (0.5 mM EGTA, 3 mM $MgCl_2 \cdot 6H_2O$, 20 mM taurine, 10 mM KH_2PO_4, 20 mM HEPES, 1 g/L BSA, 60 mM potassium-lactobionate, 110 mM sucrose, pH 7.1, adjusted at 30°C). Substrates included 10 mM glutamate plus 2 mM malate and 5mM pyruvate, 5 mM ADP and 10 mM succinate. 10 mM cytochrome c was added to ensure the outer mitochondrial membrane was intact after processing. Following the respirometry studies, the fibers were stored at -80°C until use for citrate synthase activity determination as previously outlined (137).

4.2.9 Immunoblotting

Cardiac tissue was homogenized in a lysis buffer containing 20 mM NaCl, 20 mM Tris-HCl, 0.1 mM EDTA, 1% Triton X-100, 0.5% sodium deoxycholate, and 0.1% β-mercaptoethanol (pH 7.4) in the presence of a protease inhibitor cocktail (Sigma-Aldrich, Oakville, ON, Canada) and phosphatase inhibitor cocktail (Thermo Fisher Scientific, Mississauga, ON, Canada). Tissue homogenate was centrifuged (10 minutes at 1000g and 4°C) and supernatant protein determination was assessed using the Bradford method. Cardiac (15-50 μg) proteins were separated on NuPAGE 4-12% Bis-Tris gels (Life Technologies) and transferred to a polyvinylidene fluoride membrane. Membranes were probed with peroxisome proliferator-activated receptor gamma coactivator-1alpha (PGC-1α; Santa Cruz Biotechnology, Santa Cruz, CA, USA), glucose transporter 4 (GLUT4; Abcam, Cambridge, MA, USA), hexokinase II (HKII; Chemicon, Temecula, CA, USA), UCP3 (Abcam), phospho-insulin receptor substrate 1(Tyr608) (p-IRS-1; EMD Millipore Chemicals, Billerica, MA, USA), IRS-1 (EMD Millipore Chemicals), phospho-Akt(Ser473) (p-Akt; Cell Signaling Technology, Whitby, ON, Canada), Akt (Cell Signaling Technology), nuclear respiratory factor 1 (NRF-1; Santa Cruz Biotechnology), mitochondrial transcription factor A (TFAM; Santa Cruz Biotechnology) and oxidative phosphorylation complexes I-V (OXPHOS CI-CV; Abcam) antibodies. Glyceraldehyde 3-phosphate dehydrogenase (GAPDH; Abcam) protein was utilized as a loading control.

4.2.10 Statistical analyses

One-way ANOVA or two-way repeated measures ANOVA were performed to detect statistical differences ($p < 0.05$) as appropriate followed by Tukey's post hoc tests. All data are reported as mean ± SEM.

4.3 Results

4.3.1 Stem cell administration minimizes cardiac contractile dysfunction

Echocardiography was employed in the conscious mouse to evaluate cardiac contractile function (Table 4.1). Systolic dysfunction was identified in the MI+PBS group seven and 28 days post-infarction as indicated by the depression in ejection fraction (Figure 4.2A) and fractional shortening (Figure 4.2B). The MSC administration exhibited the ability to lessen the insult induced by the MI. The MSC-treated animals displayed a reduction in ejection fraction (Figure 4.2A) and fractional shortening (Figure 4.2B) at seven and 28 days post-MI compared to the SHAM group. However, the MSC-treated hearts exhibited a greater ejection fraction (Figure 4.2A) and fractional shortening (Figure 4.2B) than the MI+PBS mice at seven and 28 days following cardiac insult. Cardiac hypertrophy was also assessed in the mice. The heart-to-body weight (Figure 4.2C) was elevated in MI+PBS mice 36 days post-MI. The MSC administration minimized the increase in heart-to-body weight (Figure 4.2C).

Table 4.1 Cardiovascular parameters in conscious C57BL/6 mice

	Baseline			7 days post-MI			28 days post-MI		
	SHAM	**MI+ PBS**	**MI+ MSC**	**SHAM**	**MI+ PBS**	**MI+ MSC**	**SHAM**	**MI+ PBS**	**MI+ MSC**
HR (bpm)	691 ± 7	646 ± 34	666 ± 13	716 ± 8	692 ± 16	678 ± 7	777 ± 43	799 ± 69	689 ± 9*†
IVSd (mm)	0.79 ± 0.01	0.77 ± 0.01	0.76 ± 0.01	0.84 ± 0.01	0.81 ± 0.05	0.78 ± 0.02*	0.77 ± 0.02	0.77 ± 0.03	0.81 ± 0.01
LVIDd (mm)	2.93 ± 0.05	3.09 ± 0.10	3.33 ± 0.09	3.02 ± 0.04	4.44 ± 0.32*	3.93 ± 0.28*	2.98 ± 0.04	4.76 ± 0.33*	4.35 ± 0.14*
LVPWd (mm)	0.78 ± 0.02	0.76± 0.03	0.74 ± 0.01	0.77 ± 0.02	0.77 ± 0.07	0.80 ± 0.02	0.74 ± 0.03	0.60 ± 0.06*	0.83 ± 0.02*†
IVSs (mm)	0.93 ± 0.02	0.89 ± 0.02	0.93 ± 0.02	0.95 ± 0.03	0.91 ± 0.04*	0.93 ± 0.02	0.88± 0.02	0.81 ± 0.03	0.93 ± 0.02†
LVIDs (mm)	1.45 ± 0.03	1.53 ± 0.06	1.73 ± 0.06	1.53 ± 0.03	3.36 ± 0.29*	2.86 ± 0.14*†	1.52 ± 0.03	3.69 ± 0.32*	2.94 ± 0.16*†
LVPWs (mm)	0.97 ± 0.02	0.97 ± 0.02	1.02 ± 0.02	0.99 ± 0.03	0.86 ± 0.07*	0.96 ± 0.02	0.92 ± 0.03	0.75 ± 0.07*	1.01 ± 0.02*†

*p<0.05 vs. SHAM at specified time point.

†p<0.05 vs. MI+PBS at specified time point.

Data are mean ± SEM for n=6-14 mice per group.

Abbreviations: HR, heart rate; IVSd, interventricular septal thickness in diastole; LVIDd, left ventricle (LV) end-diastolic dimension; LVPWd, LV posterior wall thickness in diastole; IVSs, interventricular septal thickness in systole; LVIDs, LV end-systolic dimension; LVPWs, LV posterior wall thickness in systole.

Figure 4.2 Cardiac functional and hypertrophic indices

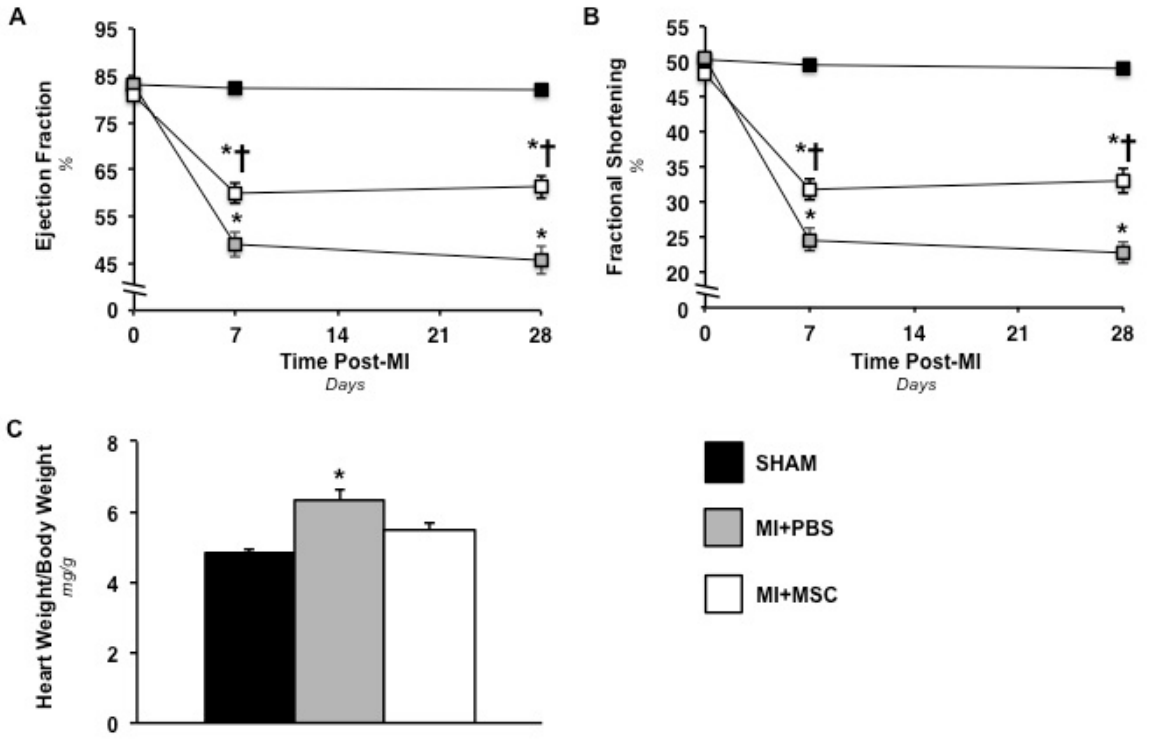

Figure 4.2: (A) Cardiac ejection fraction (%) prior to a myocardial infarction (MI), 7 and 28 days following a MI. n=6-14 mice per group. (B) Cardiac fractional shortening (%) prior to a MI, 7 and 28 days following a MI. n=6-14 mice per group. (C) Heart weight-to-body weight ratio 36 days following a MI. n=11-12 mice per group. Data are mean ± S.E.M. *p<0.05 vs. SHAM. †p<0.05 vs. MI+PBS.

4.3.2 MSC therapy dampens impairment in glucose uptake in the infarcted heart

Insulin clamps in the conscious, unrestrained mouse were employed to evaluate *in vivo* whole body glucose disposal in response to insulin and as a means of identifying a systemic effect of the MI and MSC treatment. The glucose infusion rate (GIR) required to achieve euglycemia (~7.0 mM) was similar between groups (Figure 4.3A). Blood

glucose levels were comparable between groups during the insulin clamp (Figure 4.3B). Isotopic glucose (2-[^{14}C]DG) was administered during the insulin clamps to assess insulin-stimulated, tissue-specific glucose uptake. Both the remote left ventricle (MI+PBS LV) and the peri-infarct region (MI+PBS PI) in the MI+PBS animals exhibited a lower rate of glucose utilization compared the SHAM group (Figure 4.3C and 4.3D). In contrast, a regional effect was observed in the MSC-treated mice. An intramyocardial injection of MSC preserved cardiac glucose uptake in response to insulin in the remote left ventricle (MI+MSC LV) but was not able to rescue the peri-infarct region (MI+MSC PI) from impaired glucose uptake (Figure 4.3C and 4.3D).

Figure 4.3 Insulin-stimulated whole body disposal and cardiac-specific glucose uptake

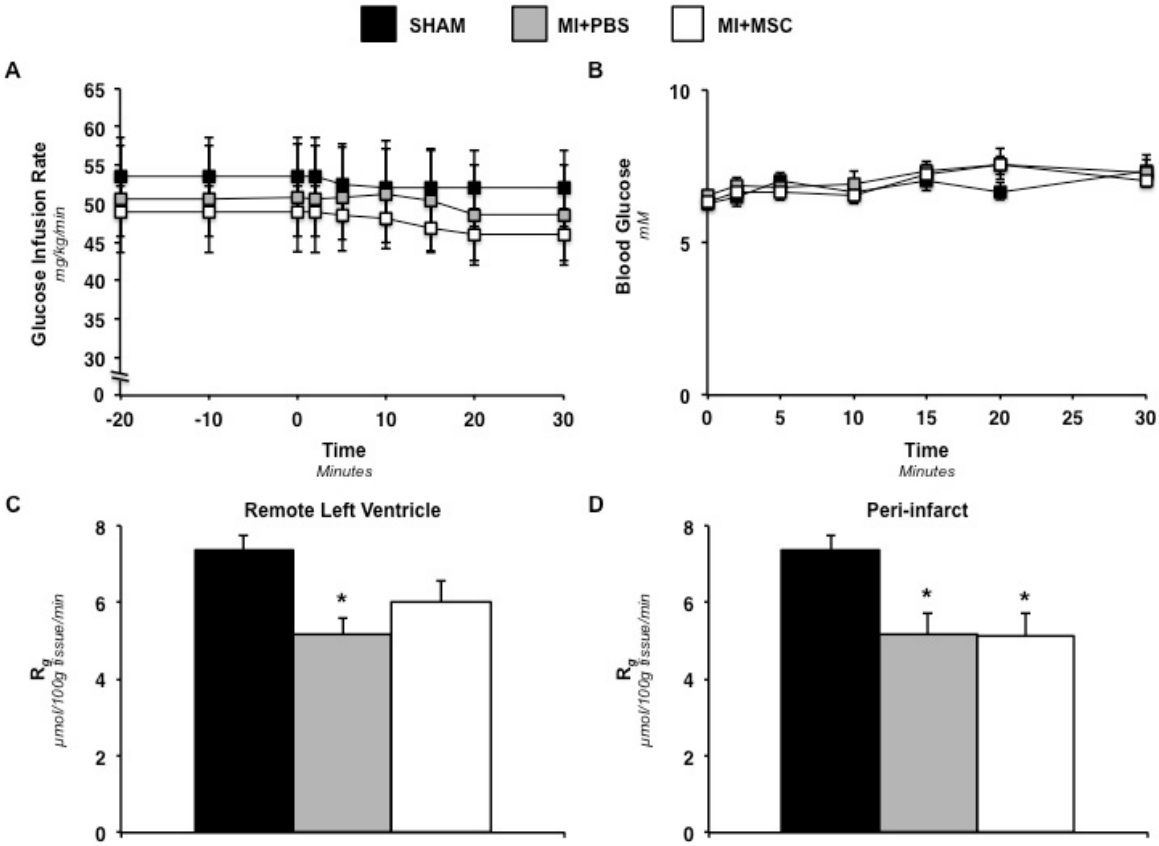

Figure 4.3: (A) Glucose infusion rate (GIR) during the insulin clamp. The GIR is equivalent to the whole body glucose disposal rate in response to venous infusion of insulin. The GIR is shown as a time course starting twenty minutes prior to administration of 2-[^{14}C]DG (-20 minute time point) to 30 minutes following 2-[^{14}C]DG infusion (30 minute time point). (B) Arterial, blood glucose concentration following 2-[^{14}C]DG for 30 minutes post-administration. Data are mean ± SEM for n=6-10 mice per group. (C) Metabolic index of glucose uptake (R_g) in the remote left ventricle (LV) and (D) metabolic index of glucose uptake in the peri-infarct region of the left ventricle (PI).

Cardiac R_g values are relative to brain R_g. n=6-8 mice per group. Data are mean ± S.E.M. *p<0.05 vs. SHAM.

4.3.3 Diminishing impairments in regulators of glucose uptake by MSC transplantation

Regulators of glucose metabolism were evaluated to identify the mechanisms by which MSC administration preserved cardiac glucose uptake in the remote left ventricle. The insulin signalling pathway was probed by determining p-IRS-1(Tyr608), total IRS-1, p-Akt(Ser473) and total Akt. Both infarct groups displayed a reduction in p-IRS-1 in the remote left ventricle and peri-infarct region (Figure 4.4A-C). Total IRS-1 was similar between groups, however, total IRS-1 may have trended towards a significant decline given the p-IRS-1/IRS-1 ratio was comparable between groups (Figure 4.4A-C). The MI event resulted in a reduction of the p-Akt/Akt ratio in the remote left ventricle of the MI+PBS mice (Figure 4.4D and 4.4F). The MSC administration minimized the p-Akt/Akt decline in the remote left ventricle (Figure 4.4D and 4.4F). The remote left ventricle region displayed similar PGC-1α between groups (Figure 4.4G and 4.4I). However, the MI-induced a depression in cardiac PGC-1α that was inhibited by the MSC treatment in the peri-infarct region (Figure 4.4H and 4.4I). Cardiac GLUT4 and HKII in the remote left ventricle and peri-infarct regions were comparable between groups (Figure 4.4G-I).

Figure 4.4 Mediators of cardiac glucose uptake

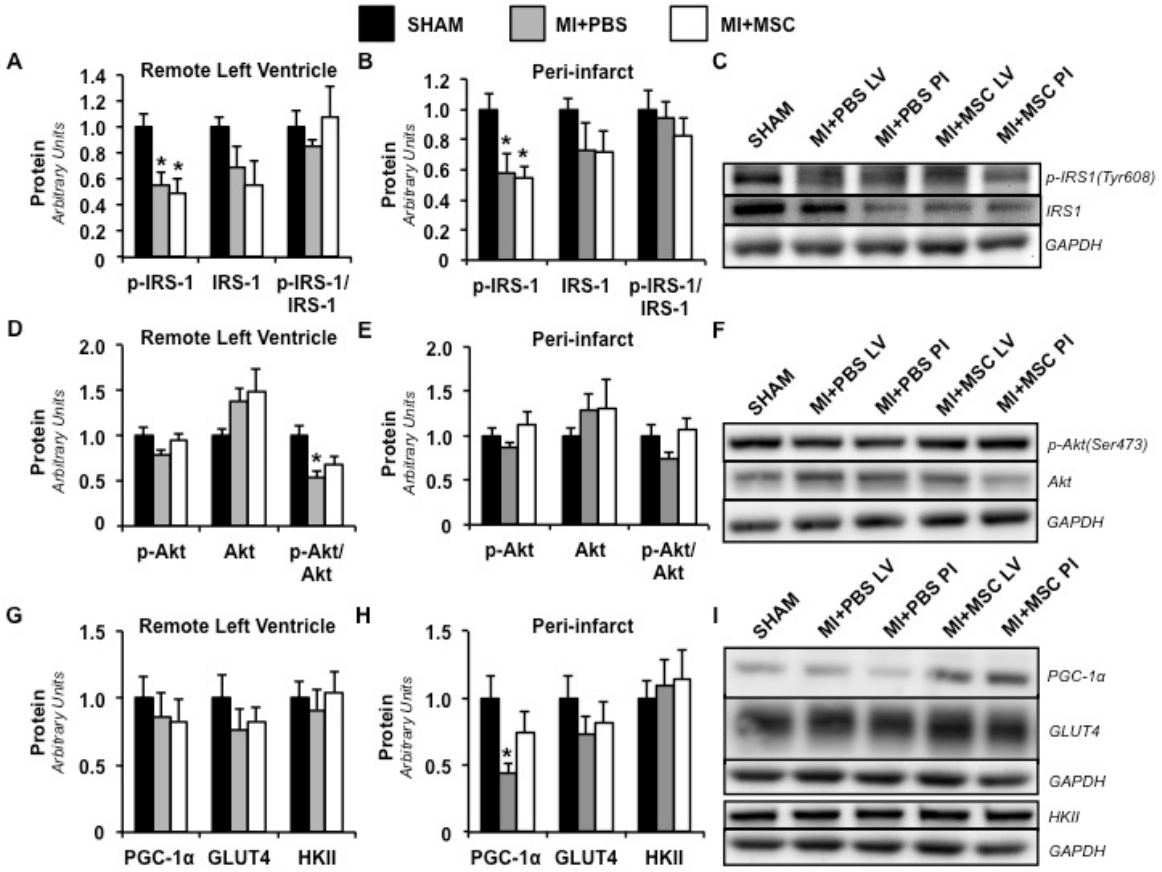

Figure 4.4: (A) Remote left ventricle and (C) peri-infarct cardiac phospho-insulin receptor substrate 1 (p-IRS-1), IRS-1 and p-IRS-1-to-total IRS-1 ratio (p-IRS-1/IRS-1) as determined by immunoblotting. (C) Representative immunoblotting performed to measure p-IRS-1 and IRS-1. (D) Remote left ventricle and (E) peri-infarct cardiac phospho-Akt (p-Akt), Akt and p-Akt-to-total Akt ratio (p-Akt/Akt) as determined by immunoblotting. (F) Representative immunoblotting performed to measure p-Akt and Akt. (G) Remote left ventricle and (H) peri-infarct cardiac peroxisome proliferator-activated receptor gamma coactivator-1alpha (PGC-1α), glucose transporter 4 (GLUT4) and hexokinase II (HKII) as determined by immunoblotting. (I) Representative immunoblotting performed to measure PGC-1α, GLUT4 and HKII. Protein levels are

normalized to glyceraldehyde-3-phosphate dehydrogenase (GAPDH) content and are relative to the SHAM group. n=5-6 mice per group. Data are mean ± S.E.M. *$p<0.05$ vs. SHAM.

4.3.4 Potential for increased peripheral tissue glucose uptake post-MSC therapy

It has been proposed that cardiomyopathy is associated with generalized energetic failure and systemic insulin resistance (271, 321). Given this, in addition to cardiac-specific glucose uptake, insulin-stimulated glucose uptake in the soleus, white adipose tissue, superficial vastus lateralis and gastrocnemius was assessed (Figure 4.5A-D). The MI+MSC soleus exhibited an elevated R_g compared to that of the SHAM and MI+PBS mice (Figure 4.5A). The rate of glucose utilization in the white adipose tissue, superficial vastus lateralis and gastrocnemius was similar between groups (Figure 4.5B-D). Also, the five-hour fasted levels of arterial glucose and non-esterified fatty acids were comparable between groups (Table 4.2).

Figure 4.5 Insulin-stimulated peripheral tissue glucose uptake

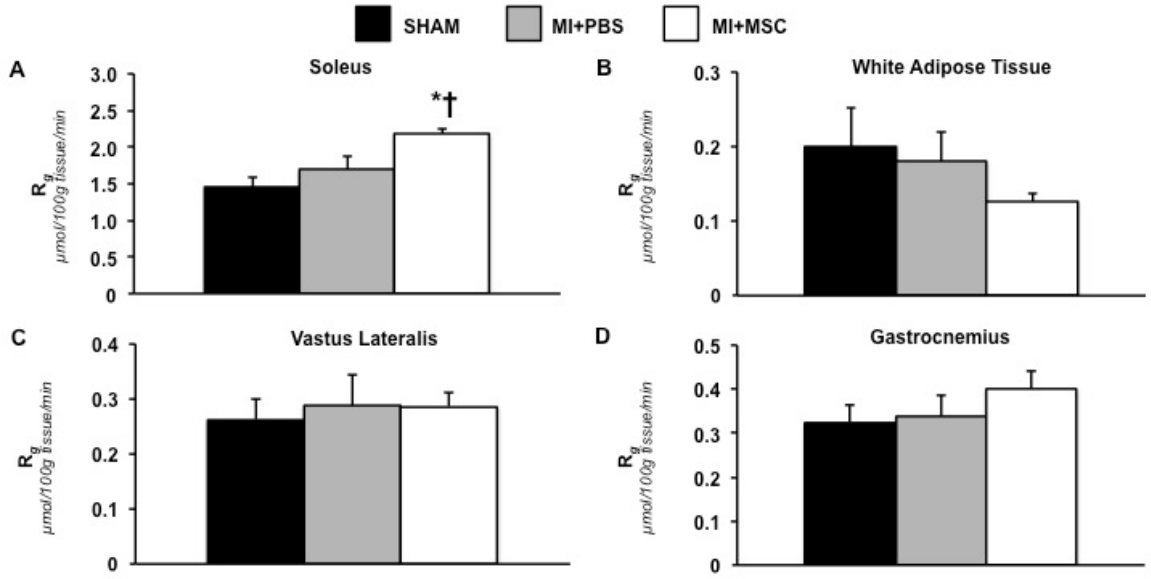

Figure 4.5: (A) Metabolic index of glucose uptake (R_g) in the soleus. (B) Metabolic index of glucose uptake (R_g) in white adipose tissue. (C) Metabolic index of glucose uptake (R_g) in the superficial vastus lateralis. (D) Metabolic index of glucose uptake (R_g) in the gastrocnemius. Tissue R_g values are relative to brain R_g. n=6-9 mice per group. *p<0.05 vs. SHAM. †p<0.05 vs. MI+PBS.

Table 4.2 Biometric characteristics of C57BL/6 mice

	SHAM	MI+PBS	MI+MSC
Fasting Plasma Glucose (mM)	9.05 ± 0.31	8.18 ± 0.37	8.43 ± 0.33
Fasting Plasma NEFA (mM)	0.9 ± 0.05	0.94 ± 0.05	1.0 ± 0.05
Experimental Plasma Insulin (µU/ml)	103.87 ± 22.32	90.25 ± 13.58	91.67 ± 12.40
Body Weight (g)	26.61 ± 0.85	25.77 ± 0.98	27.9 ± 0.55
Muscle (%)	90.88 ± 0.88	90.03 ± 0.41	89.15 ± 0.94
Fat (%)	7.66 ± 0.68	7.93 ± 0.32	8.59 ± 0.97
Free Fluid (%)	1.46 ± 0.36	2.04 ± 0.20	2.21 ± 0.17

Data are mean ± SEM for n=12-13 mice per group for plasma glucose; n=11-12 for plasma NEFA; n= 6-9 for experimental plasma insulin; n=7-9 for body weight; n=11-15 for body composition measurements.

4.3.5 MSC transplantation preserves mitochondrial content and improves efficiency

In addition to cardiac function and glucose utilization indexes, polarographic oxygen flux measurements were performed to evaluate mitochondrial OXPHOS. Basal oxygen consumption (V_0) supported by complex I substrates malate, glutamate and pyruvate was comparable between groups (Figure 4.6A). The MI-only animals displayed a reduction in maximal ADP-stimulated oxygen flux ($V_{MAX\text{-}CI}$; Figure 4.6A). In contrast, ADP-stimulated oxygen consumption through complex I in MI + MSC animals was comparable to the SHAM group (Figure 4.6A). The addition of succinate to assess ADP-stimulated oxygen flux via convergent electron flux through mitochondrial complexes I+II showed a significant reduction in the MI+PBS mice only ($V_{MAX\text{-}CI+CII}$; Figure 4.6A). The respiratory control ratio (RCR) was reduced in the MI + PBS hearts but preserved in

the MI+MSC cardiac fibers (Figure 4.6B). This suggests a decrease in ADP responsiveness in the MI+PBS mice. Intriguingly, the succinate control ratio was heightened in the MI+PBS peri-infarct region ($V_{MAX\text{-}CI + CII}$ / $V_{MAX\text{-}CI}$; Figure 4.6B). Citrate synthase activity was assessed to identify a possible effect of mitochondrial heterogeneity on potential for energy provision. Citrate synthase activity was reduced in the MI+PBS group, however, MSC transplantation protected hearts from a decline in this mitochondrial content maker (Figure 4.6C). The preservation of ADP-stimulated oxygen flux and cardiac citrate synthase activity in the MI+MSC mice prompted the evaluation of mitochondrial proteins involved in function and biogenesis. In the remote left ventricle mitochondrial OXPHOS CI–CV, NRF-1, TFAM and were similar between groups (Figure 4.6D and 4.6F). Peri-infarct complex I and TFAM were lowered in both infarct groups (Figure 4.6E and 4.6F). UCP3 in the peri-infarct region was lower in the MI+PBS mice (Figure 4.6E and 4.6F).

Figure 4.6 Cardiac mitochondrial function and characteristics

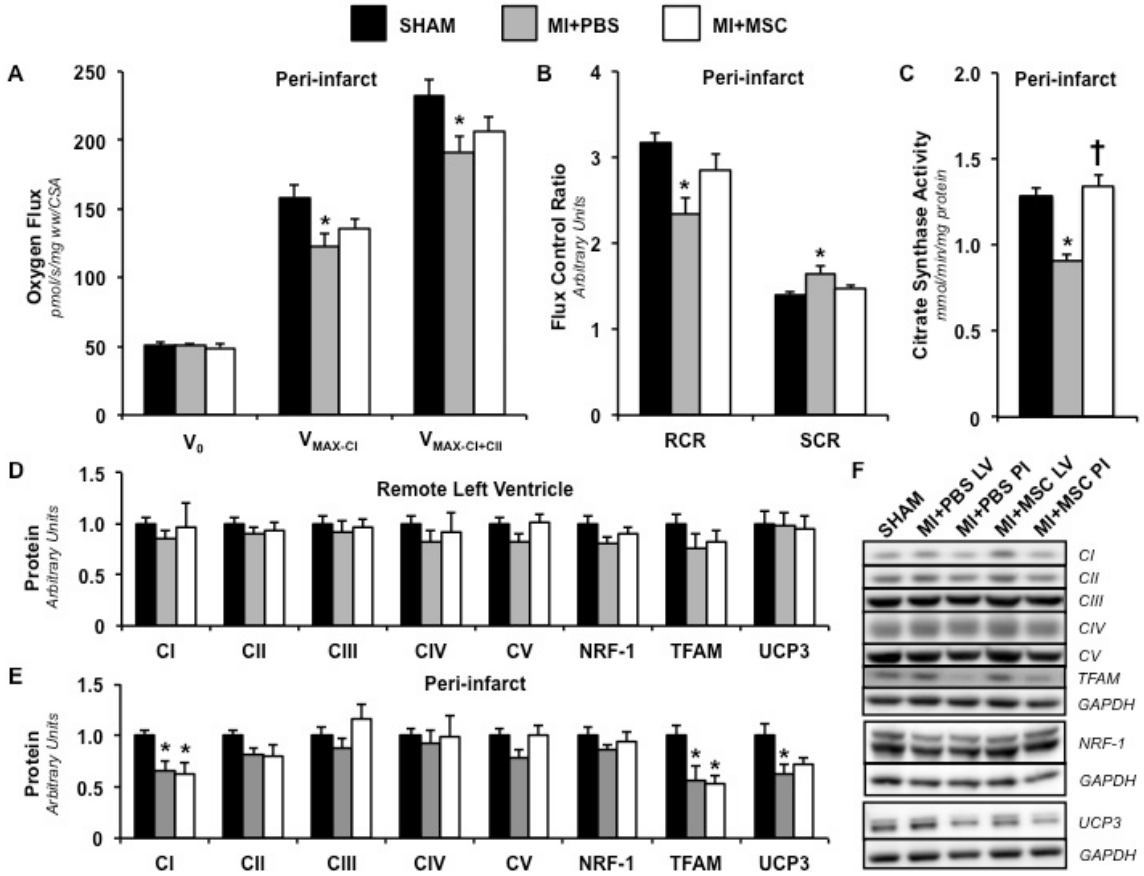

Figure 4.6: (A) Peri-infarct permeabilized cardiac fiber basal oxygen consumption supported by glutamate, malate and pyruvate (V_0), maximal oxygen consumption (ADP-stimulated) supported by glutamate, malate and pyruvate through complex I (V_{MAX-CI}) and maximal convergent oxygen flux supported by glutamate, malate, pyruvate and succinate ($V_{MAX-CI+CII}$). n=8-10 mice per group. (B) Respiratory control ratio (RCR; defined as V_{MAX-CI}/V_0) and succinate control ratio (SCR; defined as $V_{MAX-CI+CII}/V_{MAX-CI}$). n=9-10 mice per group. (C) Peri-infarct citrate synthase activity (CS) (mmol/min/mg protein). n=8-10 mice per group. (D) Remote left ventricle (LV) and (E) peri-infarct (PI) mitochondrial oxidative phosphorylation (OXPHOS) complexes I-V (CI-CV), nuclear respiratory factor 1 (NRF-1), mitochondrial transcription factor A (TFAM) and

uncoupling protein 3 (UCP3) as determined by immunoblotting. (F) Representative immunoblotting of the regional protein levels OXPHOS CI-CV, NRF-1, TFAM and UCP3. Protein levels were normalized to glyceraldehyde-3-phosphate dehydrogenase (GAPDH) content and are expressed relative to the SHAM group. n=6 mice per group. Data are mean ± S.E.M. *$p<0.05$ vs. SHAM. †$p<0.05$ vs. MI+PBS PI.

4.4 Discussion

The current study aimed to evaluate the ability of MSC therapy to attenuate aberrations in cardiac glucose utilization and mitochondria. Such disturbances may hinder energy provision required to sustain contractile performance. Experimental studies have previously reported MSC-treated hearts to exhibit elevated high-energy phosphates compared to infarct-only hearts (85). Furthermore, this improvement in the energy state of the heart was accompanied by lower cardiac dysfunction (85). However, it remains to be completely determined which metabolic processes involved in energy provision are modulated by MSC therapy to achieve these therapeutic effects.

Our results indicated systolic performance was reduced 40-55% as indicated by ejection fraction and fractional shortening following the MI. A single intramyocardial injection of MSC minimized the decline in contractile performance to approximately 25-36%. Also, the exogenous cells mediated a mild inhibition of the hypertrophic response following a MI. The improvement in cardiac function and structure was associated with the ability of the MSC transplantation to lessen irregularities in *in vivo* cardiac glucose uptake. Thirty-six days after the MI, infarct-only hearts exhibited a decline in insulin-stimulated glucose uptake in the remote left ventricle and peri-infarct regions. The MSC

treatment impeded a significant reduction in glucose utilization in the remote left ventricle. In contrast, the cell-based therapy could not prevent a decline in insulin-stimulated glucose uptake in the peri-infarct region. These results indicate that the intramyocardial injection of MSCs may exert regional influences and at the very least slow the onset of alterations in glucose utilization associated with cardiac remodelling post-MI.

Following evaluation of glucose uptake, immunoblotting was performed to identify potential mediators contributing to the maintenance of insulin-mediated glucose uptake in the MSC-treated remote left ventricle. The MSC administration did not rescue the infarcted heart from a fall in p-IRS-1. However, the stem cell transplantation did appear to provide some protection to components involved in insulin signalling through the attenuation of a significant decline in the remote left ventricle p-Akt-to-Akt ratio. This may have provided some beneficial effect on insulin-stimulated glucose uptake even in the presence of IRS-1 impairment as constitutively active Akt has been reported to almost match the effect of insulin *in vitro* (171, 232). Furthermore, the ability of MSC therapy to protect Akt phosphorylation is in agreement with previous studies that indicate the cell-based treatment enhances PI3K-Akt pathway signalling (304).

In addition to substrate flux, modulation mitochondrial OXPHOS may be a means by which the stem cell therapy may improve cardiac energetic abnormalities following a MI. The current study found MSC transplantation to minimize impairments in ADP-stimulated oxygen consumption supported by pyruvate, malate and glutamate from decline. Also, the MSC transplantation impeded an overt depression in RCR suggesting that the cell-based therapy confers modest protection to the infarcted heart from declines

in OXPHOS ADP responsiveness. These mitochondrial characteristics may contribute to the elevated high-energy phosphates previously identified following MSC transplantation in the infarcted heart. Also, the MI+PBS animals displayed an elevated SCR. While a persistent decline $V_{MAX\text{-}CI + CII}$ may indicate dysfunction downstream of complex I and II, the combination of depressed RCR, complex I protein, and elevated SCR hints that complex I could be mediating this dysfunction as there is availability for increased flux downstream of complex I.

The preservation of cardiac ADP-stimulated oxygen flux in saponin-permeabilized fibers from the peri-infarct region led us to explore PGC-1α. PGC-1α is a transcriptional co-activator that augments mitochondrial function (346). Previous studies overexpressing PGC-1α in rodent ventricular myocytes have identified that this transcription factor co-activator promotes an increase in ADP-stimulated oxygen flux supported by malate and glutamate (184). Cardiac PGC-1α is of interest in our MI-model because this master regulator of energy metabolism declines as the heart progresses towards overt failure (271). Similarly, the current study identified peri-infarct PGC-1α to be reduced in the MI-only mice.

Concurrent with its role in enhancing mitochondrial oxidative capability, PGC-1α promotes mitochondrial biogenesis (184). A loss of mitochondrial content has been observed in rodent models of heart failure (100). The current study identified a depression in citrate synthase activity, a marker of mitochondrial density, in the MI+PBS mice. However, the MSC-treated hearts exhibited no alterations in the activity of this tricarboxylic acid cycle enzyme. The preservation of cardiac mitochondria content

following MSC transplantation may play a role in the improved PCr/ATP ratio and cardiac energy homeostasis. A downstream effector of PGC-1α-mediated mitochondrial nuclear gene transcription is NRF-1 (106). Moreover, PGC-1α acts in concert with the NRFs and is proposed to be the limiting factor in NRF target gene expression (106). NRF-1 was comparable between groups suggesting the ability of the MSC treatment to diminish a decline in PGC-1α may play an important role in the conservation of mitochondrial content. Of note, our results indicate that the lowering of TFAM following a MI was not blunted by the MSCs. TFAM is a nuclear-encoded transcription factor that regulates the replication and transcription of mitochondrial DNA (86, 302). As such, caution must be exerted when it comes to conclusions concerning the ability of the cell-based treatment to prevent long-term impairments in mitochondrial density.

4.5 Conclusion

In summary (Figure 4.7), the current study found MSC transplantation for the infarcted heart to lessen declines in *in vivo*, insulin-stimulated cardiac glucose uptake. Also, the stem cell administration exhibited a protective effect on integrative OXPHOS function and mitochondrial density following a MI. These mitochondrial improvements may have been conferred by the ability of MSC therapy to prevent alterations in PGC-1α and its downstream signalling. From a therapeutic perspective, the reduction in metabolic insults induced by the MSC transplantation could assist in allowing the heart to minimize disparities in energy supply and demand.

Figure 4.7 Schematic representation of metabolic signalling pathways that may be influenced by MSC transplantation following a MI

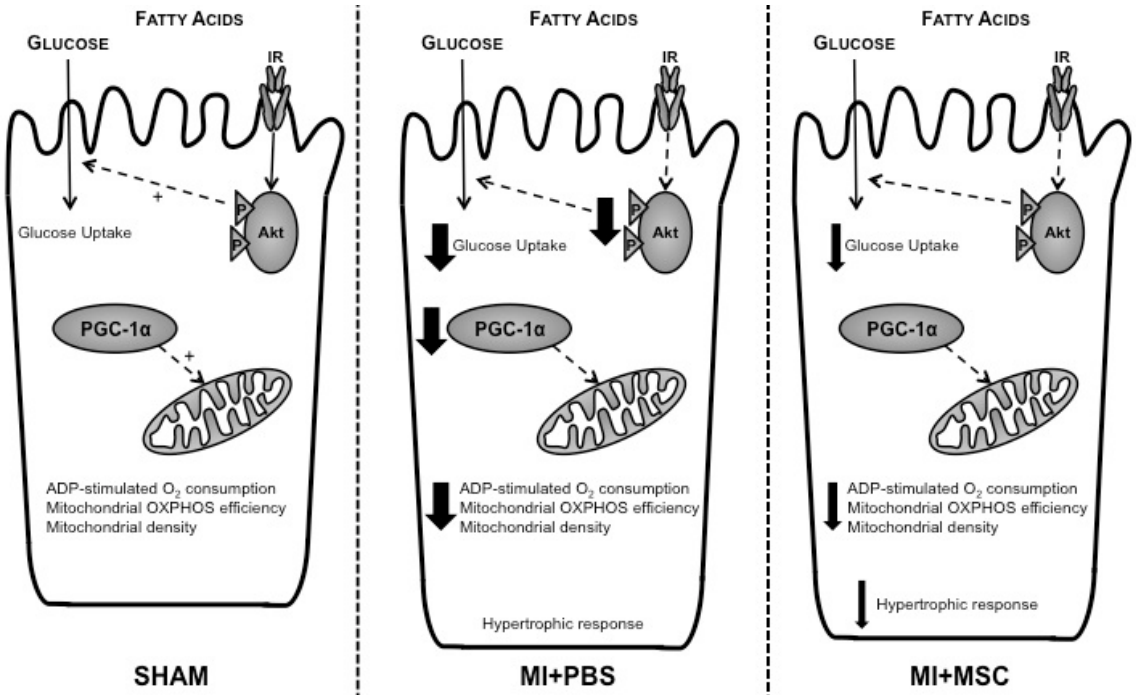

Figure 4.7: Thirty-six days following a myocardial infarction (MI), hearts exhibited a decrease in glucose uptake. The dysfunction in insulin-stimulated glucose utilization was associated with a depression in phosphorylated insulin substrate receptor 1 (p-IRS-1) and/or a phosphorylated Akt-to-total Akt ratio. Also, mitochondrial ADP-stimulated respiration, density, efficiency were reduced. Peroxisome proliferator-activated receptor γ coactivator 1α (PGC-1α), a regulator of mitochondrial function and biogenesis was lower. MSC transplantation diminished the decline in glucose uptake and p-Akt/Akt ratio in the remote left ventricle and the mitochondrial insults in the peri-infarct region.

[3]CHAPTER FIVE: THE ROLE OF MESENCHYMAL STEM CELL TRANSPLANTATION IN MINIMIZING ENERGY METABOLISM ABNORMALITIES IN THE DIET-INDUCED INSULIN RESISTANT/INFARCTED HEART

5.1 Introduction

The regional loss of cardiac myocytes following a myocardial infarction (MI) compromises the ability of the heart to pump blood to peripheral sites and may initiate compensatory mechanisms in an attempt to preserve cardiac function (322) . Researchers in regenerative medicine have become excited by the possibility of repairing and/or replacing pathological tissue via administration of exogenous cells (124, 163, 216). Experimental study and clinical trials have identified cell-based therapies to consistently improve systolic function (114, 120, 149, 150, 247, 259). However, cell transplantation has been less than adequate at replacing the lost cells; which may be, in part, due to poor cell persistence following administration in the infarcted heart (118, 269).

In the presence of poor cell survival and engraftment, the mechanisms promoting beneficial results reported following stem cell transplantation have been subject to an increasing number of studies that suggest cell-mediated paracrine effects are likely the major mediator for the improvement in cardiac function and the attenuation or slowing of the maladaptive processes (114). The release of paracrine factors have a potential

---

[3]A version of this chapter has been published. Hughey, C.C., Ma, L., James, F.D., Bracy, D.P., Wang, Z., Wasserman, D.H., Rottman, J.N., Hittel, D.S., and Shearer, J. Mesenchymal stem cell transplantation for the infarcted heart: therapeutic potential for insulin resistance beyond the heart. *Cardiovascular Diabetology*. 2013, 12(1):128.

regulatory role in various processes that influence cardiac function including anti-apoptotic signalling and neovascularization as well as the modulation of inflammation, fibrosis, cardiac contractility, host stem cell activation and metabolism (114, 360).

In terms of cardiac metabolism, animal studies indicate the ability of stem cell transplantation, specifically mesenchymal stem cell (MSC) transplantation, to lessen aberrations in glucose utilization, mitochondrial function and high-energy phosphate provision in the infarcted heart (85, 113, 137, 209, 369). Since diabetes and heart disease often co-aggregate (132, 157, 292), the absence of metabolic dysfunction associated with type 2 diabetes in previous studies may not provide a complete model in assessing the utility of cell transplantation for the infarcted heart. Of particular interest is insulin resistance, as it enhances the risk of experiencing cardiovascular disease and a MI (143, 349). Moreover, individuals with insulin resistance and type 2 diabetes exhibit a greater probability of developing heart failure and higher mortality following a MI (105, 192, 349).

From a mechanistic perspective, insulin resistance may enhance cardiac pathology following a MI by inhibiting changes in metabolic characteristics that are initially suggested to be adaptive (5, 146, 230, 328, 342). The cardiac metabolic phenotype shifts away from its predominant reliance on fatty acid oxidation towards increased glucose utilization early post-MI (5, 146, 230, 328, 342). Glucose oxidation is more oxygen efficient and may provide a more effective means of ATP provision (152). An alternative means of providing energy for cardiac contraction in an economical fashion involves the down-regulation of mitochondrial uncoupling proteins (UCPs) in the failing heart (152, 260). UCPs create an environment where oxygen consumption does not contribute to

ATP synthesis, which is achieved through the uncoupling of the electrochemical gradient and ADP phosphorylation (151). These adaptations in cardiac metabolic pathways may assist in meeting the energetic demand of contraction. However, this metabolic flexibility demonstrated by the heart is impeded in insulin resistance (359). Insulin resistance inhibits glucose uptake creating a situation of severe detriment given both fatty acid and glucose metabolism are impaired and energy provision is compromised in the insulin resistant, infarcted heart (359). Further insult occurs from hyperglycemia and hyperlipidemia (147, 354). For example, elevated circulating fatty acids promote an increase in cardiac UCP3 levels (223). The increase in UCP3 may stimulate higher mitochondrial uncoupling and further energy demand/supply disparities.

Given the deleterious impact of insulin resistance on the infarcted heart, this study aimed to identify whether the efficacy of MSC administration to minimize alterations in metabolic processes that assist in ATP provision following a MI is maintained in a murine model of diet-induced insulin resistance/MI.

5.2 Materials and methods

See Figure 5.1 for a schematic of experimental outline.

Figure 5.1 Schematic representation of experimental procedures and timeline

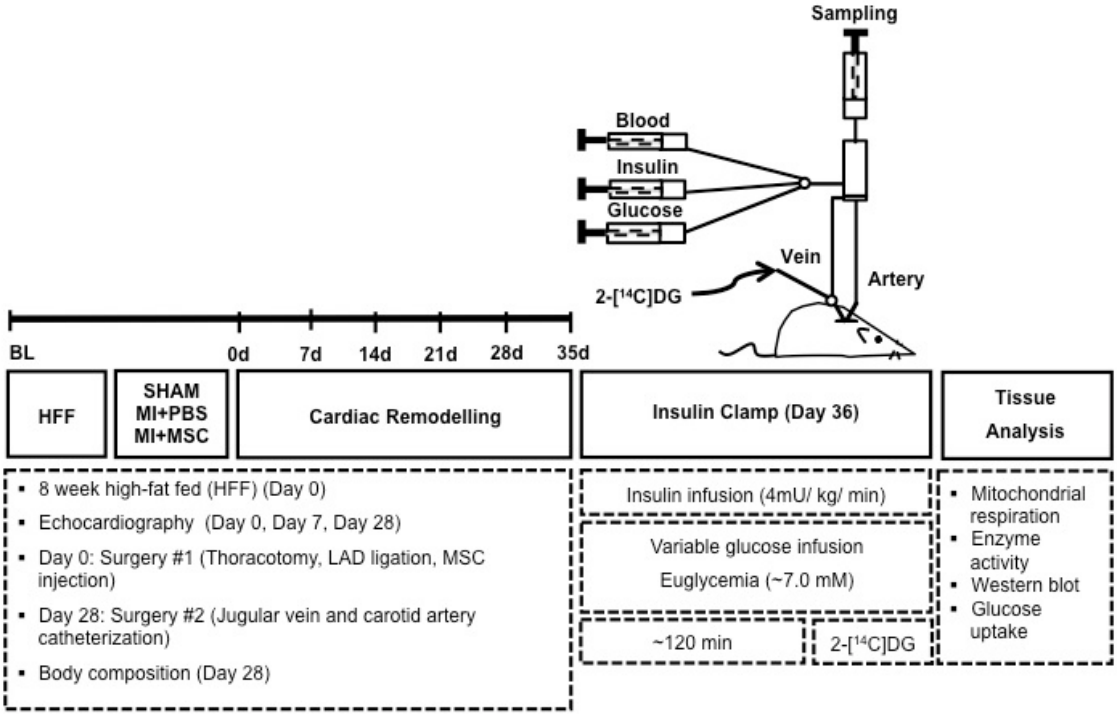

Figure 5.1: Echocardiography on conscious mice was performed prior to, seven and 28 days following ligation of the left anterior descending coronary artery (LAD). Arterial and jugular catheterization was performed 28 days following the LAD ligation for the sampling and infusion protocols of the hyperinsulinemic-euglycemic (insulin) clamp. Insulin clamps were performed following seven days of recovery from the catheterization surgeries (36 days post-LAD ligation/13 weeks of high-fat feeding) to assess insulin action in the conscious, unrestrained mouse. Isotopic tracer 2-[^{14}C]deoxyglucose (2-[^{14}C]DG) administration during the insulin clamps allowed for whole body and tissue-specific substrate uptake to be assessed *in vivo*. Additional experiments included evaluation of mitochondrial respiration in permeabilized cardiac tissue and key molecular regulators of metabolism by immunoblotting. MI+PBS, myocardial infarction + phospho-buffered saline; MI+MSC, myocardial infarction + mesenchymal stem cells.

5.2.1 Animal characteristics and myocardial infarction

Procedures were approved by the Vanderbilt University Animal Care and Use Committee and performed according to the Guide for the Care and Use of Laboratory Animals published by the National Institutes of Health (NIH Publication No. 85-23, revised 1996, A3227-01). Thirteen week-old, eight week high-fat fed (HFF) (F3282, 60% calories from fat, Bio-Serv, Frenchtown, NJ, USA), C57BL/6J, male mice (Jackson Laboratories, Bar Harbour, ME, USA) were randomly separated into three groups: SHAM, MI + phosphate buffered saline (MI+PBS) and MI + mesenchymal stem cells (MI+MSC). A left anterior descending coronary artery (LAD) chronic ligation induced a MI as described (137). Following the ligation, 25 µl of PBS (pH 7.2) or 2.5×10^5 MSCs in 25 µl of PBS (pH 7.2) were injected into the blanching peri-infarct area of the MI+PBS or MI+MSC mice, respectively.

5.2.2 Mesenchymal stem cells

Human MSCs were purchased from the Texas A&M Health Science Center College of Medicine Institute for Regenerative (Temple, TX, USA) that provides standardized MSC preparations through support from the NIH/NCRR (P40 RR 17447-06). The MSCs have been described to consistently exhibit trilineage potential and be $CD90^+$, $CD105^+$, $CD49c^+$, $CD49f^+$, $CD166^+$, $CD59^+$, $CD29^+$, $CD44^+$, $CD45^-$, $CD34^-$, $CD117^-$ and $CD36^-$ (236). MSCs were expanded in alpha minimum essential medium (αMEM) with L-glutamine (Life Technologies, Burlington, ON, Canada), 16.5% defined FBS (HyClone, Logan, UT, USA), penicillin (100 units/ml) and streptomycin (100 µg/ml). All mice received MSCs from a single donor and passages 3-8 were utilized.

5.2.3 Echocardiography

To assess cardiac contractile function, M-mode echocardiography was completed in conscious mice prior to the MI as well as seven and 28 days post-MI as previously described (79, 278).

5.2.4 Catheterization procedures

Chronic catheterization surgeries were performed 28 days post-ligation (12 weeks HFF) as those previously described for hyperinsulinemic-euglycemic (insulin clamps) (137). Post-surgery, the mice were housed individually for seven days to ensure the mice were within 10% of pre-surgical weight prior to insulin clamps.

5.2.5 Hyperinsulinemic-euglycemic clamp

Our laboratory has shown that insulin resistance is induced in 12 weeks HFF C57BL/6 mice (96, 298). Insulin clamps were performed with procedural considerations previously described (13) at 36 days post-MI (13 weeks HFF). Mice were fasted at 7:00 a.m., five hours prior to initiation of the insulin clamps. One hour prior to the experiment, the externalized mouse catheters were connected to catheter extensions attached to infusion syringes. Just prior to the onset of the insulin clamp, an arterial blood sample was obtained to evaluate levels of arterial glucose, insulin, non-esterified fatty acids (NEFA) and hematocrit. Each experiment consisted of a continuous infusion (4 mU/kg/min) of insulin. Euglycemia (blood glucose: ~7.0 mM) was maintained during the insulin clamps. Venous infusion of saline-washed erythrocytes (5 µl/min) during the insulin clamp prevented a decline in hematocrit due to arterial sampling. Insulin clamp duration averaged 122.07 ± 9.48 minutes until a stable glucose infusion rate (GIR) and euglycemia was achieved for at least 30 minutes. Arterial blood was sampled to

determine glucose levels (t=0 minutes) had achieved the steady state. Immediately following the blood sampling, a bolus containing 2-[^{14}C]deoxyglucose (2-[^{14}C]DG; 13 μCi) was administered into the jugular vein to provide an index of tissue-specific glucose uptake. At *t* = 2, 5, 10, 15, 20 minutes, arterial blood was sampled to determine glucose and 2-[^{14}C]DG. At *t* = 30 minutes, arterial blood was taken for the measurement of glucose, experimental insulin, 2-[^{14}C]DG and hematocrit. Plasma was stored at -20°C until analysis. Following the insulin clamp, mice were killed via cervical dislocation and tissues were immediately excised for analysis or stored at -80°C. The heart, soleus, gastrocnemius, superficial vastus lateralis and white adipose tissue from the epididymal fat pad were collected.

5.2.6 Plasma analyses

Arterial insulin was assayed via a double antibody method (218). Plasma NEFAs (NEFA C kit; Wako Chemicals, Richmond, VA, USA) and glucose were determined spectrophotometrically as previously described (137). Plasma 2-[^{14}C]DG was assessed as previously outlined (298).

5.2.7 Tissue-specific substrate kinetics

Tissue 2-[^{14}C]DG and tissue phosphorylated 2-[^{14}C]DG (2-[^{14}C]DG-P) were determined as previously described (298). The metabolic index of glucose (R_g) uptake was calculated (299) and expressed as previously described (276).

5.2.8 Mitochondrial respiration and enzymatic measurements

Cardiac peri-infarct fibers were prepared and saponin-permeabilized as described (136). High-resolution respirometry (Oroboros Instruments, Innsbruck, Austria) was performed in duplicate at 37°C in MiR05 (Final concentration: 0.5 mM EGTA, 3 mM

$MgCl_2 \cdot 6H_2O$, 20 mM taurine, 10 mM KH_2PO_4, 20 mM HEPES, 1 g/L BSA, 60 mM potassium-lactobionate, 110 mM sucrose, pH 7.1, adjusted at 30°C). Substrates (final concentration) included 10 mM glutamate plus 2 mM malate and 5 mM pyruvate, 5 mM ADP and 10 mM succinate. Cytochrome c (10 mM) was added to ensure the outer mitochondrial membrane was intact after processing. Peri-infarct citrate synthase activity was determined via previous methods (137).

5.2.9 Immunoblotting

Tissues were homogenized in a lysis buffer (final concentration) containing 20 mM NaCl, 20 mM Tris-HCl, 0.1 mM EDTA, 1% Triton X-100, 0.5% (wt./vol.) sodium deoxycholate, and 0.1% β-mercaptoethanol (vol./vol.) (pH 7.4) in the presence of a protease inhibitor cocktail (Sigma-Aldrich, Oakville, ON, Canada) and phosphatase inhibitor cocktail (Thermo Fisher Scientific, Mississauga, ON, Canada). Cardiac (20-30 μg), gastrocnemius (40 μg) and white adipose tissue (40 μg) proteins were resolved on NuPAGE 4-12% (vol./vol.) Bis-Tris gels (Life Technologies) and transferred to a polyvinylidene fluoride membrane. Membranes were probed with peroxisome proliferator-activated receptor gamma coactivator-1alpha (PGC-1α; Santa Cruz Biotechnology, Santa Cruz, CA, USA), glucose transporter 4 (GLUT4; Abcam, Cambridge, MA, USA), hexokinase II (HKII; Chemicon, Temecula, CA, USA), UCP3 (Abcam), phospho-Akt(Ser473) (p-Akt; Cell Signaling Technology, Whitby, ON, Canada) and Akt (Cell Signaling Technology) and oxidative phosphorylation complexes I-V (OXPHOS CI-CV; Abcam) antibodies. A goat-anti-mouse secondary antibody (Thermo Fischer Scientific) was used for the OXPHOS CI-CV primary antibody cocktail. A goat-anti rabbit secondary antibody (Cell Signaling Technologies) was used for all

other primary antibodies. Glyceraldehyde 3-phosphate dehydrogenase (GAPDH; Abcam) expression was employed as a control for all immunoblots.

5.2.10 Statistical analyses

ANOVA or two-way repeated measures ANOVA were performed to detect statistical differences ($p < 0.05$) as appropriate followed by Tukey's post hoc tests. All data are reported as means ± SEM.

5.3 Results

5.3.1 Stem cell therapy promotes improvement in cardiac contractile function

Contractile abnormalities were observed using echocardiography (Table 5.1) in the MI+PBS group seven and 28 days following a MI as indicated by the depression in ejection fraction (Figure 5.2A) and fractional shortening (Figure 5.2B). The MSC-treated animals displayed a comparable reduction in ejection fraction as the MI+PBS group at seven days post-MI (Figure 5.2A). However, the MSC-treated hearts exhibited a greater ejection fraction than the MI+PBS mice at 28 days following cardiac insult (Figure 5.2A). The MI+MSC mice, similar to the MI+PBS animals, displayed a depression in fractional shortening at seven and 28 days post-MI (Figure 5.2B).

Indices of cardiac structural alterations were also assessed. Heart weight (Figure 5.2C) and heart-to-body weight (Figure 5.2D) were increased in MI+PBS mice 36 days post-MI. A comparable elevation in these hypertrophy markers was observed in the MSC-treated mice (Figure 5.2C and 5.2D). Of note, measurement of body weight from one week prior to the ligation surgery to five weeks post-MI indicated that the MI+PBS mice were lower as a result of the MI (Figure 5.2E). In contrast, mice receiving MSC

transplantation displayed a comparable body weight to animals of the SHAM group (Figure 5.2E). Given the changes in body weight, tibial length was used to normalize heart weight and provide another index of pathological cardiac hypertrophy. Tibial length was unchanged between groups (Figure 5.2F). Both infarcted groups displayed an elevated heart-to-tibial length compared to the SHAM group (Figure 5.2F) indicating a hypertrophic response to the infarct that was not inhibited by the MSC therapy.

Table 5.1 Cardiovascular parameters in conscious high-fat fed C57BL/6 mice

	Baseline			7 days post-MI			28 days post-MI		
	SHAM	**MI+ PBS**	**MI+ MSC**	**SHAM**	**MI+ PBS**	**MI+ MSC**	**SHAM**	**MI+ PBS**	**MI+ MSC**
HR (bpm)	647 ± 16	662 ± 16	689 ± 9*	720 ± 8	699 ± 10	713 ± 12	710 ± 11	720 ± 13	731 ± 6
FS (%)	49.58 ± 0.75	48.88 ± 1.02	48.74 ± 0.46	49.12 ± 0.78	29.88 ± 3.16*	30.90 ± 2.03*	48.99 ± 0.70	27.34 ± 2.84*	32.90 ± 2.02*
EF (%)	82.07 ± 0.72	81.37 ± 1.01	81.23 ± 0.45	81.80 ± 0.76	56.51 ± 4.88*	58.48 ± 2.9*	81.48 ± 0.74	52.80 ± 2.93*	61.10 ± 2.88*†
IVSd (mm)	0.77 ± 0.02	0.81 ± 0.02	0.79 ± 0.01	0.76 ± 0.02	0.73 ± 0.04	0.84 ± 0.01*†	0.79 ± 0.01	0.76 ± 0.03	0.85 ± 0.01*†
LVIDd (mm)	3.19 ± 0.07	3.21 ± 0.08	3.28 ± 0.04	3.02 ± 0.04	4.31 ± 0.24*	4.01 ± 0.13*	3.23 ± 0.08	4.32 ± 0.21*	4.27 ± 0.13*
LVPWd (mm)	0.72 ± 0.01	0.69 ± 0.02	0.80 ± 0.02†	0.74 ± 0.02	0.68 ± 0.07	0.86 ± 0.03*†	0.77 ± 0.02	0.71 ± 0.04	0.91 ± 0.03
IVSs (mm)	0.91 ± 0.02	0.91 ± 0.02	0.90 ± 0.01	0.88 ± 0.02	0.87 ± 0.05	0.92 ± 0.02	0.88± 0.01	0.84 ± 0.02	0.96 ± 0.01*†
LVIDs (mm)	1.61 ± 0.04	1.65 ± 0.06	1.68 ± 0.03	1.54 ± 0.04	3.06 ± 0.28*	2.79 ± 0.16*	1.65 ± 0.06	3.17 ± 0.26*	2.89 ± 0.17*
LVPWs (mm)	0.97 ± 0.02	0.98 ± 0.04	1.04 ± 0.01	0.88 ± 0.02	0.83 ± 0.09	1.01 ± 0.02*†	0.96 ± 0.02	0.82 ± 0.06*	1.11 ± 0.03*†

Data are mean ± SEM for n=8-13 mice per group

*p<0.05 vs. SHAM at specified time point

†p<0.05 vs. MI+PBS at specified time point

Abbreviations: HR, heart rate; FS, fractional shortening; EF, ejection fraction; IVSd, interventricular septal thickness in diastole; LVIDd, left ventricle (LV) end-diastolic dimension; LVPWd, LV posterior wall thickness in diastole; IVSs, interventricular septal

thickness in systole; LVIDs, LV end-systolic dimension; LVPWs, LV posterior wall thickness in systole

Figure 5.2 Cardiac functional and hypertrophic indices

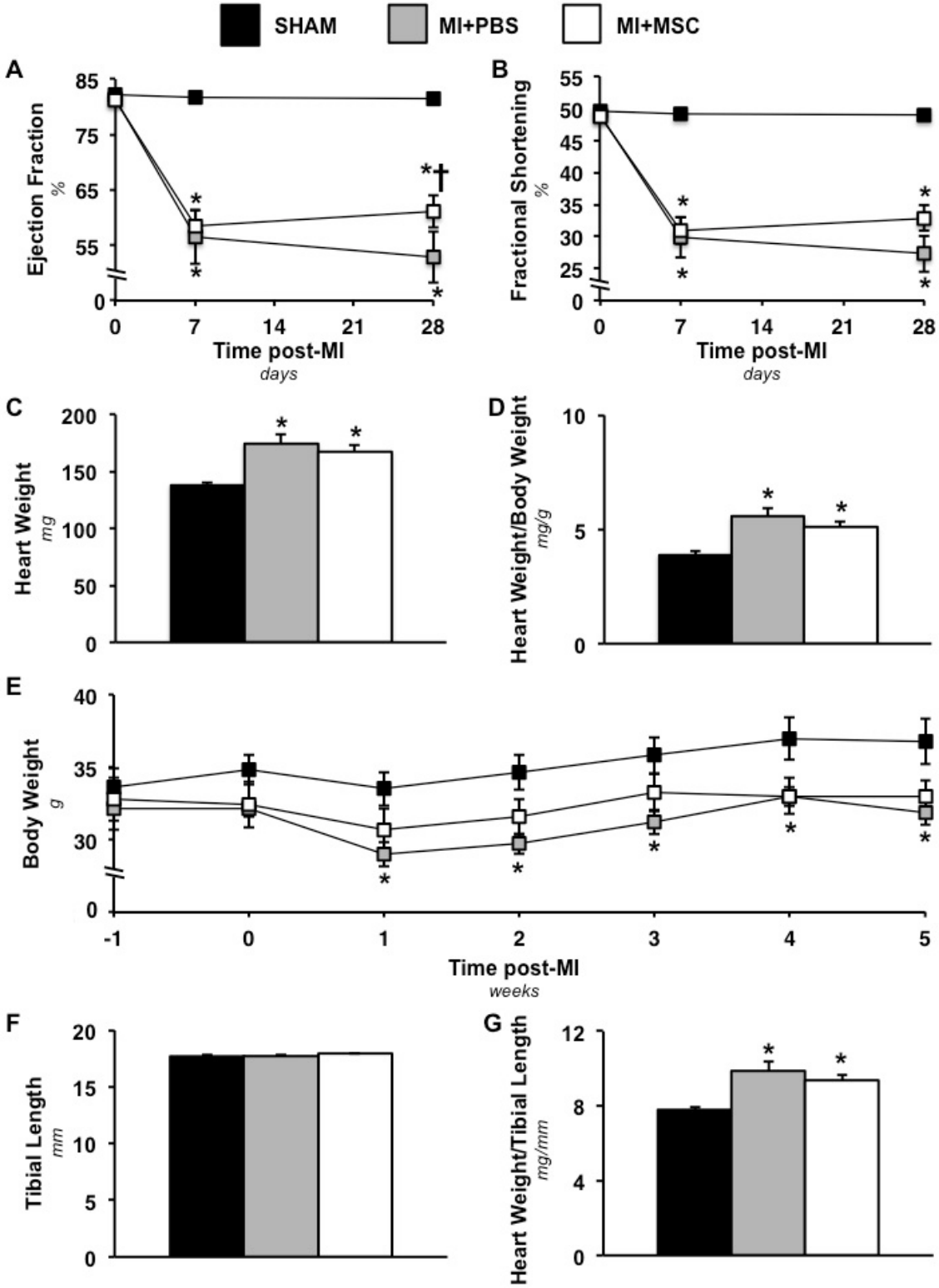

Figure 5.2: (A) Cardiac ejection fraction (%) prior to, seven and 28 days following a MI. n=8-13 mice per group. (B) Cardiac fractional shortening (%) prior to, seven and 28 days following a MI. n=8-13 mice per group. (C) Heart weight 36 days post-MI surgery. n=11-14 mice per group. (D) Heart weight-to-body weight ratio 36 days following a MI. n=11-14 mice per group. (E) Time course of body weight from one week prior to chronic left anterior descending coronary artery ligation to five weeks post-ligation. n=10-12 mice per group. (F) Tibial length 36 days following a MI. n=11-14 mice per group. (G) Heart weight-to-tibial length 36 days post-MI. n=11-14 mice per group. Data are mean ± S.E.M. *$p<0.05$ vs. SHAM. †$p<0.05$ vs. MI+PBS.

5.3.2 Enhanced insulin-stimulated cardiac glucose utilization in MSC-treated mice

Isotopic glucose (2-[^{14}C]DG) was administered during the insulin clamps to assess tissue-specific glucose uptake. A MI did not influence regional insulin-stimulated glucose uptake (R_g) in the heart. The remote left ventricle (MI+PBS LV) and the peri-infarct region (MI+PBS PI) in the MI+PBS animals were comparable the SHAM group (Figure 5.3A and 5.3B). In contrast, intramyocardial injection of MSCs enhanced cardiac R_g in response to insulin. The remote left ventricle of the MSC-treated mice (MI+MSC LV) displayed greater R_g compared to that of the MI+PBS mice (Figure 5.3A). Furthermore, the insulin-mediated response of the peri-infarct region of the MI+MSC hearts (MI+MSC PI) was more apparent. The MI+MSC PI region exhibited a higher R_g than the SHAM hearts and the peri-infarct region of the MI+PBS group (Figure 5.3B).

To identify the mechanisms by which MSC administration promoted cardiac glucose uptake key regulators of glucose metabolism were evaluated. The remote left

ventricle and peri-infarct PGC-1α, GLUT4 and HKII were comparable between groups (Figure 5.3C and 5.3D). The insulin signalling pathway was also probed by determining p-Akt(Ser473) and total Akt. Again, the regional p-Akt/Akt ratio was similar between groups (Figure 5.3E and 5.3F).

Figure 5.3 Regional insulin-stimulated cardiac glucose uptake

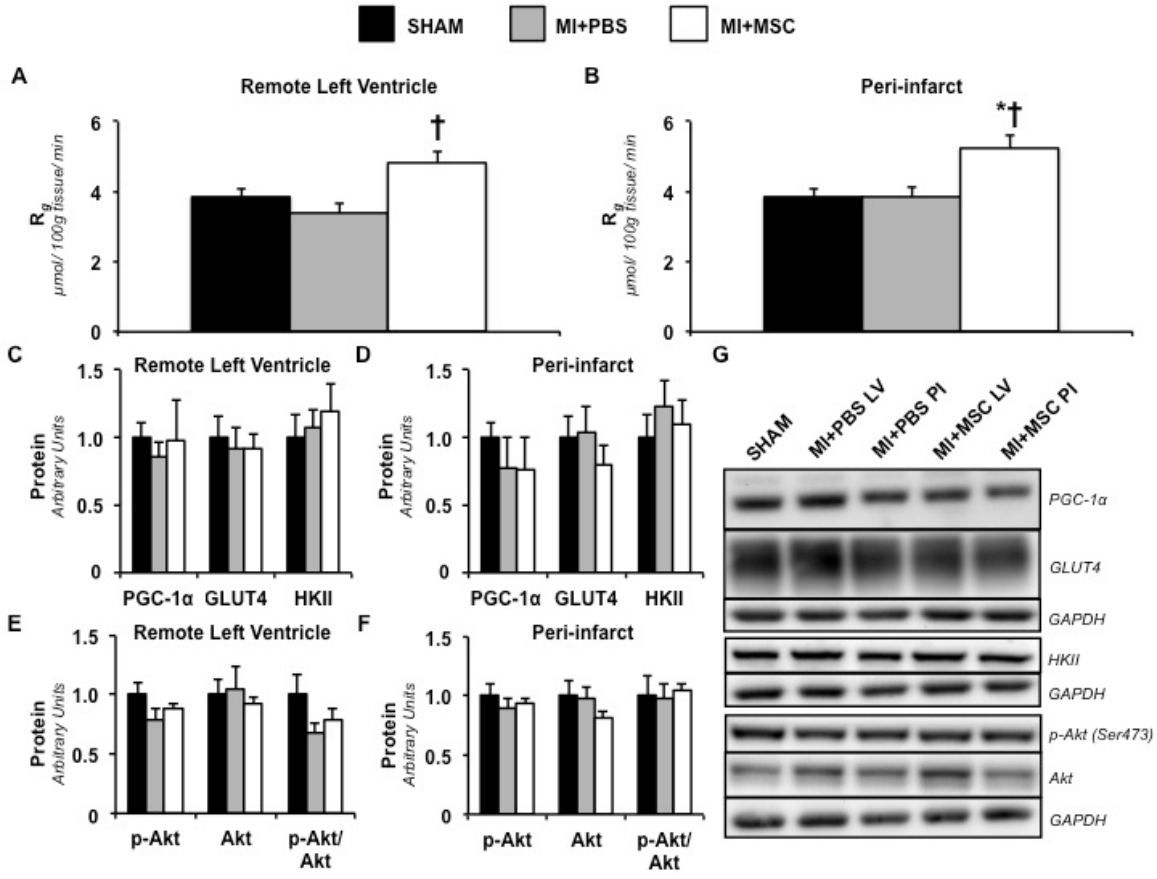

Figure 5.3: (A) Metabolic index of glucose uptake (R_g) in the remote left ventricle and (B) peri-infarct region of the left ventricle. Cardiac R_g values are relative to brain R_g. n=8-9 mice per group. (C) Remote left ventricle and (D) peri-infarct peroxisome proliferator-activated receptor gamma coactivator-1alpha (PGC-1α), glucose transporter 4 (GLUT4) and hexokinase II (HKII) as determined by immunoblotting. (E) Left ventricle

and (F) peri-infarct phospho-Akt (p-Akt), Akt and p-Akt-to-total Akt ratio (p-Akt/Akt) as determined by immunoblotting. (G) Representative immunoblotting performed to measure PGC-1α, GLUT4, HKII, p-Akt and Akt. Cardiac proteins are normalized to glyceraldehyde-3-phosphate dehydrogenase (GAPDH) content and are relative to the SHAM group. n=6 mice per group. Data are mean ± S.E.M. *$p<0.05$ vs. SHAM. †$p<0.05$ vs. MI+PBS.

5.3.3 MSC transplantation augments mitochondrial physiology

Given both contractile function and substrate utilization may be influenced by energy metabolism, respirometry measurements were performed to assess integrative mitochondrial OXPHOS. The MI+PBS peri-infarct fibers exhibited a reduced basal oxygen consumption (V_0) supported by glutamate, malate and pyruvate compared to the SHAM group (Figure 5.4A). Interestingly, MSC-treated hearts displayed an even further depression in basal oxygen flux compared to the MI+PBS and SHAM peri-infarct regions (Figure 5.4A). ADP-stimulated oxygen consumption through complex I was reduced in MI+PBS and MI+MSC animals ($V_{MAX\text{-}CI}$; Figure 5.4A). Similarly, ADP-stimulated oxygen flux via convergent electron flux through mitochondrial complexes I+II was reduced in both infarcted groups ($V_{MAX\text{-}CI+CII}$; Figure 5.4A). Intriguingly, the respiratory control ratio (RCR) was reduced in the MI+PBS hearts compared with the MI+MSC cardiac fibers (Figure 5.4B). This suggests a decrease in OXPHOS efficiency in the MI+PBS mice. Citrate synthase activity was assessed to identify differences in mitochondrial content. The MI+PBS group exhibited a decline in citrate synthase activity (Figure 5.4C). The preservation of cardiac citrate synthase activity in the

MI+MSC mice prompted the evaluation of mitochondrial proteins in an effort to identify mechanisms contributing to the reduced V_0 but greater RCR. Protein expression of mitochondrial OXPHOS complexes showed the MI+MSC mice to have a lower complex I protein in the remote left ventricle region (Figure 5.4D and 5.4F). Similarly, the MI+PBS and MI+MSC peri-infarct region exhibit a reduced complex I protein compared to the SHAM heart (Figure 5.4E and 5.4F). Surprisingly, there was an added effect of the MSC therapy. The MI+MSC peri-infarct region displayed a lower complex II and complex V compared to the SHAM hearts (Figure 5.4E and 5.4F). Another potential contributor to the lower basal oxygen flux but elevated RCR is the peri-infarct UCP3 that was lower in the MI+MSC mice (Figure 5.4E and 5.4F).

Figure 5.4 Cardiac mitochondrial function and characteristics

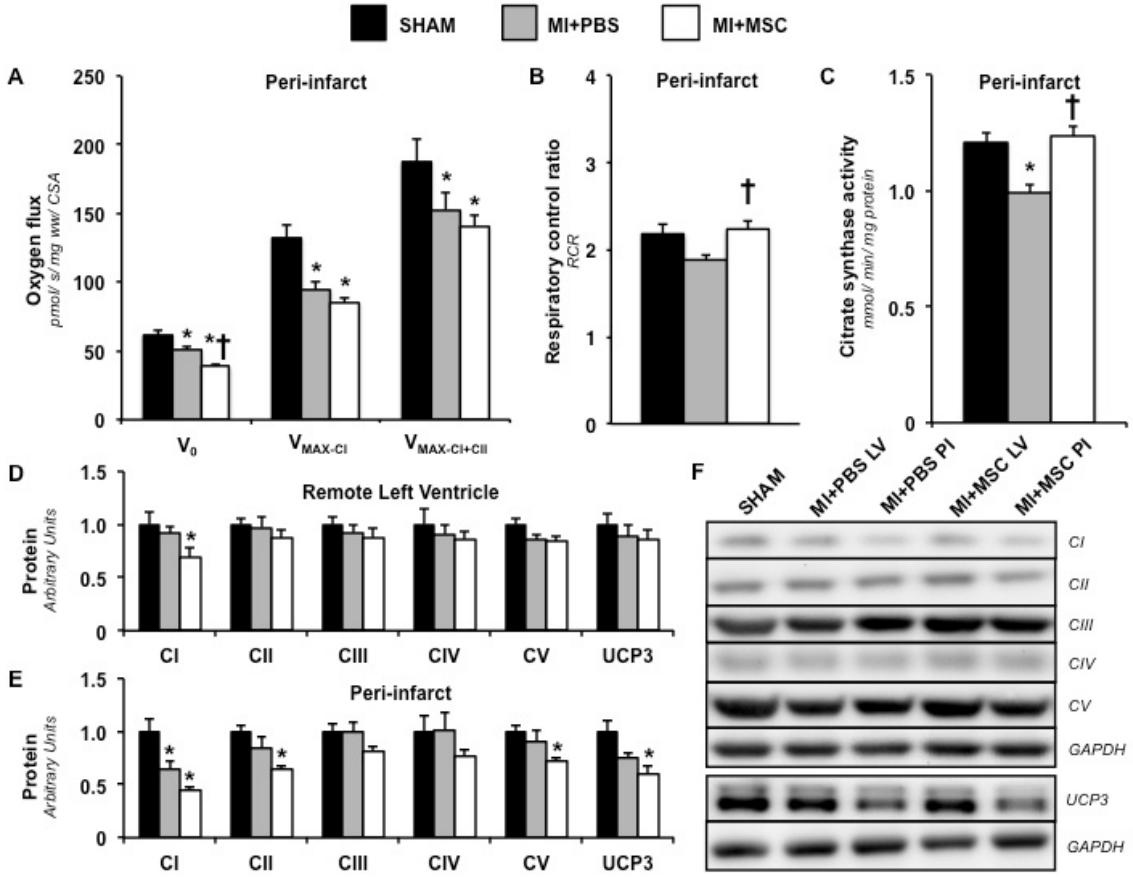

Figure 5.4: (A) Peri-infarct permeabilized cardiac fiber basal oxygen consumption supported by glutamate, malate and pyruvate (V_0), maximal oxygen consumption (ADP-stimulated) supported by glutamate, malate and pyruvate through complex I (V_{MAX-CI}) and maximal convergent oxygen flux supported by glutamate, malate, pyruvate and succinate ($V_{MAX-CI+CII}$). n=8-9 mice per group. (B) Respiratory control ratio (RCR; defined as V_{MAX-CI}/V_0). n=8-9 mice per group. (C) Peri-infarct citrate synthase activity (CSA) (mmol/min/mg protein). n=8-9 mice per group. (D) Remote Left ventricle and (E) peri-infarct mitochondrial oxidative phosphorylation (OXPHOS) complexes I-V (CI-CV) and uncoupling protein 3 (UCP3) as determined by immunoblotting. (F) Representative immunoblotting of the regional protein levels OXPHOS complexes I-V and UCP3.

Cardiac protein was normalized to glyceraldehyde-3-phosphate dehydrogenase (GAPDH) content and expressed relative to the SHAM group. n=6 mice per group. Data are mean ± S.E.M. *p<0.05 vs. SHAM. †p<0.05 vs. MI+PBS.

5.3.4 Reduced fasting plasma glucose and fatty acids following MSC administration

High-fat diets have been reported to promote an increase in tissue UCP3 protein. More specifically, cardiac UCP3 positively correlates with circulating fatty acid levels (223) . As such, we evaluated fasting plasma non-esterified fatty acid (NEFA) concentration. There was a lowering of NEFA levels in the MI+MSC mice (Table 5.2). In addition, fasting plasma glucose concentration was reduced following MSC therapy (Table 5.2). Of note, arterial insulin concentrations in the fasted state and during the insulin clamp were both similar between groups (Table 5.2).

Table 5.2 Biometric characteristics of high-fat fed C57BL/6 mice

	SHAM	MI+PBS	MI+MSC
Fasting Plasma Glucose (mM)	11.37 ± 0.48	10.81 ± 0.43	9.06 ± 0.32*†
Fasting Plasma NEFA (mM)	1.04 ± 0.05	1.09 ± 0.06	0.8 ± 0.06*†
Fasting Plasma Insulin (µU/ml)	60.08 ± 13.22	50.76 ± 16.15	42.46 ± 11.13
Experimental Plasma Insulin (µU/ml)	128.02 ± 15.77	108.17 ± 8.84	160.04 ± 24.32
Muscle (%)	68.70 ± 1.76	77.75 ± 1.96*	67.88 ± 2.38†
Fat (%)	29.53 ± 1.80	20.74 ± 2.02*	30.25 ± 2.42†
Free Fluid (%)	1.77 ± 0.11	1.51 ± 0.17	1.87 ± 0.27

Data are mean ± SEM

n=11-12 mice per group for plasma glucose, n=10-12 for plasma NEFA, n=8-9 for fasting plasma insulin, n= 8 for experimental plasma insulin, n=9-13 for body composition

*$p<0.05$ vs. SHAM

†$p<0.05$ vs. MI+PBS

5.3.5 Systemic insulin sensitivity elevated by MSC injection

The lowering of fasting plasma glucose and fatty acids suggested a systemic effect of the MSC administration. To this end, insulin clamps were performed in the conscious, unrestrained mouse to evaluate whole body glucose disposal in response to insulin *in vivo*. The GIR required to maintain an arterial glucose concentration of 7.0 mM was elevated in MI+MSC mice throughout the duration of the insulin clamp (Figure 5.5A). The GIR for the MI+PBS mice was similar to the SHAM group (Figure 5.5A). Arterial glucose was comparable between groups during the insulin clamp (Figure 5.5B).

Figure 5.5 Whole body insulin sensitivity and blood glucose during the insulin clamp

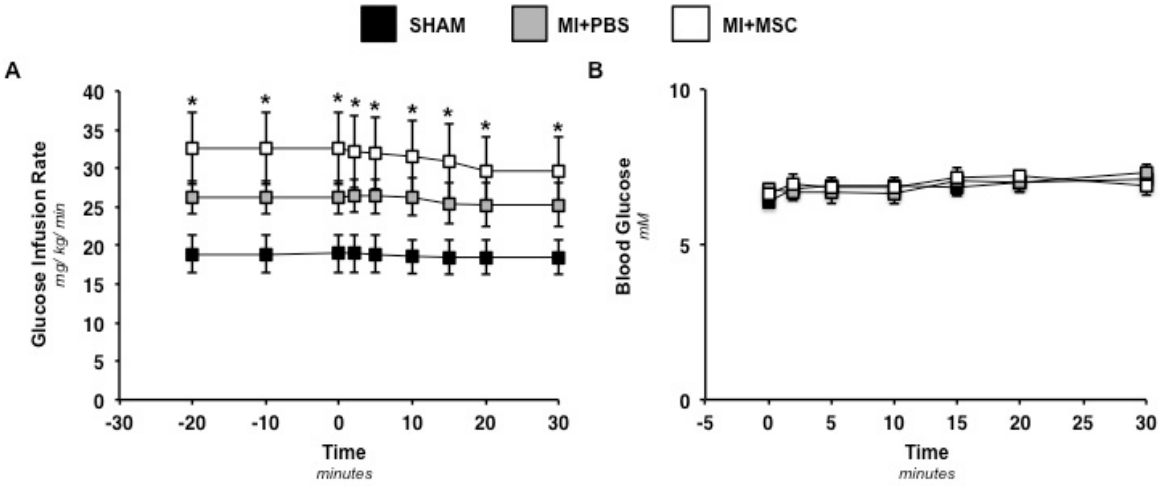

Figure 5.5: (A) Glucose infusion rate (GIR) during the insulin clamp. The GIR is equivalent to the whole body glucose disposal rate in response to venous insulin infusion. The insulin infusion was for approximately 120 minutes prior to 2-[^{14}C]deoxyglucose (2-[^{14}C]DG) administration. The GIR is displayed as a time course commencing twenty minutes prior to administration of 2-[^{14}C]DG (-20 minute time point) to 30 minutes following 2-[^{14}C]DG infusion (30 minute time point). (B) Arterial, blood glucose concentration following 2-[^{14}C]DG for 30 minutes post-administration. Data are mean ± SEM for n=9-12 mice per group. *$p<0.05$ vs. SHAM.

5.3.6 Increased peripheral tissue glucose uptake post-MSC therapy

In agreement with the increased GIR, the MSC administration increased insulin-stimulated R_g in peripheral tissues. The MI+MSC soleus, superficial vastus lateralis, gastrocnemius and white adipose tissue had a greater R_g compared to the same tissues of the SHAM group (Figure 5.6A-D). The MI+MSC gastrocnemius also exhibited an elevated R_g compared to that of the MI+PBS mice (Figure 5.6C). The MI+PBS mice

displayed a higher R_g in white adipose tissue compared to the SHAM group (Figure 5.6D). The protein expression of regulators involved in insulin-mediated R_g was evaluated in the gastrocnemius and white adipose tissue. GLUT4 was higher in the MI+MSC gastrocnemius compared to the SHAM group (Figure 5.6E and 5.6F). Also, gastrocnemius p-Akt and the p-Akt-to-Akt ratio were greater in the MI+MSC mice (Figure 5.6E and 5.6F). Both the MI+MSC and MI+PBS groups displayed higher GLUT4 in the white adipose tissue (Figure 5.6G and 5.6H). However, only the MI+MSC exhibited elevated p-Akt relative to the SHAM group in white adipose tissue (Figure 5.6G and 5.6H). Furthermore, the p-Akt-to-Akt ratio in MI+MSC white adipose tissue was greater than that of the SHAM and MI+PBS mice (Figure 5.6G).

Figure 5.6 Insulin-stimulated peripheral tissue glucose utilization

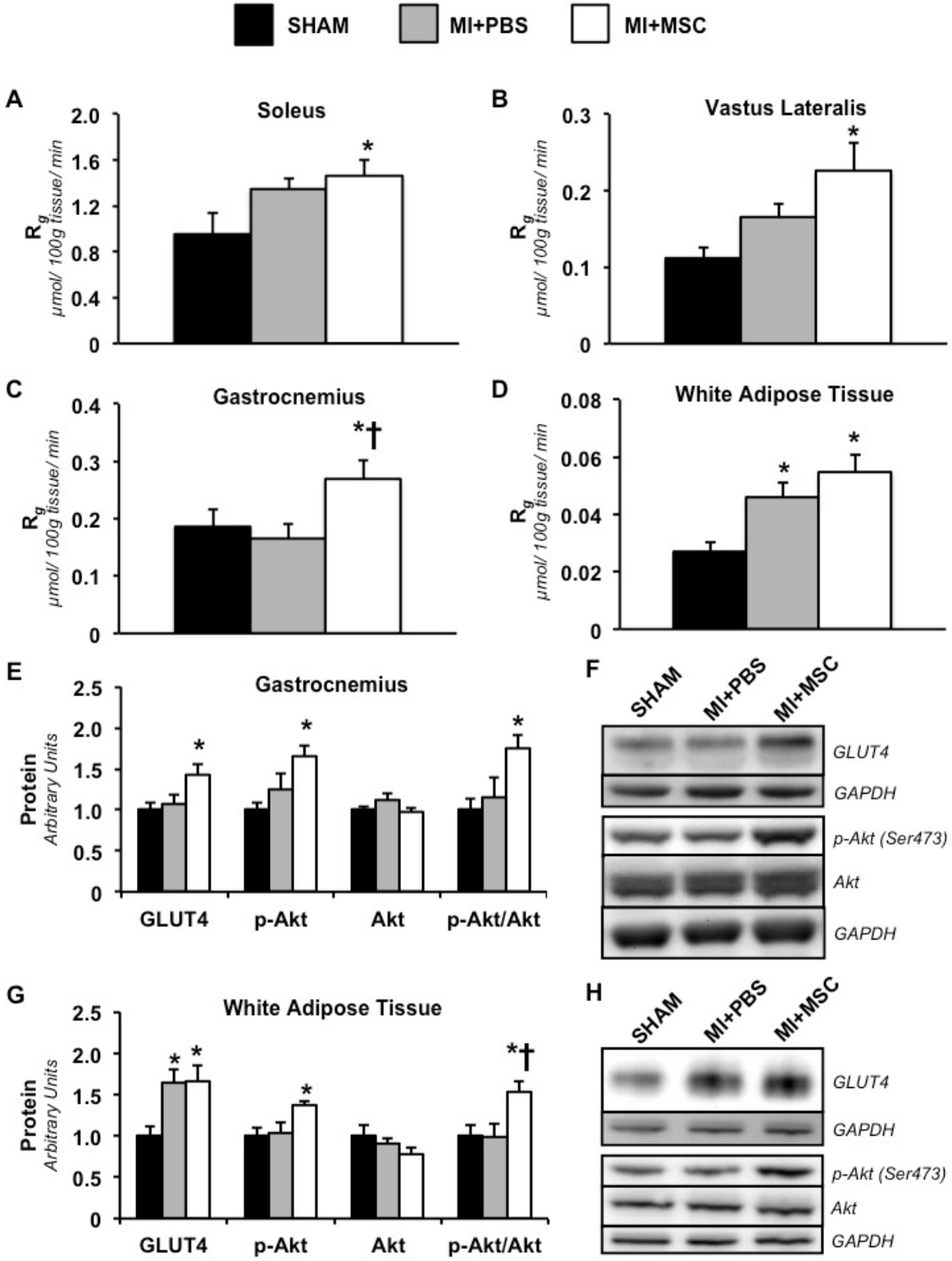

Figure 5.6: (A) Metabolic index of glucose uptake (R_g) in the soleus. (B) Metabolic index of glucose uptake (R_g) in the superficial vastus lateralis. (C) Metabolic index of glucose uptake (R_g) in the gastrocnemius. (D) Metabolic index of glucose uptake (R_g) in white adipose tissue. Tissue R_g values are relative to brain R_g. n=9 mice per group. (E) Gastrocnemius glucose transporter 4 (GLUT4), phospho-Akt (p-Akt), Akt and p-Akt-to-total Akt ratio (p-Akt/Akt) as determined by immunoblotting. n=6-8 mice per group. (F) Representative immunoblotting performed to measure gastrocnemius GLUT4, p-Akt and Akt. (G) White adipose tissue glucose transporter 4 (GLUT4), phospho-Akt (p-Akt), Akt and p-Akt-to-total Akt ratio (p-Akt/Akt) as determined by immunoblotting. n=6 mice per group. (H) Representative immunoblotting performed to measure white adipose tissue GLUT4, p-Akt and Akt. Protein levels are normalized to glyceraldehyde-3-phosphate dehydrogenase (GAPDH) content and are expressed relative to the SHAM group. Data are mean ± S.E.M. *$p<0.05$ vs. SHAM. †$p<0.05$ vs. MI+PBS.

5.4 Discussion

Numerous studies have reported that cell-based therapeutics can minimize insult to the infarcted heart, in large part, through trophic mechanisms (114, 360). However, as stem cell therapy transfers to clinical trials and ideally to routine use in the clinical setting a clearer understanding as to how the transplanted cells improve outcomes is needed. To gain greater insight into the mechanisms of action, stem cell administration in models of physiological relevance is required. Few studies have included type 2 diabetes and/or its associated metabolic dysregulation on the effect of stem cell transplantation in the infarcted heart. Yan et al. (366) assessed the influence of induced-pluripotent stem (iPS)

cell administration in the db/db mouse heart following a MI. Echocardiography revealed that 14 days post-MI left ventricle contractile dysfunction was minimized by iPS cell transplantation (366). The current study expands on the work of Yan and colleagues (366) by employing a diet-induced insulin resistant C57BL/6 mouse model and assessing the ability of MSC administration to minimize cardiac systolic abnormalities post-infarct. We report the MSC therapy to improve cardiac ejection fraction 28 days post-MI. This indicates that MSC transplantation holds similar potential in restoring left ventricle systolic function in the presence of diet-induced systemic metabolic insults. Furthermore, our experiments investigate beyond cardiac contractile function to evaluate the effect of MSC transplantation on metabolic characteristics that may minimize dysfunction.

The superior contractile function in the MSC-treated mice may be due to the ability of the hearts to more effectively utilize substrates and synthesize ATP. The current study demonstrates intramyocardial administration of MSCs to improve the ability of the heart to transport glucose in the remote left ventricle and peri-infarct region. This improvement in glucose utilization may assist in energetic provision. Molecular regulators of glucose metabolism were evaluated to provide insight into the mechanisms through which the MSC transplantation elevated cardiac glucose uptake. The current study did not expose alterations in regional cardiac levels of PGC-1α, GLUT4, HKII, p-Akt, Akt and the p-Akt-to-Akt ratio. This suggests key proteins involved in glucose uptake and insulin signalling were not augmented by the MSC treatment in the heart. The absence of changes in these proteins led us to explore mitochondrial function as a possible mechanism by which glucose would be utilized at a higher rate.

Downstream of glucose transport, phosphorylation and glycolysis, mitochondria OXPHOS acts as a link between glucose uptake and ATP generation. Early studies evaluating the effect of MSC transplantation show an improvement in the infarct border zone and whole left ventricle phosphocreatine (PCr)-to-ATP ratio (85, 113, 369). The PCr-to-ATP ratio reflects efficiency of myocardial energy provision, and correlates well with LV contractile function (85, 119, 231, 370). Furthermore, MSC therapy reduces basal mitochondrial oxygen consumption (V_0) and improves cardiac RCR ($V_{MAX\text{-}CI}/V_0$) (137). V_0 represents futile respiration that does not contribute to ATP synthesis and a lower basal oxygen flux helps increase RCR; which is indicative of a more efficient OXPHOS. Mitochondrial dysfunction has been theorized to promote insulin-resistance (324). Conversely, improved mitochondrial function may help alleviate impaired glucose uptake and assist in greater ATP synthesis. In the current study, MSC therapy was also able to lower V_0 and increase RCR. The mechanisms through which MSCs promote these alterations on mitochondrial function may be due to a direct influence on OXPHOS complexes. Jameel at al. (148) indicate that MSC administration for the infarcted heart reduces gene expression of complex I subunits. We report that in the peri-infarct region, there was a decline in complex I protein levels following a MI. However, MSC transplantation enhanced the reduction in complex I as indicated by the decline induced in the remote left ventricle and peri-infarct region. Complex II and V were also lower in the MSC-treated peri-infarct region. A reduction in OXPHOS complexes I, II and V may explain the diminished V_0 as a repressed complex number could potentially subdue electron flux and oxygen consumption. Another potential mechanism for the lower V_0 and elevated RCR is alterations in UCP3. UCP3 has been suggested to function as a

potential OXPHOS uncoupler (57). As such, a reduction in protein may promote a decline in UCP3-mediated uncoupling.

Increases in tissue UCP3 are often more pronounced with high-fat diets and with elevated circulating fatty acids (16, 223). We report that MSC-treated mice exhibited a reduction in fasted plasma NEFAs. This decline would promote a lower tissue expression of UCP3. Further systemic influence of the MSC therapy was observed in fasting plasma glucose. We found plasma glucose levels were diminished in the MSC-treated animals. In agreement, animal studies indicate that MSC therapy is capable of lowering blood glucose levels in both type 1 diabetes (80, 182) and type 2 diabetes (304). A recent pilot clinical study has reported a reduction in blood glucose in individuals with type 2 diabetes following MSC transplantation (155).

The exact mechanisms by which MSC exert these effects on metabolism have yet to be elucidated. To date, the majority of studies evaluating stem cell transplantation in diabetes have focused on the ability of the administered cells to regenerate and/or protect the insulin-producing beta cells of the pancreas as a means of providing improved glucose control and reducing diabetic complications (58). To the authors' knowledge, only a single study has evaluated the influence of cell-based therapy on peripheral tissue glucose disposal as a mechanism through which the treatment reduces hyperglycemia. Si et al. (304) employed insulin clamps to test whether MSC administration improves whole-body insulin sensitivity in streptozotocin/high-fat diet-induced diabetes rodents. It was reported that MSC therapy increased GIR but there was not a complete restoration to that of a chow fed animal (304). We achieved comparable results employing insulin clamps to show the MSC-treated animals display greater systemic insulin sensitivity.

Mice receiving MSC displayed an approximately 40% increase in the GIR compared to SHAM mice. However, the current study provides further support for a system-wide elevation in insulin-mediated glucose uptake by combining the insulin clamp with isotopic techniques to evaluate tissue-specific glucose utilization. In addition to increased cardiac glucose uptake, the soleus, superficial vastus lateralis, gastrocnemius and white adipose tissue exhibited an elevated rate of insulin-stimulated glucose uptake following MSC transplantation. The rise in glucose utilization in a range of insulin-sensitive tissues suggests the stem cell therapy is indeed acting in a systemic fashion rather than solely via tissue-specific mechanisms.

To address the mechanisms by which the MSC treatment promoted glucose uptake in the selected tissues, GLUT4 protein was examined. Both gastrocnemius and white adipose tissue total GLUT4 content was elevated in the MSC-treated mice. In the current study plasma fasting and experimental insulin concentrations were comparable between groups, however, there was an insulin-dependent influence conferred by the MSC transplantation. The gastrocnemius and white adipose tissue displayed higher p-Akt and an elevated p-Akt-to Akt ratio. This suggests the cell therapy may augment the insulin signalling pathway to enhance glucose uptake.

5.5 Conclusion

In summary (Figure 5.7), the novel findings of this study are the MSC-mediated increase in both cardiac glucose uptake and mitochondrial OXPHOS efficiency. These metabolic improvements may assist in greater ATP provision for contractile demands following a MI. Our results also demonstrate MSC transplantation to reduce

hyperglycemia, hyperlipidemia and improve peripheral tissue insulin-mediated glucose uptake. These findings differ from the effects of MSC therapy in the absence of type 2 diabetes and/or its metabolic abnormalities. Previous work by the authors evaluating the therapeutic influence of MSC transplantation on cardiac glucose utilization post-MI in chow fed mice did not identify MSC-induced alterations in cardiac glucose metabolism (137). Furthermore, no apparent whole body effect on insulin sensitivity was mediated by MSC transplantation (137). By utilizing a combined diet-induced insulin resistant/MI model the current study identifies that not only does MSC transplantation potentially lessen impairment in cardiac contractile performance via augmentation of cardiac-specific metabolism but also holds the ability to reach farther than the heart to dampen systemic dysregulation that may contribute to the maladaptive alterations in cardiac function.

Figure 5.7 Schematic representation of metabolic signalling pathways that may be influenced by MSC transplantation following a MI

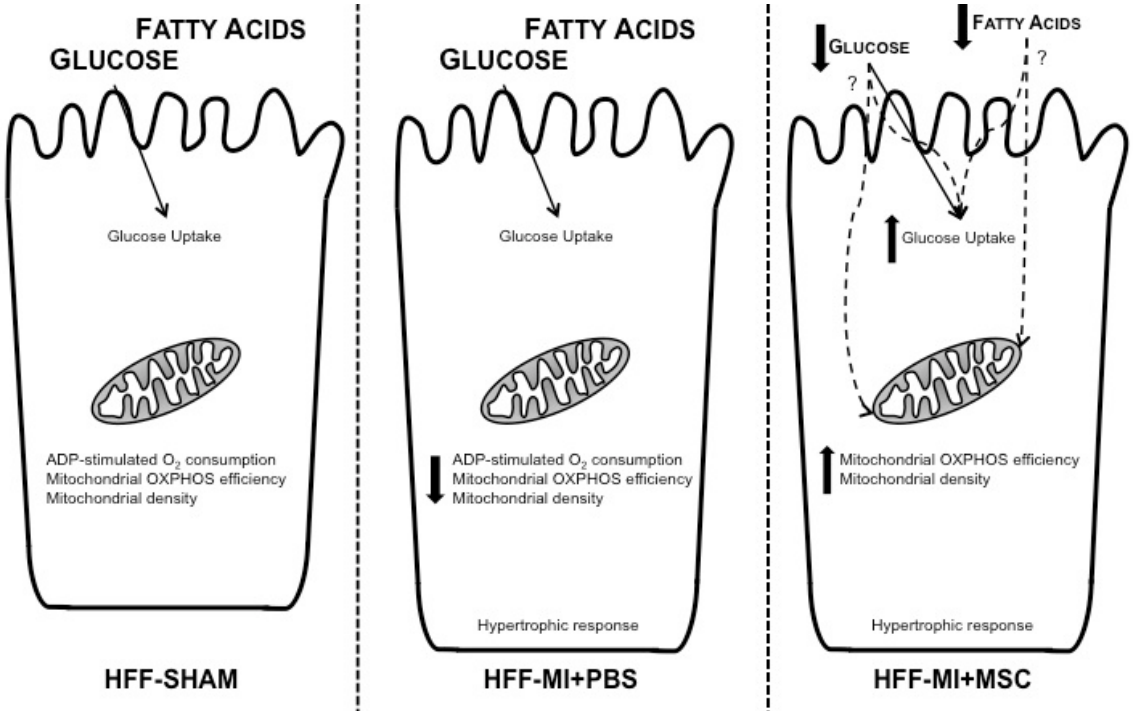

Figure 5.7: Thirty-six days following a myocardial infarction (MI), hearts of high-fat fed mice exhibited a reduction in mitochondrial ADP-stimulated respiration, density and efficiency. MSC-treated hearts displayed an increase in glucose uptake in response to insulin. Mitochondrial density and oxidative phosphorylation efficiency were preserved. These cardiac improvements may have been in response to the administered MSCs enhancing whole body, insulin-stimulated glucose uptake and/or lowering blood glucose and fatty acid concentrations in the fasted state.

[4]CHAPTER SIX: CHARACTERIZING MITOCHONDRIAL OXIDATIVE PHOSPHORYLATION IN 'SUPERHEALER' MESENCHYMAL STEM CELLS

6.1 Introduction

Advances in stem cell therapy for treating a myocardial infarction (MI) are impeded by inadequate survival and engraftment of implanted cells in the host tissue. Up to 99% of mesenchymal stem cells (MSCs) experience cell death following administration into the infarcted heart (90, 335). A predominant factor for the poor survival is ischemia (118, 269). Ischemia results in ATP depletion, a reduction in mitochondrial oxidative phosphorylation (OXPHOS) and increased reliance on glycolysis leading to cellular acidosis and cell death (269).

The bone marrow-derived '*Superhealer*' MRL/MpJ MSC (MRL-MSC) has been reported to exhibit greater engraftment in the infarcted heart (8). This improved retention promoted superior cardio-protection as indicated by increased angiogenesis, reduced infarct size and improved contractility in a murine MI model (8). The primary contributor of MRL-MSC-mediated wound repair and cardiac contractile improvements was identified as the paracrine/autocrine factor, secreted frizzled-related protein 2 (sFRP2) (8, 9). sFRP2 is a member of the secreted frizzled-related protein (sFRP) family that exhibits a cysteine-rich domain that binds Wnt glycoproteins (102). sFRP binding diminishes Wnt interactions with frizzled receptors, which propagate apoptosis through

[4] A version of this chapter has been published. Hughey, C.C., Alfaro, M.P., Belke, D.D., Rottman, J.N., Young, P.P., Wasserman, D.H., Shearer, J. Increased oxygen consumption and energetic reserve in 'superhealer' mesenchymal stem cells. *Cell Regeneration*. 2012 June 28;1:3. doi:10.1186/2045-9769-1-3.

the canonical β-catenin pathway (372). In addition to its involvement in apoptosis, Wnt/β-catenin signalling promotes a switch in glucose metabolism from OXPHOS to glycolysis (47).

Given the infarcted region of the heart receives impaired oxygen and nutrient supply, the current study evaluates MSC OXPHOS to determine whether innate differences in the MRL-MSC oxygen utilization and mitochondrial energetics could explain their enhanced viability.

6.2 Materials and methods

6.2.1 Mesenchymal stem cells and cardiac myocytes

The University of Calgary and Vanderbilt University Animal Care and Use Committees approved procedures. Murine WT- and MRL-MSCs were generated and expanded from C57BL/6 and MRL/MpJ strains, respectively, as described (8, 339). Briefly, WT- and MRL-MSCs were cultured in a humidified atmosphere containing 5% CO_2 at 37°C in low glucose Dulbecco's Modified Eagle Medium (DMEM; GIBCO) containing 1000 mg/L glucose, 110 mg/L sodium pyruvate, 10% defined fetal bovine serum (FBS; HyClone), 10% penicillin-streptomycin, 10% fungizone and 10 μg/L platelet-derived growth factor-ββ (PDGF-ββ; R&D Systems). The immunophenotype of MSCs were $CD44^+$, $LY6A/E/Sca1^+$, $CD45^-$, $CD14^-$, $CD11b^-$, $CD16/32^-$, $CD144^-$ and $CD146^-$ as previously reported (8). MSC capacity for trilineage differentiation was confirmed as previously described (8). Passages 4 through 14 were used for all measurements. Primary cardiac myocytes from ten week-old, male, CD-1 mice were isolated using a collagenase digestion method as previously described (21).

6.2.2 Mitochondrial respiration

Cellular respiration was measured using the Oxygraph-2k (Oroboros Instruments) at 37°C. Experiments evaluating intact cell respiration were performed with MSCs suspended in culture medium consisting of low glucose DMEM (GIBCO) containing 1000 mg/L glucose and 110 mg/L sodium pyruvate. Experiments evaluating permeabilized cell oxygen consumption were performed with MSCs suspended in a mitochondrial respiration medium (MiR05) containing 0.5 mM EGTA, 3 mM $MgCl_2.6H_2O$, 20 mM taurine, 10 mM KH_2P0_4, 20 mM HEPES, 1 g/L BSA, 60 mM potassium-lactobionate, 110 mM sucrose, pH 7.1 (111).

A phosphorylation control protocol was performed to assess intact cell respiration (109). Without substrate addition, routine respiration (R_{DMEM}) was determined. Oligomycin (2 μg/ml) evaluated futile oxygen flux (LEAK) (141). Maximal capacity of the electron transfer system (ETS) was evaluated via the step-wise (0.5 μM steps) titration of carbonyl cyanide-p-trifluoromethoxyphenylhydraz-one (FCCP). All respiratory states were corrected for residual/non-mitochondrial oxygen consumption (0.5 μM rotenone and 2.5 μM antimycin A).

Digitonin-permeabilized cell analysis was employed to assess complexes I and II. Optimal digitonin concentrations required to permeabilize MSCs were determined as previously outlined (110). Cardiac myocytes were permeabilized with digitonin as indicated by Liu et al. (190). Routine respiration (R_{MiR05}) was identified in MiR05. State 2 respiration (V_{CI}) was assessed by the addition of complex I substrates glutamate (10 mM) and malate (2 mM). ADP (5 mM) induced state 3 respiration/maximal oxygen consumption ($V_{MAX\text{-}CI}$). A subsequent titration of succinate (10 mM) allowed for

evaluation of state 3 respiration by convergent electron input. Convergent electron input is defined as electrons being passed through a series of oxido-reduction reactions from both complex I and II to the Q-junction which is followed by the flow of electrons through complex III, cytochrome *c* and complex IV (107). Inhibition of complex I with 0.5 μM rotenone revealed succinate-supported respiration ($V_{MAX\text{-}CII}$). The respiratory control ratio (RCR) was defined as $V_{MAX\text{-}CI}$ relative to V_{CI}. A titration of 10 μm cytochrome *c* evaluated intactness of the outer mitochondrial membrane and provided quality control for the digitonin-permabilized cell preparations.

6.2.3 Glucose deprivation and ischemic culture conditions

WT-and MRL-MSCs were plated at a density of 3000 cells/cm^2 on 58 cm^2 dishes (Nunc) for two days under the previously described conditions. The cells were washed with Dulbecco's phosphate buffered saline (GIBCO) and randomly segregated into three groups: control, glucose-deprived and ischemic. Control cells were cultured in a humidified atmosphere of 5% CO_2 and 37°C in low glucose DMEM (GIBCO) containing 1000 mg/L glucose, 110 mg/L sodium pyruvate, 10% defined fetal bovine serum (FBS; HyClone), 10% penicillin-streptomycin, 10% fungizone and 10 μg/ml platelet-derived growth factor-ββ (PDGF-ββ; R&D Systems). Glucose-deprived cells were cultured at 5% CO_2 and 37°C in no glucose DMEM (GIBCO) supplemented with 10 mg/L glucose, 1.1 mg/L sodium pyruvate, 10% penicillin-streptomycin, 10% fungizone creating conditions of 1% glucose and pyruvate compared to the control group. Ischemic conditions were identical to the glucose-deprived MSCs with the addition of 12 ml of sterile mineral oil (Sigma) creating an oil layer of approximately 5 mm over the cells to induce an oxygen-deprived environment. The WT-and MRL-MSCs remained under

these conditions for 48 hours prior to further analysis. The length of culture conditions was chosen to provide the most relevance to cell-based therapy for the infarcted heart. Intramyocardial injection of stem cells into the acutely infarcted heart has been reported to result in approximately 40-50% retention (of total transplanted cells) one to two hours following transplantation (189, 269, 332). The initial attrition of cells within two hours of delivery via direct intramyocardial injection is largely the consequence of cell leak from the injection site, being "washed away" by local bleeding resulting from the injection and/or being expelled by myocardium contraction (332). Of the cells remaining in the cardiac tissue, further cell death/loss occurs in the first 48 hours (1-25% of total transplanted cells are retained) with cell death stabilizing by seven days following delivery (189, 269, 332).

6.2.4 Flow cytometry

Flow cytometry (Guava easyCyte 6HT 2L; Millipore) was employed to measure the level of apoptosis induced by simulated glucose deprivation and ischemia. FlowCellect MitoLive Kit (Millipore) was performed according to the manufacturer's instructions to detect three cellular states: Healthy, viable cells (intact mitochondrial membrane potential and intracellular esterase activity), early apoptosis (impaired mitochondrial membrane potential) and late apoptotic/cell death events (impaired mitochondrial membrane potential and intracellular esterase activity). Mitosense red with an excitation/emission wavelength of 640/650 nm is employed by the FlowCellect MitoLive Kit (Millipore) to evaluate mitochondrial membrane potential. Calcein, acetoxymethlester (AM) is cell permeant and non-flurorescent. This compound is hydrolyzed by intracellular esterases to a fluorescent anion calcein with an

excitation/emission wavelength of 488/525 nm, which is utilized by the FlowCellect MitoLive Kit (Millipore) to assess cellular vitality.

6.2.5 Statistical analyses

One-way ANOVA and Two-way ANOVA were utilized to assess statistical differences ($p < 0.05$). Differences within the ANOVAs were determined using Tukey's post hoc. Data are reported as means ± SEM.

6.3 Results

6.3.1 Elevated intact MRL-MSC oxygen consumption

The initial incubation in culture medium allowed for determination of R_{DMEM}. R_{DMEM} in WT-MSCs was 33.1 ± 2.5 pmol O_2/s/10^6 cells (Figure 6.1A). MRL-MSC R_{DMEM} was elevated at 69.4 ± 3.9 pmol O_2/s/10^6 cells (Figure 6.1A). Oligomycin-induced LEAK respiration allowed for determination of non-ADP phosphorylating oxygen utilization. LEAK respiration was similar between WT-MSCs compared to the MRL-MSCs, 11.7 ± 1.2 vs. 20.0 ± 1.6 pmol O_2/s/10^6 cells (Figure 6.1A). Maximal capacity of the electron transport system (ETS) differed between cell types. In intact WT-MSCs, the ETS of 54.4 ± 7.4 pmol O_2/s/10^6 cells was lower than the MRL-MSCs ETS of 190.1 ± 15.3 pmol O_2/s/10^6 cells (Figure 6.1A). These results indicate that absolute oxygen flux in the routine respiratory state and maximal respiratory rate are elevated in the MRL-MSCs.

LEAK respiration operates at 0.25 ± 0.05 of ETS in the WT-MSCs compared to 0.11 ± 0.01 of ETS in MRL-MSCs (Figure 6.1B). This indicates a higher portion of maximal electron transport system capacity is used for futile reactions in WT-MSCs. The

LEAK/R_{DMEM} ratio was not altered between cell types. LEAK oxygen flux was 0.36 ± 0.04 of WT-MSC R_{DMEM} compared to 0.31 ± 0.02 of MRL-MSC R_{DMEM} (Figure 6.1B). R_{DMEM} functions at 0.65 ± 0.06 of ETS in WT-MSCs, which was significantly higher than the R_{DMEM}/ETS ratio of 0.35 ± 0.01 exhibited by MRL-MSCs (Figure 6.1B). The lower R_{DMEM}/ETS ratio in the MRL-MSCs indicates that the '*Superhealer*' cell type display a greater potential electron transport capacity in excess of routine requirements.

Figure 6.1 Oxygen flux in intact mesenchymal stem cells

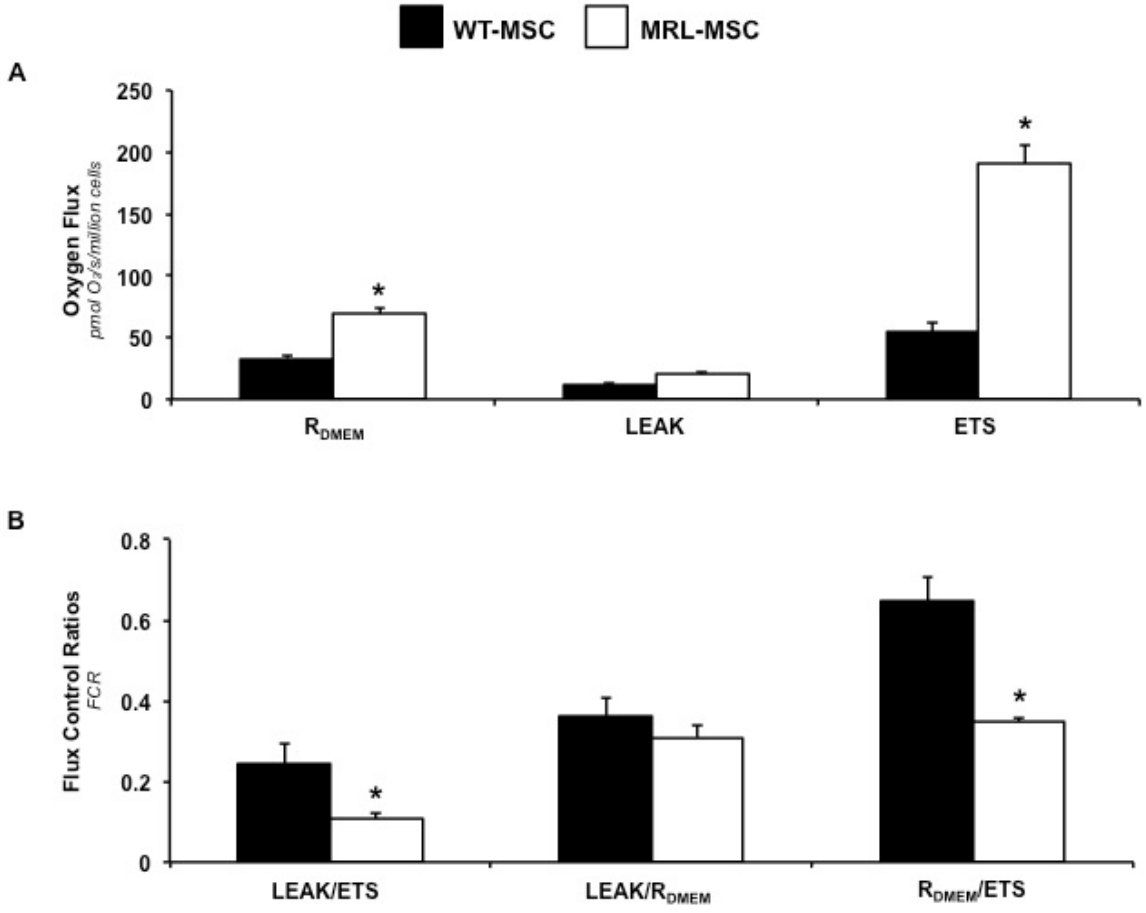

Figure 6.1: (A) R_{DMEM}, LEAK and ETS oxygen consumption in intact WT-MSC and MRL-MSC. R_{DMEM} represents routine respiration, LEAK represents oxygen consumption independent of ADP phosphorylation and ETS indicates maximal electron transport capacity. (B) Flux control ratios (FCR). Ratios of oxygen flux in differing respiratory control states, normalized to a defined reference respiratory state. n=6, data are mean ± S.E.M. *$p<0.05$ vs. WT-MSC.

6.3.2 Superior permeabilized MRL-MSC oxygen flux

Oxygen consumption in permeabilized cells was evaluated to obtain a greater understanding of the OXPHOS function. Suspension of intact MSCs in MiR05 did not change routine respiration. R_{MiR05} remained significantly lower in the WT-MSCs, 37.3 ± 4.7 vs. 63.5 ± 3.3 pmol O_2/s/10^6 cells (Figure 2A). State 2 respiration (V_{CI}), was similar between WT- and MRL-MSCs. WT-MSC state 2 respiration was 11.4 ± 0.6 pmol O_2/s/10^6 cells compared to the MRL-MSC respiration of 21.8 ± 2.7 pmol O_2/s 10^6 cells (Figure 2A). Following the addition of ADP, state 3 (V_{MAX-CI}) was lower in the WT-MSCs compared to the MRL-MSCs, 90.0 ± 13.0 vs. 112.0 ± 2.7 pmol O_2/s/10^6 cells (Figure 2A). In addition, state 3 in WT-MSCs supported by succinate alone ($V_{MAX-CII}$) was 102.0 ± 2.8 pmol O_2/s/10^6 cells. This was significantly lower than the $V_{MAX-CII}$ exhibited by MRL-MSCs, 140.1 ±5.7 pmol O_2/s/10^6 cells (Figure 2A). As a comparison, isolated cardiac myocyte oxygen flux was higher than that of both WT- and MRL-MSCs. Isolated, cardiac myocyte V_{CI}, V_{MAX-CI} and $V_{MAX-CII}$ were 1.44 ± 0.24, 6.84 ± 1.08 and 18.33 ± 2.18 nmol O_2/s/10^6 cells, respectively (Inset, Figure 2B). Additionally, the RCR did not differ between WT- and MRL-MSCs (Figure 2C).

Figure 6.2 Oxygen flux in permeabilized mesenchymal stem cells

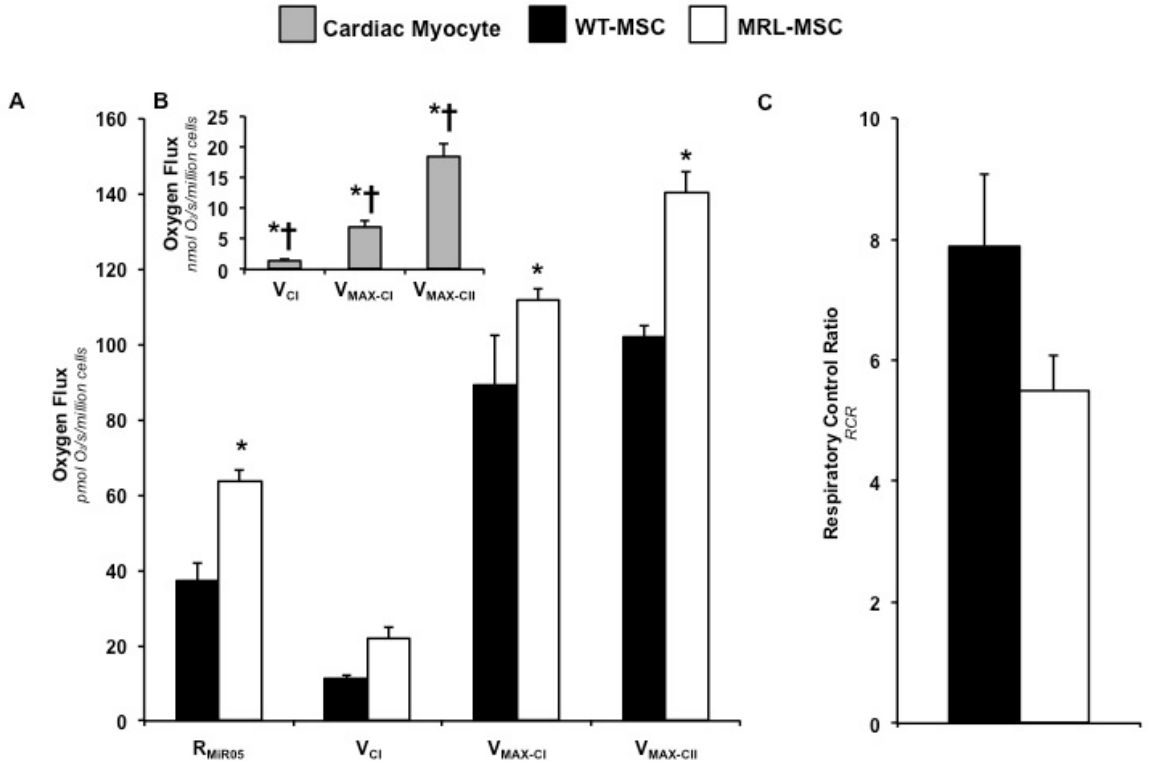

Figure 6.2: (A) Routine respiration in MiR05 (R_{MiR05}) in intact MSCs. State 2 oxygen consumption through Complex I supported by glutamate and malate (V_{CI}) in digitoin-permabilized MSCs. State 3 or maximal oxygen consumption through Complex I supported by glutamate and malate ($V_{MAX\text{-}CI}$) in digitoin-permabilized MSCs. State 3 or maximal oxygen consumption through Complex II supported by succinate ($V_{MAX\text{-}CII}$) in digitoin-permabilized MSCs. (B) Given MSCs are transplanted into the infarcted heart, isolated, primary cardiac myocyte oxygen utilization is provided as a metabolic reference state. Cardiac myocyte state 2 oxygen consumption through Complex I supported by glutamate and malate (V_{CI}) in digitoin-permabilized cardiac myocytes. State 3 or maximal oxygen consumption through Complex I supported by glutamate and malate ($V_{MAX\text{-}CI}$) in digitoin-permabilized cardiac myocytes. State 3 or maximal oxygen

consumption through Complex II supported by succinate ($V_{MAX\text{-}CII}$) in digitoin-permabilized cardiac myocytes. (C) Respiratory control ratio (RCR; defined as $V_{MAX\text{-}CI}/V_{CI}$). n=6-9, data are mean ± S.E.M. *p<0.05 vs. WT-MSC. †p<0.05 vs. MRL-MSC.

6.3.3 Increased MRL-MSC viability following glucose and oxygen deprivation

Manipulation of culture conditions to simulate 48 hours of glucose deprivation exhibit a clear induction of early apoptosis defined by mitochondrial membrane potential impairment (Figure 6.3A and 6.3B). WT-MSCs under glucose deprivation-only conditions for 48 hours resulted in a drastic increase in early apoptosis (43.61 ± 7.59% vs. 2.57 ± 0.69%; Figure 6.3B). The effect of glucose deprivation on MRL-MSCs also resulted in an increased percentage of cells undergoing early apoptosis (8.02 ± 1.37% vs. 1.16 ± 0.69%; Figure 6.3B). However, the proportion of mitochondrial membrane impaired MRL-MSCs was significantly lower than that of WT-MSCs following glucose deprivation (8.02 ± 1.37% vs. 43.61 ± 7.59%; Figure 6.3B). Interestingly, ischemic culture conditions did not promote significant increases in early apoptotic WT-MSCs or MRL-MSCs compared to control MSCs (Figure 6.3B). Furthermore, the reduced oxygen availability may have provided a mitochondrial protective effect in the presence of glucose deprivation as the WT-MSCs (43.61 ± 7.59% vs. 6.29 ± 2.55%; Figure 6.3B) and MRL-MSCs (8.02 ± 1.37% vs. 1.11 ± 0.47%; Figure 6.3B) exhibited elevated early apoptosis in the glucose-deprived condition compared to the ischemic condition.

Simulated 48 hours of glucose deprivation and ischemia *in vitro* resulted in late apoptosis/cell death defined by impaired mitochondrial membrane potential and cellular activity (Figure 6.3A and 6.3C). WT-MSC exposure to reduced glucose for two days

showed an increase in late apoptosis (7.47 ± 1.28% vs. 1.04 ± 0.69%; Figure 6.3C). Glucose deprivation did not evoke alterations in the percentage of MRL-MSC undergoing late apoptosis (2.08 ± 0.18% vs. 0.38 ± 0.21%; Figure 6.3C). The combination of decreased oxygen and substrate availability showed an increase in WT-MSCs (9.01 ± 2.19% vs. 1.04 ± 0.69%; Figure 6.3C) and MRL-MSCs (2.33 ± 0.87% vs. 0.38 ± 0.21%; Figure 6.3C) late apoptosis/cell death compared to control conditions (Figure 6.3B). However, the proportion of dead MRL-MSCs was significantly lower than that of WT-MSCs following the 48 hour ischemia (2.33 ± 0.87% vs. 9.01 ± 2.19%; Figure 6.3B). In summary, the aforementioned experiments evaluated WT-and MRL-MSCs early and late apoptosis following two days of depressed substrate availability or ischemia *in vitro*. Our results suggest MRL-MSC exhibited a lower rate of apoptosis compared to WT-MSCs under nutrient deprivation. Such characteristics may be transferable to the *in vivo* conditions of the infarcted heart allowing for greater MRL-MSC survival and a subsequent increase in their therapeutic effects.

Figure 6.3 MSC survival following 48 hours of limited glucose and oxygen

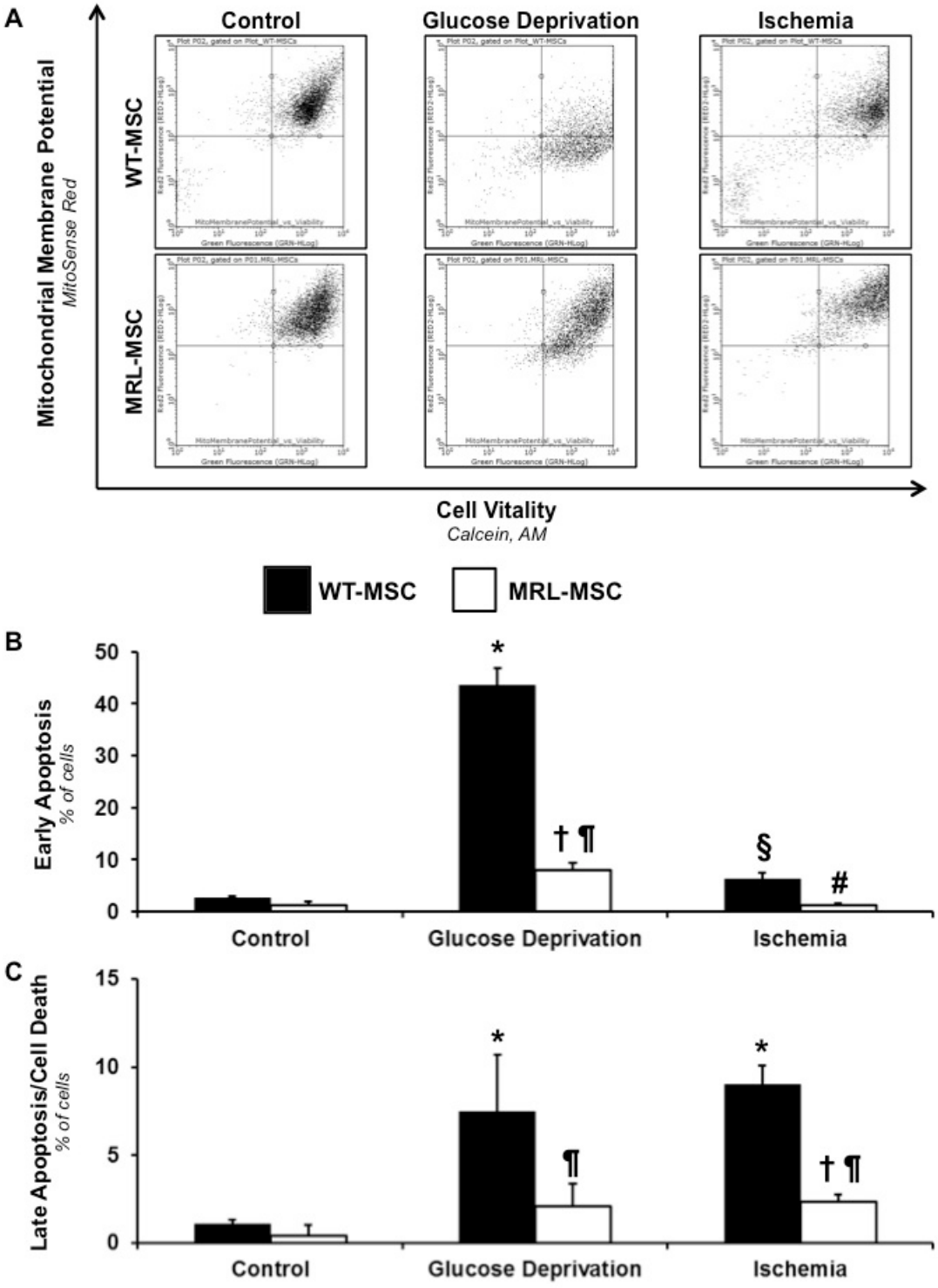

Figure 6.3: (A) Representative fluorescence-activated cell sorting analysis of apoptotic cells after mitosense red and calcein, AM staining. Healthy, viable MSCs are mitosense red^{+}/calcein, AM^{+}. The mitosense red^{-}/calcein, AM^{+} MSCs are in the early apoptotic phase, whereas the mitosense red^{-}/calcein, AM^{+} MSCs are in the late apoptotic/cell death phase. (B) Quantitation of MSC early apoptosis induced by two days of glucose deprivation and ischemia with mitosense red and calcein, AM staining. The graph shows the percentage of all MSCs that are mitosense red^{-}/calcein, AM^{+} MSCs after glucose deprivation and ischemia. (C) Quantified MSC late apoptosis/cell death induced by 48 hours of glucose deprivation and ischemia with mitosense red and calcein, AM staining. The graph shows the percentage of all MSCs that are mitosense red^{-}/calcein, AM^{-} MSCs after glucose deprivation and ischemia. n=6-7 independent experiments, data are mean ± S.E.M. *$p<0.05$ vs. WT-MSC Control. †$p<0.05$ vs. MRL-MSC Control. ¶$p<0.05$ vs. WT-MSC of identical experimental conditions. §$p<0.05$ vs. WT-MSC Glucose Deprivation. #$p<0.05$ vs. MRL-MSC Glucose Deprivation.

6.4 Discussion

Upon transplantation, MRL-MSCs exhibit increased engraftment and survival in the infarcted heart compared to WT-MSCs (8). We aimed to evaluate innate differences in mitochondrial function between these cell types to explain differences in cell viability. Novel findings identify unique energetic characteristics of MRL-MSCs that would be protective in glucose-compromised and ischemic environments.

Assessment of oxygen utilization in the intact cell allowed for the determination of physiological respiratory states. MRL-MSCs displayed similar LEAK respiration,

however, routine respiration and maximal electron transport capacity were greater. In order to eliminate the potential confounding influence of mitochondrial density, flux control ratios (FCR) were evaluated. Results revealed a lower LEAK and routine respiration as a proportion of maximal electron transport capacity in MRL-MSCs. This suggests the presence of higher electron transport capacity in MRL-MSCs. To identify regulatory factors responsible for the increased OXPHOS potential, two major sites of electron input into the electron transport system (complex I and complex II) were examined. In the presence of ADP, oxygen flux through complex I was higher in the MRL-MSCs. Because complex I is not the only site of electron input into the electron transport system, succinate-supported, maximal respiration was determined. This complex II-mediated oxygen flux was higher in the MRL-MSCs and indicates a greater aerobic energy production in the MRL-MSCs. Given the MSCs are transplanted into the heart, we also assessed the oxygen consumption of primary cardiac myocytes to provide a metabolic reference state to which MSC oxygen utilization could be compared. Relative to the WT-MSCs, cardiac myocyte V_{CI}, $V_{MAX\text{-}CI}$ and $V_{MAX\text{-}CII}$ were 127-, 77- and 180-fold greater, respectively. This indicates the oxidative capacity of MSCs is relatively minor in comparison to that of cardiac myocytes and the MRL-MSC respiration is only modestly higher than WT-MSCs. The mechanism responsible for the increased intact cell oxidative function and permeabilized cell complex I- and II-supported respiration in the MRL-MSCs is currently unknown. Given the role of sFRP2 in modulating apoptosis and glucose metabolism, future experiments evaluating the effect of sFRP2 on mitochondrial OXPHOS in the WT-and MRL-MSCs is a notable, initial mechanistic target.

Several reports conclude WT-MSCs preferentially derive energy from glycolysis with little dependence on glucose oxidation (64, 196, 228). We report MRL-MSCs exhibit elevated absolute OXPHOS function ($R_{DMEM/MiR05}$, V_{MAX-CI}, $V_{MAX-CII}$ and ETS) and higher OXPHOS potential (R_{DMEM}/ETS). Based on these observations we propose the slight elevation in OXPHOS displayed by the '*Superhealer*' MRL-MSCs is advantageous. For instance, in MSCs, there is a shift towards OXPHOS dependence under glucose deprivation (191). The increase in oxidative function is thought to be an adaptive attempt to maximize ATP synthesis in the nutrient shortage given glucose oxidation produces more ATP per mole of glucose than glycolysis (326). To evaluate this hypothesis we cultured WT-and MRL-MSCs under glucose-deprived conditions for 48 hours where oxygen was not limiting. We found that WT-and MRL-MSCs displayed a reduction in mitochondrial membrane potential; an early indicator of apoptosis (98). However, WT-MSCs exhibited a significantly higher proportion of cells with diminished mitochondrial membrane potential compared to MRL-MSCs. Additionally, the percentage of late apoptotic/dead cells was also higher in WT-MSCs compared to the MRL-MSCs following the reduced glucose conditions. The elevated routine oxygen flux and electron transport capacity in MRL-MSCs may provide benefits when faced with a lack of substrate by better accommodating the switch towards oxidative metabolism. This could assist in preservation of ATP levels and prevent energetic starvation. Furthermore, a potential for increased coupling of glycolysis to glucose oxidation in MRL-MSCs could minimize intracellular acid load and improve cell viability in the infarcted heart.

Recently, reports indicate that substrate deprivation is much more detrimental to MSC survival than hypoxia (64, 228). To expand on our glucose deprivation studies we assessed MSC apoptosis following 48 hour of ischemia (glucose and oxygen deprivation). Under the ischemic conditions, WT- and MRL-MSCs showed an elevated proportion of late apoptotic/dead cells. However, there was no added effect of depressed oxygen availability on late apoptosis/cell death over reduced glucose availability. These findings are consistent with the reports that substrate availability and not hypoxia is more influential in MSC viability. Also, the percentage of late apoptotic cells was elevated in the WT-MSCs compared to the MRL-MSCs which are in agreement with studies indicating MRL-MSC exhibit increased engraftment and survival in the infarcted heart (8).

Interestingly, ischemia had an unexpected influence on impaired mitochondrial membrane potential/early apoptosis. The portion of early apoptotic WT-and MRL-MSCs was significantly lower following 48 hours of combined substrate and oxygen reduction compared to early apoptotic cells under decreased glucose-only conditions. The mechanism for this finding is currently unclear. It is possible that the oxygen deprivation results in a compensatory reduction in MSC oxidative metabolism thereby exhibiting a protective effect on the MSCs by finding a unique compromise between OXPHOS and glycolysis that provides a more optimal balance between ATP synthesis, glycolysis-mediated acidosis from the lack of oxygen and reactive oxygen species-induced damage resulting from OXPHOS under high oxygen concentrations. Alternatively, it cannot be ignored that ischemia may primarily induce late apoptotic events independent of early mitochondrial dysfunction. Of note, a limitation of this study is the use of mineral oil to

induce hypoxia without measuring oxygen concentration in the culture medium. Future studies should more accurately control oxygen concentrations to identify the effect of various oxygen levels in combination with substrate deprivation on mitochondrial-induced apoptosis.

6.5 Conclusion

In summary (Figure 6.4), little attention has been given to the optimal metabolic characteristics that would allow transplanted cells to cope with oxygen and glucose deprivation. We found MRL-MSCs display elevated OXPHOS that may minimize metabolic stress and subsequently improve cell viability upon transplantation into the infarcted heart.

Figure 6.4 Schematic representation of mitochondrial physiology that may influence MSC viability upon transplantation into the infarcted heart

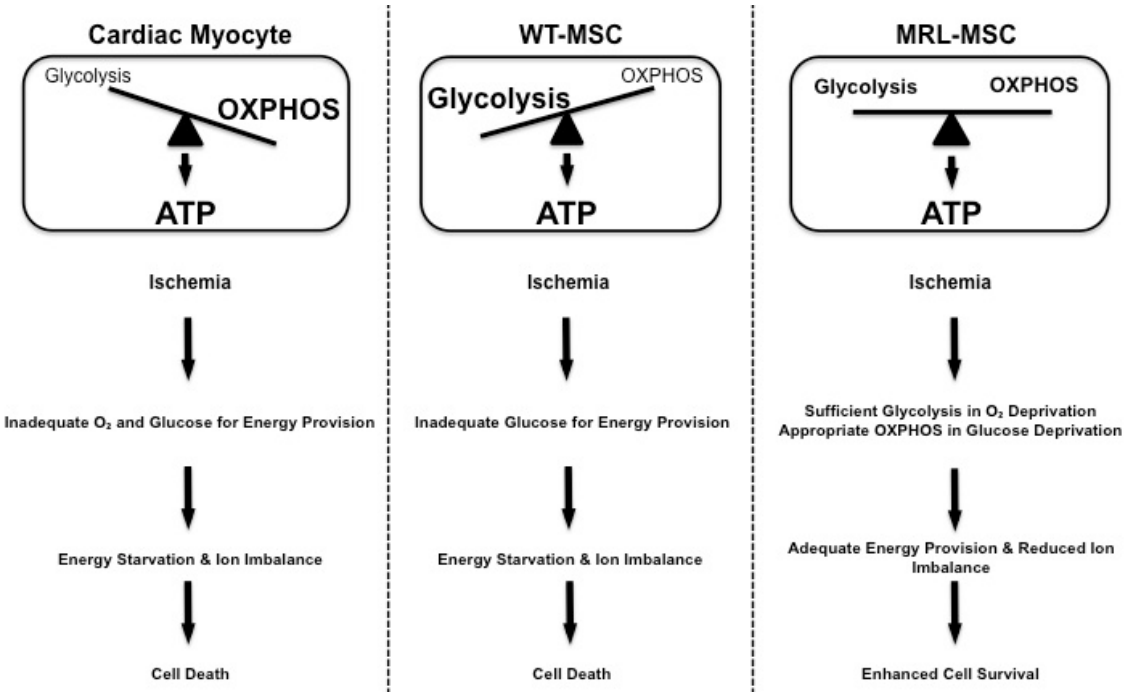

Figure 6.4: The modest increase in electron transport capacity of the MRL-MSC may provide oxidative phosphorylation (OXPHOS) flexibility to better adapt to the compromised glucose and oxygen availability characterizing the infarct region of the heart following transplantation. This phenotype may improve the ability of the MRL-MSC to meet its ATP requirements, lessen ischemia-induced dissipation of ion homeostasis and improve cell survival.

CHAPTER SEVEN: CONCLUSIONS AND GENERAL DISCUSSION

7.1 Introduction

As indicated throughout this dissertation, the infarcted heart is characterized by alterations in substrate utilization and mitochondrial oxidative phosphorylation (OXPHOS) that may compromise efficient and absolute ATP synthesis. It has been proposed that the altered metabolism limits contractile function and could exacerbate the potential transition to heart failure. Although evidence for a causal role remains elusive, there is growing appreciation for the potential importance of cardiac metabolism in ischemic heart disease. The European Society of Cardiology guidelines on the management of patients with stable angina acknowledge the use of metabolic therapies such as Trimetazidine (1-[2,3,4-trimethoxybenzyl] piperazine dihydrochloride) as an effect adjunctive therapy in improving cardiac physical performance and reducing pain (65). Trimetazidine is a pharmacological agent that lessens fatty acid β-oxidation by inhibiting long chain 3-ketoacyl-CoA thiolase (5, 193). This relieves some of the inhibitory effect that fatty acid utilization has on glucose oxidation and allows the heart to use the more oxygen efficient substrate (5, 193). While reducing cardiac metabolic flexibility and promoting the heart to utilize a single substrate such as glucose may not be an optimal long-term solution to cardiac dysfunction (173, 340), the growing acceptance that cardiac metabolism may be a viable therapeutic target in addition to current medical interventions is exciting for metabolic researchers.

Mesenchymal stem cell (MSC) transplantation as a regenerative medicine to replace lost tissue following a myocardial infarction (MI) has not achieved initial

expectations, however, the exogenous cell therapy consistently minimizes cardiac dysfunction post-MI in human and animal studies. This functional improvement is encouraging that with a greater understanding as to how the MSCs confer such benefit the MSC therapy may be optimized for further superior outcomes. As such, the major aim of work presented in this dissertation was to evaluate the efficacy of MSC therapy to lessen metabolic aberrations post-MI as a potential means through which cardiac performance is mended. Secondarily, this thesis assessed mitochondrial characteristics of MSCs that may assist in enhancing viability upon transplantation into the infarcted heart.

This final chapter will commence with a summary of the strengths, limitations, and rationale for the methodology employed. Additionally, an overview and interpretation of the findings, proposed future scientific pursuits, and the significance of the completed work are provided.

7.2 Strengths and limitations of experimental protocols

7.2.1 Left anterior descending coronary artery ligation model

Models of permanent coronary artery ligation in the mouse were initially employed to gain insight into the pathophysiology of post-MI remodelling and dysfunction (243). Given the goal of regenerative medicine is to replace the lost tissue via exogenous cell administration, stem cell therapy researchers find this MI model attractive as the chronic ligation consistently results in tissue necrosis and ventricular function is largely dependent on the infarct size induced due to the acute nature of insult onset (251).

Evidence of the ability of MSC therapy to augment cardiac glucose uptake in the post-MI heart is conflicting. Reports have indicated minimization in cardiac dysfunction following cell transplantation is associated with the reduction and elevation in cardiac glucose uptake post-MI (113, 208, 209). This may be the result of differing degrees of insult. In the C57BL/6 mouse the LAD follows a branching pattern that supplies the free wall of the left ventricle and apex (284). As such, ligating the LAD closer to the atria creates a larger infarct compared to an occlusion completed near the apex (7). This logic was employed in the current dissertation as Chapter 3 employed a LAD ligation closer to the apex than in Chapter 4. Of note, infarct size was not evaluated in the studies. However, there was a further 15-25% decline left ventricle systolic function induced by the MI event in Chapter 4 compared to Chapter 3 suggesting a larger infarct size.

Another pursuit of the current dissertation was to identify regional heterogeneity of insulin-mediated glucose uptake in the infarcted heart. One of the areas of interest was the peri-infarct region. In the clinical setting, tissue salvage and infarct size reduction is based on the assumption that the core of the infarct is severely ischemic and necrotic (121). Moreover, this core is surrounded by an area of jeopardized tissue called the peri-infarct region that can be salvaged by reperfusion efforts (121). In experimental ligation models this is not observed. Rather than a progressive transition from infarct to viable tissue there is an abrupt, but irregular, changeover from ischemic zone to perfused, viable tissue (121, 217). This is an advantage to the studies conducted in Chapter 3, 4 and 5 as this model lessens the role of compromised blood flow as a prominent regulator of insulin-stimulated glucose uptake following the MI event (352). Thus, more focus can be given to the membrane and glucose phosphorylation components of glucose uptake.

7.2.2 Dietary intervention

The first experimental documentation of high-fat feeding as a nutritional intervention was in 1959 by Masek and Fabry (39, 207). Numerous subsequent studies have displayed a high-fat diet promotes the gradual onset of hyperglycemia, hyperlipidemia, a decrease in whole body and tissue-specific insulin responsiveness, and adaptive β-cell function (12, 39, 55, 237, 297). As such, high-fat feeding is a commonly employed in rodent models to mimic metabolic phenotypes that characterize human type 2 diabetes. Chapter 5 experimental protocol involved feeding C57BL/6 mice a high-fat diet for eight weeks prior to the MI event and 13 weeks in total. The fat source was animal-based (lard) and 60% of calories consumed were by fat. The 13 weeks of high-fat feeding was chosen based on previous work in our laboratory having identified this dietary intervention to reproducibly precipitate insulin resistance, hyperglycemia, hyperlipidemia, and hyperinsulinemia compared to chow fed mice by 12 weeks of the high-fat diet being consumed (96, 298).

In addition, ad libitum feeding of mice a high-fat diet with 55-60 % of the caloric content being derived from fatty acids induces cardiovascular irregularities. After 16 weeks of high-fat feeding, systolic and diastolic blood pressure is markedly elevated compared to chow fed mice (11% calories by fat) (170). Park et al. (239) identified C57BL/6 mice to exhibit impaired systolic performance following 20 weeks of high-fat feeding as indicated by fractional shortening. The decline in fractional shortening displayed by C57BL/6 mice has also been observed in our laboratory at 20 weeks of high-fat feeding (Figure 7.1).

Figure 7.1 Fractional shortening following 20 weeks of high-fat feeding

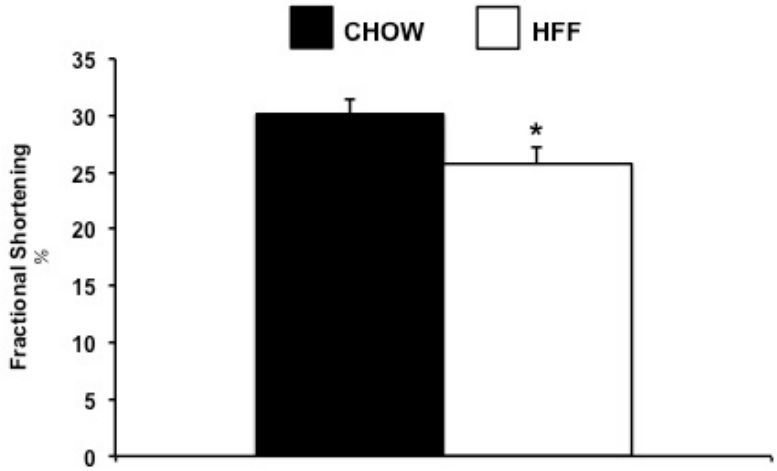

Figure 7.1: Fractional shortening (%) in chow fed (CHOW) mice (13.5% of calories from fat) compared to high-fat fed (HFF) mice (60% of calories from fat) following 20 weeks of high-fat feeding. Of note, mice were sedated with isoflurane and placed in the supine position during the acquisition of echocardiographic images. *$p<0.05$ vs. CHOW. Data are mean ± SEM for n=10 mice per group.

The above characteristics of high-fat feeding in mice provide some resemblance of the metabolic and cardiac dysfunction identified in individuals with type 2 diabetes and make it an appealing means of studying the gene-environment interactions that increase the risk of developing diabetes-related complications. However, there are obvious limitations that have often been highlighted by opponents of utilizing high-fat feeding-induced insulin resistance models. First, the source of fat such as that derived from animals or plants and the fraction (20-60 % of calories) of fat used in the literature varies extensively (233, 238). This macronutrient complexity makes interpretation of the exact metabolic aberrations promoted and the temporal onset of these alterations difficult

to summarize and compare between laboratories. Another drawback that is commonly proposed is that high-fat alone is not complex enough to adequately model the human diet (233, 238). For example, high carbohydrate composition and the use of artificial additives have been used alone or in combination with high-fat feeding to induce diabetes-associated alterations (56, 233, 238). Finally, in mice, diagnostic criteria are not generally employed to identify type 2 diabetes (211). Instead a comparative approach is used to highlight statistical differences between the intervention and control groups. Given this, McMurray et al. (211) have proposed that part of the definition of diabetes in mice be that plasma glucose concentrations following a four to six hour fast be greater than 20 mM. Such overt hyperglycemia is not regularly reported in mice fed a high-fat diet (233) and the proposed criteria would make it difficult to attribute abnormal metabolic processes to pathological glucose handling in high-fat fed mice.

7.2.3 Intramyocardial injection of mesenchymal stem cells

The route of cell delivery to the infarcted heart is an important choice as it will influence cell retention, survival and functionally as well as effect the functional outcome of the treatment and recipient safety risks (43). Several approaches to exogenous cell administration have been utilized in animal and human studies. However, intramyocardial, intracoronary and intravenous modes of delivery are the most common employed in clinical trials (43, 353, 362).

The intramyocardial injection of MSCs into the epicardial surface of the heart was utilized in the current dissertation (Chapters 3, 4 and 5). The main disadvantages associated with intramyocardial delivery of cells to the infarcted heart revolve around patient safety. This technique requires direct exposure to the heart that is obtained

through a sternotomy or thoracotomy (43, 353, 362). In patients requiring open heart surgery such as coronary artery bypass surgery, the intramyocardial injection of exogenous cells can be used in conjunction to improve cardiac functional outcomes (373). However, the invasiveness of having to gain access to the thoracic cavity renders the intramyocardial injection less appealing to use in isolation (43, 353, 362). Also, the direct injection of cells into a single location may enhance the risk of ventricular arrhythmias (43, 97, 353, 362, 373). When using MSCs as the source of exogenous cells it has been theorized that the chance of arrhythmias is due to MSCs forming connections with host myocytes and impeding impulse propagation and/or increasing sympathetic innervation (213).

Although concerns with intramyocardial administration may limit clinical use, this delivery technique remained the most optimal for employment in the experimental studies performed in Chapter 3, 4 and 5. The induction of the MI required a thoracotomy to expose the heart and complete the coronary artery ligation. This allowed for direct visualization of the epicardial surface of the heart to transplant the MSCs without added invasiveness of an additional independent surgical procedure. The intramyocardial administration also allows for targeted localization of cells to the site of injury, circumventing the need for homing of MSCs to the infarcted region (43, 353, 362). Notably, cell retention is poor and non-specific homing to organs such as the lung, spleen and liver is observed with intracoronary, intravenous and intramyocardial transplantation (43, 130). However, direct comparison suggests that intramyocardial administration exhibits the greatest engraftment and functional improvement in the infarcted heart (130, 189, 249). Additionally, the experimental objectives of Chapter 3, 4 and 5 required a

second surgery to catheterize the infarcted mice for hyperinsulinemic-euglycemic (insulin) clamps. Of the three delivery methods commonly employed in clinical trials, the intramyocardial administration of MSCs represents the least technically challenging. This was enticing as it minimized the need for further surgical expertise to conduct a third surgery and subsequently may increase the repeatability of the experimental procedures.

7.2.4 Echocardiography

M-mode echocardiography was performed in the conscious mouse in Chapters 3, 4 and 5 as a means of assessing cardiac structure and function. This dissertation focused on the fractional shortening and ejection fraction indices obtained from echocardiographic images. Under non-pathological conditions fractional shortening and ejection fraction are often used as markers of left ventricular systolic function in experimental studies (277). Utilizing these measures to make conclusions concerning cardiac function following an MI must be made with caution (99). The spatial resolution of M-mode echocardiography is poor. More specifically, echocardiographic images used to obtain fractional shortening were taken via a single line of interrogation at the level of the papillary muscles only. Thus, fractional shortening is a linear measure being utilized to convey global function (277). Also, ejection fraction is acquired via the cubic assumption of left ventricle volume (99, 323). Ultimately, fractional shortening and ejection fraction rely on geometrical presumptions that may not maintain the same accuracy in the presence of cardiac remodelling processes and regional wall motion irregularities that may characterize the post-MI heart (99, 277, 323).

Although the shortcomings of M-mode echocardiography are not easily dismissed, this technique was utilized based on several factors that were perceived to be

worthwhile. First, fractional shortening and ejection are indices that have been utilized in human echocardiography (277). Familiarity with the experimental measures allows wider audiences with limited knowledge of the specific research area to better realize the information provided. Also, echocardiography offers the opportunity to avoid terminal experimentation. The technical challenge of successfully completing two surgical procedures (MI and catheterization) and an insulin clamp heightened the desire for a methodology that could assess systolic performance in a way that did not require the animals to be sacrificed. Moreover, the non-invasiveness of M-mode echocardiography allowed for serial measurements.

An aim of the dissertation was to perform experimental procedures in the conscious mouse, where possible, to simulate more physiological relevance. While, the single line of interrogation reduces the spatial resolution, it increases the temporal resolution of echocardiographic images (323). The heart rate of the conscious C57BL/6 mouse approaches 700 beats per minute making the high temporal resolution an appreciated strength of M-mode echocardiography (277). Furthermore, evaluating cardiac function in the conscious mouse removed the cardiodepressant actions of anaesthesia (54, 277, 278). Experimental variation in duration, type and depth of sedation may introduce artificial differences in heart rate and fractional shortening (54, 277, 278). Thus, the conscious mouse model provides an opportunity for greater repeatability (277).

7.2.5 Hyperinsulinemic-euglycemic clamp

Initially developed by DeFronzo et al. (62) for human use, the insulin clamp has been adapted to laboratory animals and is often referenced as the "gold standard" for

evaluating insulin action *in vivo* (13, 135). This is largely the result of the technique reducing a number of assumptions and confounding variables (222). First, the intravenous infusion of glucose and insulin allows the experimenter to erase the effect of differing levels of these substrates on data interpretation. Second, maintenance of euglycemia prevents counter regulatory measures in instances of hypoglycaemia following insulin administration such as hepatic glucose production. Third, insulin infusion rates between 2.5-4.0 mU/kg/min in the C57BL/6 mouse are often sufficient to impede hepatic glucose production (14). The insulin clamp can also be easily coupled to the administration of isotopic glucose and fatty acids. This allows the experimenter to extend investigation beyond systemic insulin-mediated substrate disposal to tissue-specific substrate metabolism.

In mice, no standard operating procedures exist for completing an insulin clamp. There are many variations of the insulin clamp being applied to the mouse with each having their own advantages and disadvantages. Blood sampling is most commonly performed via arterial catheterization or the tail tip (14). The methodology used in this dissertation employed carotid artery catheterization for blood sampling. Arterial sampling from catheterization lowers stress from handling (13). For example, obtaining blood from the tail may require restraining the mouse and milking the tail. This results in increased catecholamine concentrations, endogenous glucose production and whole body glucose disposal (13). Anaesthesia has been used in an effort to reduce the stress response, however, many types of sedation promote hyperglycemia (37, 255, 329). Thus, the arterial catheterization allows for experimentation in a conscious, unrestrained mouse and may assist in more closely matching the actual physiology of the mouse.

Despite the benefits of arterial catheterization, the invasiveness of the procedure can deter investigators from seeking vascular access for experimental purposes. Concern is reasonable as a subset of animals will not be available for experiments due to surgical casualties and loss of catheter patency (14). For example, across all groups in this dissertation, the loss of animals due to surgical casualties and loss of catheter patency was approximately 30%. In-experiment drawbacks include increased risk of stroke during the experiment from arterial sampling (14). Also, during the execution of the insulin clamp the activity level and changes in activity of the mouse can create difficulties in achieving euglycemia. Given this, the insulin clamp performed in the conscious, unrestrained mouse is often more labour intensive and time consuming (222).

7.2.6 Permeabilized fibers and cells

This dissertation employed chemically permeabilized cardiac fibers (Chapters 3, 4 and 5) and cells (Chapter 6) to evaluate mitochondrial function via respirometric measures. The permeabilized fiber/cell technique was utilized as it offered logistical advantages over isolated mitochondria, which currently receives more widespread use (252). Chapter 3, 4 and 5 aimed to explore peri-infarct oxygen flux. The amount of tissue needed to obtain adequate yield and quality of isolated mitochondria usually requires in excess of 100 mg (178). Tissue directly surrounding the infarct is far more limited in quantity than 100 mg given the infarcted C57BL/6 mouse heart averaged less than 180 mg in this dissertation. In contrast, the permeabilized fiber model is much more feasible to study mitochondrial function in the peri-infarct tissue as only a few milligrams of cardiac tissue is needed for experimental analysis (136). The reduced cell number requirement was also an important factor in the use of permeabilized cells in Chapter 6.

Up to 120 million cells are used to obtain appropriate quality and yield of isolated mitochondria from cultured cells (91). In contrast, a million MSCs were utilized in each individual respirometric assessment in Chapter 6.

The benefits of this technique also include increased physiological relevance in comparison to isolated mitochondria as cellular architecture is preserved. While the plasma membrane is selectively degraded, many intracellular membrane structures including mitochondria (282, 345), sarcoplasmic reticulum (345), myofilaments and the cytoskeleton (215, 283) remain unaltered. Moreover, the interactions between mitochondria and these structures (215, 283) are preserved. A method that would preserve mitochondrial interactions that may influence OXPHOS function was chosen because cardiac myocyte architectural irregularities regularly accompany post-MI remodelling and mitochondria have been reported to lose functional connections with sarcoplasmic reticulum in the infarcted heart (271, 316).

Another experimental rationale for studying mitochondria in permeabilized fibers was the increased stability. Fiber preparations may be stored in preservation solutions for at least six hours and up to 24 hours (111, 308). This was of benefit as two to four insulin clamps were executed in parallel, however, only fibers from one mouse could be evaluated at any one time due to equipment limitations.

A notable drawback in the current dissertation arises when it is acknowledged that cardiac mitochondria are heterogeneous, consisting of subsarcolemmal and interfibrillar populations. There are reports that the mitochondrial subpopulations are differentially affected in the diabetic and failing heart (271). Unfortunately, *in situ* mitochondrial

respirometry is limited in that the total mitochondrial population is evaluated without the ability to distinguish between subsarcolemmal and interfibrillar mitochondria (178).

7.3 Overall summary and interpretation of results

In concert with improved cardiac systolic performance, the principle findings were (1) intramyocardial transplantation of MSCs reduced atypical insulin-stimulated, cardiac glucose uptake in the presence and absence of diet-induced insulin resistance; (2) mitochondrial function and content were provided protection by MSC administration; (3) improvements in glucose uptake and mitochondrial OXPHOS were associated with diminished alterations in insulin signalling mediators as well as fatty acid utilization and availability; and (4) MSCs displaying higher engraftment and survival upon transplantation are characterized by greater electron transport reserve capacity. This final summary will interpret the findings from Chapters 3-6 in regards to glucose uptake, cardiac mitochondria and MSC OXPHOS.

7.3.1 Insulin-stimulated glucose uptake

Insulin clamps coupled with the administration of isotopic glucose were executed in conscious, unrestrained mice to assess whole body insulin sensitivity and tissue-specific glucose uptake. A primary objective of this dissertation was to evaluate the therapeutic efficacy of MSCs for abnormalities in cardiac glucose uptake post-MI. Three studies with an increasingly greater extent of insult were performed in an attempt to clarify the conflicting reports suggesting that MSC therapy prevents an increase in glucose uptake or conversely minimizes a decline in glucose uptake following a MI (113, 208, 209). More specifically, insulin-stimulated, cardiac glucose uptake was evaluated in

chow fed, low left anterior descending coronary artery (LAD) ligated hearts (Chapter 3), in chow fed, high LAD ligated hearts (Chapter 4), and high-fat fed (HFF), high LAD ligated hearts (Chapter 5).

Consistent across all studies (Chapter 3, 4 and 5), MSC administration lowered the extent of pathological insulin-stimulated glucose uptake in the post-MI heart. In Chapter 3, the MSC transplantation prevented an increase in the metabolic index of glucose uptake (R_g) in the remote left ventricle. In chow fed mice undergoing a LAD ligation closer to the atria (Chapter 4), the metabolic index of glucose uptake was lower in both the remote left ventricle and peri-infarct region. The MSC therapy blunted the decline in the rate of glucose uptake in the remote left ventricle but did not rescue glucose utilization in the peri-infarct region. In the presence of diet-induced insulin resistance (Chapter 5), MSC transplantation elevated the R_g in both areas of the infarcted heart assessed. It should be noted that the functional improvement in Chapter 5 is very modest despite the improvement in glucose uptake. In speculation, this may be due to the mortality following the ligation procedure (APPENDIX B). The proportion of mice succumbing to the MI in Chapter 5 was 19.5% of the MI+PBS mice and 13.0% of the MSC-treated mice. There may be a critical systolic function threshold that below which life cannot be sustained. Thus, the apparent functional improvement conferred by the exogenous cells may be underestimated.

The regulation of glucose uptake is dependent of several factors including glucose transport, glucose phosphorylation, insulin signalling, substrate availability and fatty acid utilization. In all studies, cardiac GLUT4 and HKII protein were comparable between groups. This suggests the transcriptional and translational regulation of glucose transport

and phosphorylation did not play a significant role in the restoration of non-pathological insulin-stimulated glucose uptake in the heart following a MI and/or MSC therapy.

In Chapter 3, an isotopic fatty acid analog was administered during the insulin clamp to evaluate tissue-specific long chain fatty acid uptake in parallel with glucose uptake. MSC therapy prevented a depression in the insulin-mediated index of fatty acid uptake in the peri-infarct region of the post-MI heart. Additionally, PGC-1α protein, a coactivator of transcription factors involved in the expression of target genes regulating fatty acid metabolism, was preserved in the peri-infarct area. It may be that the cell-based transplantation attenuated the increase in glucose uptake, in part, by maintaining fatty acid utilization and the competitive nature of substrate utilization as described by the glucose-fatty acid cycle.

Recently, Lovell et al. (197) reported bone marrow mononuclear cell transplantation into the heart enhances the cardiac p-Akt-to-Akt ratio following ischemia-reperfusion injury. In response to the findings of Lovell and colleagues, experimental analysis in Chapter 4 focused on the potential for MSC transplantation to modulate insulin signalling in the chronically infarcted heart as a means of preventing atypical glucose uptake. While the MSC treatment did not enhance the p-Akt-to-Akt ratio, the cells did lessen the decline in this insulin signalling marker following a MI. The results of Chapter 4 indicate that a plausible MSC mode of action to mitigate glucose uptake alterations is to reduce impairments in the insulin signalling cascade(s).

Throughout all studies, substrate availability and systemic insulin sensitivity were evaluated as effectors of glucose utilization. In the chow-fed experiments (Chapter 3 and 4), plasma glucose, fatty acid and insulin concentrations were similar between groups.

Also, systemic glucose disposal in response to insulin (GIR) was unchanged following a cardiac infarction and the cell treatment. In these studies the results indicate the MSC therapy did not have a readily apparent systemic effect on metabolism that could significantly manipulate cardiac energetics. In Chapter 3, there was an increase in vascular density in the infarction that may have been extended to the peri-infarct region allowing greater substrate supply. Notably, the gastrocnemius exhibited an elevation in fatty acid uptake (Chapter 4) and the soleus displayed a heighten rate of glucose uptake (Chapter 5) in the MSC-treated mice. These observations hinted at potential for MSC transplantation to manipulate peripheral tissue substrate metabolism. In Chapter 5, mice were fed a high-fat diet to precipitate hyperglycemia, hyperlipidemia and whole body insulin resistance. The MSC-treated animals were characterized by an increase in GIR as well as skeletal muscle and adipose tissue glucose uptake in response to insulin stimulation. Furthermore, GLUT4 and the p-Akt-to-Akt ratio were higher following the MSC transplantation in skeletal muscle and adipose tissue. Although unexpected, the systemic alterations from a single intramyocardial injection of MSCs were not completely surprising. MSCs administered in this manner have been reported to home to peripheral tissues (130). Additionally, other groups have identified that the relatively thin heart wall and rapid murine heart rate can result in the experimenter erroneously injecting the exogenous cells into the lumen of the left ventricle (335). In terms of the mechanisms for the increased insulin-stimulated cardiac glucose uptake observed in the HFF mice, the MSCs did not alter insulin signalling. The improved systemic insulin sensitivity may be responsible for the lowering of plasma glucose and fatty acids in these mice. Moreover,

the lessening of hyperlipidemia could minimize the fatty acid-induced inhibition of cardiac glucose uptake.

It is currently unknown if the results observed in the three studies (Chapters 3, 4 and 5) are sustainable. Si et al. (304) evaluated the influence of MSC on whole body insulin sensitivity in a STZ/HFF rat model. The exogenously administered cells enhanced whole body insulin-mediated glucose disposal (304). However, the results were transient and required further MSC transplantation at four week intervals to maintain the metabolic effects (304). Thus, at the very least, the MSC therapy delays the onset of insulin-stimulated substrate uptake abnormalities following a MI. From a functional perspective, this conservation of a more non-pathological metabolic phenotype may provide the heart with the metabolic flexibility required to efficiently and effectively provide ATP for contractile processes in response to various physiological stressors.

7.3.2 Cardiac mitochondria

Mitochondria support cardiac function, in part, by liberating energy from oxidizable substrates (327). In the infarcted heart, high-energy phosphates derived from substrate catabolism are depressed and MSC therapy minimizes this decline (85, 369). Given this, an objective of this thesis was to identify the efficacy of MSC transplantation to preserve ATP provision via conservation of mitochondrial content and function. Similar to substrate uptake, concern existed as to the likelihood of identifying MSC therapeutic potential given aberrations in cardiac mitochondrial oxygen consumption and density have been reported to be greatly dependent on injury severity and/or the extent of progression towards heart failure post-MI. This prompted three independent studies differing in the extent of insult as a means of broadly evaluating mitochondrial protection

delivered by MSCs. Identical to glucose uptake, mitochondrial characteristics were evaluated in chow fed, low LAD ligated hearts (Chapter 3), in chow fed, high LAD ligated hearts (Chapter 4) and HFF, high LAD ligated hearts (Chapter 5).

The results provided in Chapters 3, 4 and 5 indicate that MSC administration shortly following a MI may mediate an improvement in the energetic state of the heart through maintenance of mitochondrial number. Following relatively modest cardiac injury induced by low LAD ligation (Chapter 3) a decline in PGC-1α was prevented in the MI+MSC hearts. An absence of alterations in mitochondrial density was observed in response to both the MI and MSC transplantation. Although mitochondrial content was comparable between groups, the preservation of PGC-1α by the MSC transplantation suggests the ability of the cell-based therapy to protect cardiac mitochondria from decline. In Chapter 4, mitochondrial density as indicated by citrate synthase activity, and PGC-1α protein were lower in the MI-only hearts. More importantly, the MSC treatment blunted the decline in peri-infarct mitochondria number and PGC-1α. In the presence of diet-induced insulin resistance (Chapter 5), citrate synthase activity was lower following the MI event. Similarly to the chow fed mice, the MSC transplantation attenuated this depression in this marker of mitochondria density. However, PGC-1α was comparable between groups. Thus, the preservation of mitochondria number is not solely reliant on preserving PGC-1α protein. In summary, the results of Chapter 3, 4 and 5 indicate that a conservation of total mitochondria and transcriptional regulation of these organelles may enhance ATP provision and contribute to the greater ATP-to-PCr ratio in MSC-treated hearts.

Beyond mitochondria density, MSC-treated hearts displayed a higher RCR in the peri-infarct region compared to MI-only hearts in Chapter 3 and 5. The RCR observed in Chapter 4 was not significantly elevated compared to the MI+PBS hearts, however, the mice receiving the exogenous cells were rescued from a decline in peri-infarct RCR. Together, these results suggest the MSC treatment preserves OXPHOS ADP responsiveness and potentially enhances the coupling of electron transport and ATP synthesis. Upon closer inspection, the enhanced RCR in Chapter 3 and 5 appears to be subsequent to a decline in state 2 respiration. This is particularly intriguing as it suggests the effect of MSCs on mitochondrial function is not merely secondary to reducing infarct size and structural remodelling.

Oxygen flux in the absence of ADP (state 2) can result from electron slip (33, 109). Oxygen consumption via electron slip occurs when an electron is diverted away from the electron transport chain (ETC) and reacts with oxygen to form reactive oxygen species (109). Previous work completed by Jameel et al. (148) identified a decline in three complex I subunits. It may be that a reduction in complex I subunits may reduce absolute electron flux through complex I and minimize electron slip. In Chapter 3, a lowering of complex I protein was not observed following MSC therapy, however, a depression in CI+CIII enzymatic activity was displayed. In Chapter 5, both MI+PBS and MI+MSC peri-infarct regions exhibited a decline in complex I protein. However, there may have been an added effect of the cell therapy as complex I protein in the remote left ventricle was lower as well. Of note, complex I enzymatic activity was not assessed in Chapter 5 owing to limited left ventricle peri-infarct tissue following higher ligation placement. In Chapter 4, both infarcted groups displayed a reduction in complex I

protein. The reason for a lack of MSC effect on state 2 respiration in Chapter 4 is not clear. In speculation, the influence of the MSC on cardiac mitochondrial OXPHOS may be transient and repeated cell transplantation may be required to maintain their effects. Further study is required to confirm our observations that suggest MSCs promote a reduction in complex I-mediated electron flux and/or electron slip that may improve mitochondrial efficiency.

Alternatively, proton leak, the major contributor to oxygen consumption in the absence of ADP, may be the mechanism through which the MSCs lower futile oxygen flux. In Chapter 3, ANT and UCP3 protein were comparable between groups. Given, ANT-induced proton leak depends greatly on content it appears the MSC therapy does not lower state 2 respiration via ANT manipulation (34). The majority of UCP3 uncoupling function occurs due to be activation by various inducers. Reactive oxygen species products have been reported to promote UCP3-mediated proton transport (15). The potential decline in electron slip from complex I and free radical synthesis may lower activation of UCP3. Alternatively, Chapter 3 results show the reactive oxygen species scavenger enzyme, glutathione peroxidase, to be depressed at the protein level in the MSC-treated hearts. In agreement, Jameel et al. (148) reported cardiac glutathione peroxidase mRNA to be lower following MSC therapy for the infarcted heart in a swine model. While reactive oxygen species was not measured in this dissertation, previous work from our laboratory has identified the ability of MSC transplantation to reduce hydrogen peroxide production (235). In speculation, the decline in glutathione peroxidase is in response to the ability of the MSC therapy to depress free radicals. Moreover, reduction in reactive oxygen species could lessen the activation of UCP3-

mediated proton leak. Also, as previously discussed in Chapter 2, fatty acids can promote UCP3 expression and functional activity (68, 75, 103). Chapter 5 displayed ability of MSC administration to minimize circulating fatty acids. This was associated with a dampening of UCP3 protein and possibly UCP3-mediated uncoupling as indicated by a decline in state 2 respiration. In conclusion, MSC transplantation may modulate UCP3 content and/or functional uncoupling as a means improving OXPHOS efficiency (RCR).

7.3.3 Mesenchymal stem cell oxidative phosphorylation

The majority of this dissertation was focused on the influence MSCs have on host tissue, however, the recipient environment plays a role in MSC efficacy. More specifically, the ischemia exhibited in the infarcted region contributes to the poor survival of transplanted MSCs (118, 269). The objectives of the experiments in Chapter 6 were to identify mitochondrial OXPHOS characteristics that may influence MSC survival if transplanted into the ischemic region of the infarcted heart.

The MRL-MSCs (MSCs obtained from MRL-MpJ mouse) exhibited greater resistance to cell death following 48 hours of combined glucose and oxygen deprivation compared to WT-MSCs (MSCs derived from C57BL/6 mouse). The improved viability displayed by MRL-MSCs was also very apparent under conditions of reduced glucose only. In addition to survival characteristics in response to substrate withdrawal, components of OXPHOS function were different between the cell types. In intact cells, the MRL-MSCs exhibited greater absolute oxygen consumption under culturing conditions. Also, the reserve capacity for greater electron transport was higher. In permeabilized cells, ADP-stimulated oxygen flux supported by complex I and complex II

substrates were elevated in the MRL-MSCs. Interestingly, cardiac myocyte respiration under identical conditions was far superior to that of the MSCs.

MSCs have been previously reported to contain low levels of mitochondria and rely predominantly on glycolysis for ATP synthesis (49). This may explain the lower oxygen consumption rates compared to cardiac myocytes. Moreover, the relatively low reliance on OXPHOS could benefit the transplanted MSCs in situations of low oxygen supply. Conversely, the heightened electron transport reserve capacity displayed by the MRL-MSCs may be of benefit when glucose is scare. MSCs have been reported to shift towards OXPHOS dependence under glucose reduction (191). The increase in oxidative function is thought to be an adaptive attempt to maximize ATP synthesis in the nutrient shortage. Thus, the unique MRL-MSC OXPHOS phenotype characterized by low respiration with a slight increase in maximal OXPHOS potential may afford these cells the metabolic flexibility to better maintain the energetic status and subsequently combat cell death due to cell starvation.

7.4 Future directions

The studies conducted in this dissertation are largely descriptive, however, the results stimulate many questions that may open avenues of research that define the means by which exogenous stem cells modulate cardiac metabolism following transplantation. Future endeavours must identify whether the findings are a direct effect induced by the MSCs on metabolism. As previously stated, infarct size plays a large role in the extent of cardiac dysfunction post-MI (251). Furthermore, MSCs are capable of reducing the size of this akinetic area via paracrine-mediated anti-apoptotic means. Additional

experiments should be completed to eliminate this influence of infarct severity on cardiac metabolism by comparing rodents of similar insult. Histological techniques are commonly employed to measure infarct size in cross-sectional samples. However, a non-terminal technique is required to measure tissue-specific glucose uptake, mitochondrial function, and infarct size in the same heart. Kanno et al. (158) developed a method of measuring scar size using echocardiography. Rather than taking measures at one level as done in Chapter 3, 4 and 5, echocardiographic images were taken at several levels from the base to the apex of the left ventricle. The summation of the akinetic area from each cross sectional image allowed for the estimation of infarct size that correlated extremely well with histological evaluation (158). Such a technique would be of value to the experimental protocols followed in this dissertation.

Of particular interest is the reduced state 2 respiration in Chapter 3 and 5 that suggest proton leak is lessened by the MSC therapy. UCP3-mediated proton leak is intriguing because UCP3 activity is not simply content reliant but can be activated/inactivated. Additional respiration experiments in the presence and absence of UCP inhibitor, GDP, would assist in identifying UCP3 as the facilitator of proton leak. Also, assessment of reactive oxygen species production and their by-products such as reactive alkenals would shed light on whether MSC antioxidant effects reduced UCP3 activation. In Chapter 5, it was proposed that the decline in futile respiration is the result of a reduction in fatty acid activation of UCP3 following MSC-induced depression in circulating NEFAs. Further respiration experiments should also be performed during insulin clamps or *ex vivo* experiments where exogenous lipids are infused to ensure circulating lipids are equivalent between groups.

The observations reported following MSC transplantation into the HFF/infarcted mouse heart (Chapter 5) provides the strongest support that the exogenous cells are capable of directly manipulating systemic and tissue-specific metabolism. Given MSCs predominantly confer therapeutic effects through paracrine mechanisms, future work delineating the bioactive component(s) responsible for the metabolic modulation may be most pressing.

Although only a single chapter of this dissertation was devoted to the experimental analysis of MSC metabolism and viability (Chapter 6), the results are encouraging and additional research should be performed to reduce some of the limitations of the study. Future work should be conducted with the realization that respiration assessed under air-saturated oxygen concentrations is not physiological. Chacko et al. (2009) determined that the partial pressure of oxygen (pO_2) in the ischemic region was 3.0 ± 0.7 mmHg immediately following infarction compared to 19.7 ± 1.4 mmHg in the non-infarcted control heart of rats (46). Evaluating oxygen flux at a pO_2 of 3.0 mmHg using the Oroboros oxygraph-2k would be technically challenging. However, oxygen kinetics of the MSCs at lower oxygen levels may be evaluated to provide valuable information. At oxygen levels of 8 mmHg, intact cells suspended in culture medium could be evaluated for oxygen affinity and the pO_2 at which half-maximal respiration rate (P_{50}) determined. If a lower P_{50} is exhibited by MRL-MSCs this may indicate an elevated rate of OXPHOS. In addition, further viability assays following glucose and oxygen withdrawal should be performed to identify the importance of the increased electron transport potential exhibited by MRL-MSCs. Prior to substrate deprivation, treating the MSCs with carbonyl cyanide-p-trifluoromethoxyphenylhydraz-

one (FCCP) would uncouple electron transport from ATP synthesis. This would eliminate the ability of the cells from generating ATP from OXPHOS.

7.5 Conclusions and significance

Collectively, the work presented in this dissertation identifies that energy metabolism is both influenced by and influences MSC transplantation. From an experimental perspective, the knowledge from this work provides a foundation that allows for future investigative endeavours to identify whether the metabolic changes observed in cardiac substrate uptake, mitochondrial OXPHOS and systemic insulin sensitivity following MSC administration are due to direct modulation or secondary to other modes of therapeutic action. From a clinical perspective, although energy metabolism is frequently considered trivial when evaluating cardiac pathologies and is all too often neglected as a potential cardiac stressor, the experimental results reported here add to the growing awareness that a greater understanding of metabolic processes holds potential to advance the treatment of cardiac impairments as well as stem cell efficacy in the treatment of these impairments.

REFERENCES

1. Diagnosis and classification of diabetes mellitus. *Diabetes Care* 36 Suppl 1: S67-74, 2013.

2. **Aasum E, Cooper M, Severson DL, and Larsen TS**. Effect of BM 17.0744, a PPARalpha ligand, on the metabolism of perfused hearts from control and diabetic mice. *Canadian journal of physiology and pharmacology* 83: 183-190, 2005.

3. **Aasum E, Hafstad AD, Severson DL, and Larsen TS**. Age-dependent changes in metabolism, contractile function, and ischemic sensitivity in hearts from db/db mice. *Diabetes* 52: 434-441, 2003.

4. **Abdel Aziz MT, El-Asmar MF, Haidara M, Atta HM, Roshdy NK, Rashed LA, Sabry D, Youssef MA, Abdel Aziz AT, and Moustafa M**. Effect of bone marrow-derived mesenchymal stem cells on cardiovascular complications in diabetic rats. *Medical science monitor : international medical journal of experimental and clinical research* 14: BR249-255, 2008.

5. **Abozguia K, Clarke K, Lee L, and Frenneaux M**. Modification of myocardial substrate use as a therapy for heart failure. *Nat Clin Pract Cardiovasc Med* 3: 490-498, 2006.

6. **Aerni-Flessner L, Abi-Jaoude M, Koenig A, Payne M, and Hruz PW**. GLUT4, GLUT1, and GLUT8 are the dominant GLUT transcripts expressed in the murine left ventricle. *Cardiovascular diabetology* 11: 63, 2012.

7. **Ahn D, Cheng L, Moon C, Spurgeon H, Lakatta EG, and Talan MI**. Induction of myocardial infarcts of a predictable size and location by branch pattern probability-

assisted coronary ligation in C57BL/6 mice. *Am J Physiol Heart Circ Physiol* 286: H1201-1207, 2004.

8. **Alfaro MP, Pagni M, Vincent A, Atkinson J, Hill MF, Cates J, Davidson JM, Rottman J, Lee E, and Young PP**. The Wnt modulator sFRP2 enhances mesenchymal stem cell engraftment, granulation tissue formation and myocardial repair. *Proc Natl Acad Sci U S A* 105: 18366-18371, 2008.

9. **Alfaro MP, Vincent A, Saraswati S, Thorne CA, Hong CC, Lee E, and Young PP**. sFRP2 suppression of bone morphogenic protein (BMP) and Wnt signaling mediates mesenchymal stem cell (MSC) self-renewal promoting engraftment and myocardial repair. *J Biol Chem* 285: 35645-35653, 2010.

10. **Amorim PA, Nguyen TD, Shingu Y, Schwarzer M, Mohr FW, Schrepper A, and Doenst T**. Myocardial infarction in rats causes partial impairment in insulin response associated with reduced fatty acid oxidation and mitochondrial gene expression. *J Thorac Cardiovasc Surg* 140: 1160-1167, 2010.

11. **Anderson EJ, Kypson AP, Rodriguez E, Anderson CA, Lehr EJ, and Neufer PD**. Substrate-specific derangements in mitochondrial metabolism and redox balance in the atrium of the type 2 diabetic human heart. *J Am Coll Cardiol* 54: 1891-1898, 2009.

12. **Ayala JE, Bracy DP, James FD, Burmeister MA, Wasserman DH, and Drucker DJ**. Glucagon-like peptide-1 receptor knockout mice are protected from high-fat diet-induced insulin resistance. *Endocrinology* 151: 4678-4687, 2010.

13. **Ayala JE, Bracy DP, McGuinness OP, and Wasserman DH**. Considerations in the design of hyperinsulinemic-euglycemic clamps in the conscious mouse. *Diabetes* 55: 390-397, 2006.

14. **Ayala JE, Samuel VT, Morton GJ, Obici S, Croniger CM, Shulman GI, Wasserman DH, and McGuinness OP**. Standard operating procedures for describing and performing metabolic tests of glucose homeostasis in mice. *Disease models & mechanisms* 3: 525-534, 2010.

15. **Azzu V, and Brand MD**. The on-off switches of the mitochondrial uncoupling proteins. *Trends Biochem Sci* 35: 298-307, 2010.

16. **Azzu V, Jastroch M, Divakaruni AS, and Brand MD**. The regulation and turnover of mitochondrial uncoupling proteins. *Biochim Biophys Acta* 1797: 785-791, 2010.

17. **Baddoo M, Hill K, Wilkinson R, Gaupp D, Hughes C, Kopen GC, and Phinney DG**. Characterization of mesenchymal stem cells isolated from murine bone marrow by negative selection. *J Cell Biochem* 89: 1235-1249, 2003.

18. **Baldwin JM, Gorga JC, and Lienhard GE**. The monosaccharide transporter of the human erythrocyte. Transport activity upon reconstitution. *J Biol Chem* 256: 3685-3689, 1981.

19. **Barger PM, Brandt JM, Leone TC, Weinheimer CJ, and Kelly DP**. Deactivation of peroxisome proliferator-activated receptor-alpha during cardiac hypertrophic growth. *J Clin Invest* 105: 1723-1730, 2000.

20. **Barger PM, and Kelly DP**. PPAR signaling in the control of cardiac energy metabolism. *Trends Cardiovasc Med* 10: 238-245, 2000.

21. **Belke DD, Betuing S, Tuttle MJ, Graveleau C, Young ME, Pham M, Zhang D, Cooksey RC, McClain DA, Litwin SE, Taegtmeyer H, Severson D, Kahn CR, and**

Abel ED. Insulin signaling coordinately regulates cardiac size, metabolism, and contractile protein isoform expression. *J Clin Invest* 109: 629-639, 2002.

22. **Belke DD, Larsen TS, Gibbs EM, and Severson DL**. Altered metabolism causes cardiac dysfunction in perfused hearts from diabetic (db/db) mice. *Am J Physiol Endocrinol Metab* 279: E1104-1113, 2000.

23. **Belke DD, and Severson DL**. Diabetes in mice with monogenic obesity: the db/db mouse and its use in the study of cardiac consequences. *Methods Mol Biol* 933: 47-57, 2012.

24. **Bell DS**. Diabetic cardiomyopathy. *Diabetes Care* 26: 2949-2951, 2003.

25. **Bhansali A, A P, Walia R, Bhansali S, Gupta V, Jain A, Sachdeva N, Sharma RR, Marwaha N, and Khandelwal N**. Efficacy and Safety of Autologous Bone Marrow Derived Stem Cell Transplantation in patients with Type 2 Diabetes mellitus: A randomized placebo-controlled study. *Cell Transplant* 2013.

26. **Bhansali A, Upreti V, Khandelwal N, Marwaha N, Gupta V, Sachdeva N, Sharma RR, Saluja K, Dutta P, Walia R, Minz R, Bhadada S, Das S, and Ramakrishnan S**. Efficacy of autologous bone marrow-derived stem cell transplantation in patients with type 2 diabetes mellitus. *Stem Cells Dev* 18: 1407-1416, 2009.

27. **Blum JS, Wearsch PA, and Cresswell P**. Pathways of antigen processing. *Annual review of immunology* 31: 443-473, 2013.

28. **Boss O, Samec S, Paoloni-Giacobino A, Rossier C, Dulloo A, Seydoux J, Muzzin P, and Giacobino JP**. Uncoupling protein-3: a new member of the mitochondrial carrier family with tissue-specific expression. *FEBS Lett* 408: 39-42, 1997.

29. **Boudina S, and Abel ED**. Diabetic cardiomyopathy, causes and effects. *Reviews in endocrine & metabolic disorders* 11: 31-39, 2010.

30. **Boudina S, Han YH, Pei S, Tidwell TJ, Henrie B, Tuinei J, Olsen C, Sena S, and Abel ED**. UCP3 regulates cardiac efficiency and mitochondrial coupling in high fat-fed mice but not in leptin-deficient mice. *Diabetes* 61: 3260-3269, 2012.

31. **Boudina S, Sena S, O'Neill BT, Tathireddy P, Young ME, and Abel ED**. Reduced mitochondrial oxidative capacity and increased mitochondrial uncoupling impair myocardial energetics in obesity. *Circulation* 112: 2686-2695, 2005.

32. **Boudina S, Sena S, Theobald H, Sheng X, Wright JJ, Hu XX, Aziz S, Johnson JI, Bugger H, Zaha VG, and Abel ED**. Mitochondrial energetics in the heart in obesity-related diabetes: direct evidence for increased uncoupled respiration and activation of uncoupling proteins. *Diabetes* 56: 2457-2466, 2007.

33. **Brand MD, and Nicholls DG**. Assessing mitochondrial dysfunction in cells. *Biochem J* 435: 297-312, 2011.

34. **Brand MD, Pakay JL, Ocloo A, Kokoszka J, Wallace DC, Brookes PS, and Cornwall EJ**. The basal proton conductance of mitochondria depends on adenine nucleotide translocase content. *Biochem J* 392: 353-362, 2005.

35. **Brandt JM, Djouadi F, and Kelly DP**. Fatty acids activate transcription of the muscle carnitine palmitoyltransferase I gene in cardiac myocytes via the peroxisome proliferator-activated receptor alpha. *J Biol Chem* 273: 23786-23792, 1998.

36. **Brookes PS, Rolfe DF, and Brand MD**. The proton permeability of liposomes made from mitochondrial inner membrane phospholipids: comparison with isolated mitochondria. *The Journal of membrane biology* 155: 167-174, 1997.

37. **Brown ET, Umino Y, Loi T, Solessio E, and Barlow R**. Anesthesia can cause sustained hyperglycemia in C57/BL6J mice. *Visual neuroscience* 22: 615-618, 2005.

38. **Buchanan J, Mazumder PK, Hu P, Chakrabarti G, Roberts MW, Yun UJ, Cooksey RC, Litwin SE, and Abel ED**. Reduced cardiac efficiency and altered substrate metabolism precedes the onset of hyperglycemia and contractile dysfunction in two mouse models of insulin resistance and obesity. *Endocrinology* 146: 5341-5349, 2005.

39. **Buettner R, Parhofer KG, Woenckhaus M, Wrede CE, Kunz-Schughart LA, Scholmerich J, and Bollheimer LC**. Defining high-fat-diet rat models: metabolic and molecular effects of different fat types. *Journal of molecular endocrinology* 36: 485-501, 2006.

40. **Bugger H, and Abel ED**. Mitochondria in the diabetic heart. *Cardiovasc Res* 88: 229-240, 2010.

41. **Cadenas S, Buckingham JA, Samec S, Seydoux J, Din N, Dulloo AG, and Brand MD**. UCP2 and UCP3 rise in starved rat skeletal muscle but mitochondrial proton conductance is unchanged. *FEBS Lett* 462: 257-260, 1999.

42. **Campbell CT, Kolesar JE, and Kaufman BA**. Mitochondrial transcription factor A regulates mitochondrial transcription initiation, DNA packaging, and genome copy number. *Biochim Biophys Acta* 1819: 921-929, 2012.

43. **Campbell NG, and Suzuki K**. Cell delivery routes for stem cell therapy to the heart: current and future approaches. *J Cardiovasc Transl Res* 5: 713-726, 2012.

44. **Caplan AI**. Mesenchymal stem cells. *Journal of orthopaedic research : official publication of the Orthopaedic Research Society* 9: 641-650, 1991.

45. **Carley AN, Atkinson LL, Bonen A, Harper ME, Kunnathu S, Lopaschuk GD, and Severson DL**. Mechanisms responsible for enhanced fatty acid utilization by perfused hearts from type 2 diabetic db/db mice. *Arch Physiol Biochem* 113: 65-75, 2007.

46. **Chacko SM, Khan M, Kuppusamy ML, Pandian RP, Varadharaj S, Selvendiran K, Bratasz A, Rivera BK, and Kuppusamy P**. Myocardial oxygenation and functional recovery in infarct rat hearts transplanted with mesenchymal stem cells. *Am J Physiol Heart Circ Physiol* 296: H1263-1273, 2009.

47. **Chafey P, Finzi L, Boisgard R, Cauzac M, Clary G, Broussard C, Pegorier JP, Guillonneau F, Mayeux P, Camoin L, Tavitian B, Colnot S, and Perret C**. Proteomic analysis of beta-catenin activation in mouse liver by DIGE analysis identifies glucose metabolism as a new target of the Wnt pathway. *Proteomics* 9: 3889-3900, 2009.

48. **Chandler MP, Kerner J, Huang H, Vazquez E, Reszko A, Martini WZ, Hoppel CL, Imai M, Rastogi S, Sabbah HN, and Stanley WC**. Moderate severity heart failure does not involve a downregulation of myocardial fatty acid oxidation. *Am J Physiol Heart Circ Physiol* 287: H1538-1543, 2004.

49. **Chen CT, Hsu SH, and Wei YH**. Mitochondrial bioenergetic function and metabolic plasticity in stem cell differentiation and cellular reprogramming. *Biochim Biophys Acta* 1820: 571-576, 2012.

50. **Chen Y, Wang Y, Chen J, Chen X, Cao W, Chen S, Xu S, Huang H, and Liu P**. Roles of transcriptional corepressor RIP140 and coactivator PGC-1alpha in energy state of chronically infarcted rat hearts and mitochondrial function of cardiomyocytes. *Molecular and cellular endocrinology* 362: 11-18, 2012.

51. **Cleutjens JP, Blankesteijn WM, Daemen MJ, and Smits JF**. The infarcted myocardium: simply dead tissue, or a lively target for therapeutic interventions. *Cardiovasc Res* 44: 232-241, 1999.

52. **Cohn JN, Ferrari R, and Sharpe N**. Cardiac remodeling--concepts and clinical implications: a consensus paper from an international forum on cardiac remodeling. Behalf of an International Forum on Cardiac Remodeling. *J Am Coll Cardiol* 35: 569-582, 2000.

53. **Cole MA, Murray AJ, Cochlin LE, Heather LC, McAleese S, Knight NS, Sutton E, Jamil AA, Parassol N, and Clarke K**. A high fat diet increases mitochondrial fatty acid oxidation and uncoupling to decrease efficiency in rat heart. *Basic Res Cardiol* 106: 447-457, 2011.

54. **Collins KA, Korcarz CE, and Lang RM**. Use of echocardiography for the phenotypic assessment of genetically altered mice. *Physiol Genomics* 13: 227-239, 2003.

55. **Collins S, Martin TL, Surwit RS, and Robidoux J**. Genetic vulnerability to diet-induced obesity in the C57BL/6J mouse: physiological and molecular characteristics. *Physiol Behav* 81: 243-248, 2004.

56. **Collison KS, Makhoul NJ, Zaidi MZ, Al-Rabiah R, Inglis A, Andres BL, Ubungen R, Shoukri M, and Al-Mohanna FA**. Interactive effects of neonatal exposure to monosodium glutamate and aspartame on glucose homeostasis. *Nutrition & metabolism* 9: 58, 2012.

57. **Costford SR, Seifert EL, Bezaire V, M FG, Bevilacqua L, Gowing A, and Harper ME**. The energetic implications of uncoupling protein-3 in skeletal muscle.

Applied physiology, nutrition, and metabolism = Physiologie appliquee, nutrition et metabolisme 32: 884-894, 2007.

58. **Couri CE, de Oliveira MC, and Simoes BP**. Risks, benefits, and therapeutic potential of hematopoietic stem cell transplantation for autoimmune diabetes. *Current diabetes reports* 12: 604-611, 2012.

59. **Crescenzo R, Mainieri D, Solinas G, Montani JP, Seydoux J, Liverini G, Iossa S, and Dulloo AG**. Skeletal muscle mitochondrial oxidative capacity and uncoupling protein 3 are differently influenced by semistarvation and refeeding. *FEBS Lett* 544: 138-142, 2003.

60. **Dai S, Walsh P, Wielgosz A, Gurevich Y, Bancej C, and Morrison H**. Comorbidities and mortality associated with hospitalized heart failure in Canada. *Can J Cardiol* 28: 74-79, 2012.

61. **de Brouwer KF, Degens H, Aartsen WM, Lindhout M, Bitsch NJ, Gilde AJ, Willemsen PH, Janssen BJ, van der Vusse GJ, and van Bilsen M**. Specific and sustained down-regulation of genes involved in fatty acid metabolism is not a hallmark of progression to cardiac failure in mice. *J Mol Cell Cardiol* 40: 838-845, 2006.

62. **DeFronzo RA, Tobin JD, and Andres R**. Glucose clamp technique: a method for quantifying insulin secretion and resistance. *Am J Physiol* 237: E214-223, 1979.

63. **Deng JY, Huang JP, Lu LS, and Hung LM**. Impairment of cardiac insulin signaling and myocardial contractile performance in high-cholesterol/fructose-fed rats. *Am J Physiol Heart Circ Physiol* 293: H978-987, 2007.

64. **Deschepper M, Oudina K, David B, Myrtil V, Collet C, Bensidhoum M, Logeart-Avramoglou D, and Petite H**. Survival and function of mesenchymal stem

cells (MSCs) depend on glucose to overcome exposure to long-term, severe and continuous hypoxia. *J Cell Mol Med* 15: 1505-1514, 2010.

65. **Di Napoli P**. The metabolic treatment of coronary artery disease and heart failure. *Current pharmaceutical design* 15: 826, 2009.

66. **Diamant M, Lamb HJ, Groeneveld Y, Endert EL, Smit JW, Bax JJ, Romijn JA, de Roos A, and Radder JK**. Diastolic dysfunction is associated with altered myocardial metabolism in asymptomatic normotensive patients with well-controlled type 2 diabetes mellitus. *J Am Coll Cardiol* 42: 328-335, 2003.

67. **Dinsmore JH, and Dib N**. Stem cell therapy for the treatment of acute myocardial infarction. *Cardiol Clin* 28: 127-138.

68. **Divakaruni AS, and Brand MD**. The regulation and physiology of mitochondrial proton leak. *Physiology (Bethesda)* 26: 192-205, 2011.

69. **Dominici M, Le Blanc K, Mueller I, Slaper-Cortenbach I, Marini F, Krause D, Deans R, Keating A, Prockop D, and Horwitz E**. Minimal criteria for defining multipotent mesenchymal stromal cells. The International Society for Cellular Therapy position statement. *Cytotherapy* 8: 315-317, 2006.

70. **Dong F, Li Q, Sreejayan N, Nunn JM, and Ren J**. Metallothionein prevents high-fat diet induced cardiac contractile dysfunction: role of peroxisome proliferator activated receptor gamma coactivator 1alpha and mitochondrial biogenesis. *Diabetes* 56: 2201-2212, 2007.

71. **Dressel U, Allen TL, Pippal JB, Rohde PR, Lau P, and Muscat GE**. The peroxisome proliferator-activated receptor beta/delta agonist, GW501516, regulates the

expression of genes involved in lipid catabolism and energy uncoupling in skeletal muscle cells. *Mol Endocrinol* 17: 2477-2493, 2003.

72. **Duncan JG**. Mitochondrial dysfunction in diabetic cardiomyopathy. *Biochim Biophys Acta* 1813: 1351-1359, 2011.

73. **Duncan JG, Fong JL, Medeiros DM, Finck BN, and Kelly DP**. Insulin-resistant heart exhibits a mitochondrial biogenic response driven by the peroxisome proliferator-activated receptor-alpha/PGC-1alpha gene regulatory pathway. *Circulation* 115: 909-917, 2007.

74. **Eaton S, Bartlett K, and Pourfarzam M**. Mammalian mitochondrial beta-oxidation. *Biochem J* 320 (Pt 2): 345-357, 1996.

75. **Echtay KS, Winkler E, Frischmuth K, and Klingenberg M**. Uncoupling proteins 2 and 3 are highly active H(+) transporters and highly nucleotide sensitive when activated by coenzyme Q (ubiquinone). *Proc Natl Acad Sci U S A* 98: 1416-1421, 2001.

76. **Estep JD, and Aguilar D**. Diabetes and heart failure in the post-myocardial infarction patient. *Current heart failure reports* 3: 164-169, 2006.

77. **Eun LY, Song H, Choi E, Lee TG, Moon DW, Hwang D, Byun KH, Sul JH, and Hwang KC**. Implanted bone marrow-derived mesenchymal stem cells fail to metabolically stabilize or recover electromechanical function in infarcted hearts. *Tissue Cell* 43: 238-245.

78. **Evans MJ, and Scarpulla RC**. Interaction of nuclear factors with multiple sites in the somatic cytochrome c promoter. Characterization of upstream NRF-1, ATF, and intron Sp1 recognition sequences. *J Biol Chem* 264: 14361-14368, 1989.

79. **Exil VJ, Roberts RL, Sims H, McLaughlin JE, Malkin RA, Gardner CD, Ni G, Rottman JN, and Strauss AW**. Very-long-chain acyl-coenzyme a dehydrogenase deficiency in mice. *Circ Res* 93: 448-455, 2003.

80. **Ezquer FE, Ezquer ME, Parrau DB, Carpio D, Yanez AJ, and Conget PA**. Systemic administration of multipotent mesenchymal stromal cells reverts hyperglycemia and prevents nephropathy in type 1 diabetic mice. *Biol Blood Marrow Transplant* 14: 631-640, 2008.

81. **Fam BC, Rose LJ, Sgambellone R, Ruan Z, Proietto J, and Andrikopoulos S**. Normal muscle glucose uptake in mice deficient in muscle GLUT4. *The Journal of endocrinology* 214: 313-327, 2012.

82. **Fedak PW, Verma S, Weisel RD, and Li RK**. Cardiac remodeling and failure: from molecules to man (Part I). *Cardiovasc Pathol* 14: 1-11, 2005.

83. **Ferguson SJ**. ATP synthase: from sequence to ring size to the P/O ratio. *Proc Natl Acad Sci U S A* 107: 16755-16756.

84. **Feygin J, Hu Q, Swingen C, and Zhang J**. Relationships between regional myocardial wall stress and bioenergetics in hearts with left ventricular hypertrophy. *Am J Physiol Heart Circ Physiol* 294: H2313-2321, 2008.

85. **Feygin J, Mansoor A, Eckman P, Swingen C, and Zhang J**. Functional and bioenergetic modulations in the infarct border zone following autologous mesenchymal stem cell transplantation. *Am J Physiol Heart Circ Physiol* 293: H1772-1780, 2007.

86. **Fisher RP, Lisowsky T, Parisi MA, and Clayton DA**. DNA wrapping and bending by a mitochondrial high mobility group-like transcriptional activator protein. *J Biol Chem* 267: 3358-3367, 1992.

87. **Fitchett DH, Theroux P, Brophy JM, Cantor WJ, Cox JL, Gupta M, Kertland H, Mehta SR, Welsh RC, and Goodman SG**. Assessment and management of acute coronary syndromes (ACS): a Canadian perspective on current guideline-recommended treatment--part 1: non-ST-segment elevation ACS. *Can J Cardiol* 27 Suppl A: S387-401, 2011.

88. **Flores JE, McFarland LM, Vanderbilt A, Ogasawara AK, and Williams SP**. The effects of anesthetic agent and carrier gas on blood glucose and tissue uptake in mice undergoing dynamic FDG-PET imaging: sevoflurane and isoflurane compared in air and in oxygen. *Mol Imaging Biol* 10: 192-200, 2008.

89. **Frangogiannis NG**. The mechanistic basis of infarct healing. *Antioxid Redox Signal* 8: 1907-1939, 2006.

90. **Freyman T, Polin G, Osman H, Crary J, Lu M, Cheng L, Palasis M, and Wilensky RL**. A quantitative, randomized study evaluating three methods of mesenchymal stem cell delivery following myocardial infarction. *Eur Heart J* 27: 1114-1122, 2006.

91. **Frezza C, Cipolat S, and Scorrano L**. Organelle isolation: functional mitochondria from mouse liver, muscle and cultured fibroblasts. *Nat Protoc* 2: 287-295, 2007.

92. **Friedenstein AJ, Chailakhjan RK, and Lalykina KS**. The development of fibroblast colonies in monolayer cultures of guinea-pig bone marrow and spleen cells. *Cell and tissue kinetics* 3: 393-403, 1970.

93. **Friedenstein AJ, Petrakova KV, Kurolesova AI, and Frolova GP**. Heterotopic of bone marrow. Analysis of precursor cells for osteogenic and hematopoietic tissues. *Transplantation* 6: 230-247, 1968.

94. **Fueger PT**. Glucose phosphorylation as a barrier to muscle glucose uptake. *Clin Exp Pharmacol Physiol* 32: 314-318, 2005.

95. **Fueger PT, Hess HS, Bracy DP, Pencek RR, Posey KA, Charron MJ, and Wasserman DH**. Regulation of insulin-stimulated muscle glucose uptake in the conscious mouse: role of glucose transport is dependent on glucose phosphorylation capacity. *Endocrinology* 145: 4912-4916, 2004.

96. **Fueger PT, Lee-Young RS, Shearer J, Bracy DP, Heikkinen S, Laakso M, Rottman JN, and Wasserman DH**. Phosphorylation barriers to skeletal and cardiac muscle glucose uptakes in high-fat fed mice: studies in mice with a 50% reduction of hexokinase II. *Diabetes* 56: 2476-2484, 2007.

97. **Fukushima S, Varela-Carver A, Coppen SR, Yamahara K, Felkin LE, Lee J, Barton PJ, Terracciano CM, Yacoub MH, and Suzuki K**. Direct intramyocardial but not intracoronary injection of bone marrow cells induces ventricular arrhythmias in a rat chronic ischemic heart failure model. *Circulation* 115: 2254-2261, 2007.

98. **Galluzzi L, Zamzami N, de La Motte Rouge T, Lemaire C, Brenner C, and Kroemer G**. Methods for the assessment of mitochondrial membrane permeabilization in apoptosis. *Apoptosis* 12: 803-813, 2007.

99. **Gao S, Ho D, Vatner DE, and Vatner SF**. Echocardiography in Mice. *Current protocols in mouse biology* 1: 71-83, 2011.

100. **Garnier A, Fortin D, Delomenie C, Momken I, Veksler V, and Ventura-Clapier R**. Depressed mitochondrial transcription factors and oxidative capacity in rat failing cardiac and skeletal muscles. *J Physiol* 551: 491-501, 2003.

101. **Garnier A, Zoll J, Fortin D, N'Guessan B, Lefebvre F, Geny B, Mettauer B, Veksler V, and Ventura-Clapier R**. Control by circulating factors of mitochondrial function and transcription cascade in heart failure: a role for endothelin-1 and angiotensin II. *Circ Heart Fail* 2: 342-350, 2009.

102. **Gaur T, Lengner CJ, Hovhannisyan H, Bhat RA, Bodine PV, Komm BS, Javed A, van Wijnen AJ, Stein JL, Stein GS, and Lian JB**. Canonical WNT signaling promotes osteogenesis by directly stimulating Runx2 gene expression. *J Biol Chem* 280: 33132-33140, 2005.

103. **Georgiadi A, Boekschoten MV, Muller M, and Kersten S**. Detailed transcriptomics analysis of the effect of dietary fatty acids on gene expression in the heart. *Physiol Genomics* 44: 352-361, 2012.

104. **Gheorghiade M, and Bonow RO**. Chronic heart failure in the United States: a manifestation of coronary artery disease. *Circulation* 97: 282-289, 1998.

105. **Glass CE, Singal PK, and Singla DK**. Stem cells in the diabetic infarcted heart. *Heart Fail Rev* 15: 581-588, 2010.

106. **Gleyzer N, Vercauteren K, and Scarpulla RC**. Control of mitochondrial transcription specificity factors (TFB1M and TFB2M) by nuclear respiratory factors (NRF-1 and NRF-2) and PGC-1 family coactivators. *Mol Cell Biol* 25: 1354-1366, 2005.

107. **Gnaiger E**. Capacity of oxidative phosphorylation in human skeletal muscle: new perspectives of mitochondrial physiology. *Int J Biochem Cell Biol* 41: 1837-1845, 2009.

108. **Gnaiger E**. Oxygen conformance of cellular respiration. A perspective of mitochondrial physiology. *Adv Exp Med Biol* 543: 39-55, 2003.

109. **Gnaiger E**. Polarographic oxygen sensors, the oxygraph and high-resolution respirometry to assess mitochondrial function. In: *Drug-Induced Mitochondrial Dysfunction*, edited by Dykens J, and Will Y. Hoboken, NJ: John Wiley & Sons, Inc., 2008, p. 327-352.

110. **Gnaiger E, Kuznetsov A, Lassing B, Fuchs A, Reck M, Renner K, Stadlmann S, Rieger G, and Margeiter R**. High-resolution respirometry-Optimum permeabilization of the cell membrane by digitonin. In: *BioThermoKinetics in the Post Genomic Era*, edited by Larsson C, Pahlman IL, and Gustafsson L. Goteborg: Chalmers Reproservice, 1998, p. 89-95.

111. **Gnaiger E, Kuznetsov AV, Schneeberger S, Seiler R, Brandacher G, Steurer W, and Margreiter R**. Mitochondria in the cold. In: *Life in the Cold*, edited by Heldmaier G, and Klingenspor M. Berlin, Heidelberg, New York: Springer, 2000, p. 431-442.

112. **Gnecchi M, Danieli P, and Cervio E**. Mesenchymal stem cell therapy for heart disease. *Vascular pharmacology* 57: 48-55, 2012.

113. **Gnecchi M, He H, Melo LG, Noiseaux N, Morello F, de Boer RA, Zhang L, Pratt RE, Dzau VJ, and Ingwall JS**. Early beneficial effects of bone marrow-derived mesenchymal stem cells overexpressing Akt on cardiac metabolism after myocardial infarction. *Stem Cells* 27: 971-979, 2009.

114. **Gnecchi M, Zhang Z, Ni A, and Dzau VJ**. Paracrine mechanisms in adult stem cell signaling and therapy. *Circ Res* 103: 1204-1219, 2008.

115. **Gray S, and Kim JK**. New insights into insulin resistance in the diabetic heart. *Trends in endocrinology and metabolism: TEM* 22: 394-403, 2011.

116. **Gulick T, Cresci S, Caira T, Moore DD, and Kelly DP**. The peroxisome proliferator-activated receptor regulates mitochondrial fatty acid oxidative enzyme gene expression. *Proc Natl Acad Sci U S A* 91: 11012-11016, 1994.

117. **Hafstad AD, Solevag GH, Severson DL, Larsen TS, and Aasum E**. Perfused hearts from Type 2 diabetic (db/db) mice show metabolic responsiveness to insulin. *Am J Physiol Heart Circ Physiol* 290: H1763-1769, 2006.

118. **Haider H, and Ashraf M**. Strategies to promote donor cell survival: combining preconditioning approach with stem cell transplantation. *J Mol Cell Cardiol* 45: 554-566, 2008.

119. **Hamman BL, Bittl JA, Jacobus WE, Allen PD, Spencer RS, Tian R, and Ingwall JS**. Inhibition of the creatine kinase reaction decreases the contractile reserve of isolated rat hearts. *Am J Physiol* 269: H1030-1036, 1995.

120. **Hare JM, Traverse JH, Henry TD, Dib N, Strumpf RK, Schulman SP, Gerstenblith G, DeMaria AN, Denktas AE, Gammon RS, Hermiller JB, Jr., Reisman MA, Schaer GL, and Sherman W**. A randomized, double-blind, placebo-controlled, dose-escalation study of intravenous adult human mesenchymal stem cells (prochymal) after acute myocardial infarction. *J Am Coll Cardiol* 54: 2277-2286, 2009.

121. **Hearse DJ**. Models and problems in the study of myocardial ischemia and tissue protection. *Eur Heart J* 4 Suppl C: 43-48, 1983.

122. **Heather LC, Carr CA, Stuckey DJ, Pope S, Morten KJ, Carter EE, Edwards LM, and Clarke K**. Critical role of complex III in the early metabolic changes following myocardial infarction. *Cardiovasc Res* 85: 127-136, 2010.

123. **Heather LC, Cole MA, Lygate CA, Evans RD, Stuckey DJ, Murray AJ, Neubauer S, and Clarke K**. Fatty acid transporter levels and palmitate oxidation rate correlate with ejection fraction in the infarcted rat heart. *Cardiovasc Res* 72: 430-437, 2006.

124. **Henning RJ**. Stem cells in cardiac repair. *Future cardiology* 7: 99-117, 2011.

125. **Hepple RT, Baker DJ, Kaczor JJ, and Krause DJ**. Long-term caloric restriction abrogates the age-related decline in skeletal muscle aerobic function. *Faseb J* 19: 1320-1322, 2005.

126. **Hers I, Vincent EE, and Tavare JM**. Akt signalling in health and disease. *Cellular signalling* 23: 1515-1527, 2011.

127. **Ho KK, Pinsky JL, Kannel WB, and Levy D**. The epidemiology of heart failure: the Framingham Study. *J Am Coll Cardiol* 22: 6A-13A, 1993.

128. **Horwitz EM, and Keating A**. Nonhematopoietic mesenchymal stem cells: what are they? *Cytotherapy* 2: 387-388, 2000.

129. **Horwitz EM, Le Blanc K, Dominici M, Mueller I, Slaper-Cortenbach I, Marini FC, Deans RJ, Krause DS, and Keating A**. Clarification of the nomenclature for MSC: The International Society for Cellular Therapy position statement. *Cytotherapy* 7: 393-395, 2005.

130. **Hou D, Youssef EA, Brinton TJ, Zhang P, Rogers P, Price ET, Yeung AC, Johnstone BH, Yock PG, and March KL**. Radiolabeled cell distribution after

intramyocardial, intracoronary, and interstitial retrograde coronary venous delivery: implications for current clinical trials. *Circulation* 112: I150-156, 2005.

131. **How OJ, Aasum E, Kunnathu S, Severson DL, Myhre ES, and Larsen TS**. Influence of substrate supply on cardiac efficiency, as measured by pressure-volume analysis in ex vivo mouse hearts. *Am J Physiol Heart Circ Physiol* 288: H2979-2985, 2005.

132. **Howard BV, Rodriguez BL, Bennett PH, Harris MI, Hamman R, Kuller LH, Pearson TA, and Wylie-Rosett J**. Prevention Conference VI: Diabetes and Cardiovascular disease: Writing Group I: epidemiology. *Circulation* 105: e132-137, 2002.

133. **Hu Q, Wang X, Lee J, Mansoor A, Liu J, Zeng L, Swingen C, Zhang G, Feygin J, Ochiai K, Bransford TL, From AH, Bache RJ, and Zhang J**. Profound bioenergetic abnormalities in peri-infarct myocardial regions. *Am J Physiol Heart Circ Physiol* 291: H648-657, 2006.

134. **Hue L, and Taegtmeyer H**. The Randle cycle revisited: a new head for an old hat. *Am J Physiol Endocrinol Metab* 297: E578-591, 2009.

135. **Hughey CC, Hittel DS, Johnsen VL, and Shearer J**. Hyperinsulinemic-euglycemic clamp in the conscious rat. *Journal of visualized experiments : JoVE* 2011.

136. **Hughey CC, Hittel DS, Johnsen VL, and Shearer J**. Respirometric oxidative phosphorylation assessment in saponin-permeabilized cardiac fibers. *Journal of visualized experiments : JoVE* 2011.

137. **Hughey CC, Johnsen VL, Ma L, James FD, Young PP, Wasserman DH, Rottman JN, Hittel DS, and Shearer J**. Mesenchymal stem cell transplantation for the

infarcted heart: a role in minimizing abnormalities in cardiac-specific energy metabolism. *Am J Physiol Endocrinol Metab* 302: E163-172, 2012.

138. **Huikuri HV, Kervinen K, Niemela M, Ylitalo K, Saily M, Koistinen P, Savolainen ER, Ukkonen H, Pietila M, Airaksinen JK, Knuuti J, and Makikallio TH**. Effects of intracoronary injection of mononuclear bone marrow cells on left ventricular function, arrhythmia risk profile, and restenosis after thrombolytic therapy of acute myocardial infarction. *Eur Heart J* 29: 2723-2732, 2008.

139. **Hunt SA, Abraham WT, Chin MH, Feldman AM, Francis GS, Ganiats TG, Jessup M, Konstam MA, Mancini DM, Michl K, Oates JA, Rahko PS, Silver MA, Stevenson LW, and Yancy CW**. 2009 focused update incorporated into the ACC/AHA 2005 Guidelines for the Diagnosis and Management of Heart Failure in Adults: a report of the American College of Cardiology Foundation/American Heart Association Task Force on Practice Guidelines: developed in collaboration with the International Society for Heart and Lung Transplantation. *Circulation* 119: e391-479, 2009.

140. **Huss JM, and Kelly DP**. Nuclear receptor signaling and cardiac energetics. *Circ Res* 95: 568-578, 2004.

141. **Hutter E, Unterluggauer H, Garedew A, Jansen-Durr P, and Gnaiger E**. High-resolution respirometry--a modern tool in aging research. *Exp Gerontol* 41: 103-109, 2006.

142. **Ikeuchi M, Matsusaka H, Kang D, Matsushima S, Ide T, Kubota T, Fujiwara T, Hamasaki N, Takeshita A, Sunagawa K, and Tsutsui H**. Overexpression of mitochondrial transcription factor a ameliorates mitochondrial deficiencies and cardiac failure after myocardial infarction. *Circulation* 112: 683-690, 2005.

143. **Ingelsson E, Sundstrom J, Arnlov J, Zethelius B, and Lind L**. Insulin resistance and risk of congestive heart failure. *JAMA : the journal of the American Medical Association* 294: 334-341, 2005.

144. **Ingwall JS**. Energy metabolism in heart failure and remodelling. *Cardiovasc Res* 81: 412-419, 2009.

145. **Ingwall JS**. On substrate selection for ATP synthesis in the failing human myocardium. *Am J Physiol Heart Circ Physiol* 293: H3225-3226, 2007.

146. **Ingwall JS, and Weiss RG**. Is the failing heart energy starved? On using chemical energy to support cardiac function. *Circ Res* 95: 135-145, 2004.

147. **Issad T, Masson E, and Pagesy P**. O-GlcNAc modification, insulin signaling and diabetic complications. *Diabetes & metabolism* 36: 423-435, 2010.

148. **Jameel MN, Li Q, Mansoor A, Qiang X, Sarver A, Wang X, Swingen C, and Zhang J**. Long-term functional improvement and gene expression changes after bone marrow-derived multipotent progenitor cell transplantation in myocardial infarction. *Am J Physiol Heart Circ Physiol* 298: H1348-1356, 2010.

149. **Janssens S**. Stem cells in the treatment of heart disease. *Annu Rev Med* 61: 287-300, 2010.

150. **Janssens S, Dubois C, Bogaert J, Theunissen K, Deroose C, Desmet W, Kalantzi M, Herbots L, Sinnaeve P, Dens J, Maertens J, Rademakers F, Dymarkowski S, Gheysens O, Van Cleemput J, Bormans G, Nuyts J, Belmans A, Mortelmans L, Boogaerts M, and Van de Werf F**. Autologous bone marrow-derived stem-cell transfer in patients with ST-segment elevation myocardial infarction: double-blind, randomised controlled trial. *Lancet* 367: 113-121, 2006.

151. **Jastroch M, Divakaruni AS, Mookerjee S, Treberg JR, and Brand MD**. Mitochondrial proton and electron leaks. *Essays in biochemistry* 47: 53-67, 2010.

152. **Jaswal JS, Keung W, Wang W, Ussher JR, and Lopaschuk GD**. Targeting fatty acid and carbohydrate oxidation--a novel therapeutic intervention in the ischemic and failing heart. *Biochim Biophys Acta* 1813: 1333-1350, 2011.

153. **Javadov S, Huang C, Kirshenbaum L, and Karmazyn M**. NHE-1 inhibition improves impaired mitochondrial permeability transition and respiratory function during postinfarction remodelling in the rat. *J Mol Cell Cardiol* 38: 135-143, 2005.

154. **Javadov S, Purdham DM, Zeidan A, and Karmazyn M**. NHE-1 inhibition improves cardiac mitochondrial function through regulation of mitochondrial biogenesis during postinfarction remodeling. *Am J Physiol Heart Circ Physiol* 291: H1722-1730, 2006.

155. **Jiang R, Han Z, Zhuo G, Qu X, Li X, Wang X, Shao Y, Yang S, and Han ZC**. Transplantation of placenta-derived mesenchymal stem cells in type 2 diabetes: a pilot study. *Frontiers of medicine* 5: 94-100, 2011.

156. **Kang HJ, Lee HY, Na SH, Chang SA, Park KW, Kim HK, Kim SY, Chang HJ, Lee W, Kang WJ, Koo BK, Kim YJ, Lee DS, Sohn DW, Han KS, Oh BH, Park YB, and Kim HS**. Differential effect of intracoronary infusion of mobilized peripheral blood stem cells by granulocyte colony-stimulating factor on left ventricular function and remodeling in patients with acute myocardial infarction versus old myocardial infarction: the MAGIC Cell-3-DES randomized, controlled trial. *Circulation* 114: I145-151, 2006.

157. **Kannel WB, and McGee DL**. Diabetes and cardiovascular disease. The Framingham study. *JAMA : the journal of the American Medical Association* 241: 2035-2038, 1979.

158. **Kanno S, Lerner DL, Schuessler RB, Betsuyaku T, Yamada KA, Saffitz JE, and Kovacs A**. Echocardiographic evaluation of ventricular remodeling in a mouse model of myocardial infarction. *J Am Soc Echocardiogr* 15: 601-609, 2002.

159. **Karnieli E, and Armoni M**. Transcriptional regulation of the insulin-responsive glucose transporter GLUT4 gene: from physiology to pathology. *Am J Physiol Endocrinol Metab* 295: E38-45, 2008.

160. **Kasahara M, and Hinkle PC**. Reconstitution and purification of the D-glucose transporter from human erythrocytes. *J Biol Chem* 252: 7384-7390, 1977.

161. **Katome T, Obata T, Matsushima R, Masuyama N, Cantley LC, Gotoh Y, Kishi K, Shiota H, and Ebina Y**. Use of RNA interference-mediated gene silencing and adenoviral overexpression to elucidate the roles of AKT/protein kinase B isoforms in insulin actions. *J Biol Chem* 278: 28312-28323, 2003.

162. **Keating A**. Mesenchymal stromal cells: new directions. *Cell Stem Cell* 10: 709-716, 2012.

163. **Keats EC, and Khan ZA**. Vascular stem cells in diabetic complications: evidence for a role in the pathogenesis and the therapeutic promise. *Cardiovascular diabetology* 11: 37, 2012.

164. **Kelly DP, and Scarpulla RC**. Transcriptional regulatory circuits controlling mitochondrial biogenesis and function. *Genes Dev* 18: 357-368, 2004.

165. **Kemi OJ, Hoydal MA, Haram PM, Garnier A, Fortin D, Ventura-Clapier R, and Ellingsen O**. Exercise training restores aerobic capacity and energy transfer systems in heart failure treated with losartan. *Cardiovasc Res* 76: 91-99, 2007.

166. **Kerner J, and Hoppel C**. Fatty acid import into mitochondria. *Biochim Biophys Acta* 1486: 1-17, 2000.

167. **Khan M, Kwiatkowski P, Rivera BK, and Kuppusamy P**. Oxygen and oxygenation in stem-cell therapy for myocardial infarction. *Life Sci* 87: 269-274.

168. **Kikuchi K, and Poss KD**. Cardiac regenerative capacity and mechanisms. *Annual review of cell and developmental biology* 28: 719-741, 2012.

169. **Kim WS, Park BS, Kim HK, Park JS, Kim KJ, Choi JS, Chung SJ, Kim DD, and Sung JH**. Evidence supporting antioxidant action of adipose-derived stem cells: protection of human dermal fibroblasts from oxidative stress. *J Dermatol Sci* 49: 133-142, 2008.

170. **Kobayasi R, Akamine EH, Davel AP, Rodrigues MA, Carvalho CR, and Rossoni LV**. Oxidative stress and inflammatory mediators contribute to endothelial dysfunction in high-fat diet-induced obesity in mice. *Journal of hypertension* 28: 2111-2119, 2010.

171. **Kohn AD, Summers SA, Birnbaum MJ, and Roth RA**. Expression of a constitutively active Akt Ser/Thr kinase in 3T3-L1 adipocytes stimulates glucose uptake and glucose transporter 4 translocation. *J Biol Chem* 271: 31372-31378, 1996.

172. **Kolios G, and Moodley Y**. Introduction to stem cells and regenerative medicine. *Respiration; international review of thoracic diseases* 85: 3-10, 2013.

173. **Kolwicz SC, Jr., and Tian R**. Metabolic therapy at the crossroad: how to optimize myocardial substrate utilization? *Trends Cardiovasc Med* 19: 201-207, 2009.

174. **Korvald C, Elvenes OP, and Myrmel T**. Myocardial substrate metabolism influences left ventricular energetics in vivo. *Am J Physiol Heart Circ Physiol* 278: H1345-1351, 2000.

175. **Kraljevic J, Marinovic J, Pravdic D, Zubin P, Dujic Z, Wisloff U, and Ljubkovic M**. Aerobic interval training attenuates remodelling and mitochondrial dysfunction in the post-infarction failing rat heart. *Cardiovasc Res* 2013.

176. **Kuhn NZ, and Tuan RS**. Regulation of stemness and stem cell niche of mesenchymal stem cells: implications in tumorigenesis and metastasis. *J Cell Physiol* 222: 268-277.

177. **Kuo TH, Moore KH, Giacomelli F, and Wiener J**. Defective oxidative metabolism of heart mitochondria from genetically diabetic mice. *Diabetes* 32: 781-787, 1983.

178. **Kuznetsov AV, Veksler V, Gellerich FN, Saks V, Margreiter R, and Kunz WS**. Analysis of mitochondrial function in situ in permeabilized muscle fibers, tissues and cells. *Nat Protoc* 3: 965-976, 2008.

179. **Larsen S, Nielsen J, Hansen CN, Nielsen LB, Wibrand F, Stride N, Schroder HD, Boushel R, Helge JW, Dela F, and Hey-Mogensen M**. Biomarkers of mitochondrial content in skeletal muscle of healthy young human subjects. *J Physiol* 590: 3349-3360, 2012.

180. **Le FP**. Evidence of active transfer of certain non-electrolytes across the human red cell membrane. *The Journal of general physiology* 31: 505-527, 1948.

181. **Lee J, Xu Y, Lu L, Bergman B, Leitner JW, Greyson C, Draznin B, and Schwartz GG**. Multiple abnormalities of myocardial insulin signaling in a porcine model of diet-induced obesity. *Am J Physiol Heart Circ Physiol* 298: H310-319, 2010.

182. **Lee RH, Seo MJ, Reger RL, Spees JL, Pulin AA, Olson SD, and Prockop DJ**. Multipotent stromal cells from human marrow home to and promote repair of pancreatic islets and renal glomeruli in diabetic NOD/scid mice. *Proc Natl Acad Sci U S A* 103: 17438-17443, 2006.

183. **Lee-Young RS, Griffee SR, Lynes SE, Bracy DP, Ayala JE, McGuinness OP, and Wasserman DH**. Skeletal muscle AMP-activated protein kinase is essential for the metabolic response to exercise in vivo. *J Biol Chem* 284: 23925-23934, 2009.

184. **Lehman JJ, Barger PM, Kovacs A, Saffitz JE, Medeiros DM, and Kelly DP**. Peroxisome proliferator-activated receptor gamma coactivator-1 promotes cardiac mitochondrial biogenesis. *J Clin Invest* 106: 847-856, 2000.

185. **Lehman JJ, Boudina S, Banke NH, Sambandam N, Han X, Young DM, Leone TC, Gross RW, Lewandowski ED, Abel ED, and Kelly DP**. The transcriptional coactivator PGC-1alpha is essential for maximal and efficient cardiac mitochondrial fatty acid oxidation and lipid homeostasis. *Am J Physiol Heart Circ Physiol* 295: H185-196, 2008.

186. **Lemieux H, and Hoppel CL**. Mitochondria in the human heart. *J Bioenerg Biomembr* 41: 99-106, 2009.

187. **Leto D, and Saltiel AR**. Regulation of glucose transport by insulin: traffic control of GLUT4. *Nature reviews Molecular cell biology* 13: 383-396, 2012.

188. **Li L, Zeng H, and Chen JX**. Apelin-13 increases myocardial progenitor cells and improves repair postmyocardial infarction. *Am J Physiol Heart Circ Physiol* 303: H605-618, 2012.

189. **Li SH, Lai TY, Sun Z, Han M, Moriyama E, Wilson B, Fazel S, Weisel RD, Yau T, Wu JC, and Li RK**. Tracking cardiac engraftment and distribution of implanted bone marrow cells: Comparing intra-aortic, intravenous, and intramyocardial delivery. *J Thorac Cardiovasc Surg* 137: 1225-1233 e1221, 2009.

190. **Liu B, Wang LC, and Belke DD**. Effect of low temperature on the cytosolic free Ca2+ in rat ventricular myocytes. *Cell Calcium* 12: 11-18, 1991.

191. **Lo T, Ho JH, Yang MH, and Lee OK**. Glucose reduction prevents replicative senescence and increases mitochondrial respiration in human mesenchymal stem cells. *Cell Transplant* 20: 813-825, 2011.

192. **Lomuscio A, Castagnone M, Vergani D, Verzoni A, Beltrami A, Ravaglia R, and Pozzoni L**. Clinical correlation between diabetic and non diabetic patients with myocardial infarction. *Acta cardiologica* 46: 543-554, 1991.

193. **Lopaschuk GD, Barr R, Thomas PD, and Dyck JR**. Beneficial effects of trimetazidine in ex vivo working ischemic hearts are due to a stimulation of glucose oxidation secondary to inhibition of long-chain 3-ketoacyl coenzyme a thiolase. *Circ Res* 93: e33-37, 2003.

194. **Lopaschuk GD, Ussher JR, Folmes CD, Jaswal JS, and Stanley WC**. Myocardial fatty acid metabolism in health and disease. *Physiol Rev* 90: 207-258, 2010.

195. **Lopaschuk GD, Ussher JR, Folmes CD, Jaswal JS, and Stanley WC**. Myocardial fatty acid metabolism in health and disease. *Physiol Rev* 90: 207-258.

196. **Lord-Dufour S, Copland IB, Levros LC, Jr., Post M, Das A, Khosla C, Galipeau J, Rassart E, and Annabi B**. Evidence for transcriptional regulation of the glucose-6-phosphate transporter by HIF-1alpha: Targeting G6PT with mumbaistatin analogs in hypoxic mesenchymal stromal cells. *Stem Cells* 27: 489-497, 2009.

197. **Lovell MJ, Yasin M, Lee KL, Cheung KK, Shintani Y, Collino M, Sivarajah A, Leung KY, Takahashi K, Kapoor A, Yaqoob MM, Suzuki K, Lythgoe MF, Martin J, Munroe PB, Thiemermann C, and Mathur A**. Bone marrow mononuclear cells reduce myocardial reperfusion injury by activating the PI3K/Akt survival pathway. *Atherosclerosis* 213: 67-76, 2010.

198. **Lowell BB, V SS, Hamann A, Lawitts JA, Himms-Hagen J, Boyer BB, Kozak LP, and Flier JS**. Development of obesity in transgenic mice after genetic ablation of brown adipose tissue. *Nature* 366: 740-742, 1993.

199. **Ludwig B, Bender E, Arnold S, Huttemann M, Lee I, and Kadenbach B**. Cytochrome C oxidase and the regulation of oxidative phosphorylation. *Chembiochem* 2: 392-403, 2001.

200. **Luiken JJ, Arumugam Y, Dyck DJ, Bell RC, Pelsers MM, Turcotte LP, Tandon NN, Glatz JF, and Bonen A**. Increased rates of fatty acid uptake and plasmalemmal fatty acid transporters in obese Zucker rats. *J Biol Chem* 276: 40567-40573, 2001.

201. **Lunde K, Solheim S, Aakhus S, Arnesen H, Abdelnoor M, Egeland T, Endresen K, Ilebekk A, Mangschau A, Fjeld JG, Smith HJ, Taraldsrud E, Grogaard HK, Bjornerheim R, Brekke M, Muller C, Hopp E, Ragnarsson A,**

Brinchmann JE, and Forfang K. Intracoronary injection of mononuclear bone marrow cells in acute myocardial infarction. *N Engl J Med* 355: 1199-1209, 2006.

202. **Madrazo JA, and Kelly DP**. The PPAR trio: regulators of myocardial energy metabolism in health and disease. *J Mol Cell Cardiol* 44: 968-975, 2008.

203. **Majewski N, Nogueira V, Bhaskar P, Coy PE, Skeen JE, Gottlob K, Chandel NS, Thompson CB, Robey RB, and Hay N**. Hexokinase-mitochondria interaction mediated by Akt is required to inhibit apoptosis in the presence or absence of Bax and Bak. *Mol Cell* 16: 819-830, 2004.

204. **Maki M, Luotolahti M, Nuutila P, Iida H, Voipio-Pulkki LM, Ruotsalainen U, Haaparanta M, Solin O, Hartiala J, Harkonen R, and Knuuti J**. Glucose uptake in the chronically dysfunctional but viable myocardium. *Circulation* 93: 1658-1666, 1996.

205. **Makino S, Fukuda K, Miyoshi S, Konishi F, Kodama H, Pan J, Sano M, Takahashi T, Hori S, Abe H, Hata J, Umezawa A, and Ogawa S**. Cardiomyocytes can be generated from marrow stromal cells in vitro. *J Clin Invest* 103: 697-705, 1999.

206. **Marshall BA, and Mueckler MM**. Differential effects of GLUT-1 or GLUT-4 overexpression on insulin responsiveness in transgenic mice. *Am J Physiol* 267: E738-744, 1994.

207. **Masek J, and Fabry P**. High-fat diet and the development of obesity in albino rats. *Experientia* 15: 444-445, 1959.

208. **Mazo M, Gavira JJ, Abizanda G, Moreno C, Ecay M, Soriano M, Aranda P, Collantes M, Alegria E, Merino J, Penuelas I, Garcia Verdugo JM, Pelacho B, and Prosper F**. Transplantation of mesenchymal stem cells exerts a greater long-term effect

than bone marrow mononuclear cells in a chronic myocardial infarction model in rat. *Cell Transplant* 19: 313-328, 2010.

209. **Mazo M, Planat-Benard V, Abizanda G, Pelacho B, Leobon B, Gavira JJ, Penuelas I, Cemborain A, Penicaud L, Laharrague P, Joffre C, Boisson M, Ecay M, Collantes M, Barba J, Casteilla L, and Prosper F**. Transplantation of adipose derived stromal cells is associated with functional improvement in a rat model of chronic myocardial infarction. *Eur J Heart Fail* 10: 454-462, 2008.

210. **Mazumder PK, O'Neill BT, Roberts MW, Buchanan J, Yun UJ, Cooksey RC, Boudina S, and Abel ED**. Impaired cardiac efficiency and increased fatty acid oxidation in insulin-resistant ob/ob mouse hearts. *Diabetes* 53: 2366-2374, 2004.

211. **McMurray F, and Cox RD**. Mouse models and type 2 diabetes: translational opportunities. *Mamm Genome* 22: 390-400, 2011.

212. **Meluzin J, Mayer J, Groch L, Janousek S, Hornacek I, Hlinomaz O, Kala P, Panovsky R, Prasek J, Kaminek M, Stanicek J, Klabusay M, Koristek Z, Navratil M, Dusek L, and Vinklarkova J**. Autologous transplantation of mononuclear bone marrow cells in patients with acute myocardial infarction: the effect of the dose of transplanted cells on myocardial function. *Am Heart J* 152: 975 e979-915, 2006.

213. **Menasche P**. Stem cell therapy for heart failure: are arrhythmias a real safety concern? *Circulation* 119: 2735-2740, 2009.

214. **Michael LF, Wu Z, Cheatham RB, Puigserver P, Adelmant G, Lehman JJ, Kelly DP, and Spiegelman BM**. Restoration of insulin-sensitive glucose transporter (GLUT4) gene expression in muscle cells by the transcriptional coactivator PGC-1. *Proc Natl Acad Sci U S A* 98: 3820-3825, 2001.

215. **Milner DJ, Mavroidis M, Weisleder N, and Capetanaki Y**. Desmin cytoskeleton linked to muscle mitochondrial distribution and respiratory function. *J Cell Biol* 150: 1283-1298, 2000.

216. **Minicucci MF, Azevedo PS, Polegato BF, Paiva SA, and Zornoff LA**. Heart failure after myocardial infarction: clinical implications and treatment. *Clinical cardiology* 34: 410-414, 2011.

217. **Miura T, and Miki T**. Limitation of myocardial infarct size in the clinical setting: current status and challenges in translating animal experiments into clinical therapy. *Basic Res Cardiol* 103: 501-513, 2008.

218. **Morgan CR, and Lazarow A**. Immunoassay of pancreatic and plasma insulin following alloxan injection of rats. *Diabetes* 14: 669-671, 1965.

219. **Morgan HE, Henderson MJ, Regen DM, and Park CR**. Regulation of glucose uptake in muscle. I. The effects of insulin and anoxia on glucose transport and phosphorylation in the isolated, perfused heart of normal rats. *J Biol Chem* 236: 253-261, 1961.

220. **Motojima K, Passilly P, Peters JM, Gonzalez FJ, and Latruffe N**. Expression of putative fatty acid transporter genes are regulated by peroxisome proliferator-activated receptor alpha and gamma activators in a tissue- and inducer-specific manner. *J Biol Chem* 273: 16710-16714, 1998.

221. **Mueckler M, Caruso C, Baldwin SA, Panico M, Blench I, Morris HR, Allard WJ, Lienhard GE, and Lodish HF**. Sequence and structure of a human glucose transporter. *Science* 229: 941-945, 1985.

222. **Muniyappa R, Lee S, Chen H, and Quon MJ**. Current approaches for assessing insulin sensitivity and resistance in vivo: advantages, limitations, and appropriate usage. *Am J Physiol Endocrinol Metab* 294: E15-26, 2008.

223. **Murray AJ, Anderson RE, Watson GC, Radda GK, and Clarke K**. Uncoupling proteins in human heart. *Lancet* 364: 1786-1788, 2004.

224. **Murray AJ, Cole MA, Lygate CA, Carr CA, Stuckey DJ, Little SE, Neubauer S, and Clarke K**. Increased mitochondrial uncoupling proteins, respiratory uncoupling and decreased efficiency in the chronically infarcted rat heart. *J Mol Cell Cardiol* 44: 694-700, 2008.

225. **Murray AJ, Knight NS, Little SE, Cochlin LE, Clements M, and Clarke K**. Dietary long-chain, but not medium-chain, triglycerides impair exercise performance and uncouple cardiac mitochondria in rats. *Nutrition & metabolism* 8: 55, 2011.

226. **Murray AJ, Lygate CA, Cole MA, Carr CA, Radda GK, Neubauer S, and Clarke K**. Insulin resistance, abnormal energy metabolism and increased ischemic damage in the chronically infarcted rat heart. *Cardiovasc Res* 71: 149-157, 2006.

227. **Murray AJ, Panagia M, Hauton D, Gibbons GF, and Clarke K**. Plasma free fatty acids and peroxisome proliferator-activated receptor alpha in the control of myocardial uncoupling protein levels. *Diabetes* 54: 3496-3502, 2005.

228. **Mylotte LA, Duffy AM, Murphy M, O'Brien T, Samali A, Barry F, and Szegezdi E**. Metabolic flexibility permits mesenchymal stem cell survival in an ischemic environment. *Stem Cells* 26: 1325-1336, 2008.

229. **Neel S, and Singla DK**. Induced pluripotent stem (iPS) cells inhibit apoptosis and fibrosis in streptozotocin-induced diabetic rats. *Molecular pharmaceutics* 8: 2350-2357, 2011.

230. **Neubauer S**. The failing heart--an engine out of fuel. *N Engl J Med* 356: 1140-1151, 2007.

231. **Neubauer S, Horn M, Cramer M, Harre K, Newell JB, Peters W, Pabst T, Ertl G, Hahn D, Ingwall JS, and Kochsiek K**. Myocardial phosphocreatine-to-ATP ratio is a predictor of mortality in patients with dilated cardiomyopathy. *Circulation* 96: 2190-2196, 1997.

232. **Ng Y, Ramm G, Lopez JA, and James DE**. Rapid activation of Akt2 is sufficient to stimulate GLUT4 translocation in 3T3-L1 adipocytes. *Cell Metab* 7: 348-356, 2008.

233. **Nilsson C, Raun K, Yan FF, Larsen MO, and Tang-Christensen M**. Laboratory animals as surrogate models of human obesity. *Acta pharmacologica Sinica* 33: 173-181, 2012.

234. **Norhammar A, Malmberg K, Diderholm E, Lagerqvist B, Lindahl B, Ryden L, and Wallentin L**. Diabetes mellitus: the major risk factor in unstable coronary artery disease even after consideration of the extent of coronary artery disease and benefits of revascularization. *J Am Coll Cardiol* 43: 585-591, 2004.

235. **Nyamandi VZ, Johnsen VL, Hughey CC, Hittel DS, Khan A, Newell C, and Shearer J**. Enhanced stem cell engraftment and modulation of hepatic reactive oxygen species production in diet-induced obesity. *Obesity (Silver Spring)* 2013.

236. **Oh JY, Lee RH, Yu JM, Ko JH, Lee HJ, Ko AY, Roddy GW, and Prockop DJ**. Intravenous mesenchymal stem cells prevented rejection of allogeneic corneal transplants by aborting the early inflammatory response. *Mol Ther* 20: 2143-2152, 2012.

237. **Omar B, Pacini G, and Ahren B**. Differential development of glucose intolerance and pancreatic islet adaptation in multiple diet induced obesity models. *Nutrients* 4: 1367-1381, 2012.

238. **Panchal SK, and Brown L**. Rodent models for metabolic syndrome research. *Journal of biomedicine & biotechnology* 2011: 351982, 2011.

239. **Park SY, Cho YR, Kim HJ, Higashimori T, Danton C, Lee MK, Dey A, Rothermel B, Kim YB, Kalinowski A, Russell KS, and Kim JK**. Unraveling the temporal pattern of diet-induced insulin resistance in individual organs and cardiac dysfunction in C57BL/6 mice. *Diabetes* 54: 3530-3540, 2005.

240. **Passonneau JV, and Lowry OH**. Phosphofructokinase and the Pasteur effect. *Biochem Biophys Res Commun* 7: 10-15, 1962.

241. **Pastorino JG, Hoek JB, and Shulga N**. Activation of glycogen synthase kinase 3beta disrupts the binding of hexokinase II to mitochondria by phosphorylating voltage-dependent anion channel and potentiates chemotherapy-induced cytotoxicity. *Cancer research* 65: 10545-10554, 2005.

242. **Paternostro G, Pagano D, Gnecchi-Ruscone T, Bonser RS, and Camici PG**. Insulin resistance in patients with cardiac hypertrophy. *Cardiovasc Res* 42: 246-253, 1999.

243. **Patten RD, and Hall-Porter MR**. Small animal models of heart failure: development of novel therapies, past and present. *Circ Heart Fail* 2: 138-144, 2009.

244. **Pecqueur C, Alves-Guerra MC, Gelly C, Levi-Meyrueis C, Couplan E, Collins S, Ricquier D, Bouillaud F, and Miroux B**. Uncoupling protein 2, in vivo distribution, induction upon oxidative stress, and evidence for translational regulation. *J Biol Chem* 276: 8705-8712, 2001.

245. **Peister A, Mellad JA, Larson BL, Hall BM, Gibson LF, and Prockop DJ**. Adult stem cells from bone marrow (MSCs) isolated from different strains of inbred mice vary in surface epitopes, rates of proliferation, and differentiation potential. *Blood* 103: 1662-1668, 2004.

246. **Pelletier C, Dai S, Roberts KC, Bienek A, Onysko J, and Pelletier L**. Report summary. Diabetes in Canada: facts and figures from a public health perspective. *Chronic diseases and injuries in Canada* 33: 53-54, 2012.

247. **Penn MS, Ellis S, Gandhi S, Greenbaum A, Hodes Z, Mendelsohn FO, Strasser D, Ting AE, and Sherman W**. Adventitial delivery of an allogeneic bone marrow-derived adherent stem cell in acute myocardial infarction: phase I clinical study. *Circ Res* 110: 304-311, 2012.

248. **Pepine CJ, and Nichols WW**. The pathophysiology of chronic ischemic heart disease. *Clinical cardiology* 30: I4-9, 2007.

249. **Perin EC, Silva GV, Assad JA, Vela D, Buja LM, Sousa AL, Litovsky S, Lin J, Vaughn WK, Coulter S, Fernandes MR, and Willerson JT**. Comparison of intracoronary and transendocardial delivery of allogeneic mesenchymal cells in a canine model of acute myocardial infarction. *J Mol Cell Cardiol* 44: 486-495, 2008.

250. **Peterson LR, Herrero P, Schechtman KB, Racette SB, Waggoner AD, Kisrieva-Ware Z, Dence C, Klein S, Marsala J, Meyer T, and Gropler RJ**. Effect of

obesity and insulin resistance on myocardial substrate metabolism and efficiency in young women. *Circulation* 109: 2191-2196, 2004.

251. **Pfeffer MA, Pfeffer JM, Fishbein MC, Fletcher PJ, Spadaro J, Kloner RA, and Braunwald E**. Myocardial infarct size and ventricular function in rats. *Circ Res* 44: 503-512, 1979.

252. **Picard M, Taivassalo T, Ritchie D, Wright KJ, Thomas MM, Romestaing C, and Hepple RT**. Mitochondrial structure and function are disrupted by standard isolation methods. *PLoS One* 6: e18317, 2011.

253. **Pittenger MF, Mackay AM, Beck SC, Jaiswal RK, Douglas R, Mosca JD, Moorman MA, Simonetti DW, Craig S, and Marshak DR**. Multilineage potential of adult human mesenchymal stem cells. *Science* 284: 143-147, 1999.

254. **Pittenger MF, and Martin BJ**. Mesenchymal stem cells and their potential as cardiac therapeutics. *Circ Res* 95: 9-20, 2004.

255. **Pomplun D, Mohlig M, Spranger J, Pfeiffer AF, and Ristow M**. Elevation of blood glucose following anaesthetic treatment in C57BL/6 mice. *Hormone and metabolic research = Hormon- und Stoffwechselforschung = Hormones et metabolisme* 36: 67-69, 2004.

256. **Puigserver P, Wu Z, Park CW, Graves R, Wright M, and Spiegelman BM**. A cold-inducible coactivator of nuclear receptors linked to adaptive thermogenesis. *Cell* 92: 829-839, 1998.

257. **Randle PJ**. Regulatory interactions between lipids and carbohydrates: the glucose fatty acid cycle after 35 years. *Diabetes/metabolism reviews* 14: 263-283, 1998.

258. **Randle PJ, Garland PB, Hales CN, and Newsholme EA**. The glucose fatty-acid cycle. Its role in insulin sensitivity and the metabolic disturbances of diabetes mellitus. *Lancet* 1: 785-789, 1963.

259. **Ranganath SH, Levy O, Inamdar MS, and Karp JM**. Harnessing the mesenchymal stem cell secretome for the treatment of cardiovascular disease. *Cell Stem Cell* 10: 244-258, 2012.

260. **Razeghi P, Young ME, Ying J, Depre C, Uray IP, Kolesar J, Shipley GL, Moravec CS, Davies PJ, Frazier OH, and Taegtmeyer H**. Downregulation of metabolic gene expression in failing human heart before and after mechanical unloading. *Cardiology* 97: 203-209, 2002.

261. **Regan TJ, Lyons MM, Ahmed SS, Levinson GE, Oldewurtel HA, Ahmad MR, and Haider B**. Evidence for cardiomyopathy in familial diabetes mellitus. *J Clin Invest* 60: 884-899, 1977.

262. **Remondino A, Rosenblatt-Velin N, Montessuit C, Tardy I, Papageorgiou I, Dorsaz PA, Jorge-Costa M, and Lerch R**. Altered expression of proteins of metabolic regulation during remodeling of the left ventricle after myocardial infarction. *J Mol Cell Cardiol* 32: 2025-2034, 2000.

263. **Ren JM, Marshall BA, Mueckler MM, McCaleb M, Amatruda JM, and Shulman GI**. Overexpression of Glut4 protein in muscle increases basal and insulin-stimulated whole body glucose disposal in conscious mice. *J Clin Invest* 95: 429-432, 1995.

264. **Rennison JH, McElfresh TA, Chen X, Anand VR, Hoit BD, Hoppel CL, and Chandler MP**. Prolonged exposure to high dietary lipids is not associated with lipotoxicity in heart failure. *J Mol Cell Cardiol* 46: 883-890, 2009.

265. **Rennison JH, McElfresh TA, Okere IC, Patel HV, Foster AB, Patel KK, Stoll MS, Minkler PE, Fujioka H, Hoit BD, Young ME, Hoppel CL, and Chandler MP**. Enhanced acyl-CoA dehydrogenase activity is associated with improved mitochondrial and contractile function in heart failure. *Cardiovasc Res* 79: 331-340, 2008.

266. **Rennison JH, McElfresh TA, Okere IC, Vazquez EJ, Patel HV, Foster AB, Patel KK, Chen Q, Hoit BD, Tserng KY, Hassan MO, Hoppel CL, and Chandler MP**. High-fat diet postinfarction enhances mitochondrial function and does not exacerbate left ventricular dysfunction. *Am J Physiol Heart Circ Physiol* 292: H1498-1506, 2007.

267. **Resnick HE, Foster GL, Bardsley J, and Ratner RE**. Achievement of American Diabetes Association clinical practice recommendations among U.S. adults with diabetes, 1999-2002: the National Health and Nutrition Examination Survey. *Diabetes Care* 29: 531-537, 2006.

268. **Rimbaud S, Garnier A, and Ventura-Clapier R**. Mitochondrial biogenesis in cardiac pathophysiology. *Pharmacological reports : PR* 61: 131-138, 2009.

269. **Robey TE, Saiget MK, Reinecke H, and Murry CE**. Systems approaches to preventing transplanted cell death in cardiac repair. *J Mol Cell Cardiol* 45: 567-581, 2008.

270. **Rosca MG, and Hoppel CL**. Mitochondria in heart failure. *Cardiovasc Res* 88: 40-50.

271. **Rosca MG, and Hoppel CL**. Mitochondrial dysfunction in heart failure. *Heart Fail Rev* 2012.

272. **Rosca MG, and Hoppel CL**. New aspects of impaired mitochondrial function in heart failure. *J Bioenerg Biomembr* 41: 107-112, 2009.

273. **Rosca MG, Tandler B, and Hoppel CL**. Mitochondria in cardiac hypertrophy and heart failure. *J Mol Cell Cardiol* 55: 31-41, 2013.

274. **Rosca MG, Vazquez EJ, Kerner J, Parland W, Chandler MP, Stanley W, Sabbah HN, and Hoppel CL**. Cardiac mitochondria in heart failure: decrease in respirasomes and oxidative phosphorylation. *Cardiovasc Res* 80: 30-39, 2008.

275. **Rosenblatt-Velin N, Montessuit C, Papageorgiou I, Terrand J, and Lerch R**. Postinfarction heart failure in rats is associated with upregulation of GLUT-1 and downregulation of genes of fatty acid metabolism. *Cardiovasc Res* 52: 407-416, 2001.

276. **Rottman JN, Bracy D, Malabanan C, Yue Z, Clanton J, and Wasserman DH**. Contrasting effects of exercise and NOS inhibition on tissue-specific fatty acid and glucose uptake in mice. *Am J Physiol Endocrinol Metab* 283: E116-123, 2002.

277. **Rottman JN, Ni G, and Brown M**. Echocardiographic evaluation of ventricular function in mice. *Echocardiography* 24: 83-89, 2007.

278. **Rottman JN, Ni G, Khoo M, Wang Z, Zhang W, Anderson ME, and Madu EC**. Temporal changes in ventricular function assessed echocardiographically in conscious and anesthetized mice. *J Am Soc Echocardiogr* 16: 1150-1157, 2003.

279. **Rubler S, Dlugash J, Yuceoglu YZ, Kumral T, Branwood AW, and Grishman A**. New type of cardiomyopathy associated with diabetic glomerulosclerosis. *The American journal of cardiology* 30: 595-602, 1972.

280. **Sack MN, Disch DL, Rockman HA, and Kelly DP**. A role for Sp and nuclear receptor transcription factors in a cardiac hypertrophic growth program. *Proc Natl Acad Sci U S A* 94: 6438-6443, 1997.

281. **Saito Y**. Roles of atrial natriuretic peptide and its therapeutic use. *J Cardiol* 56: 262-270.

282. **Saks VA, Vasil'eva E, Belikova Yu O, Kuznetsov AV, Lyapina S, Petrova L, and Perov NA**. Retarded diffusion of ADP in cardiomyocytes: possible role of mitochondrial outer membrane and creatine kinase in cellular regulation of oxidative phosphorylation. *Biochim Biophys Acta* 1144: 134-148, 1993.

283. **Saks VA, Veksler VI, Kuznetsov AV, Kay L, Sikk P, Tiivel T, Tranqui L, Olivares J, Winkler K, Wiedemann F, and Kunz WS**. Permeabilized cell and skinned fiber techniques in studies of mitochondrial function in vivo. *Mol Cell Biochem* 184: 81-100, 1998.

284. **Salto-Tellez M, Yung Lim S, El-Oakley RM, Tang TP, ZA AL, and Lim SK**. Myocardial infarction in the C57BL/6J mouse: a quantifiable and highly reproducible experimental model. *Cardiovasc Pathol* 13: 91-97, 2004.

285. **Sanbe A, Tanonaka K, Hanaoka Y, Katoh T, and Takeo S**. Regional energy metabolism of failing hearts following myocardial infarction. *J Mol Cell Cardiol* 25: 995-1013, 1993.

286. **Scarpulla RC**. Nuclear activators and coactivators in mammalian mitochondrial biogenesis. *Biochim Biophys Acta* 1576: 1-14, 2002.

287. **Scarpulla RC**. Nucleus-encoded regulators of mitochondrial function: integration of respiratory chain expression, nutrient sensing and metabolic stress. *Biochim Biophys Acta* 1819: 1088-1097, 2012.

288. **Scarpulla RC**. Transcriptional paradigms in mammalian mitochondrial biogenesis and function. *Physiol Rev* 88: 611-638, 2008.

289. **Scarpulla RC, Vega RB, and Kelly DP**. Transcriptional integration of mitochondrial biogenesis. *Trends in endocrinology and metabolism: TEM* 23: 459-466, 2012.

290. **Schachinger V, Erbs S, Elsasser A, Haberbosch W, Hambrecht R, Holschermann H, Yu J, Corti R, Mathey DG, Hamm CW, Suselbeck T, Assmus B, Tonn T, Dimmeler S, and Zeiher AM**. Intracoronary bone marrow-derived progenitor cells in acute myocardial infarction. *N Engl J Med* 355: 1210-1221, 2006.

291. **Scheuermann-Freestone M, Madsen PL, Manners D, Blamire AM, Buckingham RE, Styles P, Radda GK, Neubauer S, and Clarke K**. Abnormal cardiac and skeletal muscle energy metabolism in patients with type 2 diabetes. *Circulation* 107: 3040-3046, 2003.

292. **Sethi SS, Akl EG, and Farkouh ME**. Diabetes mellitus and acute coronary syndrome: lessons from randomized clinical trials. *Current diabetes reports* 12: 294-304, 2012.

293. **Severson DL**. Diabetic cardiomyopathy: recent evidence from mouse models of type 1 and type 2 diabetes. *Canadian journal of physiology and pharmacology* 82: 813-823, 2004.

294. **Shake JG, Gruber PJ, Baumgartner WA, Senechal G, Meyers J, Redmond JM, Pittenger MF, and Martin BJ**. Mesenchymal stem cell implantation in a swine myocardial infarct model: engraftment and functional effects. *Ann Thorac Surg* 73: 1919-1925; discussion 1926, 2002.

295. **Sharov VG, Goussev A, Lesch M, Goldstein S, and Sabbah HN**. Abnormal mitochondrial function in myocardium of dogs with chronic heart failure. *J Mol Cell Cardiol* 30: 1757-1762, 1998.

296. **Sharov VG, Todor AV, Silverman N, Goldstein S, and Sabbah HN**. Abnormal mitochondrial respiration in failed human myocardium. *J Mol Cell Cardiol* 32: 2361-2367, 2000.

297. **Shearer J, Duggan G, Weljie A, Hittel DS, Wasserman DH, and Vogel HJ**. Metabolomic profiling of dietary-induced insulin resistance in the high fat-fed C57BL/6J mouse. *Diabetes Obes Metab* 10: 950-958, 2008.

298. **Shearer J, Fueger PT, Bracy DP, Wasserman DH, and Rottman JN**. Partial gene deletion of heart-type fatty acid-binding protein limits the severity of dietary-induced insulin resistance. *Diabetes* 54: 3133-3139, 2005.

299. **Shearer J, Fueger PT, Wang Z, Bracy DP, Wasserman DH, and Rottman JN**. Metabolic implications of reduced heart-type fatty acid binding protein in insulin resistant cardiac muscle. *Biochim Biophys Acta* 1782: 586-592, 2008.

300. **Shearer J, Ross KD, Hughey CC, Johnsen VL, Hittel DS, and Severson DL**. Exercise training does not correct abnormal cardiac glycogen accumulation in the db/db mouse model of type 2 diabetes. *Am J Physiol Endocrinol Metab* 301: E31-39.

301. **Shearer J, Severson DL, Su L, Belardinelli L, and Dhalla AK**. Partial A1 adenosine receptor agonist regulates cardiac substrate utilization in insulin-resistant rats in vivo. *J Pharmacol Exp Ther* 328: 306-311, 2009.

302. **Shi Y, Dierckx A, Wanrooij PH, Wanrooij S, Larsson NG, Wilhelmsson LM, Falkenberg M, and Gustafsson CM**. Mammalian transcription factor A is a core component of the mitochondrial transcription machinery. *Proc Natl Acad Sci U S A* 109: 16510-16515, 2012.

303. **Shimokawa H, and Yasuda S**. Myocardial ischemia: current concepts and future perspectives. *Journal of cardiology* 52: 67-78, 2008.

304. **Si Y, Zhao Y, Hao H, Liu J, Guo Y, Mu Y, Shen J, Cheng Y, Fu X, and Han W**. Infusion of mesenchymal stem cells ameliorates hyperglycemia in type 2 diabetic rats: identification of a novel role in improving insulin sensitivity. *Diabetes* 61: 1616-1625, 2012.

305. **Siegel G, Krause P, Wohrle S, Nowak P, Ayturan M, Kluba T, Brehm BR, Neumeister B, Kohler D, Rosenberger P, Just L, Northoff H, and Schafer R**. Bone marrow-derived human mesenchymal stem cells express cardiomyogenic proteins but do not exhibit functional cardiomyogenic differentiation potential. *Stem Cells Dev* 21: 2457-2470, 2012.

306. **Sielaff H, and Borsch M**. Twisting and subunit rotation in single F(O)(F1)-ATP synthase. *Philos Trans R Soc Lond B Biol Sci* 368: 20120024, 2013.

307. **Siu CW, Liao SY, Liu Y, Lian Q, and Tse HF**. Stem cells for myocardial repair. *Thromb Haemost* 104: 6-12.

308. **Skladal D, Sperl W, Schranzhofer R, Krismer M, Gnaiger E, Margreiter R, and Gellerich F**. Preservation of mitochondrial functions in human skeletal muscle during storage in high energy preservation solution (HEPS). In: What is Controlling Life? In: *Modern Trends in BioThermoKinetics* edited by Gnaiger E, Gellerich F, and Wyss MInnsbruck Univ. Press, 1994, p. 268-271.

309. **Slot JW, Geuze HJ, Gigengack S, James DE, and Lienhard GE**. Translocation of the glucose transporter GLUT4 in cardiac myocytes of the rat. *Proc Natl Acad Sci U S A* 88: 7815-7819, 1991.

310. **Solanes G, Pedraza N, Iglesias R, Giralt M, and Villarroya F**. Functional relationship between MyoD and peroxisome proliferator-activated receptor-dependent regulatory pathways in the control of the human uncoupling protein-3 gene transcription. *Mol Endocrinol* 17: 1944-1958, 2003.

311. **Song H, Song BW, Cha MJ, Choi IG, and Hwang KC**. Modification of mesenchymal stem cells for cardiac regeneration. *Expert Opin Biol Ther* 10: 309-319.

312. **Southworth R**. Hexokinase-mitochondrial interaction in cardiac tissue: implications for cardiac glucose uptake, the 18FDG lumped constant and cardiac protection. *J Bioenerg Biomembr* 41: 187-193, 2009.

313. **Southworth R, Davey KA, Warley A, and Garlick PB**. A reevaluation of the roles of hexokinase I and II in the heart. *Am J Physiol Heart Circ Physiol* 292: H378-386, 2007.

314. **Stanley WC, and Chandler MP**. Energy metabolism in the normal and failing heart: potential for therapeutic interventions. *Heart Fail Rev* 7: 115-130, 2002.

315. **Stanley WC, Recchia FA, and Lopaschuk GD**. Myocardial substrate metabolism in the normal and failing heart. *Physiol Rev* 85: 1093-1129, 2005.

316. **Su X, Sekiguchi M, and Endo M**. An ultrastructural study of cardiac myocytes in postmyocardial infarction ventricular aneurysm representative of chronic ischemic myocardium using semiquantitative and quantitative assessment. *Cardiovasc Pathol* 9: 1-8, 2000.

317. **Suga H**. Ventricular energetics. *Physiol Rev* 70: 247-277, 1990.

318. **Sugden MC**. In appreciation of Sir Philip Randle: the glucose-fatty acid cycle. *The British journal of nutrition* 97: 809-813, 2007.

319. **Sun CK, Chang LT, Sheu JJ, Wang CY, Youssef AA, Wu CJ, Chua S, and Yip HK**. Losartan preserves integrity of cardiac gap junctions and PGC-1 alpha gene expression and prevents cellular apoptosis in remote area of left ventricular myocardium following acute myocardial infarction. *International heart journal* 48: 533-546, 2007.

320. **Sun Y, and Weber KT**. Infarct scar: a dynamic tissue. *Cardiovasc Res* 46: 250-256, 2000.

321. **Swan JW, Anker SD, Walton C, Godsland IF, Clark AL, Leyva F, Stevenson JC, and Coats AJ**. Insulin resistance in chronic heart failure: relation to severity and etiology of heart failure. *J Am Coll Cardiol* 30: 527-532, 1997.

322. **Swynghedauw B**. Molecular mechanisms of myocardial remodeling. *Physiol Rev* 79: 215-262, 1999.

323. **Syed F, Diwan A, and Hahn HS**. Murine echocardiography: a practical approach for phenotyping genetically manipulated and surgically modeled mice. *J Am Soc Echocardiogr* 18: 982-990, 2005.

324. **Szendroedi J, Phielix E, and Roden M**. The role of mitochondria in insulin resistance and type 2 diabetes mellitus. *Nature reviews Endocrinology* 8: 92-103, 2012.

325. **Szkudelski T**. Streptozotocin-nicotinamide-induced diabetes in the rat. Characteristics of the experimental model. *Exp Biol Med (Maywood)* 237: 481-490, 2012.

326. **Taegtmeyer H**. Energy metabolism of the heart: from basic concepts to clinical applications. *Curr Probl Cardiol* 19: 59-113, 1994.

327. **Taegtmeyer H**. Switching metabolic genes to build a better heart. *Circulation* 106: 2043-2045, 2002.

328. **Taha M, and Lopaschuk GD**. Alterations in energy metabolism in cardiomyopathies. *Ann Med* 39: 594-607, 2007.

329. **Tanaka K, Kawano T, Tomino T, Kawano H, Okada T, Oshita S, Takahashi A, and Nakaya Y**. Mechanisms of impaired glucose tolerance and insulin secretion during isoflurane anesthesia. *Anesthesiology* 111: 1044-1051, 2009.

330. **Tarquini R, Lazzeri C, Pala L, Rotella CM, and Gensini GF**. The diabetic cardiomyopathy. *Acta diabetologica* 48: 173-181, 2011.

331. **Tendera M, Wojakowski W, Ruzyllo W, Chojnowska L, Kepka C, Tracz W, Musialek P, Piwowarska W, Nessler J, Buszman P, Grajek S, Breborowicz P, Majka M, and Ratajczak MZ**. Intracoronary infusion of bone marrow-derived selected CD34+CXCR4+ cells and non-selected mononuclear cells in patients with acute STEMI and reduced left ventricular ejection fraction: results of randomized, multicentre Myocardial Regeneration by Intracoronary Infusion of Selected Population of Stem Cells in Acute Myocardial Infarction (REGENT) Trial. *Eur Heart J* 30: 1313-1321, 2009.

332. **Terrovitis JV, Smith RR, and Marban E**. Assessment and optimization of cell engraftment after transplantation into the heart. *Circ Res* 106: 479-494, 2010.

333. **Thorens B, and Mueckler M**. Glucose transporters in the 21st Century. *Am J Physiol Endocrinol Metab* 298: E141-145, 2010.

334. **Tian R, Gaudron P, Neubauer S, Hu K, and Ertl G**. Alterations of performance and oxygen utilization in chronically infarcted rat hearts. *J Mol Cell Cardiol* 28: 321-330, 1996.

335. **Toma C, Pittenger MF, Cahill KS, Byrne BJ, and Kessler PD**. Human mesenchymal stem cells differentiate to a cardiomyocyte phenotype in the adult murine heart. *Circulation* 105: 93-98, 2002.

336. **Traba J, Satrustegui J, and del Arco A**. Adenine nucleotide transporters in organelles: novel genes and functions. *Cellular and molecular life sciences : CMLS* 68: 1183-1206, 2011.

337. **Trachtenberg B, Velazquez DL, Williams AR, McNiece I, Fishman J, Nguyen K, Rouy D, Altman P, Schwarz R, Mendizabal A, Oskouei B, Byrnes J, Soto V, Tracy M, Zambrano JP, Heldman AW, and Hare JM**. Rationale and design of the Transendocardial Injection of Autologous Human Cells (bone marrow or mesenchymal) in Chronic Ischemic Left Ventricular Dysfunction and Heart Failure Secondary to Myocardial Infarction (TAC-HFT) trial: A randomized, double-blind, placebo-controlled study of safety and efficacy. *Am Heart J* 161: 487-493, 2011.

338. **Treadway JL, Hargrove DM, Nardone NA, McPherson RK, Russo JF, Milici AJ, Stukenbrok HA, Gibbs EM, Stevenson RW, and Pessin JE**. Enhanced peripheral

glucose utilization in transgenic mice expressing the human GLUT4 gene. *J Biol Chem* 269: 29956-29961, 1994.

339. **Tropel P, Noel D, Platet N, Legrand P, Benabid AL, and Berger F**. Isolation and characterisation of mesenchymal stem cells from adult mouse bone marrow. *Exp Cell Res* 295: 395-406, 2004.

340. **Tuunanen H, Engblom E, Naum A, Nagren K, Hesse B, Airaksinen KE, Nuutila P, Iozzo P, Ukkonen H, Opie LH, and Knuuti J**. Free fatty acid depletion acutely decreases cardiac work and efficiency in cardiomyopathic heart failure. *Circulation* 114: 2130-2137, 2006.

341. **Tuunanen H, Engblom E, Naum A, Scheinin M, Nagren K, Airaksinen J, Nuutila P, Iozzo P, Ukkonen H, and Knuuti J**. Decreased myocardial free fatty acid uptake in patients with idiopathic dilated cardiomyopathy: evidence of relationship with insulin resistance and left ventricular dysfunction. *J Card Fail* 12: 644-652, 2006.

342. **van Bilsen M, van Nieuwenhoven FA, and van der Vusse GJ**. Metabolic remodelling of the failing heart: beneficial or detrimental? *Cardiovasc Res* 81: 420-428, 2009.

343. **van der Lee KA, Vork MM, De Vries JE, Willemsen PH, Glatz JF, Reneman RS, Van der Vusse GJ, and Van Bilsen M**. Long-chain fatty acid-induced changes in gene expression in neonatal cardiac myocytes. *J Lipid Res* 41: 41-47, 2000.

344. **Vega RB, Huss JM, and Kelly DP**. The coactivator PGC-1 cooperates with peroxisome proliferator-activated receptor alpha in transcriptional control of nuclear genes encoding mitochondrial fatty acid oxidation enzymes. *Mol Cell Biol* 20: 1868-1876, 2000.

345. **Veksler VI, Kuznetsov AV, Sharov VG, Kapelko VI, and Saks VA**. Mitochondrial respiratory parameters in cardiac tissue: a novel method of assessment by using saponin-skinned fibers. *Biochim Biophys Acta* 892: 191-196, 1987.

346. **Ventura-Clapier R, Garnier A, and Veksler V**. Transcriptional control of mitochondrial biogenesis: the central role of PGC-1alpha. *Cardiovasc Res* 79: 208-217, 2008.

347. **Virbasius JV, and Scarpulla RC**. Activation of the human mitochondrial transcription factor A gene by nuclear respiratory factors: a potential regulatory link between nuclear and mitochondrial gene expression in organelle biogenesis. *Proc Natl Acad Sci U S A* 91: 1309-1313, 1994.

348. **Virbasius JV, and Scarpulla RC**. Transcriptional activation through ETS domain binding sites in the cytochrome c oxidase subunit IV gene. *Mol Cell Biol* 11: 5631-5638, 1991.

349. **von Bibra H, and St John Sutton M**. Impact of diabetes on postinfarction heart failure and left ventricular remodeling. *Current heart failure reports* 8: 242-251, 2011.

350. **Wasserman DH**. Four grams of glucose. *Am J Physiol Endocrinol Metab* 296: E11-21, 2009.

351. **Wasserman DH, and Ayala JE**. Interaction of physiological mechanisms in control of muscle glucose uptake. *Clin Exp Pharmacol Physiol* 32: 319-323, 2005.

352. **Wasserman DH, Kang L, Ayala JE, Fueger PT, and Lee-Young RS**. The physiological regulation of glucose flux into muscle in vivo. *J Exp Biol* 214: 254-262, 2011.

353. **Wei H, Ooi TH, Tan G, Lim SY, Qian L, Wong P, and Shim W**. Cell delivery and tracking in post-myocardial infarction cardiac stem cell therapy: an introduction for clinical researchers. *Heart Fail Rev* 15: 1-14, 2010.

354. **Wende AR, Symons JD, and Abel ED**. Mechanisms of lipotoxicity in the cardiovascular system. *Current hypertension reports* 14: 517-531, 2012.

355. **Westerhof N**. Cardiac work and efficiency. *Cardiovasc Res* 48: 4-7, 2000.

356. **Williams AR, and Hare JM**. Mesenchymal stem cells: biology, pathophysiology, translational findings, and therapeutic implications for cardiac disease. *Circ Res* 109: 923-940, 2011.

357. **Wilson JE**. Hexokinases. *Reviews of physiology, biochemistry and pharmacology* 126: 65-198, 1995.

358. **Wilson JE**. Isozymes of mammalian hexokinase: structure, subcellular localization and metabolic function. *J Exp Biol* 206: 2049-2057, 2003.

359. **Witteles RM, and Fowler MB**. Insulin-resistant cardiomyopathy clinical evidence, mechanisms, and treatment options. *J Am Coll Cardiol* 51: 93-102, 2008.

360. **Wollert KC, and Drexler H**. Cell therapy for the treatment of coronary heart disease: a critical appraisal. *Nat Rev Cardiol* 7: 204-215, 2010.

361. **Wright JJ, Kim J, Buchanan J, Boudina S, Sena S, Bakirtzi K, Ilkun O, Theobald HA, Cooksey RC, Kandror KV, and Abel ED**. Mechanisms for increased myocardial fatty acid utilization following short-term high-fat feeding. *Cardiovasc Res* 82: 351-360, 2009.

362. **Wu KH, Han ZC, Mo XM, and Zhou B**. Cell delivery in cardiac regenerative therapy. *Ageing research reviews* 11: 32-40, 2012.

363. **Wu KK, and Huan Y**. Diabetic atherosclerosis mouse models. *Atherosclerosis* 191: 241-249, 2007.

364. **Wu Z, Puigserver P, Andersson U, Zhang C, Adelmant G, Mootha V, Troy A, Cinti S, Lowell B, Scarpulla RC, and Spiegelman BM**. Mechanisms controlling mitochondrial biogenesis and respiration through the thermogenic coactivator PGC-1. *Cell* 98: 115-124, 1999.

365. **Xu W, Zhang X, Qian H, Zhu W, Sun X, Hu J, Zhou H, and Chen Y**. Mesenchymal stem cells from adult human bone marrow differentiate into a cardiomyocyte phenotype in vitro. *Exp Biol Med (Maywood)* 229: 623-631, 2004.

366. **Yan B, Abdelli LS, and Singla DK**. Transplanted induced pluripotent stem cells improve cardiac function and induce neovascularization in the infarcted hearts of db/db mice. *Molecular pharmaceutics* 8: 1602-1610, 2011.

367. **Yan J, Young ME, Cui L, Lopaschuk GD, Liao R, and Tian R**. Increased glucose uptake and oxidation in mouse hearts prevent high fatty acid oxidation but cause cardiac dysfunction in diet-induced obesity. *Circulation* 119: 2818-2828, 2009.

368. **Yeih DF, Yeh HI, Lin LY, Tsay YG, Chiang FT, Tseng CD, and Tseng YZ**. Enhanced activity and subcellular redistribution of myocardial hexokinase after acute myocardial infarction. *Int J Cardiol* 149: 74-79, 2011.

369. **Zeng L, Hu Q, Wang X, Mansoor A, Lee J, Feygin J, Zhang G, Suntharalingam P, Boozer S, Mhashilkar A, Panetta CJ, Swingen C, Deans R, From AH, Bache RJ, Verfaillie CM, and Zhang J**. Bioenergetic and functional consequences of bone marrow-derived multipotent progenitor cell transplantation in hearts with postinfarction left ventricular remodeling. *Circulation* 115: 1866-1875, 2007.

370. **Zhang J, and McDonald KM**. Bioenergetic consequences of left ventricular remodeling. *Circulation* 92: 1011-1019, 1995.

371. **Zhang L, Ussher JR, Oka T, Cadete VJ, Wagg C, and Lopaschuk GD**. Cardiac diacylglycerol accumulation in high fat-fed mice is associated with impaired insulin-stimulated glucose oxidation. *Cardiovasc Res* 89: 148-156, 2011.

372. **Zhang Z, Deb A, Zhang Z, Pachori A, He W, Guo J, Pratt R, and Dzau VJ**. Secreted frizzled related protein 2 protects cells from apoptosis by blocking the effect of canonical Wnt3a. *J Mol Cell Cardiol* 46: 370-377, 2009.

373. **Zhao Q, Sun Y, Xia L, Chen A, and Wang Z**. Randomized study of mononuclear bone marrow cell transplantation in patients with coronary surgery. *Ann Thorac Surg* 86: 1833-1840, 2008.

374. **Zoll J, Monassier L, Garnier A, N'Guessan B, Mettauer B, Veksler V, Piquard F, Ventura-Clapier R, and Geny B**. ACE inhibition prevents myocardial infarction-induced skeletal muscle mitochondrial dysfunction. *J Appl Physiol* 101: 385-391, 2006.

APPENDIX A

Figure A.1 Representative saponin-permeabilized, left ventricle, fiber bundle oxygen consumption experiment

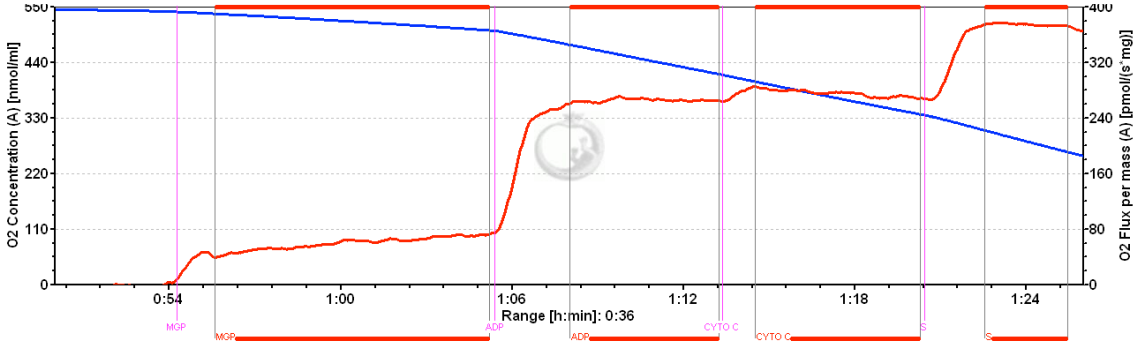

Figure A.1: Representative saponin-permeabilized cardiac fiber oxygen consumption/flux trace (red line) from a chow fed SHAM mouse utilized in Chapter 4. Oxygen consumption is the negative time-derivative of oxygen concentration (blue line) in a closed 2 ml chamber. Oxygen levels are held at a hyper-saturated concentration to prevent it from being rate limiting. Malate (2mM), glutamate (10mM), pyruvate (5mM) (MGP) supported respiration in the absence of ADP indicates respiration resulting from proton leak, electron slip, and ATPase activity (33). Saturating (5mM) adenosine diphosphate (ADP)-stimulated respiration supported by nicotinamide adenine dinucleotide reducing equivalents (MGP) represents maximal respiration through complex I. This respiratory state is influenced by ATP turnover (ANT, phosphate transporter and ATP synthase) and substrate oxidation (substrate uptake, substrate catabolism, electron transport through the ETC, oxygen concentration and pool sizes of cytochrome c and ubiquinone) (33). A cytochrome c (CYTO C) (10mM) test acts as a quality control index to identify damaged preparations. There is not an elevation in oxygen consumption that exceeds 15% suggesting appropriate sample preparation (178).

A titration of succinate (S) (10 mM) results in ADP-stimulated respiration from convergent electron input through complex I and II.

APPENDIX B

Table B.1 Proportion of mouse mortality following the ligation surgery in chapter four and five

	SHAM	MI+PBS	MI+MSC
Chapter 4 Mortality Post-infarct (%)	0.0	7.4	0.0
Chapter 5 Mortality Post-infarct (%)	0.0	19.5	13.0

Chapter four mice: n=13 for SHAM, n=27 for MI+PBS, and n=22 for MI+MSC. Chapter five mice: n=18 for SHAM, n=41 for MI+PBS, and n=23 for MI+MSC.